NATIONAL TECHNICAL UNIVERSITY OF ATHENS
School of Civil Engineering
Department of Structural Engineering
Institute of Steel Structure

DUCTILE SEISMIC DESIGN, PERFORMANCE ASSESSMENT AND TAXONOMIC CHARACTERIZATION OF STEEL RACKING SYSTEMS

DOCTORAL THESIS OF
DIMITRIOS A. TSARPALIS

Supervised by
I. VAYAS
Professor (ret.) NTUA

Athens, May 2022

ΕΘΝΙΚΟ ΜΕΤΣΟΒΙΟ ΠΟΛΥΤΕΧΝΕΙΟ
Σχολή Πολιτικών Μηχανικών
Τομέας Δομοστατικής
Εργαστήριο Μεταλλικών Κατασκευών

ΠΛΑΣΤΙΜΟΣ ΣΕΙΣΜΙΚΟΣ ΣΧΕΔΙΑΣΜΟΣ, ΑΠΟΤΙΜΗΣΗ ΕΠΙΤΕΛΕΣΤΙΚΟΤΗΤΑΣ ΚΑΙ ΤΑΞΙΝΟΜΙΚΟΣ ΧΑΡΑΚΤΗΡΙΣΜΟΣ ΣΥΣΤΗΜΑΤΩΝ ΜΕΤΑΛΛΙΚΩΝ ΡΑΦΙΩΝ

ΔΙΔΑΚΤΟΡΙΚΗ ΔΙΑΤΡΙΒΗ
ΔΗΜΗΤΡΙΟΥ Α. ΤΣΑΡΠΑΛΗ

Επιβλέπων
Ι. ΒΑΓΙΑΣ
τ. Καθηγητής ΕΜΠ

Αθήνα, Μάιος 2022

NATIONAL TECHNICAL UNIVERSITY OF ATHENS
School of Civil Engineering
Department of Structural Engineering
Institute of Steel Structure

DUCTILE SEISMIC DESIGN, PERFORMANCE ASSESSMENT, AND TAXONOMIC CHARACTERIZATION OF STEEL RACKING SYSTEMS

DOCTORAL THESIS OF
DIMITRIOS A. TSARPALIS
Diploma in Civil Engineering, NTUA (2016)
MSc, NTUA (2018)
«Analysis and Design of Earthquake Resistant Structures»

The thesis is submitted to the School of Civil Engineering of the National Technical University of Athens in fulfilment of the requirement for the Degree of Doctor of Philosophy

ADVISORY COMMITTEE:
1. I. VAYAS, Professor (ret.), NTUA (supervisor)
2. D. VAMVATSIKOS, Associate Professor, NTUA
3. P. THANOPOULOS, Lecturer, NTUA

EXAMINATION COMMITTEE:
1. I. VAYAS, Professor (ret.), NTUA (supervisor)
2. D. VAMVATSIKOS, Associate Professor, NTUA
3. P. THANOPOULOS, Lecturer, NTUA
4. C. GANTES, Professor, NTUA
5. A. AVRAAM, Assistant Professor, NTUA
6. F. MORELLI, Assistant Professor, UNIPI
7. C.A. CASTIGLIONI, Professor, POLIMI

Athens, May 2022

© Copyright 2022 by Dimitrios Tsarpalis
All Rights Reserved

Neither the whole nor any part of this doctoral thesis may be copied, stored in a retrieval system, distributed, reproduced, translated, or transmitted for commercial purposes, in any form or by any means now or hereafter known, electronic or mechanical, without the written permission from the author. Reproducing, storing and distributing this doctoral thesis for non-profitable, educational or research purposes is allowed, without prejudice to reference to its source and to inclusion of the present text. Any queries in relation to the use of the present doctoral thesis for commercial purposes must be addressed to its author.

Approval of this doctoral thesis by the School of Civil Engineering of the National Technical University of Athens (NTUA) does not constitute in any way an acceptance of the views of the author contained herein by the said academic organization (L. 5343/1932, art. 202).

ΕΘΝΙΚΟΣ ΜΕΤΣΟΒΙΟ ΠΟΛΥΤΕΧΝΕΙΟ
Σχολή Πολιτικών Μηχανικών
Τομέας Δομοστατικής
Εργαστήριο Μεταλλικών Κατασκευών

ΠΛΑΣΤΙΜΟΣ ΣΕΙΣΜΙΚΟΣ ΣΧΕΔΙΑΣΜΟΣ, ΑΠΟΤΙΜΗΣΗ ΕΠΙΤΕΛΕΣΤΙΚΟΤΗΤΑΣ ΚΑΙ ΤΑΞΙΝΟΜΙΚΟΣ ΧΑΡΑΚΤΗΡΙΣΜΟΣ ΣΥΣΤΗΜΑΤΩΝ ΜΕΤΑΛΛΙΚΩΝ ΡΑΦΙΩΝ

ΔΙΔΑΚΤΟΡΙΚΗ ΔΙΑΤΡΙΒΗ
ΔΗΜΗΤΡΙΟΥ Α. ΤΣΑΡΠΑΛΗ
Δίπλωμα Πολιτικού Μηχανικού, ΕΜΠ (2016)
Μεταπτυχιακό Δίπλωμα, ΕΜΠ (2018)
«Δομοστατικός Σχεδιασμός & Ανάλυση των Κατασκευών»

Η διατριβή υποβλήθηκε στη Σχολή Πολιτικών Μηχανικών του Εθνικού Μετσόβιου Πολυτεχνείου προς εκπλήρωση των προϋποθέσεων του τίτλου του Διδάκτορος Μηχανικού

ΤΡΙΜΕΛΗΣ ΣΥΜΒΟΥΛΕΥΤΙΚΗ ΕΠΙΤΡΟΠΗ:
1. Ι. ΒΑΓΙΑΣ, τ. Καθηγητής, ΕΜΠ (επιβλέπων)
2. Δ. ΒΑΜΒΑΤΣΙΚΟΣ, Αν. Καθηγητής, ΕΜΠ
3. Π. ΘΑΝΟΠΟΥΛΟΣ, Λέκτορας, ΕΜΠ

ΕΠΤΑΜΕΛΗΣ ΕΞΕΤΑΣΤΙΚΗ ΕΠΙΤΡΟΠΗ:
1. Ι. ΒΑΓΙΑΣ, τ. Καθηγητής, ΕΜΠ (επιβλέπων)
2. Δ. ΒΑΜΒΑΤΣΙΚΟΣ, Αν. Καθηγητής, ΕΜΠ
3. Π. ΘΑΝΟΠΟΥΛΟΣ, Λέκτορας, ΕΜΠ
4. Χ. ΓΑΝΤΕΣ, Καθηγητής, ΕΜΠ
5. Α. ΑΒΡΑΑΜ, Επ. Καθηγητής, ΕΜΠ
6. F. MORELLI, Επ. Καθηγητής, UNIPI
7. C.A. CASTIGLIONI, Καθηγητής, POLIMI

Αθήνα, Μάιος 2022

© Copyright 2022 by Δημήτριος Τσαρπαλής

Με επιφύλαξη παντός δικαιώματος

Απαγορεύεται η αντιγραφή, αποθήκευση σε αρχείο πληροφοριών, διανομή, αναπαραγωγή, μετάφραση ή μετάδοση της παρούσας εργασίας, εξ ολοκλήρου ή τμήματος αυτής, για εμπορικό σκοπό, υπό οποιαδήποτε μορφή και με οποιοδήποτε μέσο επικοινωνίας, ηλεκτρονικό ή μηχανικό, χωρίς την προηγούμενη έγγραφη άδεια του συγγραφέα. Επιτρέπεται η αναπαραγωγή, αποθήκευση και διανομή για σκοπό μη κερδοσκοπικό, εκπαιδευτικής ή ερευνητικής φύσης, υπό την προϋπόθεση να αναφέρεται η πηγή προέλευσης και να διατηρείται το παρόν μήνυμα. Ερωτήματα που αφορούν στη χρήση της εργασίας για κερδοσκοπικό σκοπό πρέπει να απευθύνονται προς το συγγραφέα.

Η έγκριση της διδακτορικής διατριβής από την Ανώτατη Σχολή Πολιτικών Μηχανικών του Εθνικού Μετσόβιου Πολυτεχνείου δεν υποδηλώνει αποδοχή των απόψεων του συγγραφέως (Ν. 5343/1932, Άρθρο 202).

Το έργο συγχρηματοδοτείται από την Ελλάδα και την Ευρωπαϊκή Ένωση (Ευρωπαϊκό Κοινωνικό Ταμείο) μέσω του Επιχειρησιακού Προγράμματος «Ανάπτυξη Ανθρώπινου Δυναμικού, Εκπαίδευση και Διά Βίου Μάθηση», στο πλαίσιο της Πράξης «Ενίσχυση του ανθρώπινου ερευνητικού δυναμικού μέσω της υλοποίησης διδακτορικής έρευνας» (MIS-5000432), που υλοποιεί το Ίδρυμα Κρατικών Υποτροφιών (ΙΚΥ).

Ευρωπαϊκή Ένωση
Ευρωπαϊκό Κοινωνικό Ταμείο

Επιχειρησιακό Πρόγραμμα
Ανάπτυξη Ανθρώπινου Δυναμικού,
Εκπαίδευση και Διά Βίου Μάθηση
Με τη συγχρηματοδότηση της Ελλάδας και της Ευρωπαϊκής Ένωσης

ΕΣΠΑ
2014-2020
ανάπτυξη - εργασία - αλληλεγγύη

This research is co-financed by Greece and the European Union (European Social Fund- ESF) through the Operational Programme «Human Resources Development, Education and Lifelong Learning» in the context of the project “Strengthening Human Resources Research Potential via Doctorate Research” (MIS-5000432), implemented by the State Scholarships Foundation (ΙΚΥ).

Ευρωπαϊκή Ένωση
European Social Fund

Operational Programme
Human Resources Development,
Education and Lifelong Learning
Co-financed by Greece and the European Union

ΕΣΠΑ
2014-2020
ανάπτυξη - εργασία - αλληλεγγύη

Ευχαριστίες

Σε αυτό το σημείο θα ήθελα να ευχαριστήσω πρωτίστως τους Ι. Βάγια, τ. Καθηγητή ΕΜΠ και Δ. Βαμβάτσικο, Αναπληρωτή Καθηγητή ΕΜΠ για την επιστημονική καθοδήγηση και τις πολύτιμες συμβουλές τους σε θέματα Στατικής, Αντισεισμικής Μηχανικής και επιστήμης των Μεταλλικών Κατασκευών. Επίσης θα ήθελα να ευχαριστήσω τον Π. Θανόπουλο, Λέκτορα ΕΜΠ και μέλος της τριμελούς συμβουλευτικής επιτροπής καθώς και τα υπόλοιπα μέλη της επταμελούς επιτροπής που συνέβαλαν σημαντικά στη βελτίωση της ποιότητας της παρούσας διατριβής με ενδιαφέρουσες παρατηρήσεις, διορθώσεις και συμβουλές.

Θα ήθελα ακόμη να ευχαριστήσω τους συναδέλφους μηχανικούς με τους οποίους συνεργάστηκα στα πλαίσια του ερευνητικού προγράμματος STEELWAR και με βοήθησαν καθοριστικά στην κατανόηση του αντικειμένου των μεταλλικών ραφιών. Ιδιαιτέρως θα ήθελα να ευχαριστήσω τους Filippo Delladonna, Agnese Natali, Cristian Vulcu και Fransesco Morelli για το ευχάριστο και φιλικό κλίμα που αναπτύξαμε σε όλα τα χρόνια της συνεργασίας μας.

Σε προσωπικό επίπεδο θα ήθελα να ευχαριστήσω τους φίλους μου Απόστολο Σ., Αναστάση Α., Βασίλη Γκ., Γιώργο Δ., Γιώργο Χ., Δημήτρη Α. και Νεκτάριο Β. που με στηρίζουν και με συντροφεύουν με την παρέα τους. Ευχαριστίες θα ήθελα να δώσω και στη φίλη μου Στέλλα Ξ. για την ηρεμία και την υπομονή της που με βοήθησαν σημαντικά τους τελευταίους μήνες στη συγγραφή της διατριβής. Ακόμη θα ήθελα να ευχαριστήσω τους συναδέλφους και Υποψήφιους Διδάκτορες του εργαστηρίου Μεταλλικών Κατασκευών Α. Χατζηδάκη, Κ. Βλαχάκη, Π. Τσαρπαλή και Χ. Λαχανά, για τη συνεργασία μας τα τελευταία πέντε χρόνια και να τους ευχηθώ γρήγορη και επιτυχή ολοκλήρωση των διδακτορικών τους διατριβών.

Θα ήθελα να ευχαριστήσω την οικογένειά μου για την ανιδιοτελή στήριξή της σε όλες μου τις αποφάσεις. Ιδιαίτερα θα ήθελα να ευχαριστήσω τη μητέρα μου Ουρανία και τον πατέρα μου Αναστάσιο, με τον οποίο είχαμε μια ενδιαφέρουσα συζήτηση στο πρόβλημα της ολίσθησης των παλετών του Κεφαλαίου 6 της διατριβής. Τέλος θα ήθελα να ευχαριστήσω τα αδέρφια μου Παναγιώτη και Ηλία για την βοήθειά τους σε ό,τι χρειαστώ και να τους ευχηθώ συνεχή πρόοδο και ανέλιξη.

Στους γονείς μου, Ουρανία και Αναστάσιο

Abstract

Steel racking systems are Civil Engineering structures used to store the goods and materials of a warehousing unit. In order to facilitate the construction process and to minimize the weight of the steel members, racks are characterized by a number of peculiarities that distinguish them from ordinary buildings. Due to their loose connections and lightness, racks are flexible structures, characterized by significant geometric nonlinearities and local buckling phenomena that significantly deteriorate their lateral-loading response. Indeed, past earthquake events have revealed the vulnerability of racks against strong ground motions, underlining the need for novel design approaches in order to increase their resilience.

Research so far has focused on understanding the cyclic behaviour of members and joints that belong to the most common rack configuration, namely adjustable pallet racking systems. However, in order to serve different logistic needs, a variety of rack typologies with different uses and salient characteristics has evolved over time. As a result, racks can range from large independent buildings in the form of the automated rack supported warehouses (ARSWs), down to compact sub-structures. Along these lines, the macro-characteristics of various rack typologies are discussed for the first time, identifying their idiosyncrasies and commonalities to other systems, which are then summarized in a flexible and collapsible taxonomy.

In view of better understanding the behaviour of ARSWs to earthquake excitations, a comprehensive seismic assessment is conducted on five multi-depth case studies, designed by professional engineers according to the current European standards. The impact of the design assumptions on the definition of the seismic loads is highlighted and aggregated in a cumulative seismic load multiplier. Consequently, a series of linear response history analyses is performed, in order to assess the vulnerability of the ARSWs to non-ductile failure modes and to define a hierarchy of criticalities for each case study.

Following the current tendency in the earthquake engineering community for resilient infrastructure, a ductile seismic design framework is proposed for the cross-aisle direction of racks, so-called plastic ovalization strategy (POS). POS relies on the bearing deformation of the diagonal bolt hole to introduce ductility and reduce seismic demands, employing capacity design to avoid non-ductile failure modes. Analytical equations and finite element models are used to determine the key factors that influence the ductility of the connection and to calibrate the uniaxial springs in a beam element model. Finally, to assess the performance of POS, two ARSWs are examined.

To achieve frugal performance assessment of racking systems, a reduced-order modelling approach is proposed that replaces the entire cross-aisle frame with a single/double built-up column, equivalent Timoshenko beams or link elements. The resulting model can support 2D/3D elastic and inelastic analyses, allowing rapid structural analysis of massive racking systems.

Finally, the dissertation attempts to fill a gap in the problem of content-structure-sliding interaction (CSSI), a multi-faceted phenomenon that offers both detrimental and beneficial effects to the racking structure. Three approaches are investigated to capture CSSI, each characterized by its own modelling needs and level of accuracy. Simplified alternatives are calibrated using single degree of freedom systems and realistic rack case studies, offering a reliable tool for structural engineers to (a) accurately determine the expected pallet sliding displacements, and (b) correctly reduce the design seismic loads thanks the seismic isolation mechanism offered by CSSI.

Περίληψη

Τα μεταλλικά συστήματα ραφιών αποτελούν κατασκευές Πολιτικού Μηχανικού που χρησιμοποιούνται στην αποθήκευση προϊόντων και υλικών μιας αποθηκευτικής μονάδας. Προκειμένου να μειωθεί το κόστος και ο χρόνος κατασκευής, τα ράφια χαρακτηρίζονται από μια πληθώρα ιδιαιτεροτήτων που τα ξεχωρίζει από τα συμβατικά κτήρια. Η απόκρισή τους σε πλευρικά φορτία επηρεάζεται από τις εύκαμπτες συνδέσεις μεταξύ των μελών και τη χρήση λεπτότοιχων διατομών, οδηγώντας σε σημαντικές γεωμετρικές μη γραμμικότητες και φαινόμενα τοπικού λυγισμού. Πράγματι, παλαιότερες καταγραφές έχουν δείξει την τρωτότητα των συστημάτων αυτών σε έντονες σεισμικές διεγέρσεις, κάνοντας επιτακτική την ανάγκη για αναζήτηση καινοτόμων σχεδιαστικών προσεγγίσεων με σκοπό την αύξηση της ανταξιμότητάς τους.

Η ερεύνα έως τώρα έχει επικεντρωθεί στην κατανόηση της ανακυκλιζόμενης συμπεριφοράς μελών και κόμβων που ανήκουν στον πιο συνήθη τύπο ραφιών, τα προσαρμοσμένα συστήματα παλετόραφων. Ωστόσο, προκειμένου να εξυπηρετηθούν διαφορετικές υλικοτεχνικές ανάγκες, έχουν αναπτυχθεί στο πέρασμα του χρόνου ποικίλες τυπολογίες ραφιών με διαφορετικές χρήσεις και βασικά χαρακτηριστικά. Ως αποτέλεσμα, τα ράφια μπορεί να κυμαίνονται από μεγάλα ανεξάρτητα κτήρια στη μορφή των αυτοματοποιημένων ραφοϊστάμενων αποθηκών (ΑΡΑ) μέχρι συμπαγείς υπο-κατασκευές. Για το λόγο αυτό πραγματοποιείται για πρώτη φορά ένας ολοκληρωμένος σχολιασμός των μακρο-χαρακτηριστικών διάφορων τυπολογιών ραφιών, εντοπίζοντας τις ιδιοσυγκρασίες αλλά και τις ομοιότητές τους με άλλα συστήματα, τα οποία στη συνέχεια συνοψίζονται σε μια ευέλικτη και πτυσσόμενη ταξινομία.

Ενόψει της καλύτερης κατανόησης της συμπεριφοράς των ΑΡΑ σε σεισμικές διεγέρσεις, πραγματοποιείται μια ολιστική σεισμική αποτίμηση σε πέντε παραδείγματα σχεδιασμού ραφιών πολλαπλού βάθους, σχεδιασμένα από επαγγελματίες μηχανικούς σύμφωνα με τα τρέχοντα Ευρωπαϊκά πρότυπα. Υπογραμμίζεται η επίπτωση των σχεδιαστικών υποθέσεων κατά τον προσδιορισμό των σεισμικών φορτίων, οι οποίοι στη συνέχεια συγκεντρώνονται σε έναν σωρευτικό πολλαπλασιαστή σεισμικών δυνάμεων. Έπειτα πραγματοποιείται μια σειρά γραμμικών αναλύσεων χρονοϊστορίας προκειμένου να εκτιμηθεί η τρωτότητα των ΑΡΑ σε ψαθυρούς μηχανισμούς αστοχίας και να προσδιοριστεί η ιεραρχία κρισιμοτήτων για κάθε παράδειγμα σχεδιασμού.

Ακολουθώντας την τρέχουσα τάση της κοινότητας αντισεισμικής μηχανικής για ανατάξιμες υποδομές, προτείνεται μια πλάστιμη σεισμική σχεδίαση κατά την εγκάρσια διεύθυνση των ραφιών, η λεγόμενη στρατηγική πλαστικής οβαλοποίησης (ΣΠΟ). Η ΣΠΟ βασίζεται στην παραμόρφωση λόγω σύνθλιψης άντυγας της οπής της διαγωνίου ώστε να εξασφαλιστεί επαρκής πλαστιμότητα και να μειωθούν οι σεισμικές απαιτήσεις, εισάγοντας έναν ικανοτικό σχεδιασμό για να αποφευχθούν μη πλάστιμες μορφές αστοχίας. Στη συνέχεια γίνεται χρήση αναλυτικών εξισώσεων και μοντέλων πεπερασμένων στοιχείων ώστε να προσδιοριστούν οι βασικοί παράγοντες που επηρεάζουν την πλαστιμότητα της σύνδεσης και να βαθμονομηθούν τα μονοαξονικά ελατήρια που χρησιμοποιούνται για την προσομοίωση του φαινομένου σε γραμμικά μοντέλα δοκού. Τέλος, προκειμένου να εκτιμηθεί η επίδοση της ΣΠΟ, εξετάζονται δύο παραδείγματα σχεδιασμού ΑΡΑ.

Για την επίτευξη μιας φειδωλής αποτίμησης επιτελεστικότητας συστημάτων ραφιών, προτείνεται μια μεθοδολογία απλοποίησης του αριθμητικού μοντέλου η οποία αντικαθιστά ολόκληρο το πλαίσιο της εγκάρσιας διεύθυνσης είτε με ένα μονό/διπλό σύνθετο υποστύλωμα, είτε με ισοδύναμες δοκούς Timoshenko, είτε με στοιχεία συνδέσμου κόμβων. Το μοντέλο που προκύπτει μπορεί να υποστηρίξει 2Δ/3Δ ελαστικές και ανελαστικές αναλύσεις, επιτρέποντας την ταχεία δομική ανάλυση μεγάλων και πολύπλοκων συστημάτων ραφιών.

Τέλος, η διατριβή επιχειρεί να καλύψει κενά στο πρόβλημα της αλληλεπίδρασης περιεχομένων-κατασκευής λόγω ολίσθησης (ΑΠΚΟ), ένα πολύπλευρο φαινόμενο που έχει επιζήμιες αλλά και ευεργετικές επιδράσεις σε ένα σύστημα ραφιών. Τρεις προσεγγίσεις εξετάζονται για να ληφθεί υπόψη η ΑΠΚΟ, καθεμία χαρακτηριζόμενη από τις δικές της απαιτήσεις μοντελοποίησης και επίπεδο ακρίβειας. Οι απλοποιημένες εναλλακτικές βαθμονομούνται χρησιμοποιώντας μονοβάθμια συστήματα και πραγματικά παραδείγματα ραφιών, προσφέροντας ένα αξιόπιστο εργαλείο στους δομοστατικούς μηχανικούς προκειμένου (α) να προσδιορίσουν με ακρίβεια τις αναμενόμενες μετατοπίσεις των παλετών λόγω ολίσθησης, και (β) να απομειώσουν κατάλληλα τα σεισμικά φορτία σχεδιασμού χάρη στο μηχανισμό σεισμικής μόνωσης που προσφέρει η ΑΠΚΟ.

Πίνακας Περιεχομένων Εκτενούς Περίληψης

I. Εισαγωγή i

II. Μακρο-χαρακτηριστικά και Ταξινομία Συστημάτων Μεταλλικών Ραφιών ii

III. Σεισμική Αποτίμηση των Αυτοματοποιημένων Ραφοϊστάμενων Αποθηκών v

IV. Στρατηγική Πλαστικής Οβαλοποίησης vii

V. Απλοποιημένη Μοντελοποίηση των Αυτοματοποιημένων Ραφοϊστάμενων Αποθηκών ix

VI. Μέθοδοι για τη Σεισμική Αποτίμηση της Ολίσθησης Περιεχομένων σε Ράφια Αποθήκευσης.. xi

VII. Συμπεράσματα xiii

VIII. Βιβλιογραφικές αναφορές xiv

Εκτενής Περίληψη

I. Εισαγωγή

Τα συστήματα μεταλλικών ραφιών αποτελούν κατασκευές Πολιτικού Μηχανικού με σκοπό την αποθήκευση των προϊόντων και υλικών μιας αποθήκης. Προκειμένου να εξυπηρετηθούν διαφορετικές υλικοτεχνικές ανάγκες, μια μεγάλη ποικιλία τυπολογιών ραφιών έχει αναπτυχθεί τα τελευταία χρόνια (Tilburgs, 2013), με σημαντικές δομικές διαφορές μεταξύ τους. Έτσι τα ράφια κυμαίνονται από μικρού ύψους υπο-κατασκευές εντός μιας αποθηκευτικής μονάδας, μέχρι πελώριες μεταλλικές κατασκευές που στηρίζουν τόσο τις παλέτες όσο και την ίδια την αποθήκη. Οι καινοτομίες δε περιορίζονται μόνο στο στατικό φορέα αλλά εκτείνονται και στον τρόπο διαχείρισης των αγαθών, όπου αυξάνεται συνεχώς η ζήτηση για την ενσωμάτωση αυτοματοποιημένων διαδικασιών συλλογής & αποθήκευσης, με τη χρήση τεχνικής νοημοσύνης και ρομποτικής.

Λόγω της ανάγκης για γρήγορη εγκατάσταση, μεταβαλλόμενη γεωμετρία και χαμηλό κόστος, τα συστήματα μεταλλικών ραφιών χαρακτηρίζονται από κάποιες ιδιαιτερότητές που τα ξεχωρίζουν από τα συμβατικά κτήρια. Η πιο παραδοσιακή τυπολογία ραφιών είναι τα λεγόμενα ρυθμιζόμενα συστήματα παλετόραφων (ΡΣΠ), στα οποία η διαχείριση των παλετών γίνεται μέσω περονοφόρων οχημάτων και επομένως απαιτείται ο σχηματισμός διαδρόμων ανάμεσά τους. Έτσι, στα ΡΣΠ (αλλά και στα ράφια γενικά), ορίζονται δύο κύριες κατευθύνσεις: η διαμήκης (down-aisle) και η εγκάρσια (cross-aisle), όπως φαίνεται στο Σχήμα 1(α). Και στις δύο κύριες διευθύνσεις τυπικά χρησιμοποιούνται μέλη από λεπτότοιχες διατομές με πολύ απλές κοχλιωτές (Σχήμα 1(β)) ή γαντζωτές συνδέσεις (Σχήμα 1(γ)), τα οποία έχουν πολύ μεγάλη επιρροή στην απόκριση του ραφιού σε σεισμικές διεγέρσεις. Επίσης, σε αντίθεση με τα συμβατικά κτήρια, το βάρος των μεταλλικών αυτών μελών είναι ένα πολύ μικρό ποσοστό, π.χ. της τάξης του 5-10%, των ωφέλιμων φορτίων. Για τους λόγους αυτούς, έχουν αναπτυχθεί εξιδικευμένοι κώδικες σχεδιασμού για ράφια, όπως το EN 15512 (2005) στην Ευρώπη, το RMI (2012) στις ΗΠΑ, ή το AS 4084 (2012) στην Αυστραλία.

Η σεισμική συμπεριφορά των συστημάτων ραφιών έχει διερευνηθεί από πολλούς ερευνητές παγκοσμίως. Στην Ευρώπη, τα ευρωπαϊκά ερευνητικά έργα SEISRACKS (Rosin et al., 2007) και SEISRACKS2 (Castiglioni et al., 2014) εξέτασαν τη σεισμική απόκριση των ΡΣΠ με ή χωρίς συνδέσμους δυσκαμψίας μέσω πειραματικών και αριθμητικών δοκιμών (Adamakos, 2018; Kanyilmaz, et al., 2016). Στην Αυστραλία, οι Gilbert and Rasmussen (2012) και οι Gilbert et al. (2014) παρουσίασαν την τρισδιάστατη απόκριση των ραφιών drive-in, όπου φάνηκε ότι η τριβή μεταξύ παλετών-δοκών παρέχει ένα είδος πρόσθετου οριζόντιου διαφράγματος στην κατασκευή. Η παρούσα διατριβή περιλαμβάνει μια συλλογή επιστημονικών διερευνήσεων που επιχειρεί να επεκτείνει την τρέχουσα γνώση σχετικά με τη σεισμική συμπεριφορά των συστημάτων μεταλλικών ραφιών. Ενώ η έρευνα επικεντρώνεται κυρίως στη σεισμική αποτίμηση των καινοτόμων αυτοματοποιημένων ραφοϊστάμενων αποθηκών (ΑΡΑ), δεν περιορίζεται σε μια μεμονωμένη τυπολογία ραφιών αλλά προσφέρει μια πολύπλευρη συνεισφορά που δεν είναι μόνο ακαδημαϊκού ενδιαφέροντος, αλλά και πρακτικής χρήσης, βοηθώντας τους δομοστατικούς μηχανικούς και τους αναλυτές κινδύνου να βελτιώσουν το σχεδιασμό, την αξιολόγηση και την υποστήριξη αποφάσεων.

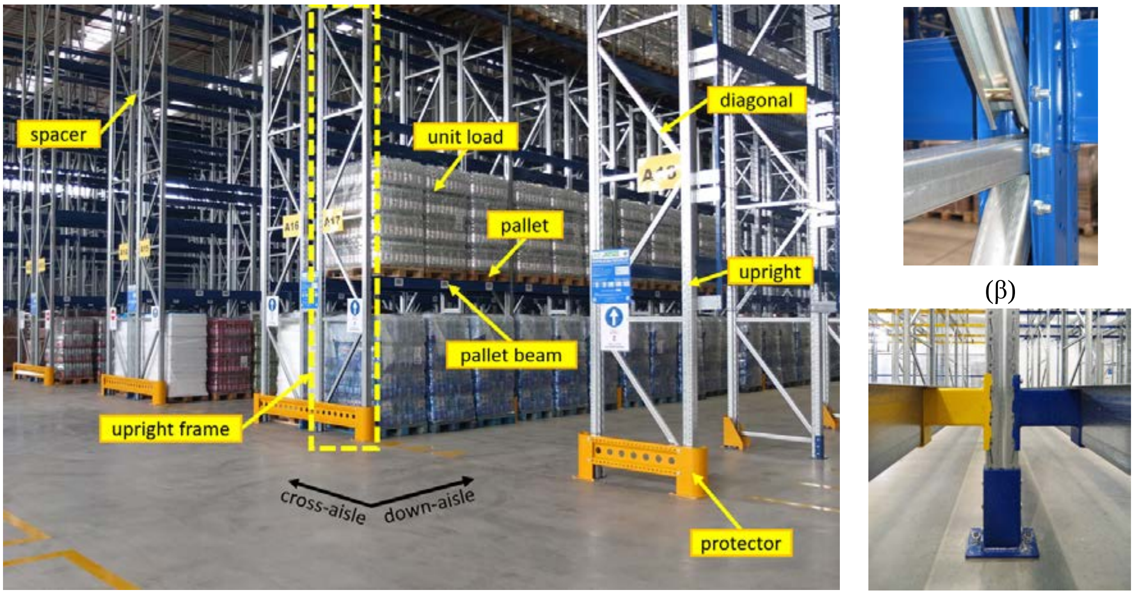

(β)

(α) (γ)

Σχήμα 1: Τυπική μορφολογία ενός ρυθμιζόμενου συστήματος παλετόραφων (ΡΣΠ), δείχνοντας (α) τον ορισμό των κύριων διευθύνσεων και τα βασικά δομικά μέλη, (β) την κοχλιωτή σύνδεση διαγώνιου-υποστυλώματος και (γ) την γαντζωτή σύνδεση δοκού-υποστυλώματος.

Ο στόχος της διατριβής είναι: (α) να δημιουργηθεί μια επεκτάσιμη, φιλική προς τον χρήστη και διαισθητική ταξινομία για συστήματα μεταλλικών ραφιών, προσφέροντας ένα κοινό λεξιλόγιο στους αναλυτές κινδύνου για αποτελεσματική αναγνώριση και αποτίμηση, (β) να πραγματοποιηθεί, για πρώτη φορά, μια ολοκληρωμένη σεισμική αποτίμηση των ΑΡΑ εγκατεστημένων σε περιοχές υψηλής σεισμικότητας, (γ) να προτείνει μια νέα προσέγγιση σεισμικού σχεδιασμού που αυξάνει αξιόπιστα την πλαστιμότητα των ραφιών κατά την εγκάρσια διεύθυνσή τους, (δ) να προσφέρει απλοποιημένες προσεγγίσεις μοντελοποίησης για ταχεία αποτίμηση και σχεδιασμό των ΑΡΑ και (ε) να καθορίσει αξιόπιστες μεθόδους για τη σεισμική αποτίμηση της ολίσθησης περιεχομένων.

II. Μακρο-χαρακτηριστικά και Ταξινομία Συστημάτων Μεταλλικών Ραφιών

Η μεγάλη ποικιλία χαρακτηριστικών μεταξύ διαφορετικών συστημάτων ραφιών σημαίνει ότι συγχώνευση όλων των τύπων σε μια ενιαία κλάση «συστήματα ραφιών» θα αποτελούσε μια χονδρική υπεραπλούστευση. Αυτό μπορεί να γίνει αντιληπτό αν κανείς εξετάσει τον στατικό φορέα διαφορετικών τυπολογιών κατά τη διαμήκη διεύθυνση. Έτσι για παράδειγμα στο τυπικό ΡΣΠ (Σχήμα 1(α)) ή στα ράφια ελαφρού τύπου (Σχήμα 2(δ)) η διαμήκης διεύθυνση αποτελείται από ένα εύκαμπτο πλαίσιο ροπής, στο σύστημα drive-in (Σχήμα 2(α)) σχηματίζεται ένα τρισδιάστατο δικτυωτό πλαίσιο, ενώ στις ΑΡΑ (Σχήμα 2(β)) είναι απαραίτητη η χρήση δύσκαμπτων χιαστί πύργων. Οι διαφορές δεν περιορίζονται μόνο το δομικό φορέα, αλλά σχετίζονται και με το τρόπο διαχείρισης των προϊόντων (π.χ. στα ΡΣΠ χειρωνακτικός, στις ΑΡΑ αυτοματοποιημένος (Σχήμα 2(β)), τη θέση του ραφιού (π.χ. τα drive-in είναι εντός της αποθήκης, τα σύστηματα ραφιών-προβόλων (Σχήμα 2(γ)) εκτός), κ.λπ.

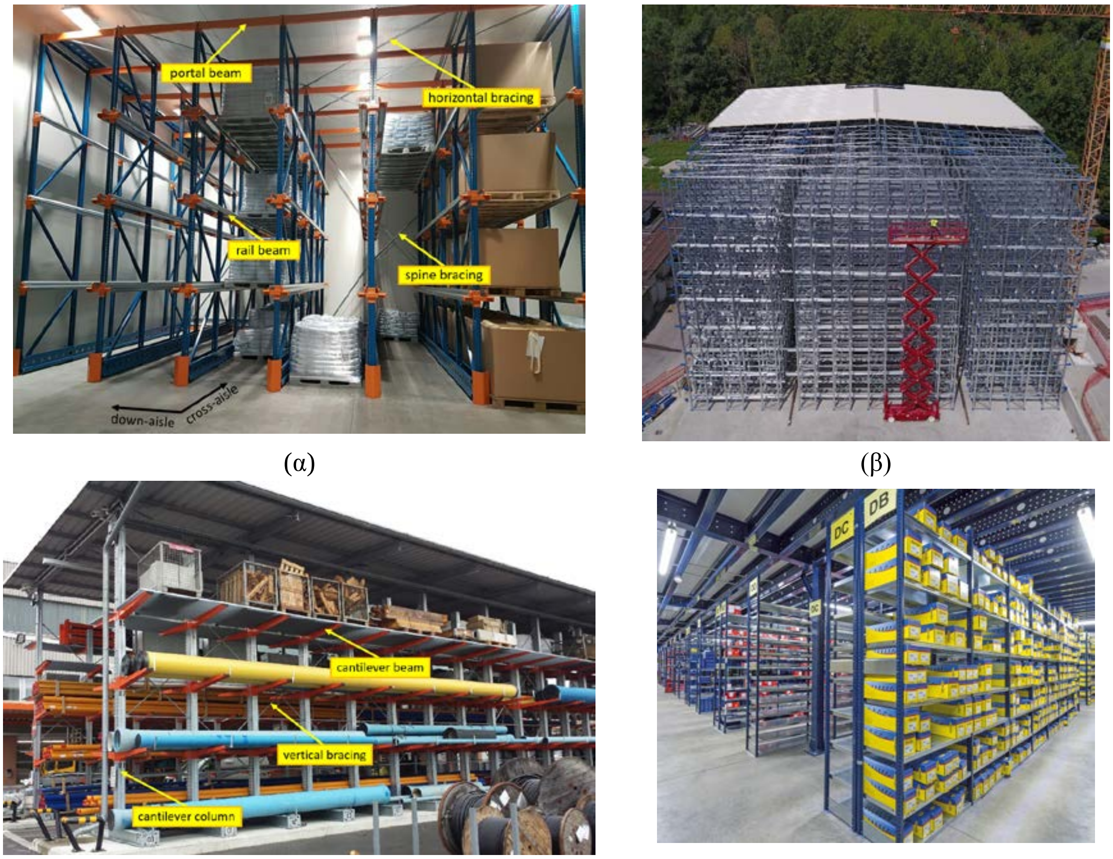

(α) (β)

(γ) (δ)

Σχήμα 2: Παραδείγματα συστημάτων ραφιών: (α) σύστημα ραφιών drive-in, (β) σύστημα APA πολλαπλού βάθους, (γ) σύστημα ραφιών-προβόλων και (δ) σύστημα ραφιών ελαφρού τύπου.

Ενώ οι κατασκευαστές και οι σχεδιαστές μεταλλικών ραφιών χρησιμοποιούν μια αρκετά ευρεία κατηγοριοποίηση των προϊόντων τους, τείνουν επίσης να εστιάζουν στη λειτουργικότητα, τη χρηστικότητα και την απόδοση από την άποψη της υλικοτεχνικής υποστήριξης· τέτοια χαρακτηριστικά δεν είναι απαραίτητα σημαντικά κατά τη διαδικασία αποτίμησης επικινδυνότητας. Ομοίως, οι κώδικες σχεδιασμού για ράφια μπορεί να χρησιμοποιούν ορισμένα στοιχεία ταξινομίας (π.χ. το EN 16681), ωστόσο αυτά δεν πληρούν τους σκοπούς μίας πλήρους ταξινομίας με σκοπό την αποτίμηση επικινδυνότητας. Προκειμένου να αντιμετωπιστούν τα ανωτέρω προβλήματα, είναι απαραίτητη η δημιουργία μιας ομοιόμορφης ταξινομίας για τα συστήματα ραφιών, η οποία οδηγεί στα ακόλουθα πλεονεκτήματα: (α) διευκόλυνση της σύγκρισης των αποτελεσμάτων μεταξύ διαφορετικών μελετών, (β) επιλογή συναρτήσεων επικινδυνότητας/τρωτότητας για μελέτες αξιολόγησης χαρτοφυλακίου ή κινδύνων/ζημιών περιφερειών και (γ) συλλογή αξιοποιήσιμων δεδομένων κατά τη διαδικασία καταγραφής των σεισμικών ζημιών/απωλειών.

Η προτεινόμενη ταξινομία εστιάζει στη δομική συμπεριφορά των ραφιών υπό σεισμικές δράσεις, έχοντας ως βάση την Ταξινομία Κτηρίων του Global Earthquake Model (Brzev et al., 2013). Είναι σχεδιασμένη να είναι επεκτάσιμη (γρήγορη προσθήκη νέων συστημάτων), φιλική προς το χρήστη και διαισθητική, με τα θεωρούμενα μακρο-χαρακτηριστικά να είναι εύκολα αναγνωρίσιμα από μη ειδικούς. Περιλαμβάνει πέντε βασικές «Ιδιότητες» για το χαρακτηρισμό ενός συστήματος ραφιών: (α) δομική τυπολογία, (β) τοποθέτηση και κάλυψη, (γ) ύψος, (δ) σύστημα αποθήκευσης και (ε) επίπεδο κώδικα σχεδιασμού . Κάθε «Ιδιότητα» μπορεί να αναλύεται σε πολλά «Επίπεδα Ιδιοτήτων», για τα οποία στη συνέχεια δίνονται διάφορες «Επιλογές» (ή παραδείγματα). Ο λεπτομερής σχολιασμός των επιμέρους «Ιδιοτήτων» παρατίθεται στη συνέχεια.

Α) Δομική Τυπολογία, αναλύεται σε τρία «Επίπεδα»:
   1. Το σύστημα παραλαβής κατακόρυφων φορτίων (π.χ. «στύλοι+δοκοί», «στύλοι+ράγες», «πρόβολοι»);
   2. Το σύστημα παραλαβής οριζόντιων φορτίων στη διαμήκη διεύθυνση (π.χ. πλαίσια ροπής, σύνδεσμοι δυσκαμψίας, χιαστί πύργοι);
   3. Τον τύπο χάλυβα (π.χ. ψυχρής έλασης, θερμής έλασης, μεικτός).

Β) Τοποθέτηση και κάλυψη (π.χ. εσωτερικού/εξωτερικού χώρου, ραφοϊστάμενα). Αναλόγως της θέσης τοποθέτησης του ραφιού, μπορεί να υπάρχουν πρόσθετοι κίνδυνοι (π.χ. τα εξωτερικού χώρου πλήττονται από άνεμου, βροχή, χαλάζι, κ.λπ.).

Γ) Ύψος (π.χ. χαμηλά < 8 m, μέτριου ύψους 8-12 m, ψηλά 12-20 m, πολύ ψηλά > 20 m). Ιδιαίτερα στα συστήματα ραφιών, με μεγαλύτερο ύψος αυξάνονται όχι μόνο τα φαινόμενα Ρ-Δ, αλλά και οι κίνδυνος πτώσης προϊόντων από τα ανώτερα επίπεδα.

Δ) Σύστημα αποθήκευσης, αναλύεται σε τρία «Επίπεδα»:
   1. Το βάρος του φορτίου μονάδας (π.χ. ελαφρύ < 200 kg, μεσαίου βάρους 200-1000 kg, βαρύ 1000-2000 kg);
   2. Η επιφάνεια επαφής (π.χ. ξύλο/πλαστικό//χάλυβας+χάλυβας, κρεμαστά εμπορεύματα). Οι ξύλινες παλέτες έχουν πιο τραχεία επιφάνεια σε σχέση με τις πλαστικές ή τις μεταλλικές, άρα μικρότερό ο κίνδυνος ολίσθησης προϊόντων;
   3. Το σύστημα διαχείρισης (π.χ. χειρωνακτικό, ημι-αυτοματοποιημένο, πλήρως αυτοματοποιημένο. Στο χειρωνακτικό σύστημα υπάρχει ο κίνδυνος σύγκρουσης περονοφόρου οχήματος στο ράφι λόγω λάθος του οδηγού.

Ε) Επίπεδο κώδικα σχεδιασμού (π.χ. άνευ κώδικα, μεσαίου κώδικα, υψηλού κώδικα). Παλαιότερα, πολλές περιπτώσεις ραφιών είχαν κατασκευαστεί χωρίς καθόλου σεισμικό σχεδιασμού, ενώ άλλα με σεισμικούς κώδικες για συμβατικά κτήρια, υιοθετώντας υψηλά q. Πλέον, τόσο στην Ευρώπη όσο και στις ΗΠΑ υπάρχουν σεισμικά πρότυπα εξειδικευμένα για ράφια (κυρίως για τα ΡΣΠ), τα οποία προτείνουν χαμηλά q λόγω της χαμηλής πλαστιμότητας που έχει παρατηρηθεί τόσο πειραματικά όσο και σε πραγματικούς σεισμούς.

Τέλος η προτεινόμενη ταξινομία χρησιμοποιήθηκε για την κατηγοριοποίηση επιστημονικών δημοσιεύσεων που μελετούσαν την καθολική συμπεριφορά συστήματων ραφιών. Όπως διαπιστώθηκε, η διεθνής βιβλιογραφία έχει επικεντρωθεί κυρίως στην ανάλυση και την κατανόηση της σεισμικής συμπεριφοράς των συμβατικών ΡΣΠ, τα οποία είναι χαμηλού ύψους, φορτωμένα με παλέτες μεσαίου βάρους και διαχειριζόμενα με χειρωνακτικές μεθόδους. Αντίθετα, άλλα συστήματα όπως οι καινοτόμες ΑΡΑ δεν έχουν λάβει ακόμη την προσοχή της επιστημονικής κοινότητας, παρόλο που είναι πολύ δημοφιλείς στο εμπόριο.

III. Σεισμική Αποτίμηση των Αυτοματοποιημένων Ραφοϊστάμενων Αποθηκών

Η κατηγοριοποίηση πολλών αναλυτικών και πειραματικών δημοσιεύσεων που πραγματοποιήθηκε στο Κεφάλαιο ΙΙ, κατέδειξε ότι η επιστημονική κοινότητα έχει δώσει περιορισμένη προσοχή στη σεισμική απόκριση των πολυώροφων ΑΡΑ, αφήνοντας πολλά αναπάντητα ερωτήματα, όπως (α) τι q/R θα πρέπει να χρησιμοποιείται κατά την εγκάρσια και διαμήκη διεύθυνση του ραφιού, (β) ποια είναι τα κρισιμότερα μέλη/συνδέσεις, (γ) πώς λαμβάνονται υπόψη τα φαινόμενα δευτέρας τάξης και (δ) είναι η δυναμική φασματική ανάλυση μια κατάλληλη μέθοδος για τον υπολογισμό των σεισμικών δυνάμεων/παραμορφώσεων;

Ως ένα πρώτο βήμα προς την καλύτερη κατανόηση της σεισμικής συμπεριφοράς των ΑΡΑ, πραγματοποιήθηκε στα πλαίσια του ερευνητικού προγράμματος STEELWAR (2017) μια ολοκληρωμένη σεισμική αποτίμηση σε παραδείγματα εφαρμογών ραφιών πολλαπλού βάθους (βλ. Σχήμα 2(β)). Συγκεκριμένα, δόθηκε μια δεδομένη αποθηκευτική διάταξη (αριθμός επίπεδων, βάρος παλετών) ΑΡΑ και θέση εγκατάστασης (η πόλη Van στην Τουρκία, a_g = 0.3 g) σε πέντε επαγγελματίες μηχανικούς ραφιών και τους ζητήθηκε να σχεδιάσουν την αποθήκη με βάση τις σχεδιαστικές πρακτικές που χρησιμοποιούν. Λόγω των γεωμετρικών περιορισμών, όλοι οι σχεδιαστές κατέληξαν σε παρόμοιες διαστάσεις στην εγκάρσια διεύθυνση [64.84 – 65.05 m], στη διαμήκη [70.94 – 73.92 m] και στο ύψος [25.31 – 26.71 m] της αποθήκης. Επίσης σε όλα τα παραδείγματα ο δομικός φορέας αποτελούταν κατά την εγκάρσια διεύθυνση από πολλά σύνθετα υποστυλώματα συνδεόμενα στην κορυφή τους με μια δικτυωτή στέγη, ενώ κατά τη διαμήκη από δύο ή τρεις δύσκαμπτους χιαστί πύργους.

Λόγω της έλλειψης ενός σχεδιαστικού προτύπου εξειδικευμένο για τις ΑΡΑ, οι μελετητές αναγκάστηκαν να χρησιμοποιήσουν ως βάση το σεισμικό κώδικα EN 16681 (2016), ο οποίος όμως αφορά τα συμβατικά ΡΣΠ. Έτσι, υιοθετήθηκαν χαμηλοί συντελεστές συμπεριφοράς, της τάξης του 1.5 έως 2.0, θεωρώντας ότι τα ράφια είναι κατασκευές περιορισμένης πλαστιμότητας και επομένως δε λήφθηκαν υπόψη κανόνες ικανοτικού σχεδιασμού. Αυτό είχε ως αποτέλεσμα την εμφάνιση ψαθυρών μηχανισμών αστοχίας στα μέλη και στις συνδέσεις, όπως διαπιστώθηκε κατά τον υπολογισμό των αντοχών σύμφωνα με τα EN 1993-1-1 (2005), EN 1993-1-3 (2006) και EN 15512 (2009). Συγκεκριμένα, κατά την εγκάρσια διεύθυνση οι στύλοι των σύνθετων υποστυλωμάτων ήταν επιρρεπείς σε στρεπτοκαμπτικό και τοπικό λυγισμό, ενώ τα διαγώνια μέλη σε λυγισμό και αστοχία της κοχλιωτής σύνδεσής τους με τους στύλους. Επειδή η σύνδεση αυτή υλοποιείται τυπικά με έναν κοχλία M10 ή M12, η αντοχή σε σύνθλιψη άντυγας ή αστοχίας του κοχλία σε διάτμηση ήταν πάντοτε μικρότερη από την πλαστική αντοχή διαρροής του μέλους. Όσον αφορά τις βάσεις των στύλων, σε όλα τα παραδείγματα περιλάμβαναν 2 ή 4 χημικά αγκύρια τα οποία ήταν επιρρεπή σε αστοχία κώνου σκυροδέματος. Παρόμοια ψαθυρή συμπεριφορά παρατηρήθηκε και στη διαμήκη διεύθυνση των ραφιών.

Για τη σεισμική αποτίμηση των παραδειγμάτων εφαρμογής χρησιμοποιήθηκε ένα σετ 15 πραγματικών σεισμικών καταγράφων (Kohrangi et al., 2018) που σέβονται την καμπύλη σεισμικής επικινδυνότητας της πόλης Van, χρησιμοποιώντας το γεωμετρικό μέσο των φασματικών επιταχύνσεων ($AvgSa$) ως μέτρο έντασης (Kohrangi et al., 2017). Συνεπώς, για κάθε παράδειγμα ΑΡΑ εκτελέστηκαν 15 αναλύσεις χρονοϊστορίας στην εγκάρσια και 15 στη διαμήκη διεύθυνση. Ο διαχωρισμός των αναλύσεων στις δύο κύριες διευθύνσεις έγινε για λόγους υπολογιστικής απλότητας, αφού τα 3Δ μοντέλα των ΑΡΑ είναι πολύ δύσχρηστα. Επίσης, λόγω της επικράτησης ψαθυρών μηχανισμών αστοχίας στις κατασκευές, δε λήφθηκαν υπόψη μη γραμμικότητες υλικού στους διαγώνιους συνδέσμους. Ωστόσο, οι γεωμετρικές μη γραμμικότητες προσομοιώθηκαν στα μοντέλα μέσω της χρήσης του γεωμετρικού μητρώου δυσκαμψίας P-Δ, αφού η χαμηλή πλευρική δυσκαμψία των ΑΡΑ τις καθιστά επιρρεπείς σε φαινόμενα δευτέρας τάξης.

Μετά την εκτέλεση των αναλύσεων, πραγματοποιήθηκε μια μετεπεξεργασία των αποτελεσμάτων για τον υπολογισμό των συντελεστών εκμετάλλευσης (ΣΕ) των συστατικών μερών των ραφιών. Συγκεκριμένα, χρησιμοποιήθηκαν οι χρονοϊστορίες των εντατικών μεγεθών (δυνάμεις και ροπές) που αναπτύσσονταν στα μέλη και στις συνδέσεις και με βάση τις αντοχές σχεδιασμού πραγματοποιήθηκαν οι έλεγχοι υπέρβασης σε κάθε χρονική στιγμή, με βάση τους αντίστοιχους Ευρωκώδικες. Με τον τρόπο αυτό καθορίστηκε μια *ιεραρχία κρισιμοτήτων* για κάθε παράδειγμα ραφιού, όπου πιο κρίσιμο θεωρούταν ένα συστατικό μέρος του οποίου η διάμεση τιμη των ΣΕ από τις 15 αναλύσεις ήταν υψηλότερη. Τα αποτελέσματα συνοψίζονται παραστατικά με τη χρήση διαγραμμάτων boxplot, όπως δίνεται στο Σχήμα 3 για το πρώτο ράφι (CS1).

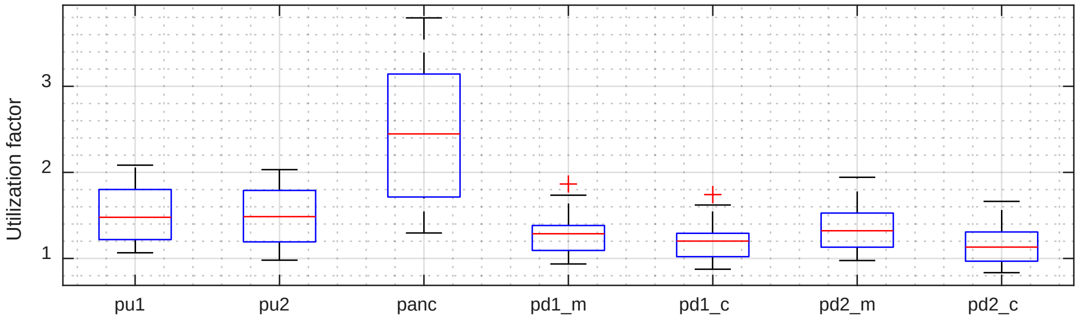

Σχήμα 3: Διαγράμματα boxplot των ΣΕ των συστατικών μερών (εγκάρσια διεύθυνση, παράδειγμα εφαρμογής CS1). Οι οριζόντιες κόκκινες γραμμές αναφέρονται στη διάμεσο των 15 αναλύσεων.

Με βάση το Σχήμα 3, το πιο κρίσιμα συστατικά μέρη στην εγκάρσια διεύθυνση του ραφιού CS1 είναι τα χημικά αγκύρια της βάσης (panc), ενώ ακολουθούν οι στύλοι των σύνθετων υποστυλωμάτων (pu1+pu2). Λιγότερο κρίσιμα ήταν τα διαγώνια μέλη (pd1_m+pd2_m) και οι συνδέσεις τους με τους στύλους (pd1_c+pd2_c). Παρόμοια συμπεριφορά παρατηρήθηκε και στα άλλα παραδείγματα εφαρμογών, τόσο στην εγκάρσια όσο και στη διαμήκη διεύθυνση. Ως αποτέλεσμα, οι καινοτόμες ΑΡΑ σχεδιασμένες με βάση τα τρέχοντα σεισμικά πρότυπα ραφιών είναι επιρρεπείς σε μη πλάστιμους μηχανισμούς αστοχίας και επομένως η ανακατανομή εντάσεων κατά τη διάρκεια ενός σεισμικού συμβάντος είναι πολύ περιορισμένη. Επίσης, παρατηρήθηκε ότι οι διάμεσες τιμές των ΣΕ σχεδόν όλων των συστατικών μερών ήταν κατά πολύ μεγαλύτερες της μονάδας. Αυτό οφείλεται στο γεγονός ότι κατά το σχεδιασμό οι μελετητές χρησιμοποίησαν διάφορους μειωτικούς συντελεστές τους φάσματος σχεδιασμού, οι οποίοι δε λήφθηκαν υπόψη στις αναλύσεις χρονοϊστορίας. Προκειμένου να εξεταστεί η επιρροή των συντελεστών αυτών, υλοποιήθηκαν πέντε υποθετικά σενάρια, όπου κάθε σενάριο κάνει δεκτές κάποιες μειώσεις ενώ άλλες όχι. Προέκυψε ότι ακόμη και αν γίνουν δεκτές όλες οι ευνοϊκές θεωρήσεις, τα χημικά αγκύρια των βάσεων εξακολουθούν να είναι κρίσιμα, έχοντας διάμεση τιμή ΣΕ μεγαλύτερη του 1.0.

IV. Στρατηγική Πλαστικής Οβαλοποίησης

Η σημαντικότητα των εγκαταστάσεων αποθήκευσης στον τομέα της εφοδιαστικής αλυσίδας δημιουργεί την απαίτηση για κατασκευές ραφιών που είναι ανατάξιμες σε ακραίους κινδύνους. Μια διακοπή της αλυσίδας εφοδιασμού, ή ακόμη χειρότερα, η καταστροφή των αποθηκευμένων αγαθών, μπορεί να οδηγήσει σε οικονομικές απώλειες που είναι πολύ μεγαλύτερες από το αρχικό κόστος του ραφιού. Αυτό ισχύει ιδιαίτερα για τις καινοτόμες ΑΡΑ, καθώς διαδραματίζουν διπλό ρόλο στη διαδικασία αποθήκευσης, υποστηρίζοντας τα εμπορεύματα και ταυτόχρονα προσφέροντας προστασία από το εξωτερικό περιβάλλον. Υπό αυτή την έννοια, οι ιδιοκτήτες πολυώροφων ΑΡΑ μπορεί να είναι πρόθυμοι να πληρώσουν για έναν ελαφρώς πιο ακριβό, αλλά λιγότερο ευάλωτο δομικό φορέα, προκειμένου να μετριάσουν τον κίνδυνο προσωρινής διακοπής λειτουργίας ή πλήρους απώλειας της περιουσίας τους.

Μια ευέλικτη προσέγγιση σε αυτό το πρόβλημα είναι η αύξηση της πλαστιμότητας του ραφιού, μέσω αξιοποίησης της πλάστιμης συμπεριφοράς συγκεκριμένων τμημάτων του φορέα, διατηρώντας παράλληλα την υπόλοιπη δομή στην ελαστική περιοχή. Ωστόσο, μια τέτοια νέα στρατηγική σχεδιασμού θα πρέπει να σέβεται τη φιλοσοφία της βιομηχανίας ραφιών, η οποία απαιτεί λεπτότοιχες μεταλλικές διατομές με πολύ απλές συνδέσεις με κοχλίες/γάντζους, ελαχιστοποιώντας τις εργασίες κατά τη διαδικασία εγκατάστασης και αποσυναρμολόγησης. Ως αποτέλεσμα, προτείνεται μια νέα προσέγγιση πλάστιμου σχεδιασμού κατά την εγκάρσια διεύθυνση των ραφιών, η λεγόμενη στρατηγική πλαστικής οβαλοποίησης (ΣΠΟ). Η ΣΠΟ βασίζεται στην πλαστική οβαλοποίηση λόγω σύνθλιψης άντυγας των διαγώνιων προκειμένου να αποφευχθούν άλλοι, πιο ψαθυροί, μηχανισμοί αστοχίας. Αυτό επιτυγχάνεται με την εισαγωγή των 10 νέων ικανοτικών κανόνων, οι οποίοι προσφέρουν υπεραντοχή στην κατασκευή, όπως στην αντοχή των κοχλιών σε διάτμηση, στη σύνθλιψη άντυγας των στύλων, στα χημικά αγκύρια, κ.λπ. Με τον τρόπο αυτό, οι σεισμικές ζημίες περιορίζονται κυρίως στις οπές των διαγώνιων, τα οποία είναι εύκολα αντικαταστάσιμα μέλη.

Ενώ η οβαλοποίηση λόγω σύνθλιψης άντυγας θεωρείται μια πλάστιμη μορφή αστοχίας σε στατικές φορτίσεις, εντούτοις δεν έχει διερευνηθεί για δυναμικά φορτία, κυρίως επειδή σε συμβατικές κατασκευές οι συνδέσεις σχεδιάζονται με υπεραντοχή. Για τον ορισμό της μονοτονικής καμπύλης δύναμης/παραμόρφωσης, το προσχέδιο prEN1993-1-8:2021 (2021) προσφέρει μια αναλυτική σχέση μεταξύ της τάσης άντυγας και του ανοίγματος της οπής. Ωστόσο, η σχέση αυτή έχει αναπτυχθεί με βάση πειραματικά και αναλυτικά αποτελέσματα σε χαλύβδινα ελάσματα μεσαίο/μεγάλου πάχους και επομένως μπορεί να μην είναι κατάλληλη για λεπτότοιχες διατομές, όπως αυτές στα διαγώνια μέλη των ραφιών. Προκειμένου να διερευνηθεί η εφαρμοσιμότητα των σχέσεων του Ευρωκώδικα, εκτελέστηκε μια σειρά παραμετρικών αναλύσεων στο λογισμικό πεπερασμένων στοιχείων ABAQUS v6.14 (2014), μεταβάλλοντας το πάχος ενός διαγώνιου από 3 mm στα 1.5 mm.

Παρατηρήθηκε ότι για τις διατομές με πάχη 3 mm και 2.5 mm η σχέση του prEN1993-1-8 έχει πολύ καλή ακρίβεια (Σχήμα 4(α)), ενώ για τις 2 mm και 1.5 mm η αναλυτική σχέση υπερεκτιμά την πλαστιμότητα της σύνδεσης, η οποία μειώνεται σημαντικά λόγω της εμφάνισης τοπικού λυγισμού στον κορμό του διαγώνιου (Σχήμα 4(β)).

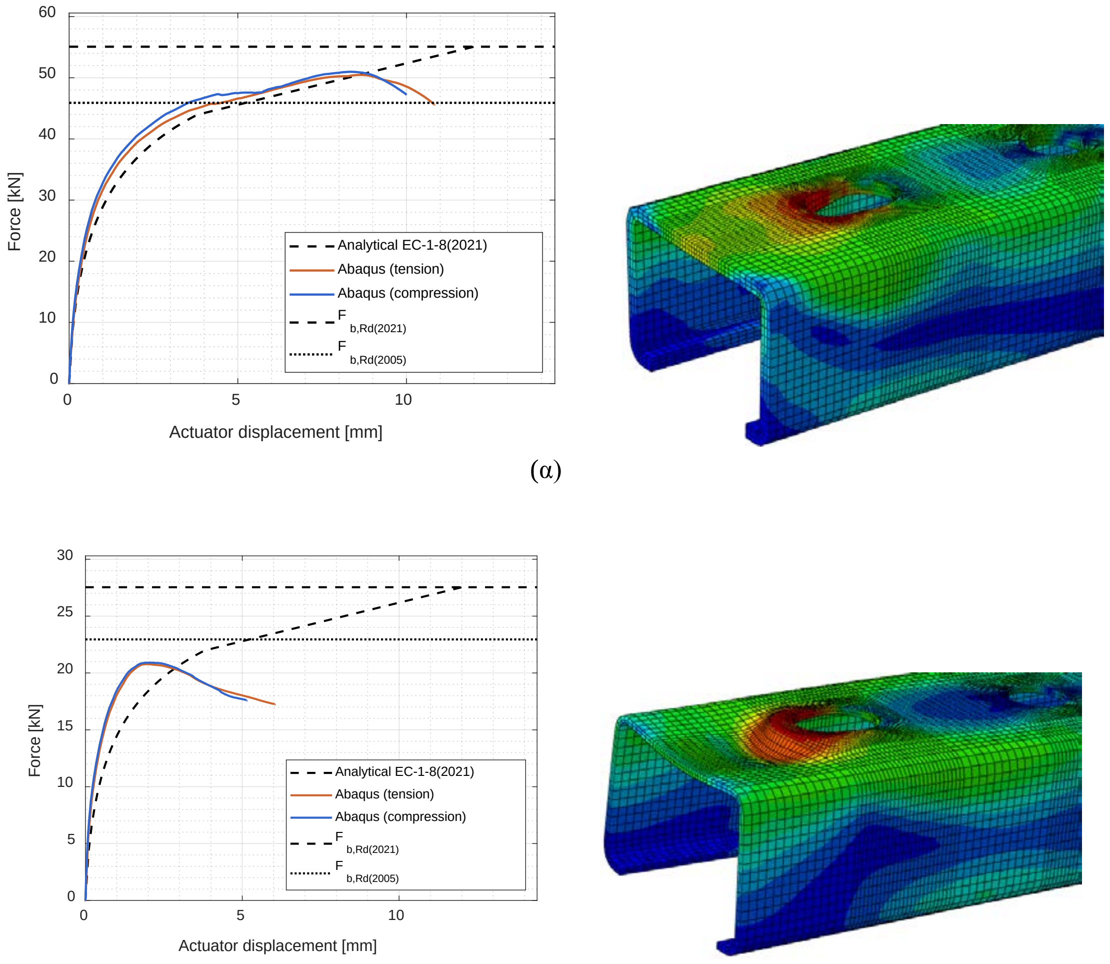

(α)

(β)

Σχήμα 4: Αποτελέσματα αναλύσεων πεπερασμένων στοιχείων και σύγκριση με αναλυτικές σχέσεις του Ευρωκώδικα για: (α) το διαγώνιο με πάχος 3 mm και (β) το διαγώνιο με πάχος 1.5 mm.

Στη συνέχεια, με βάση τους νέους ικανοτικούς κανόνες σχεδιασμού για τη ΣΠΟ, επανασχεδιάστηκαν δύο μελέτες εφαρμογής, μίας ΑΡΑ διπλού και μίας πολλαπλού βάθους. Παρατηρήθηκε ότι η σχεδίαση με βάση τη ΣΠΟ δεν οδήγησε σε σημαντική αύξηση των διατομών των ραφιών, ενώ σε ορισμένες περιπτώσεις τα διαγώνια ήταν ελαφρύτερα. Προκειμένου να συγκριθεί η ΣΠΟ με τον τυπικό σχεδιασμό, πραγματοποιήθηκε για κάθε ράφι μια ολοκληρωμένη σεισμική αποτίμηση στο λογισμικό OpenSees (McKenna et al., 2000), με τη χρήση 30 καταγραφών και 6 επιπέδων έντασης (60% έως 3%/50 χρόνια). Στα αριθμητικά μοντέλα του τυπικού σχεδιασμού όλα τα μέλη και οι συνδέσεις προσομοιώθηκαν ελαστικά λόγω της κυριαρχίας ψαθυρών μηχανισμών αστοχίας. Αντίθετα, για τα μοντέλα της ΣΠΟ χρησιμοποιήθηκε ένα καινοτόμο μακρο-στοιχείο για την προσομοίωση του διαγώνιου και της σύνδεσής του. Συγκεκριμένα, το διαγώνιο προσομοιώθηκε ως ελαστική δοκός, ενώ η σύνθλιψη άντυγας των κοχλιωτών συνδέσεων από ένα ανελαστικό στοιχείο μηδενικού μήκους, με ενσωματωμένο ένα βαθμονομημένο μη γραμμικό ελατήριο «ανοίγματος».

Όπως και στην περίπτωση του Κεφαλαίου III, τα αποτελέσματα των αναλύσεων χρονοϊστορίας μετεπεξεργάστηκαν προκειμένου να υπολογιστούν οι ΣΕ κάθε συστατικού μέρους. Στα δύο πρώτα επίπεδα έντασης, τόσο η ΣΠΟ όσο και ο τυπικός σχεδιασμός συμπεριφέρθηκαν άψογα, με πολύ λίγες χρονοϊστορίες να οδηγούν σε αστοχία κάποιου μέλους/σύνδεσης. Αντίθετα, στα 20%/50χρ., το οποίο είναι το επίπεδο σχεδίασης των ΑΡΑ, η ΣΠΟ έδειξε βελτιωμένη απόκριση, αφού 1 και 3 από τις 30 αναλύσεις εμφάνισαν κάποια αστοχία στην διπλή και πολλαπλή ΑΡΑ, αντίστοιχα, σε αντίθεση με τις 7 και 16 στον τυπικό σχεδιασμό. Η υπεροχή της ΣΠΟ ήταν εμφανής και σε υψηλότερα επίπεδα έντασης, το οποίο υπογραμμίζει ότι μια πλάστιμη σχεδίαση των ραφιών αυξάνει την επαναταξιμότητά τους και σε σεισμούς σπανιότερους από αυτούς του σχεδιασμού.

V. Απλοποιημένη Μοντελοποίηση των Αυτοματοποιημένων Ραφοϊστάμενων Αποθηκών

Το πλήρες τρισδιάστατο στατικό μοντέλο μιας ΑΡΑ τυπικά περιλαμβάνει εκατοντάδες χιλιάδες στοιχεία δοκού-στύλου, με σχεδόν μισό εκατομμύριο βαθμούς ελευθερίας (β.ε.). Αυτό έχει ως αποτέλεσμα οι αναλύσεις να γίνονται ιδιαίτερα δυσχερείς ακόμα και σε επίπεδο σχεδιασμού, με τους μελετητές να προσομοιώνουν μόνο ένα τμήμα της κατασκευής ή να χρησιμοποιούν δισδιάστατα μοντέλα. Σε επίπεδο μιας ολοκληρωμένης σεισμικής αποτίμησης όπου απαιτούνται εκατοντάδες μη γραμμικές αναλύσεις χρονοϊστορίας, γίνεται αντιληπτό ότι η λεπτομερής προσομοίωση μιας ΑΡΑ είναι πρακτικώς αδύνατη. Η μόνη λύση σε αυτές τις περιπτώσεις είναι η ανάπτυξη μιας μεθοδολογίας για την απλοποίηση του αριθμητικού προσομοιώματος, η οποία θα ισορροπεί μεταξύ της αριθμητικής ευρωστίας/ταχύτητας και της ακρίβειας των αποτελεσμάτων. Το απλοποιημένο μοντέλο που προτείνεται στην παρούσα διατριβή βασίζεται στην αντικατάσταση των σύνθετων υποστυλωμάτων με ισοδύναμα στοιχεία Timoshenko/συνδέσμου και επιτρέπει τόσο γραμμικές όσο και μη γραμμικές 2Δ και 3Δ αναλύσεις.

Η ιδέα της αντικατάστασης δικτυωτών δοκών και στύλων με ισοδύναμα ελαστικά στοιχεία έχει χρησιμοποιηθεί εκτενώς στη βιβλιογραφία. Για παράδειγμα, οι Belleri et al. (2017) ανέπτυξαν μια μεθοδολογία απλοποιημένου σεισμικού σχεδιασμού για βιομηχανικά κτήρια, η οποία βασίζεται στη χρήση ισοδύναμων δοκών σε παράλληλη σύνδεση με ελαστικά ελατήρια. Από την άλλη πλευρά, οι Kalochairetis and Gantes (2012) χρησιμοποίησαν ελαστικά στοιχεία Timoshenko για να προσδιορίσουν το φορτίο λυγισμού σύνθετων υποστυλωμάτων και να πραγματοποιήσουν ταχείες παραμετρικές αναλύσεις για τον προσδιορισμό της επίδρασης των ατελειών. Με βάση αυτές τις ιδέες, προτείνεται στην περίπτωση των ραφιών η χρήση γραμμικών στοιχείων Timoshenko για την αντικατάσταση των σύνθετων στύλων όταν δε μελετάται η μη γραμμικότητα του υλικού, καθώς επίσης και χρήση μη γραμμικών στοιχείων συνδέσμου σε πιο πλάστιμες κατασκευές.

Το πρώτο βήμα της απλοποίησης περιλαμβάνει τον προσδιορισμό των ελαστικών ιδιοτήτων των ισοδύναμων στοιχείων Timoshenko. Συγκεκριμένα, το εμβαδόν της ισοδύναμης διατομής ισούται με το άθροισμα των εμβαδών των επιμέρους στύλων που μορφώνουν το σύνθετο υποστύλωμα, ενώ η ισοδύναμη ροπή αδρανείας μπορεί να υπολογιστεί με τη χρήση του κανόνα Steiner. Επιπλέον, επειδή τα σύνθετα υποστυλώματα (και γενικά τα δικτυωτά μέλη) χαρακτηρίζονται από σημαντική διατμητική παραμόρφωση, είναι απαραίτητος ο υπολογισμός του διατμητικού εμβαδού του ισοδύναμου στοιχείου Timoshenko. Για τυπικές μορφές δικτύωσης (π.χ. D, Z, K, X), το EN 1993-1-1 (2005) προσφέρει κλειστούς τύπους για τον υπολογισμό του διατμητικού εμβαδού, ενώ σε περιπτώσεις όπου η δικτύωση δεν είναι σταθερή καθ' ύψος, μπορεί να ακολουθηθεί ένα απλό αριθμητικό τεστ προβόλου.

Το δεύτερο βήμα της απλοποίησης περιλαμβάνει τον προσδιορισμό των ελαστικών και ανελαστικών ιδιοτήτων των ισοδύναμων στοιχείων συνδέσμου. Ένα στοιχείο συνδέσμου συνδέει δύο κόμβους με διακριτά, συνήθως χωρίς αλληλεπίδραση μεταξύ τους, ελατήρια που λαμβάνουν υπόψη όλες τις μορφές σχετικής παραμόρφωσης. Για παράδειγμα, το 2Δ πεπερασμένο στοιχείο two-node link του λογισμικού OpenSees (McKenna et al., 2000) περιλαμβάνει τρία ελατήρια, ένα αξονικό, ένα διατμητικό και ένα καμπτικό. Οι ελαστικές δυσκαμψίες των ελατηριών υπολογίζονται έτσι ώστε το στοιχείο συνδέσμου να έχει το ίδιο μητρώο δυσκαμψίας με το ισοδύναμο ελαστικό στοιχείο Timoshenko. Στην ανελαστική περιοχή, υπολογίζεται μια μέγιστη ροπή αντοχής του καμπτικού ελατηρίου με βάση την αντοχή των στύλων σε λυγισμό. Όταν η ροπή αυτή ξεπεραστεί στην ανάλυση, το καμπτικό ελατήριο χάνει πλήρως την αντοχή του. Αντίθετα, το διατμητικό ελατήριο έχει μια πιο πλάστιμη συμπεριφορά, αφού λαμβάνει υπόψη τη διαρροή και το λυγισμό των διαγώνιων στοιχείων. Για τον προσδιορισμό της υστερητικής συμπεριφοράς του πραγματοποιείται ένα αριθμητικό «διατμητικό» τεστ σε ένα μικρό τμήμα της κατασκευής, το οποίο στη συνέχεια χρησιμοποιείται για τη βαθμονόμηση του μη γραμμικού υστερητικού υλικού του ελατηρίου.

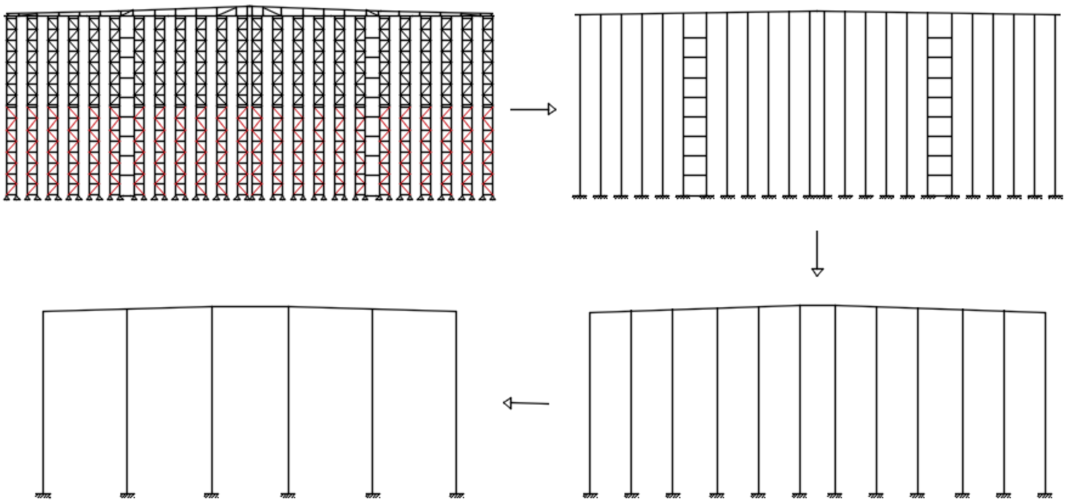

Σχήμα 5: Στάδια απλοποίησης μιας ΑΡΑ: υποθέτοντας αμελητέα διατμητική δυσκαμψία της στέγης, πολλαπλά σύνθετα υποστυλώματα μπορούν να αντικατασταθούν από ένα μόνο μακρο-στοχείο.

Το τρίτο βήμα της απλοποίησης περιλαμβάνει την αντικατάσταση της δικτυωτής στέγης της ΑΡΑ. Επειδή η στέγη δε συμμετέχει σημαντικά στο μηχανισμό αστοχίας της κατασκευής, αντικαθίσταται από γραμμικά στοιχεία Timoshenko, σύμφωνα με το πρώτο βήμα. Επίσης, λόγω της μειωμένης διατμητικής της δυσκαμψίας, συνήθως δεν αναπτύσσεται σημαντική ροπή ανατροπής στις ΑΡΑ, γεγονός που επιτρέπει τη συγχώνευση πολλών σύνθετων στύλων σε ένα ισοδύναμο μακρο-στοχείο, όπως δίνεται στο Σχήμα 5. Αυτή η διαδικασία απλοποίησης μπορεί να αξιοποιηθεί για να μειωθεί σημαντικά η πολυπλοκότητα του μοντέλου, δεδομένου του υψηλού επιπέδου ομοιοτήτων μεταξύ των σύνθετων στύλων, με την αναπόφευκτη αδυναμία να χάνεται η χωρική κατανομή της μάζας σε περιπτώσεις ανομοιόμορφης φόρτισης.

Τέλος η προτεινόμενη μεθοδολογία απλοποίησης πιστοποιήθηκε στην ελαστική περιοχή μέσω γραμμικών αναλύσεων σε μια ΑΡΑ πολλαπλού βάθους. Το πλήρες 3Δ μοντέλο περιλάμβανε 647,000 β.ε. και 200,000 στοιχεία δοκού-στύλου, ενώ το απλοποιημένο μόλις 17,000 β.ε. και 7,500 ισοδύναμα στοιχεία Timoshenko. Η σύγκριση των ιδιομορφών και ιδιοπεριόδων έδειξε ότι το απλοποιημένο μοντέλο μπορούσε να λάβει υπόψη με ακρίβεια τα δυναμικά χαρακτηριστικά της κατασκευής. Στη συνέχεια η μεθοδολογία πιστοποιήθηκε και στην ανελαστική περιοχή, με την εκτέλεση γραμμικών στατικών και δυναμικών 2Δ αναλύσεων σε μια ΑΡΑ διπλού βάθους. Η διαφορά των αποτελεσμάτων μεταξύ του πλήρους και του απλοποιημένου μοντέλου ήταν τις περισσότερες φορές πολύ μικρή (η μέγιστη που παρατηρήθηκε ήταν 10%), ενώ τα οφέλη σε επίδοση ήταν πολύ σημαντικά, αφού ο χρόνος κάθε ανάλυση χρονοϊστορίας μειώθηκε από 90 λεπτά σε 30 δευτερόλεπτα.

VI. Μέθοδοι για τη Σεισμική Αποτίμηση της Ολίσθησης Περιεχομένων σε Ράφια Αποθήκευσης

Επειδή τα περιεχόμενα ενός συστήματος ραφιών δεν είναι μηχανικά συνδεμένα με το δομικό φορέα, έντονες σεισμικές κινήσεις οδηγούν αναπόφευκτα στη σχετική μετατόπιση/ολίσθηση των περιεχομένων. Σε συμβατικές κατασκευές το βάρος των περιεχομένων είναι πολύ μικρό σε σχέση με το ίδιο βάρος της κατασκευής και επομένως δε λαμβάνεται υπόψη η αλληλεπίδραση των δύο, γεγονός που επιτρέπει το διαχωρισμό της σεισμικής αποτίμησης σε δύο στάδια. Στο πρώτο στάδιο πραγματοποιούνται αναλύσεις χρονοϊστορίας στην κατασκευή, θεωρώντας ότι δεν υπάρχει σχετική μετακίνηση κατασκευής-περιεχομένων. Στο δεύτερο στάδιο γίνεται μια μετεπεξεργασία των αποτελεσμάτων των αναλύσεων, όπου χρησιμοποιούνται οι χρονοϊστορίες απόλυτων επιταχύνσεων ορόφου για τον προσδιορισμό της ολίσθησης των περιεχομένων, μια διαδικασία που είναι γνωστή στη βιβλιογραφία ως Newmark’s sliding block analysis (NSBA) (Newmark, 1965). Στην ουσία η NSBA περιλαμβάνει τη διπλή ολοκλήρωση των επιταχύνσεων ορόφου που ξεπερνάνε τη λεγόμενη *επιτάχυνση διαρροής* $a_y = \mu g$, όπου μ η σταθερά τριβής της επιφάνειας κατασκευής-περιεχομένου και g η επιτάχυνση της βαρύτητας.

Ενώ η NSBA είναι μια αξιόπιστη μέθοδος για τον υπολογισμό της ολίσθησης περιεχομένων σε συμβατικές κατασκευές, η ακρίβειά της μειώνεται σημαντικά σε περιπτώσεις όπου το βάρος των περιεχομένων γίνεται η κύρια πηγή σεισμικής μάζας. Αυτό μπορεί να γίνει αντιληπτό με τη σύγκριση της NSBA με ένα αριθμητικό μοντέλο που περιλαμβάνει ένα πεπερασμένο στοιχείο *ολισθητήρα τριβής*. Ένας ολισθητήρας τριβής μπορεί να λάβει υπόψη τη σχετική παραμόρφωση δύο κόμβων, όταν η ασκούμενη διατμητική δύναμη στο στοιχείο ξεπεράσει την κρίσιμη δύναμη ολίσθησης. Για τη σύγκριση των δύο μεθόδων χρησιμοποιήθηκε ένα απλό μοντέλο που περιλάμβανε μια μάζα m πάνω σε ένα μονοβάθμιο ταλαντωτή περιόδου $T > 0$ sec με σταθερά τριβής μ μεταξύ τους. Στο πρώτο μοντέλο της NSBA εκτελέστηκε η ανάλυση χρονοϊστορίας στον ταλαντωτή και με μια διπλή ολοκλήρωση υπολογίστηκε η ολίσθηση της μάζας. Στο δεύτερο μοντέλο χρησιμοποιήθηκε μεταξύ μάζας-ταλαντωτή ένας ολισθητήρας τριβής ο οποίος λαμβάνει υπόψη κατά την ανάλυση την επιρροή της ολίσθησης. Η σύγκριση των δύο αναλύσεων δείχνει ότι η NSBA υπερεκτιμά σημαντικά (της τάξης του +100%) την ολίσθηση της μάζας. Αυτό οφείλεται στο γεγονός ότι στο πρώτο μοντέλο δε λαμβάνεται υπόψη η λεγόμενη αλληλεπίδραση περιεχομένων-κατασκευής λόγω ολίσθησης (ΑΠΚΟ).

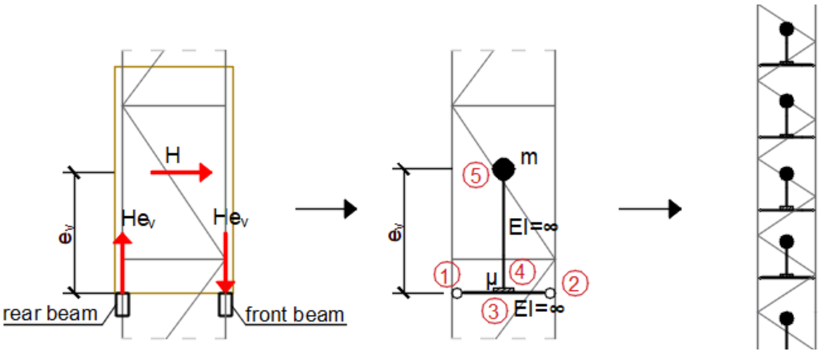

Σχήμα 6: Προσομοίωση των παλετών κατά την εγκάρσια διεύθυνση του ραφιού με τη χρήση ολισθητήρων τριβής και πλασματικών στοιχείων.

Η πιο αξιόπιστη μέθοδος για την προσομοίωση της ΑΠΚΟ είναι η χρήση ενός ολισθητήρα τριβής για κάθε παλέτα, μαζί με πλασματικά δύσκαμπτα στοιχεία προκειμένου να μοντελοποιηθεί η εκκεντρότητα παλέτας-δοκών (Σχήμα 6). Ωστόσο, η μέθοδος αυτή απαιτεί μη γραμμικές αναλύσεις χρονοϊστορίας σε εξιδεικευμένα λογισμικά και επομένως δεν προτείνεται κατά τη διαδικασία σχεδιασμού ενός ραφιού. Ως μια εναλλακτική λύση για την αποτίμηση της ολίσθησης περιεχομένων προτείνεται η εκτέλεση γραμμικών αναλύσεων χρονοϊστορίας και η μετεπεξεργασία των επιταχύνσεων ορόφου με την NSBA. Για να ληφθεί υπόψη η ΑΠΚΟ αναπτύχθηκε η ακόλουθη εμπειρική σχέση για την αύξηση της ιξώδους απόσβεσης της κατασκευής, μέσα από την εκτέλεση παραμετρικών αναλύσεων σε μονοβάθμιους ταλατωντές:

$$\xi_{eq} = min\left\{3\%,\ \ 5.82\%\frac{Sa(T)}{\mu} - 3.97\%\right\} \qquad \text{Εξ. (1)}$$

Σύμφωνα με την Εξ. (1), για κάθε ανάλυση χρονοϊστορίας υπολογίζεται η φασματική επιτάχυνση $Sa(T)$ του ταλαντωτή και με βάση το συντελεστή τριβής μ αυξάνεται αριθμητικά η ισοδύναμη απόσβεση του μοντέλου. Ένα ράφι ωστόσο είναι ένα πολυβάθμιο σύστημα όπου η επιρροή των ανώτερων ιδιομορφών είναι σημαντική. Για το λόγο αυτό πραγματοποιήθηκε μια ολοκληρωμένη σεισμική αποτίμηση σε τρία παραδείγματα σχεδιασμού ραφιών, από συμβατικά ΡΣΠ χαμηλού ύψους μέχρι μια ΑΡΑ μεγάλου ύψους. Η σύγκριση των απλοποιημένων μεθόδων με τα ακριβή μοντέλα με τους ολισθητήρες τριβής έδειξαν ότι η χρήση μιας μέσης απόσβεσης $\bar{\xi}_{eq} = (\xi_{1,eq} + \xi_{2,eq})/2$, όπου $\xi_{1,eq}$ και $\xi_{2,eq}$ η ισοδύναμη απόσβεση της πρώτης και δεύτερης ιδιομορφής του ραφιού σύμφωνα με την Εξ. (1), μειώνει σημαντικά τη μεροληψία και αυξάνει την ακρίβεια της NSBA.

Τέλος, για πρακτικές εφαρμογές συμβατές με τους κώδικες σχεδιασμού, προτείνεται η μείωση του φάσματος σχεδιασμού για την προσομοίωση της ΑΠΚΟ. Το σεισμικό πρότυπο ραφιών EN 16681 (2016) προσφέρει το μειωτικό συντελεστή E_{D1} για τη μείωση των σεισμικών δράσεων λόγω ολίσθησης. Ο E_{D1} αποτελεί συνάρτηση του λόγου $Sa(T_1)/\mu$ και επομένως εξαρτάται μόνο από τη πρώτη ιδιομορφή του ραφιού. Ωστόσο, από τις αναλύσεις χρονοϊστορίας προέκυψε ότι, ιδιαίτερα στις ψηλές ΑΡΑ, η μείωση της σεισμικής τέμνουσας λόγω της ΑΠΚΟ εξαρτάται όχι μόνο από την πρώτη αλλά και από τη δεύτερη ιδιομορφή. Για το λόγο αυτό προτάθηκε ένας νέος μειωτικός συντελεστής, ο λεγόμενος E_{N1}, ο οποίος χρησιμοποιεί το γεωμετρικό μέσο των φασματικών επιταχύνσεων $\sqrt{Sa(T_1)Sa(T_2)}/\mu$:

$$E_{N1} = max\left\{0.4, \ -0.1966 \cdot \sqrt{Sa(T_1)Sa(T_2)}/\mu + 1.0995\right\} \leq 1.0 \qquad \text{Εξ. (2)}$$

Προκειμένου να συγκριθεί ο προτεινόμενος συντελεστής E_{N1} με τον E_{D1} του κανονισμού, χρησιμοποιήθηκε μια πολυώροφη ΑΡΑ και 30 σεισμικές καταγραφές κλιμακωμένες σε τρία επίπεδα έντασης που αντιστοιχούν σε 3%, 5% και 10% στα 50 χρόνια πιθανότητα υπέρβασης. Για κάθε καταγραφή και επίπεδο έντασης πραγματοποιήθηκε μια μη γραμμική ανάλυση χρονοϊστορίας με ολισθητήρες τριβής, η οποία χρησιμοποιήθηκε για την αξιολόγηση των άλλων μεθόδων. Στη συνέχεια εκτελέστηκαν δύο φασματικές αναλύσεις με CQC συνδυασμό των ιδιομορφών: η πρώτη με τη χρήση του συντελεστή E_{D1} και η δεύτερη με τον E_{N1}. Οι ανάλυσεις με τον E_{D1} υπερεκτιμούσαν την τέμνουσα βάσης, τις αξονικές δυνάμεις στους στύλους/διαγώνια και τη μετατόπιση της οροφής, κατά 20% έως 40%. Αντίθετά οι αναλύσεις με τον E_{N1} προσέφεραν πολύ καλύτερη συνολική απόδοση, τόσο από άποψη αμερόληπτης μέσης τιμής όσο και από την άποψη μικρότερου συντελεστή διακύμανσης. Αυτό σημαίνει ότι η χρήση του E_{N1} μπορεί εν δυνάμει να οδηγήσει σε μια ελαφρύτερη (και επομένως πιο οικονομική) κατασκευή.

VII. Συμπεράσματα

Στην παρούσα διδακτορική διατριβή εξετάστηκε η σεισμική συμπεριφορά των συστημάτων ραφιών, κατασκευές που χρησιμοποιούνται για την αποθήκευση των αγαθών/προϊόντων μιας αποθήκης. Συνοπτικά, τα κύρια συμπεράσματα είναι τα ακόλουθα:

- Διαφορετικές τυπολογίες ραφιών μοιράζονται κοινά μακρο-χαρακτηριστικά τα οποία μπορούν να συμπεριληφθούν σε μια ευέλικτη ταξινομία για την υποστήριξη μελετών αξιολόγησης χαρτοφυλακίου ή κινδύνων/ζημιών περιφερειών;
- Οι αυτοματοποιημένες ραφοϊστάμενες αποθήκες (ΑΡΑ) σχεδιασμένες με βάση τα σεισμικά πρότυπα για συμβατικά ράφια είναι επιρρεπείς σε ψαθυρούς μηχανισμούς αστοχίας, όπως αστοχία των αγκυρίων, αστοχίας κοχλιωτών συνδέσεων, λυγισμός στύλων, κ.λπ.;
- Η στρατηγική πλαστικής οβαλοποίησης (ΣΠΟ) είναι ένας πλάστιμος σεισμικός σχεδιασμός για την εγκάρσια διεύθυνση των ραφιών και βασίζεται στην παραμόρφωση λόγω σύνθλιψης άντυγας του διαγώνιου για να «απορροφήσει» την εισερχόμενη σεισμική ενέργεια;

- Αναλύσεις πεπερασμένων στοιχείων έδειξαν ότι η κοχλιωτή σύνδεση διαγώνιου-στύλου μπορεί να έχει επαρκεί πλαστιμότητα, εφόσον τα πάχος του διαγώνιου είναι αρκετά μεγάλο ώστε να αποφευχθεί ο τοπικός λυγισμός του κορμού του;
- Για ταχεία αποτίμηση και σχεδιασμό των ΑΡΑ, μια πολύ αξιόπιστη μεθοδολογία απλοποίησης του αριθμητικού προσομοιώματος αποτελεί η αντικατάσταση των σύνθετων υποστυλωμάτων με ισοδύναμα στοιχεία Timoshenko (ελαστική ανάλυση) ή με στοιχεία συνδέσμου (ανελαστική ανάλυση);
- Η πιο ακριβής μέθοδος για να ληφθεί υπόψη η αλληλεπίδραση περιεχομένων-κατασκευής λόγω ολίσθησης (ΑΠΚΟ) είναι η χρήση μη γραμμικών στοιχείων ολισθητήρων τριβής για την προσομοίωση της κίνησης κάθε παλέτας;
- Μια εναλλακτική λύση για την μοντελοποίηση της ΑΠΚΟ σε ελαστικά μοντέλα αποτελεί η χρήση ενός ισοδύναμου αυξημένου συντελεστή απόσβεσης της κατασκευής και η μετεπεξεργασία των επιταχύνσεων ορόφου με τη μέθοδο Newmark's sliding block analysis (NSBA);
- Μια αποτελεσματική μεθοδολογία για να ληφθεί υπόψη η ΑΠΚΟ σε επίπεδο σχεδιασμού είναι η χρήση ενός μειωτικού συντελεστή στο φάσμα σχεδιασμού με βάση τη πρώτη και δεύτερη ιδιομορφή ταλάντωσης του ραφιού. Ωστόσο η μέθοδος αυτή δεν μπορεί να υπολογίσει την ολίσθηση των περιεχομένων.

VIII. Βιβλιογραφικές αναφορές

ABAQUS v6.14 (2014). *“ABAQUS Documentation (6.14)”*, Dassault Systèmes Simulia Corp., Providence, RI, USA.

Adamakos K. (2018). *“Seismic actions and response of steel storage pallet racks - A numerical investigation”*, Doctoral Thesis, National Technical University of Athens, School of Civil Engineering.

AS 4084 (2012). *“Steel storage racking”*, Standard Australia.

Belleri A., Torquati M., Marini A., Riva P. (2017). *“Simplified building models as advanced seismic screening tools for steel industrial buildings”*, Journal of Constructional Steel Research, **138**, 51-64. https://doi.org/10.1016/j.jcsr.2017.06.027

Brzev S., Scawthorn C., Charleson A.W., Allen L., Greene M., Jaiswal K., and Silva V. (2013). *“GEM Building Taxonomy Version 2.0”*, GEM Technical Report 2013-02 V1.0.0, 188 pp., GEM Foundation, Pavia, Italy.

Castiglioni C.A. et al. (2014). *“Seismic behavior of steel storage pallet racking systems (SEISRACKS2)”*, Final Report, RFSR-PR-03114, European Commission, DG Research, Brussels, Belgium.

EN 15512 (2009). *“Steel static storage systems - Adjustable pallet racking systems - Principles for structural design”*, European Committee for Standardization (CEN), Brussels, Belgium.

EN 16681 (2016). *“Steel static storage systems - Adjustable pallet racking systems - Principles for seismic design”*, European Committee for Standardization (CEN), Brussels, Belgium.

EN 1993-1-1 (2005). *“Eurocode 3: Design of Steel Structures - Part 1-1: General rules and rules for buildings”*, European Committee for Standardization, Brussels, Belgium.

EN 1993-1-3 (2006). *“Eurocode 3: Design of Steel Structures - Part 1-3: General rules - Supplementary rules for cord-formed members and sheeting”*, European Committee for Standardization, Brussels, Belgium.

Gilbert B.P., Rasmussen K.J.R. (2012). *“Drive-in Steel Storage Racks I: Stiffness Tests and 3D Load-Transfer Mechanisms”*, Journal of Structural Engineering, **138**(2). https://doi.org/10.1061/(ASCE)ST.1943-541X.0000449

Gilbert B.P., Teh L.H., Badet R.X., Rasmussen K.J.R. (2014). *“Influence of pallets on behaviour and design of steel drive-in racks”*, Journal of Constructional Steel Research, **97**, 10-23. https://doi.org/10.1016/j.jcsr.2014.01.013

Kalochairetis K. Gantes C.J. (2012). *“Axially and transversely loaded Timoshenko and laced built-up columns with arbitrary supports”*, Journal of Constructional Steel Research, **77**, 95-106. https://doi.org/10.1016/j.jcsr.2012.05.004

Kanyilmaz A., Castiglioni C.A., Brambilla G., Chiarelli G.P. (2016). *“Experimental assessment of the seismic behavior of unbraced steel storage pallet racks”*, Thin-Walled Structures, **108**, 391-405. https://doi.org/10.1016/j.tws.2016.09.001

Kohrangi M., Bazzurro P., Vamvatsikos D., Spillatura A. (2017). *“Conditional spectrum-based ground motion record selection using average spectral acceleration”*, Earthquake Engineering and Structural Dynamics, **46**(10), 1667-1685. https://doi.org/10.1002/eqe.2876

Kohrangi M., Tsarpalis D., Vamvatsikos D. (2018). *“CS(AvgSA) consistent Records and Hazard curves for Van and Montopoli”*. STEELWAR Project. Link: http://users.ntua.gr/divamva/resources/SteelWAR_MontopoliVanRecords_2in50.rar

McKenna F., Fenves G.L., Scott M.H., Jeremic B. (2000). *“Open System for Earthquake Engineering Simulation (OpenSees)”*, Pacific Earthquake Engineering Research Center, University of California, Berkeley, CA.

Newmark N.M. (1965). *“Effects of Earthquakes on Dams and Embankments”*, Géotechnique, **15**(12), 139-160. https://doi.org/10.1680/geot.1965.15.2.139

prEN 1993-1-8 (2021). *“Eurocode 3: Design of Steel Structures - Part 1-8: Design of joints”*, European Committee for Standardization, Brussels, Belgium.

RMI, ANSI MH16.1.12 (2012). *“Specification for the Design, Testing and Utilization for Industrial Steel Storage Racks”*, Rack Manufacturer’s Institute, Charlotte, NC.

Rosin I., Calado L., Proença J., Carydis P., Mouzakis H., Castiglioni C., Brescianini J.C., Plumier A., Degee H., Negro P., Molina F. (2007). *“Storage racks in seismic areas (SEISRACKS)”*, Final Report, RFSR-PR-03114, European Commission, DG Research, Brussels, Belgium.

STEELWAR (2017). *“Advanced structural solutions for automated STEELrack supported WARehouses”*, The Steelwar Project Consortium, Pisa, Italy. https://www.unipi.it/index.php/risultati-e-prodotti/item/10663-steelwar

Tilburgs K. (2013). *“Those peculiar structures in cold-formed steel: “racking & shelving””*, Steel Construction **6**(2). https://doi.org/10.1002/stco.201310016

Table of Contents

1 Introduction 1
  1.1 Problem statement 1
  1.2 Objectives and Scope 4
  1.3 Outline 4
  1.4 References 6

2 Macro-characteristics and Taxonomy of Steel Racking Systems 9
  2.1 Introduction 9
  2.2 Morphology of racking systems 9
  2.3 Seismic behaviour and design of racks 16
  2.4 Proposed taxonomy 19
    2.4.1 Structural typology 21
    2.4.2 Placement and cladding 23
    2.4.3 Height 24
    2.4.4 Storage system 25
    2.4.5 Design code level 28
    2.4.6 Available literature per proposed taxonomy 29
  2.5 Conclusions 31
  2.6 References 31

3 Seismic Assessment of Automated Rack Supported Warehouses 35
  3.1 Introduction 35
  3.2 Description of case studies 35
    3.2.1 Structural configuration 35
    3.2.2 Seismic design assumptions 44
    3.2.3 Cumulative seismic load multiplier 47
  3.3 Seismic hazard and record selection 49
    3.3.1 Hazard analysis 49
    3.3.2 Disaggregation analysis 50
    3.3.3 Record selection 51
  3.4 Response History Analyses 52
    3.4.1 Modelling and analysis parameters 52
    3.4.2 Verification checks and resistances 53
    3.4.3 Hierarchy of criticalities 57
    3.4.4 Effect of seismic design assumptions 57
  3.5 Conclusions 63
  3.6 References 64

4 Plastic Ovalization Strategy 67
  4.1 Introduction 67
  4.2 Theoretical concept and design rules 69
    4.2.1 Failure modes of a shear bolted connection 69
    4.2.2 Proposed capacity design rules 71
  4.3 Numerical study on the behaviour of the diagonal bolt hole in bearing 74
    4.3.1 Existing analytical expressions 74
    4.3.2 Numerical simulation of tension/compression quasi-static tests 75
  4.4 Response History Analyses 80
    4.4.1 Description of case studies 80
    4.4.2 Numerical modelling 83
    4.4.3 Comparison of design approaches 87
  4.5 Conclusions 91
  4.6 References 91

5 Simplified Modelling of Automated Rack Supported Warehouses 95
5.1 Introduction 95
5.2 Proposed simplified model 95
5.3 Elastic model validation on single upright frames 103
5.4 Case study A: Elastic model of a multi-depth ARSW 105
5.4.1 Structure and model description 105
5.4.2 Model validation 107
5.4.3 Fragility assessment 110
5.5 Case study B: Nonlinear model of a double-depth ARSW 112
5.5.1 Structure and model description 112
5.5.2 Model validation 114
5.5.3 Fragility assessment 116
5.6 Conclusions 117
5.7 References 117

6 Seismic Assessment Approaches for Sliding Contents in Storage Racks 121
6.1 Introduction 121
6.2 RHA for SDOF systems 123
6.2.1 Newmark’s sliding block analysis 123
6.2.2 CSSI for SDOF structures 125
6.2.3 Equivalent damping ratio 127
6.3 RHA for MDOF systems 130
6.3.1 CSSI for MDOF structures 130
6.3.2 Five modelling approaches 132
6.3.3 Description of case studies 134
6.3.4 Seismic hazard and record selection 136
6.3.5 Comparison of modelling approaches 137
6.4 MRSA for MDOF systems 139
6.4.1 Reduction of lateral loads for simplified CSSI 139
6.4.2 Comparison of MRSA approaches 141
6.5 Conclusions 143
6.6 References 144

7 Conclusions 147
7.1 Summary 147
7.2 Limitations and future work 149
7.3 References 150

Annex A: Spring stiffnesses of two-node link element 153

Annex B: MATLAB function for performing NSBA on an idealized body sliding on a moving platform 155

List of Figures

Figure 1.1: Typical configuration of a warehousing unit, comprising (a) the racking systems used to store the goods and materials of the warehouse (herein it contains a series of shelving racks and a series of adjustable pallet racks), and (b) the independent external shell structure (photo courtesy of Nedcon B.V). 1

Figure 1.2: Plan and side views of a typical racking system. Two directions are defined, the down-aisle, which is used by the forklift trucks and, perpendicularly, the cross-aisle. 2

Figure 1.3: Failure of indoor racking structures during seismic motions, showing (a): partial collapse of an adjustable steel rack during the Christchurch earthquake of 2011 (Clifton et al., 2011) and (b): collapse of cantilever-like racks used for Parmigiano Reggiano cheese wheels in a warehouse in Emilia Romagna (Franco et al., 2015). 2

Figure 1.4: Collapse of Ceramic Storage warehouse in Sant' Agostino due to 2012 Emilia-Romagna earthquake, Italy (Kanyilmaz et al., 2016). 3

Figure 2.1: Primary structural components of an adjustable pallet racking (APR) system and definition of the down- and cross-aisle directions (photo courtesy of SACMA S.p.a.). 10

Figure 2.2: Component connections of an APR system showing: (a) a diagonal-to-upright bolted connection and (b) a beam-to-column hooked connection and an upright-to-floor connection (photos courtesy of SACMA S.p.a.). 11

Figure 2.3: Primary structural components of a drive-in steel racking system. In drive-in racks, the forklifts enter inside the rack in order to deposit and withdraw the pallets (photo courtesy of Nedcon B.V.). 11

Figure 2.4: Configuration of a multi-depth pallet shuttle racking system. Pallets are stored in long storage tunnels serviced by mechanized shuttles running on rails (photo courtesy of MECALUX S.A.). 12

Figure 2.5: Example of a double-depth ARSW in the construction stage (photo courtesy of SACMA S.p.a.). 13

Figure 2.6: Example of a multi-depth ARSW in the construction stage (photo courtesy of SACMA S.p.a.). 13

Figure 2.7: Example of a mini-load automated racking system (photo courtesy of Nedcon B.V.). 14

Figure 2.8: Example of a heavy-duty cantilever rack (photo courtesy of Modulblok). 14

Figure 2.9: Example of a light-duty shelving rack (photo courtesy of MECALUX S.A.) 15

Figure 2.10: Typical shelving rack and key components (adopted from Bernuzzi et al., 2016a). ... 15

Figure 2.11: Example of a mobile racking system (photo courtesy of Modulblok) 16

Figure 2.12: Example of a push-back gravity flow racking system (photo courtesy of MECALUX S.A.). 16

Figure 2.13: Spine bracing layout (adopted from FEM 10.2.08, 2011). 18

Figure 2.14: The GLRS Attribute-Level of the structural typology Attribute comprises three Options: (a) “uprights+beams”, (b) “uprights+rails” and (c) “cantilever”.. 21

Figure 2.15: The LLRS Attribute-Level of the structural typology Attribute comprises three Options: (a) MRF, (b) spine bracing and (c) bracing tower.. 22

Figure 2.16: The placement and cladding Attribute comprises three Options: (a) indoor, (b) outdoor and (c) clad-supporting racks (photos courtesy of MECALUX S.A.). 23

Figure 2.17: The height Attribute comprises four Options: (a) low-, (b) medium- (c) high- and (d) very high-rise racks (photos courtesy of MECALUX S.A.). 24

Figure 2.18: The weight of the unit load Attribute-Level of the storage system Attribute consists of three Options: (a) low-, (b) medium- and (c) high-weight (photos courtesy of MECALUX S.A.). 25

Figure 2.19: The contact surface Attribute-Level of the storage system Attribute consists of four Options: (a) wood+steel, (b) plastic+steel, (c) steel+steel and (d) hanging goods (photos courtesy of MECALUX S.A.)... 26

Figure 2.20: Material/goods handling Attribute-Level of the storage system Attribute consists of three Options: (a) manual, (b) semi-automated, and (c) fully-automated (photos courtesy of MECALUX S.A.)... 27

Figure 3.1: Structural configuration of CS1, showing plan, down- and cross-aisle views............... 36

Figure 3.2: Structural configuration of CS2, showing plan, down- and cross-aisle views............... 37

Figure 3.3: Structural configuration of CS3, showing plan, down- and cross-aisle views............... 38

Figure 3.4: Structural configuration of CS4, showing plan, down- and cross-aisle views............... 39

Figure 3.5: Structural configuration of CS5, showing plan, down- and cross-aisle views............... 40

Figure 3.6: Side views with the structural components considered in the tag list of Table 3.1, for the (a) cross-aisle, and (b) down-aisle direction.. 42

Figure 3.7: Hazard curve for the city of Van in Turkey, using $AvgSa$ as an IM............................ 50

Figure 3.8: Disaggregation analysis for 60% to 1% in 50 years probability of exceedance for the city of Van in Turkey, using $AvgSa$ as an IM. 51

Figure 3.9: Set of 15 records and 2.5/50/97.5th percentiles of the CS at 2475 years return period, for the city of Van in Turkey, using $AvgSa$ as the conditioning IM. 52

Figure 3.10: Normalized member and connection resistances for the cross-aisle direction: (a)+(b), (c)+(d), (e)+(f), (g)+(h), and (i)+(f) are for CS1, CS2, CS3, CS4, and CS5 multi-depth ARSWs, respectively (see Table 3.1 for the description of the tag of each structural component). 55

Figure 3.11: Normalized member and connection resistances for the down-aisle direction: (a)+(b), (c)+(d), (e)+(f), (g)+(h), and (i)+(f) are for CS1, CS2, CS3, CS4, and CS5 multi-depth ARSWs, respectively (see Table 3.1 for the description of the tag of each structural component). 56

Figure 3.12: Boxplots with the utilization factors of the critical structural components along the cross-aisle direction for 15 RHAs scaled to IM that corresponds 10% in 50 years probability of exceedance, showing the: (a) CS1, (b) CS2, (c) CS3, (d) CS4, and (e) CS5 multi-depth ARSW (the suffixes “_m” and “_c” indicate member and connection resistances, respectively). 58

Figure 3.13: Boxplots with the utilization factors of the critical structural components along the down-aisle direction for 15 RHAs scaled to IM that corresponds 10% in 50 years probability of exceedance, showing the: (a) CS1, (b) CS2, (c) CS3, (d) CS4, and (e) CS5 multi-depth ARSW (the suffixes "_m" and "_c" indicate member and connection resistances, respectively)....................... 59

Figure 3.14: Boxplots with the utilization factors of the five scenarios of accepted seismic design assumptions, for the: (a) "pu1" and "pu2", (b) "panc", (c) "pd1" and "pd2", (d) "bu1" and "bu2", (e) "buanc", and (f) "bd1" and "bd2" structural components (each boxplot has a size of 75 UFs, containing the results of all 5 case studies and 15 RHAs per case study)....................................... 61

Figure 4.1: Typical diagonal-to-upright bolted connection, using an M12 bolt with two shear planes. 68

Figure 4.2: Failure modes on a shear bolted connection (Draganić et al., 2014)............................ 69

Figure 4.3: Edge and inner distances of a bolt layout according to EN 1993-1-8 (2005)............... 71

Figure 4.4: Bearing deformation behaviour (adopted from Može et al., 2021). 75

Figure 4.5: Test setup of quasi-static tension/compression numerical tests on a UTM. 76

Figure 4.6: Numerical model of the UTM numerical tests: a) model assembly, b) model mesh, c) mesh refinement near the holes, and d) bolt mesh. 77

Figure 4.7: Analytical (EN 1993-1-8:2005 and 2021) versus numerical (ABAQUS) force-displacement curves of the quasi-static compression/tension tests, for diagonals of (a) 3 mm, (b) 2.5 mm, (c) 2 mm, and (d) 1.5 mm thickness.. 77

Figure 4.8: Deformed shapes and stress fields near the bolt hole for the (a) 3 mm and (b) the 1.5 mm diagonal thickness. 79

Figure 4.9: Numerical force-displacement curves of the (virtual) UTM tension tests, for the 40 mm, 50 mm, 60 mm, and 70 mm width of the diagonal's web.. 79

Figure 4.10: Deformed shapes and stress fields near the bolt hole at 5 mm of (virtual) actuator displacement for the (a) 40 mm, (b) 50 mm, (c) 60 mm, and (d) 70 mm width of the diagonal's web. 80

Figure 4.11: Cross-aisle view of case study DD (dimensions in m). 81

Figure 4.12: Cross-aisle view of case study MD (dimensions in m)... 81

Figure 4.13: Simulating the plastic ovalization of a bolt hole under cyclic loading, using the elastic-perfectly-plastic gap material of OpenSees (McKenna et al., 2000). F_y is the yield force, E_0 is the elastic tangent, and E_1 is the hardening tangent. The gap opens by the amount of plastic strain the material accumulates at each excursion. In the left side of the figure, the loading, unloading, and reloading states of the bolt hole are shown schematically, along with the numbered points corresponding to the right diagram (the gray and black circles indicate the initial and final position of the bolt, respectively)... 85

Figure 4.14: Fitting the parameters F_y, E_0, and E_1 of the elastic-perfectly-plastic gap material, to match the analytical predictions of Eq. (4.12), Eq. (4.13), and Eq. (4.14). F_y is calculated so that the hatched areas below and under the bilinear fit are approximately equal. 86

Figure 4.15: Numerical modelling of a diagonal element with bearing failure behaviour in OpenSees (McKenna et al., 2000). Nodes i and j are connected by a zero-length element with an elastic-perfectly-plastic gap material, and nodes j and k by an elastic beam element with stiffness EA'/L. The cross-section area of the beam element is numerically reduced to A', to achieve the elastic shear stiffness of the upright frame taken from experimental shear tests. 87

Figure 4.16: Multi stripe analysis for double-depth case study DD, using a set of 30 records scaled to six IM levels. Two pie charts are given per stripe, showing the number of times a failure mode was observed on the standard (left) and the POS (right) design. If multiple failure modes were observed on a single record, the one with the highest utilization factor is considered..................... 88

Figure 4.17: Multi stripe analysis for multi-depth case study MD, using a set of 30 records scaled to six IM levels. Two pie charts are given per stripe, showing the number of times a failure mode was observed on the standard (left) and the POS (right) design. If multiple failure modes were observed on a single record, the one with the highest utilization factor is considered. 89

Figure 5.1: OpenSees' two-node link element for 2D analysis (McKenna et al., 2000). Nodes i and j are connected via three independent uniaxial springs to capture the axial, shear and rotational DOFs. 98

Figure 5.2: Transformation of member uprights' axial forces to stress resultants on the equivalent column, showing (a) a numerical example of an upright frame comprising two columns, and (b) the interaction between bending moment and axial force and the corresponding failure surface.......... 98

Figure 5.3: Simplification stages for a multi-depth cross-aisle frame; assuming negligible shear stiffness of the roof truss, multiple two- or three- member upright frames can be substituted by a single link element... 99

Figure 5.4: Numerical shear testing of a triple-upright segment. Bow-type imperfections of $L/200$ are applied to the diagonals, while rotational springs stiffen the pin/roll end supports. The derived force-displacement curve is employed to define the shear spring of the link element.................. 100

Figure 5.5: Cycle shear testing of the upright frame segment showing, the loading protocol (left) and the calibrated force-deformation response of the shear spring (right)... 101

Figure 5.6: Each roof beam element comprises two rigid parts at the two ends and one elastic in the middle, as its clear span is significantly different from the centreline length. 102

Figure 5.7: Calibration procedure for the grid formed by the rail and pallet beams in multi-depth systems. A small part of the rack is considered (the black lines in the figure) and the torsional constant of the equivalent pallet beam is calibrated until the first few modes of vibration of the simplified model match those of the full model. 103

Figure 5.8: Full and simplified models of (a) "uniform" Upright Frame 1 and (b) "nonuniform" Upright Frame 2. 104

Figure 5.9: Modes of vibration of "uniform" Upright Frame 1, showing (a) the first mode: T_1^{full} = 1.025 sec, T_1^{simpl} = 1.024 sec, (b) the second mode: T_2^{full} = 0.198 sec, T_2^{simpl} = 0.197 sec, and (c) the third mode: T_3^{full} = 0.087 sec, T_3^{simpl} = 0.087 sec. 105

Figure 5.10: Modes of vibration of "nonuniform" Upright Frame 2, showing (a) the first mode: T_1^{full} = 0.195 sec, T_1^{simpl} = 0.195 sec, (b) the second mode: T_2^{full} = 0.088 sec, T_2^{simpl} = 0.088 sec, and (c) the third mode: T_3^{full} = 0.056 sec, T_3^{simpl} = 0.055 sec. 105

Figure 5.11: Down-aisle view of the multi-depth 3D Case Study A. Each of the 44 vertical lines represents a single cross-aisle frame running perpendicularly to this figure. The 6 column-lines connected by X-braces correspond to heavy “tower” frames, while the remaining 38 are lighter “pallet” frames (units in meters). 106

Figure 5.12: Cross-aisle view of the multi-depth 3D Case Study A, comprising 24 “K-type” upright frames and a connecting shallow roof truss (units in meters). Along the vertical there are 9 load levels, while along the horizonal direction, four storage cells are distinguished comprising 6 upright frames each.. 107

Figure 5.13: Detail drawings for multi-depth Case Study A, showing (a): a reinforced upright Ω+U section, (b): a standard upright Ω section and (c): an upright-to-beam hooked connection. 107

Figure 5.14: Numerical models of the multi-depth Case Study A, showing (a) the full 3D beam-column model (647,000 DOFs), and (b) the simplified 3D Timoshenko-beam model (17,000 DOFs) 108

Figure 5.15: Modal analysis results of the 3D multi-depth Case Study A showing the dominant modes along the cross- and down-aisle direction as well as diaphragm shearing for the full model (left) and the simplified one (right).. 109

Figure 5.16: Response history results for the 2D cross-aisle frame of Case Study A, showing the peak interstory drift profiles for the four models (left) and the relative error of the maximum (over all stories) interstory drifts versus the DOFs of each model (right). 110

Figure 5.17: Response spectra of selected ground motions for high seismicity European sites, scaled at 2% in 50 years level (Kohrangi and Vamvatsikos, 2016). 111

Figure 5.18: Multi stripe analysis for the multi-depth Case Study A, showing the IM-EDP stripes for the three intensity levels (left), and the fragility curves for the three examined limit states (right). 112

Figure 5.19: The cross-aisle view of the ARSW double-depth frame of Caprili et al. (2018), showing (a) the full model, and (b) the reduced-order one (units in meters). 112

Figure 5.20: Axial compression-tension numerical test for a distributed plasticity beam-column representation of diagonal brace. The derived force-deformation curve is employed to characterize the equivalent nonlinear truss element. 114

Figure 5.21: Capacity curves for the three numerical models of Case Study B, showing the base shear versus the roof displacement (left), and versus the maximum interstory drift (right). 114

Figure 5.22: Maximum inter-story drift profile for the three numerical models of Case Study B (full, truss and link model). Four record scales were considered corresponding scale factors of 0.89, 1.00, 2.41 and 4.44. 115

Figure 5.23: IDA analysis results for the link model of Case Study B, showing (a) the individual IDA curves of each record, and (b) the corresponding 16%, 50% and 84% fractiles. 116

Figure 5.24: Fragility curves for Light Damage, Moderate Damage and Collapse Prevention limit states of Case Study B. 117

Figure 6.1: Partial collapse of an adjustable steel rack due to pallet falling during the Christchurch earthquake of 2011 (Clifton et al., 2011). 121

Figure 6.2: Idealized model of a body with mass m sliding with a friction constant μ on a moving rigid platform.. 123

Figure 6.3: NSBA of an idealized body sliding with a_y = 5 $\mathrm{m/s^2}$ on top of a rigid platform that is subjected to two rectangular pulses... 124

Figure 6.4: NSBA of an idealized body sliding with a_y = 5 $\mathrm{m/s^2}$ on top of a rigid platform that is subjected to two-and-a-half sinusoidal pulses.. 124

Figure 6.5: Numerical model of a 2DOF system of a cantilever beam with a flat slider at the top, showing (a) a case where the whole mass can slide (m = M), and (b) a case where only a portion m of the total mass M can slide, while $M - m$ is attached to the beam.. 125

Figure 6.6: Absolute acceleration and sliding diagrams of a mass sliding with friction coefficient μ = 0.3 on top of a rigid platform (period T = 0 sec), comparing the predictions of NSBA (SDOF system with rigidly connected mass, where sliding is estimated in post-processing) against the 2DOF flat slider model of Figure 6.5(a) (Landers 1992, Station BAKER FIRE, PEER NGA2 (Ancheta et al., 2013), scaled by 3.28). 126

Figure 6.7: Absolute acceleration and sliding diagrams of a 2DOF system with period T = 0.7 sec, μ = 0.3, and m = M (100% of mass can slide) comparing the predictions of NSBA (SDOF system with rigidly connected mass, where sliding is estimated in post-processing) against the 2DOF flat slider model of Figure 6.5(a) (Landers 1992, Station BAKER FIRE, PEER NGA2 (Ancheta et al., 2013), scaled by 3.28). 126

Figure 6.8: Comparison of NSBA (“Approximated”) with a 2DOF slider-on-cantilever (“Exact”), in terms of the predicted sliding for a system with T = 0.7 sec and μ = 0.3. The 16%, 50% and 84% fractiles of 30 ground-motions are shown, for m/M within 1% and 100%. 127

Figure 6.9: Boxplots of the ratio of the sliding displacement predicted by NSBA (“Approximated”) over the estimate of the 2DOF slider-on-cantilever (“Exact”), for a system with T = 0.75 sec, μ = 0.3 and $Sa(T)/\mu$ = 2.25, using 105 ground motions (red asterisks indicate the mean values). The optimal ξ_{eq} = 9.5% results to a mean ratio ~1.0... 129

Figure 6.10: Linear regression analysis for the relation of $Sa(T)/\mu$ with the equivalent damping ratio, ξ_{eq}, selected to optimally match NSBA with the 2DOF slider-on-cantilever............................... 129

Figure 6.11: Mean values of sliding displacement for 11 2DOF systems with different periods of vibration and μ = 0.3, subjected to 105 ground motions and 8 levels of IM................................. 130

Figure 6.12: Modelling of pallets along the cross-aisle direction of an APR system using flat sliders and rigid elements. 130

Figure 6.13: When multiple pallets are resting on pallet/rail beams, the pair of overturning forces $H \cdot e_V$ produced by the vertical eccentricity of the pallet and the supporting beams is cancelled by its adjacent pallets. 131

Figure 6.14: Substitution of the full cross-aisle frame of multi-depth systems with a single upright frame or a single stick that employs horizontal axial springs at the top, to simulate the lateral restraint offered by the roofing system... 131

Figure 6.15: Rayleigh damping coefficients for ξ_1 = 3% and ξ_2 varying from 3% to 30%........... 133

Figure 6.16: Cross-aisle view of the multi-depth Case Study 1, consisting of 24 “K-type” upright frames and a connecting shallow roof truss (units in meters). 134

Figure 6.17: Cross-aisle view of: (a) the medium-rise APR Case Study 2 and (b) the low-rise APR Case Study 3 (units in meters)... 135

Figure 6.18: Hazard curves for the sites of Athens and Van, using $AvgSa$ as an IM.................... 137

Figure 6.19: Boxplots of the “Approximated/Exact” ratio of (a) Base Shear, (b) Roof Drift, (c) Interstorey Drift and (d) Sliding, for all the 30x12 = 360 RHAs shown in Table 6.4 (the FM approach was considered the “Exact” solution, and the rest four “Approximated” were compared against it). 138

Figure 6.20: Linear regression analysis for $EN1$ (FM/NM base shear reduction) given the IM of (a) $Sa(T_1)/\mu$, (b) $Sa(T_2)/\mu$, and (c) $\sqrt{Sa(T_1)Sa(T_2)}/\mu$. 140

Figure 6.21: FM/NM roof drift reduction given the IM of (a) $Sa(T_1)/\mu$, (b) $Sa(T_2)/\mu$, and (c) $\sqrt{Sa(T_1)Sa(T_2)}/\mu$.. 140

Figure 6.22: FM/NM maximum interstorey drift reduction given the IM of (a) $Sa(T_1)/\mu$, (b) $Sa(T_2)/\mu$, and (c) $\sqrt{Sa(T_1)Sa(T_2)}/\mu$. 141

Figure 6.23: Pallet sliding prediction via RHA with flat sliders given the IM of (a) $Sa(T_1)/\mu$, (b) $Sa(T_2)/\mu$, and (c) $\sqrt{Sa(T_1)Sa(T_2)}/\mu$. 141

Figure 6.24: Boxplots of the MRSA/RHA ratio of (a) maximum bottom upright axial force, (b) maximum bottom diagonal force, (c) maximum top upright axial force, (d) maximum top diagonal axial force, (e) base shear and (f) roof drift, for the upright frame of Case Study 1, using the 30-records set #1, scaled to 3%, 5% and 10% in 50 years probability of exceedance (red asterisks indicate the mean value while red horizontal lines the median). 143

List of Tables

Table 2.1: Proposed Rack taxonomy following the GEM breakdown to Attributes/Attribute-Levels/Options. 20

Table 2.2: Publications related to the seismic performance of racks, categorized according to the proposed taxonomy. 30

Table 3.1: Tag list of structural components used for the seismic assessment of the five multi-depth ARSW case studies. 42

Table 3.2: Section scheme and height of the structural components given in Table 3.1. 43

Table 3.3: Seismic design assumptions adopted for each multi-depth ARSW case study.......... 44

Table 3.4: Sensitivity factors and cumulative seismic load multipliers for each multi-depth ARSW case study. 48

Table 3.5: IM value, mean magnitude, distance and epsilon obtained from disaggregation analysis for Van in terms of $AvgSa$ at nine selected return periods.......... 50

Table 3.6: Periods and mass participation factors for the five multi-depth ARSW case studies. 53

Table 3.7: Element/connection verification checks conducted during the seismic assessment of the five multi-depth ARSW case studies. 54

Table 3.8: Statistics for the utilization factors displayed in Figure 3.14(a)-(f) and scenario checks. 62

Table 4.1: Seismic design assumptions adopted in case studies DD and MD according to the standard design (STD), and the POS re-design (POS). 82

Table 4.2: Member and connection properties of case study DD according to the standard design (STD), and the POS re-design (POS). Section areas are given normalized to the bottommost elements of the STD design.......... 83

Table 4.3: Member and connection properties of case study MD according to the standard design (STD), and the POS re-design (POS). Section areas are given normalized to the bottommost elements of the STD design.......... 83

Table 4.4: Periods and mass participation factors for the case studies DD and MD according to the standard design (STD), and the POS re-design (POS).......... 84

Table 5.1: Cross-section shear area for bracing patterns D, Z, K, and X per EN 1993-1-1 (2005). 96

Table 5.2: Unit load weight and cross-sectional properties of “uniform” Upright Frame 1 and “nonuniform” Upright Frame 2.......... 104

Table 5.3: Cross-section properties of structural members (multi-depth, Case Study A). Cross-section areas are rounded to the third digit while moments of inertia to the fifth.......... 107

Table 5.4: Structural member cross-sections and steel grade for interior and exterior upright frames (Case B). Per EN 1993 (2005), steel grade Sxxx has a characteristic yield strength of xxx MPa. 113

Table 6.1: Selected modelling approaches, indicating the use of flat slider elements, equivalent damping, or none. 133

Table 6.2: Cross-section properties of structural members. Cross-section areas are rounded to the 3rd digit while moments of inertia to the 5th. 135

Table 6.3: Periods and mass participation factors for the three considered case studies along the cross-aisle direction. 135

Table 6.4: Selection of seismic input for Case Studies 1, 2 and 3. 137

Nomenclature

2D	two-dimensional
2DOF	two-degree-of-freedom
3D	three-dimensional
A	nominal cross-section area
APR	adjustable pallet rack
ARSW	automated rack supported warehouse
$AvgSa$	average spectral acceleration
A_{eff}	effective cross-section area
A_{mult}	cross-section area reduction multiplier
A_{net}	net cross-section area
b	width of steel profile
CA	cross-aisle
CoV	coefficient of variance
CS	conditional spectrum
CSSI	content-structure-sliding interaction
d	bolt diameter
d_0	bolt hole diameter
DA	down-aisle
DOF	degree of freedom
E	young’s modulus
EDP	engineering demand parameter
E_{D1}	design spectrum modification factor 1
E_{D2}	unit load weight modificatory factor 2
E_{D3}	design spectrum modification factor 3
E_{N1}	new design spectrum modification factor 1
FEM	Federation Européenne de la Manutention
FM	full model
f_u	nominal ultimate tensile strength
f_{ub}	nominal ultimate tensile strength of the bolt
f_y	yield stress
$F_{v,Rd}$	design bolt shear resistance
$F_{b,Rd}$	design bearing resistance
g	gravity acceleration
G	dead loads
GEM	Global Earthquake Model
GLRS	gravity load-resisting system
I	second moment of inertia
IDA	incremental dynamic analysis
IM	intensity measure
I_t	polar moment of inertia
I_y	cross-aisle second moment of inertia

I_z	down-aisle second moment of inertia
k	constant slope of hazard curve
K_D	design spectral acceleration factor
LLRS	lateral load-resisting system
MAF	mean annual frequency
MDOF	multi degree of freedom
MRF	moment resisting frame
MRSA	modal response spectrum analysis
M_{Ed}	design bending moment
$M_{E,tot}$	total seismic mass of rack
$M_{E,G}$	total seismic mass coming from the self-weight of the rack
$M_{E,UL}$	unit load seismic mass
NDM	Newmark’s block with equivalent damping model
NDWM	Newmark’s block with weighted mean equivalent damping model
NM	Newmark’s block model
NSBA	Newmark’s sliding block analysis
$N_{anc,Rd}$	design anchorage uplift resistance
$N_{b,Rd}$	design buckling resistance
N_{Ed}	design axial force
$N_{pl,Rd}$	design plastic resistance
$N_{t,Rd}$	design tensile resistance
$N_{u,Rd}$	design ultimate resistance
POS	plastic ovalization strategy
P_E	total seismic weight of rack
$P_{E,prod}$	total seismic product weight stored in the rack
q	behaviour factor
Q	live/unit loads
q_d	ductility behaviour factor
$Q_{P,rated}$	specified weight of unit loads
R	response modification coefficient
RHA	response history analysis
RHS	rectangular hollow section
RMI	Rack Manufacturer Institute
RSW	rack supported warehouse
R_{cum}	cumulative seismic load multiplier
R_F	rack filling grade reduction factor
R_m	mass seismic load multiplier
R_q	behaviour factor seismic load multiplier
S	soil factor
Sa	(pseudo) spectral acceleration
SDOF	single degree of freedom
SKU	stock keeping unit

SM	stick model
SPO	static pushover
t	thickness of steel profile
T_1	fundamental period of vibration
T_2	second period of vibration
UF	utilization factor
UTM	universal testing machine
$V_{eff,1,Rd}$	design block tear-out resistance
V_{Ed}	design shear force
a_g	ground acceleration
a_y	yield acceleration
γ_I	importance factor
γ_M	partial safety factor
γ_{ov}	overstrength factor
Γ_i	modal participation factor of mode i
η	damping correction factor
θ	interstory drift sensitivity coefficient
λ	mean annual frequency
μ	friction coefficient
μ_{UF}	mean value of utilization factor
ν	Poisson’s ratio
ξ	viscous damping ratio
ξ_{eq}	equivalent viscous damping ratio
ψ_2	seismic mass combination coefficient
Ω	overstrength factor

1 Introduction

1.1 Problem statement

Warehousing and transportation support activities are a subsector of the transport and storage services business sector, with a significant impact on the global economy. For instance, in the European Union, this sector generated €487.1 billion of value added in 2018, the fifth greater in EU's economy, representing 7.4% of the wealth generated in the non-financial business economy (EuroStat). Specifically, the warehousing subsector employed nearly 2.5 million persons, most of them working in Germany, Netherlands, Belgium, France, Italy, and Spain. In other words, warehouses are civil engineering structures that play an important role in the society, providing a safe place for the goods to be stored before their large distribution to the public (Gu et al., 2007). At the same time, they are concentrated points of failure in an otherwise widely distributed logistics system.

In order to provide flexibility in the handling process and to accommodate a large variety of stored goods, warehouses come in all kinds of structural configurations (Tilburgs, 2013). Typically, one considers a warehouse as a combination of (a) an external shell and (b) a series of racks or shelves that support the merchandise (Figure 1.1); however, this is not always the case (Vujanac et al., 2017). Integrated solutions are proliferating, where the racks also support the cladding and facade in the so-called rack supported warehouses (RSWs). Innovation is not limited in the structural configuration but also extends to the handling process, providing automated management systems for storage and retrieval using integrated artificial intelligence and robotics. Considering also the nature of the stockpiled wares, there is a virtually "infinite" number of warehouse configurations, each characterized by specific attributes such as dimensions, used material, automation, etc.

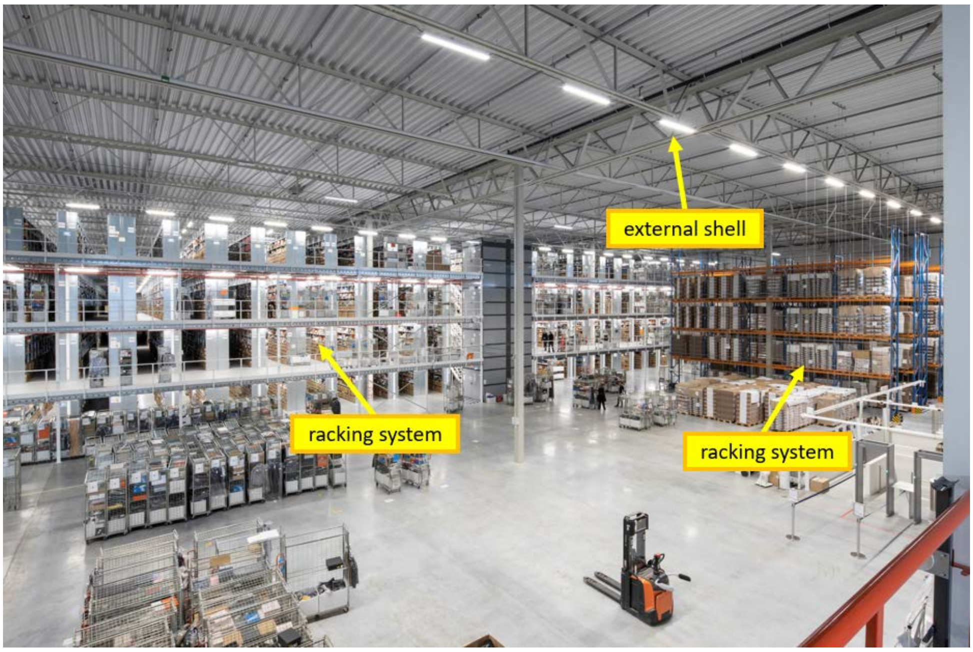

Figure 1.1: Typical configuration of a warehousing unit, comprising (a) the racking systems used to store the goods and materials of the warehouse (herein it contains a series of shelving racks and a series of adjustable pallet racks), and (b) the independent external shell structure (photo courtesy of Nedcon B.V).

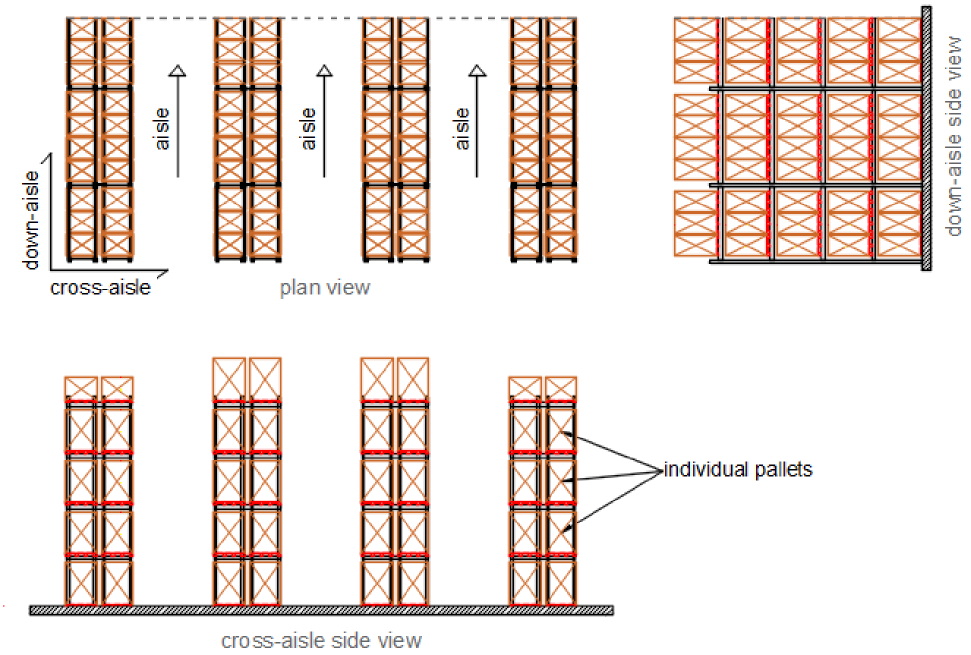

Figure 1.2: Plan and side views of a typical racking system. Two directions are defined, the down-aisle, which is used by the forklift trucks and, perpendicularly, the cross-aisle.

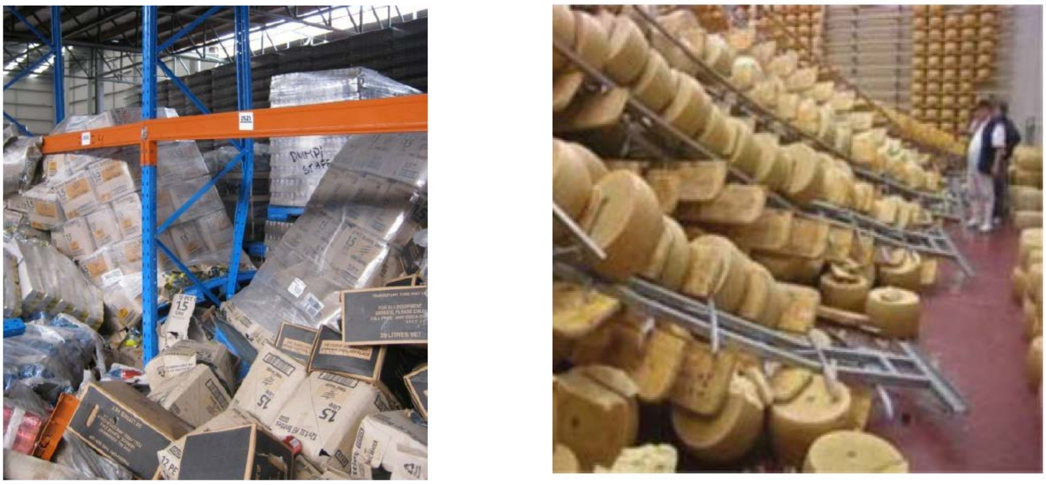

(a) (b)

Figure 1.3: Failure of indoor racking structures during seismic motions, showing (a): partial collapse of an adjustable steel rack during the Christchurch earthquake of 2011 (Clifton et al., 2011) and (b): collapse of cantilever-like racks used for Parmigiano Reggiano cheese wheels in a warehouse in Emilia Romagna (Franco et al., 2015).

Arising from the need of easy assembly, adjustable geometry and low cost, steel pallet racking systems exhibit a number of peculiarities that distinguish them from ordinary building structures. A typical rack configuration consists of two directions, the down-aisle, which is used by the forklift trucks in order to deposit and withdraw the goods and, perpendicularly, the cross-aisle (Figure 1.2). Both directions are typically realized using thin-walled steel members with simple hooked or bolted connections, which significantly affect the response of the rack to lateral loads, such as seismic or wind actions. Moreover, unlike typical buildings, the weight of these steel members is only a small fraction, e.g., 5-10%, of the live loads. For these reasons, their design is not based on codes for regular steel structures, e.g., EN 1993 (2005) (Eurocode 3), but on special standards, such as EN 15512 (2009) in Europe, RMI (2012) in the US, or AS 4084 (2012) in Australia. These specifications call for design assisted by testing to acknowledge that the response of members and joints to loading cannot be covered exclusively by numerical analysis.

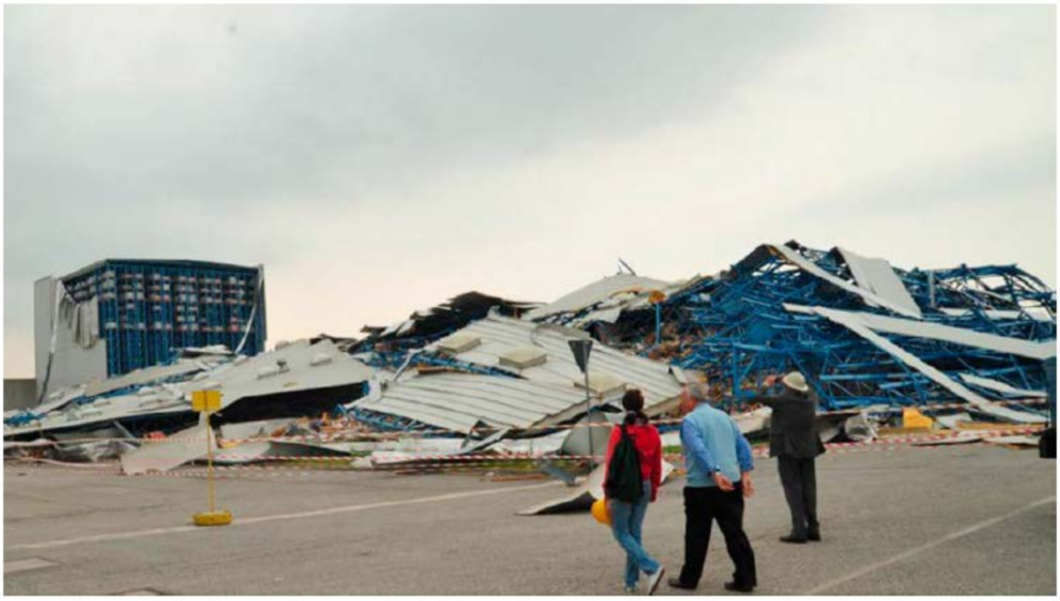

Figure 1.4: Collapse of Ceramic Storage warehouse in Sant' Agostino due to 2012 Emilia-Romagna earthquake, Italy (Kanyilmaz et al., 2016).

Seismic events on industrial areas over the past years have showed the vulnerability of many warehouses to lateral loads (Bournas et al., 2014). Storage racks, whether they support the whole building or not (i.e., indoor racks), are made of slender members that carry high live-loads; this renders them susceptible to various types of member buckling and global geometric non-linearities (i.e. P-Δ effects). During the Christchurch earthquake series of 2010 and 2011 (Clifton et al., 2011), several indoor storage racks collapsed (Figure 1.3(a)), despite the fact that the owners of the warehouses took measures or retrofitted the racks between the two events. In the Emilia-Romagna earthquake of 2012, it was estimated that 633,700 wheels of Parmigiano Reggiano and Grana Padano cheese were damaged by falling off factory shelves where they were maturing (Franco et al., 2015), with the cost of the damage estimated at €150 million (Figure 1.3(b)). Partial or even global collapses of RSWs were also reported (Figure 1.4).

The behaviour of racking systems to seismic excitations has been investigated by many researchers worldwide. In Europe, the European research projects SEISRACKS (Rosin et al., 2007) and SEISRACKS2 (Castiglioni et al., 2014) examined the seismic performance of braced and unbraced racks by means of experimental and numerical tests (Adamakos, 2018; Kanyilmaz, 2016). The full-scale tests revealed the sensitivity of racks to construction details and to system-level effects not completely detected during the code-mandated component and subassembly tests. In Australia, Gilbert and Rasmussen (2012) and Gilbert et al. (2014) presented the three-dimensional response of drive-in storage racks, where it was shown that the friction between pallet bases and rail beams provides additional horizontal bracing restraints on the system. In China, Yin et al. (2016; 2018) conducted several monotonic and cyclic loading tests on beam-to-column connections and found that by introducing additional bolts and welds, the hysteretic response of the joint can be improved in terms of stiffness degradation and deformability.

So far, the research has mainly focused on the seismic behaviour of low/medium-rise racking systems, and in particular on the response along the down-aisle direction. As a result, current design codes are available almost solely for the adjustable pallet racks (APRs) (Figure 1.2), and it is the designer's responsibility to extend them to other systems. For instance, no official provisions exist for the design of automated rack supported warehouses (ARSWs); designers are obliged to treat them as APRs, adopting low-ductility concepts and disregarding capacity-design rules. There is also a large percentage of racks that are not even designed for seismic loads, despite being installed in earthquake-prone areas. However, considering the economic impact that a collapse of a warehouse has, it is questionable whether low cost outweighs resilience.

Apart from the explicit increase of internal actions during the seismic excitation, racking systems may also suffer damages due to the implicit hazard of content sliding. As the wares are not mechanically connected to the rack, but are stored on pallets, boxes, containers, etc., floor accelerations can initiate excessive content sliding, leading to localized damages due to impact on the structural members, or even complete collapse of the structure due to contents falling off (Figure 1.3(a)) and crushing adjacent frames. Currently, seismic design codes for racks (e.g., EN 16681, 2016; RMI, 2012) do not offer a tool to predict sliding displacements, as it is related to absolute floor accelerations for which a conventional modal response spectrum analysis (MRSA) is not able to provide any information.

1.2 Objectives and Scope

The present thesis comprises a collection of research studies that attempt to expand the current knowledge on the seismic behaviour of steel racking systems. While mainly focusing on the seismic assessment of the innovative ARSWs, research is not limited to a single rack typology; it offers a multi-faceted contribution that is not only of academic interest, but also of practical usage, assisting structural engineers and risk analysts to improve on design, assessment, and decision-support.

Ultimately the goal is to: (a) establish an expandable, user-friendly, and intuitive taxonomy for steel racking systems, offering a common glossary to risk analysts for efficient identification and assessment, (b) perform, for the first time, a comprehensive seismic assessment of ARSWs installed in high-seismicity areas, (c) propose a new seismic design approach that reliably increases the ductility of the racks along their cross-aisle direction, (d) offer simplified modelling approaches for rapid assessment and design of ARSWs, and (e) delineate a solid methodology for the assessment of content sliding under seismic excitations.

1.3 Outline

Most chapters are designed to be autonomous, each being a self-contained, single paper that has either been published in a scientific journal or is being planned as a future publication, augmented herein with additional information and figures. The only exceptions of interconnections among the chapters consist of few references on figures/tables/equations, in an attempt to minimize the size of the thesis.

Chapter 2 discusses the morphology and the macro-characteristics of various racking typologies, focusing on their structural behaviour under lateral loading conditions. Subsequently, these individual attributes are summarized in a flexible and collapsible taxonomy, which adopts the same terminology as the Building Taxonomy of the Global Earthquake Model, comprising five basic classes or “Attributes”, capable of characterizing any existing, contemporary, and upcoming rack typology.

Chapter 3 presents a comprehensive study on the seismic performance of five multi-depth ARSWs, designed by professional engineers within the context of the STEELWAR (2017) project to be installed in the city of Van, Turkey. Using a state-of-the-art methodology for record selection, a series of linear response history analyses is performed for each case study, in order to specify the most vulnerable members and connections of the structures and define a *hierarchy of criticalities*. Finally, the effect of the *cumulative seismic load multiplier* is assessed, by realizing a series of “what-if” scenarios, where each scenario exploits a certain level of seismic load reduction as implied by the relevant design codes.

Chapter 4 proposes a new “dissipative” (as per EN 1998-1:2005 parlance) approach for seismic design along the cross-aisle direction, the so-called plastic ovalization strategy (POS). POS relies on the bearing deformation of the diagonal bolt hole, while adjacent components are designed to be over-resistant. Ten capacity design rules inspired by EN 1998-1 (2005) are introduced, but appropriately modified to respect the philosophy of the rack industry that demands light steel members with very simple bolted connections. The advantage of the POS over the standard design approaches is illustrated by performing a multi stripe analysis (Jalayer and Cornell, 2009) on the cross-aisle direction of two ARSW case studies. A subsystem of a beam element in tandem with nonlinear springs is employed to simulate the bearing failure of the diagonal-to-upright connection, calibrated by finite element models and existing analytical equations.

Chapter 5 presents a reduced-order modelling approach for the seismic analysis of ARSWs. It is based on the well-established substitution of built-up columns and truss beams with equivalent Timoshenko beam elements, reducing the size of the numerical problem by orders of magnitude. The proposed simplified model goes one step beyond by providing the capability for inelastic static and dynamic simulations with negligible loss of accuracy. This is achieved with the use of link elements that can capture the shear, axial and rotational stiffness degradation of the substituted upright frames. The accuracy and numerical efficiency of the proposed simplified method is then demonstrated in a series of 2D and 3D elastic and inelastic analyses on two high-rise ARSWs.

Chapter 6 discusses the phenomenon of content-structure-sliding interaction (CSSI) on structures with mass-dominant contents, focusing on the case of racking systems. Three approaches are investigated to capture CSSI: (i) introducing friction sliders per pallet and running nonlinear response-history analysis, (ii) increasing the model viscous damping and using elastic response-history analysis, and (iii) reducing the horizontal seismic loads in tandem with modal response spectrum analysis. Three case studies are employed to calibrate empirical relationships for damping amplification and seismic load reduction, largely removing the bias of simpler alternatives (ii) and (iii), respectively, to level the ground for future code applications.

Finally, Chapter 7 provides the overall conclusions and scientific contribution of the thesis, summarises the virtues and limitations of the proposed methods, and sets directions for future work and improvements.

1.4 References

Adamakos K. (2018). “*Seismic actions and response of steel storage pallet racks - A numerical investigation*”, Doctoral Thesis, National Technical University of Athens, School of Civil Engineering.

AS 4084 (2012). “*Steel storage racking*”, Standard Australia.

Bournas D.A., Negro P., Taucer F.F. (2014). “*Performance of industrial buildings during the Emilia earthquakes in Northern Italy and recommendations for their strengthening*”, Bulletin of Earthquake Engineering, **12**, 2383-2404. https://doi.org/10.1007/s10518-013-9466-z

Castiglioni C.A. et al. (2014). “*Seismic behavior of steel storage pallet racking systems (SEISRACKS2)*”, Final Report, RFSR-PR-03114, European Commission, DG Research, Brussels, Belgium.

Clifton G.C., Bruneau M., Macrae G.A. (2011). “*Steel structures damage from the Christchurch earthquake series of 2010 and 2011*”, Bulletin of the New Zealand Society for Earthquake Engineering, **44**(4), 297-318. https://doi.org/10.5459/bnzsee.44.4.297-318

EN 15512 (2009). “*Steel static storage systems - Adjustable pallet racking systems - Principles for structural design*”, European Committee for Standardization (CEN), Brussels, Belgium.

EN 16681 (2016). “*Steel static storage systems - Adjustable pallet racking systems - Principles for seismic design*”, European Committee for Standardization (CEN), Brussels, Belgium.

EN 1993 (2005). “*Eurocode 3: Design of Steel Structures*”, European Committee for Standardization, Brussels, Belgium.

EN 1998-1 (2004). “*Eurocode 8: Design of structures for earthquake resistance - Part 1: General rules, seismic actions and rules for buildings*”, European Committee for Standardization, Brussels, Belgium.

Eurostat, homepage: https://ec.europa.eu/eurostat/web/main/home

Franco A., Massimiani S., Carfagni G.R. (2015). “*Passive Control of Steel Storage Racks for Parmigiano Reggiano Cheese under Seismic Accelerations*”, Journal of Earthquake Engineering, **19**(8), 1222-1259. https://doi.org/10.1080/13632469.2015.1049386

Gilbert B.P., Rasmussen K.J.R. (2012). “*Drive-in Steel Storage Racks I: Stiffness Tests and 3D Load-Transfer Mechanisms*”, Journal of Structural Engineering, **138**(2). https://doi.org/10.1061/(ASCE)ST.1943-541X.0000449

Gilbert B.P., Teh L.H., Badet R.X., Rasmussen K.J.R. (2014). “*Influence of pallets on behaviour and design of steel drive-in racks*”, Journal of Constructional Steel Research, **97**, 10-23. https://doi.org/10.1016/j.jcsr.2014.01.013

Gu J., Goetschalckx M., McGinnis L.F. (2007). “*Research on warehouse operation: A comprehensive review*”, European Journal of Operational Research, **177**(1), 1-12. https://doi.org/10.1016/j.ejor.2006.02.025

Jalayer F., Cornell C.A. (2009). “*Alternative non-linear demand estimation methods for probability-based seismic assessments*”, Earthquake Engineering and Structural Dynamics **38**(8), 951-972. https://doi.org/10.1002/eqe.876

Kanyilmaz A., Castiglioni C.A., Brambilla G., Chiarelli G.P. (2016). “*Experimental assessment of the seismic behavior of unbraced steel storage pallet racks*”, Thin-Walled Structures, **108**, 391-405. https://doi.org/10.1016/j.tws.2016.09.001

RMI, ANSI MH16.1.12 (2012). “*Specification for the Design, Testing and Utilization for Industrial Steel Storage Racks*”, Rack Manufacturer’s Institute, Charlotte, NC.

Rosin I., Calado L., Proença J., Carydis P., Mouzakis H., Castiglioni C., Brescianini J.C., Plumier A., Degee H., Negro P., Molina F. (2007). “*Storage racks in seismic areas (SEISRACKS)*”, Final Report, RFSR-PR-03114, European Commission, DG Research, Brussels, Belgium.

STEELWAR (2017). “*Advanced structural solutions for automated STEELrack supported WARehouses*”, The Steelwar Project Consortium, Pisa, Italy. https://www.unipi.it/index.php/risultati-e-prodotti/item/10663-steelwar

Tilburgs K. (2013). “*Those peculiar structures in cold-formed steel: “racking & shelving”*”, Steel Construction **6**(2). https://doi.org/10.1002/stco.201310016

Vujanac R., Živković M., Slavković R., Vulović S. (2017). "*Steel frame versus rack supported warehouse structures*", Tehnički vjesnik **24**(4). https://doi.org/10.17559/TV-20140226220936

Yin L., Tang G., Zhang M., Wang B., Feng B. (2016). “*Monotonic and cyclic response of speed-lock connections with bolts in storage racks*”, Engineering Structures, **116**, 40-55. https://doi.org/10.1016/j.engstruct.2016.02.032

Yin L., Tang G., Li Z., Zhang M. (2018). “*Responses of cold-formed steel storage racks with spine bracings using speed-lock connections with bolts II: Nonlinear dynamic response history analysis*”, Thin-Walled Structures, **125**, 89-99. https://doi.org/10.1016/j.tws.2018.01.002

2 Macro-characteristics and Taxonomy of Steel Racking Systems[1]

2.1 Introduction

The large variation of characteristics among different racking systems, not unlike the differences among types of conventional buildings, means that lumping all types into a single "warehouse class" can become a gross oversimplification. Instead, by defining a uniform taxonomy, there are distinct advantages to be had: (a) by facilitating the comparison of results between different studies, (b) selecting vulnerability/fragility functions for portfolio or regional risk/loss assessment studies, and (c) collecting usable damage/loss data in post-earthquake surveys. While manufacturers and designers of steel racks do employ a fairly wide categorization of structural systems, they also tend to focus on functionality, usability and performance from a logistics point of view; such attributes are not necessarily important for guiding vulnerability assessment. Similarly, rack design codes may employ some elements of classification (e.g., EN 16681, 2016), yet these are not comprehensive enough to fit the purposes of a full taxonomy for vulnerability assessment. Instead, we propose distilling current industrial classifications to delineate a collapsible, flexible and extensible set of classes that can encode the salient structural characteristics of existing, contemporary and upcoming racking systems, akin to literature taxonomies for typical buildings, e.g., by the Global Earthquake Model (GEM, Brzev et al., 2013) or the Earthquake Engineering Research Institute (EERI) and International Association for Earthquake Engineering (IAEE) World Housing Encyclopedia (Brzev and Greene, 2004). In turn we offer perspective regarding the expected behaviour, as well as a common glossary to support efficient identification and assessment by risk analysts.

2.2 Morphology of racking systems

Steel racking systems commonly comprise cold-formed members that can be easily assembled and adjusted to serve the continuously changing needs of a warehouse. While some members can be made of hot-rolled steel, such as some angle-L sections in the bracing system, a rack completely made of hot-rolled sections is not considered to be economically viable, due to the heavy connections needed with respect to the cold-formed solutions. Typically, in a racking system one defines two primary directions, the down-aisle direction which is used by the forklift trucks in order to deposit and withdraw the goods and, perpendicularly, the cross-aisle (EN 15512, 2009).

---

[1] This work contains material from "Tsarpalis D., Vamvatsikos D., Deladonna F., Fabini M., Hermanek J., Dot Margotan P., Sesana S., Vantusso E., Vayas I. (2022). *Macro-characteristics and taxonomy of steel racking systems for seismic vulnerability assessment*, Bulletin of Earthquake Engineering. https://doi.org/10.1007/s10518-022-01326-x", reproduced here with permission.

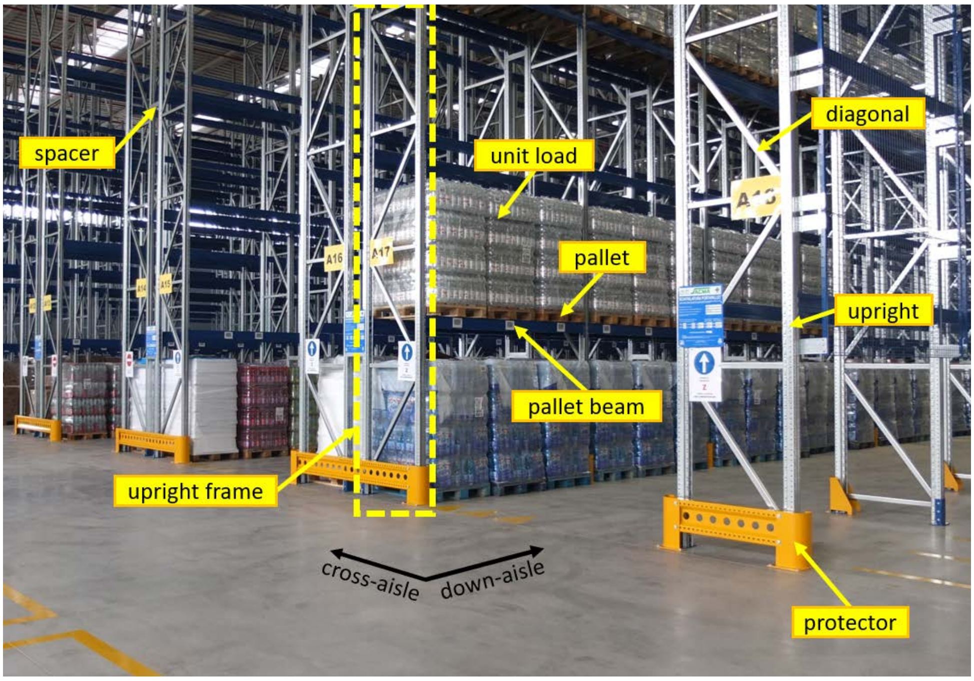

Figure 2.1: Primary structural components of an adjustable pallet racking (APR) system and definition of the down- and cross-aisle directions (photo courtesy of SACMA S.p.a.).

Figure 2.1 illustrates the primary components of the most common rack configuration, the adjustable pallet racking (APR) system (also referred to as “selective” system). Individual or boxed items are combined into single “units”, so-called unit loads, that can be moved easily with a pallet jack or forklift truck. They typically consist of corrugated fiberboard boxes stacked on a pallet or slip sheet and stabilized with stretch wrap. Each unit load is characterized by a stock keeping unit (SKU), a unique identifier that is used to classify the stored goods inside a warehouse. Unit loads of the same SKU are considered identical and thus, interchangeable. In APR systems, the pallets are accommodated by the pallet beams that are hooked (Figure 2.2(b)) or bolted to the uprights, creating a moment resisting frame (MRF) in the down-aisle direction (Bernuzzi and Simoncelli, 2016b). In the cross-aisle direction, the uprights are connected by a bracing system (Figure 2.2(a)) with a D, Z, K or X bracing pattern (EN 15512, 2009), defining the so-called upright frames (Figure 2.1). Racking systems are typically fixed on a concrete ground slab using a base plate and post-installed anchors (Figure 2.2(b)), however there are some exceptional cases where the racks are installed on asphalt, tiles or even suspended floors.

Other traditional types of storage racks are the drive-in and the drive-through systems. Drive-in racks allow a lift truck to enter the rack from one side to pick up or lay down pallets, which are placed on a continuous rail beam (Figure 2.3). From a logistics point of view, drive-in racks are efficient when one has a large number of similar items that can be stored in a single “input/output” pallet position and accessed via the Last-In, First-Out method. Access is provided through a single aisle in the front of the rack. The fact that the forklifts need to drive into the racks leads to the absence of pallet beams, with the exception of the “portal” beams at the highest level of the rack. As a result, drive-in racks cannot rely on this extremely weak MRF to resist the lateral loads and a bracing system is always mandatory. When the vertical bracing is placed eccentrically at the one end of the rack, so called spine bracing, horizontal braces are also placed in order to provide an in-plane stiffness diaphragm at the top level (Cheng and Wu, 2016), as shown in Figure 2.3. On the other hand, some manufacturers prefer to sacrifice one bay and install a concentric vertical bracing system, the so-called bracing towers, a lateral force resisting system that is used also in other racking systems. Finally, the drive-through system is identical to the drive-in from a structural point of view; the only difference is that drive-through racks allow the lift truck to enter through both ends of the system allowing for a First-In, First-Out storage option, but requiring aisles on both the front and the back of the rack.

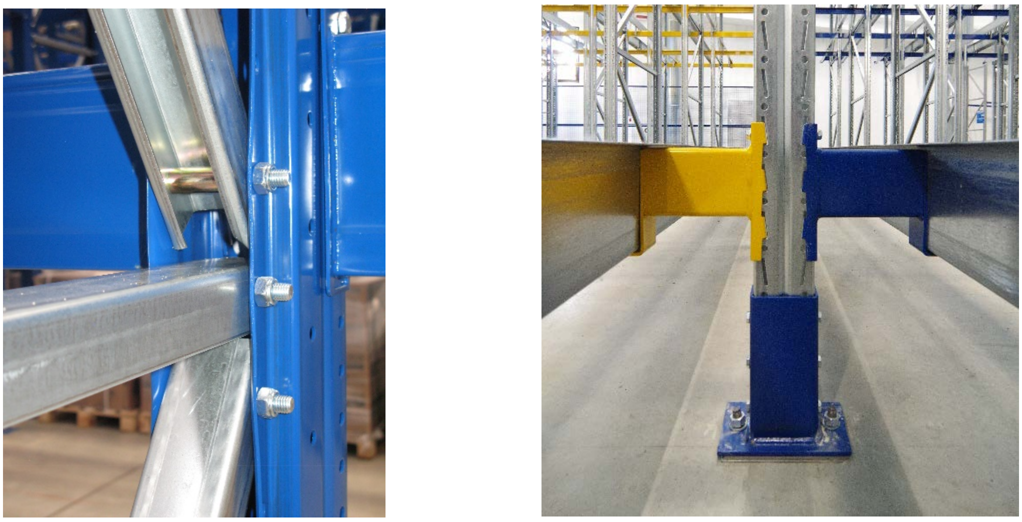
(a) (b)

Figure 2.2: Component connections of an APR system showing: (a) a diagonal-to-upright bolted connection and (b) a beam-to-column hooked connection and an upright-to-floor connection (photos courtesy of SACMA S.p.a.).

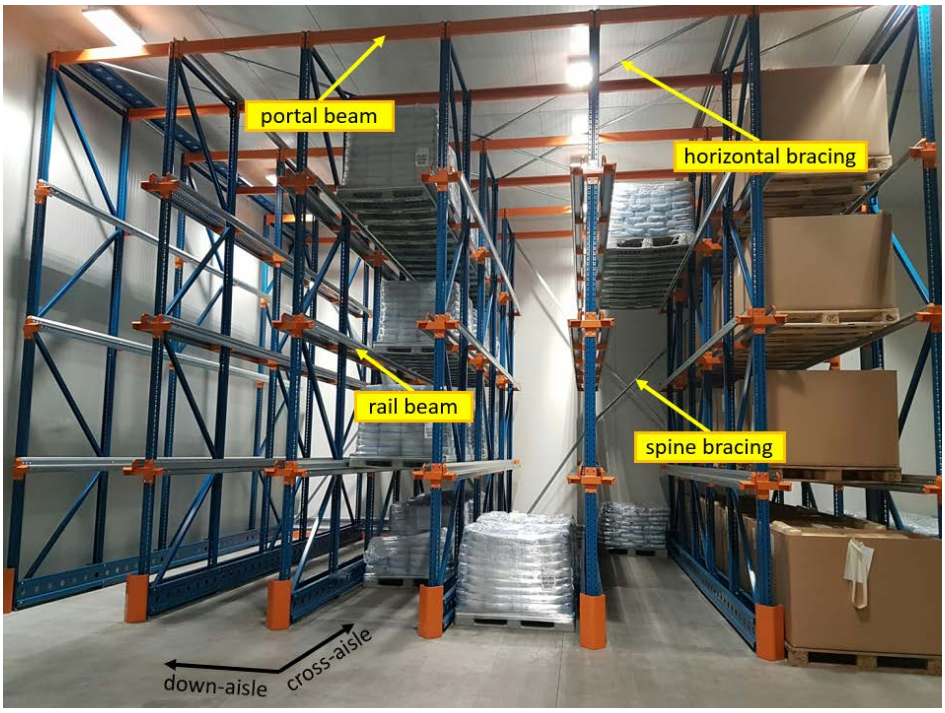

Figure 2.3: Primary structural components of a drive-in steel racking system. In drive-in racks, the forklifts enter inside the rack in order to deposit and withdraw the pallets (photo courtesy of Nedcon B.V.).

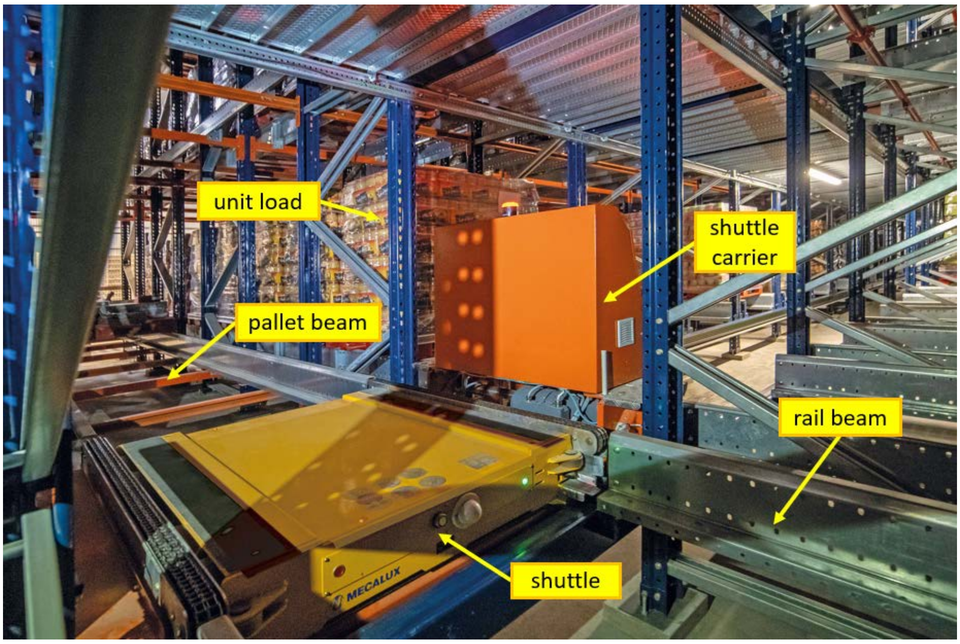

Figure 2.4: Configuration of a multi-depth pallet shuttle racking system. Pallets are stored in long storage tunnels serviced by mechanized shuttles running on rails (photo courtesy of MECALUX S.A.).

A more modern approach to the Last-In, First-Out method, is the pallet shuttle racking system (Huang et al., 2012). Lately, these systems are preferred over the traditional drive-in, as they allow working on each load level individually, while in the drive-in each bay must have items with the same SKU. The pallet shuttle racks are characterized by a multi-depth structure, where the unit loads are stored in long storage tunnels, serviced by mechanical shuttles which are positioned by traditional forklift trucks or cranes (Figure 2.4). As the shuttles are moving along the cross-aisle direction, like the lift trucks do in the drive-in system, rail beams are also mandatory in this system, with the difference that they are not connected directly to the uprights but on pallet beams. As the pallet beams now need only to accommodate one pallet per bay, their cross-sections are lighter with respect to those of the APR system and thus the formed MRF is somewhat flexible. Thus, in seismic areas bracing towers are frequently placed at the one or both ends of the racking system.

The state of the art in storage technology are the automated rack supported warehouses (ARSWs), racking systems that employ automated storage procedures, while supporting both the stored pallets and the external cladding shell (Tsarpalis et al., 2021). ARSWs maximize the exploitation of the available footprint by achieving far greater heights than the traditional systems (e.g., 30 meters tall). This is achieved by connecting the upright frames by a roof truss, avoiding the construction of an independent shell-supporting structure. Two main types can be distinguished based on their configuration and handling system, namely the automated double-depth cranes (Figure 2.5) and the automated multi-depth shuttles (Figure 2.6). Double-depth cranes belong to direct-access systems and provide easy accessibility to the pallets, stored with a maximum number of two units for each row in the cross-aisle direction, but decrease the use of the available footprint of the warehouse by needing more aisles. Recently, the mini-load automated racking systems have become a popular solution for storing light and small wares with high stock turnover ratios (Figure

2.7), which essentially comprise a scaled-down version of the double-depth ARSWs. On the other hand, multi-depth shuttles are more compact systems that maximize the storage density, while losing accessibility to the pallets that are stored in long storage tunnels serviced by mechanized shuttles running on rails, which renders them more suitable for handling a reduced number of SKUs.

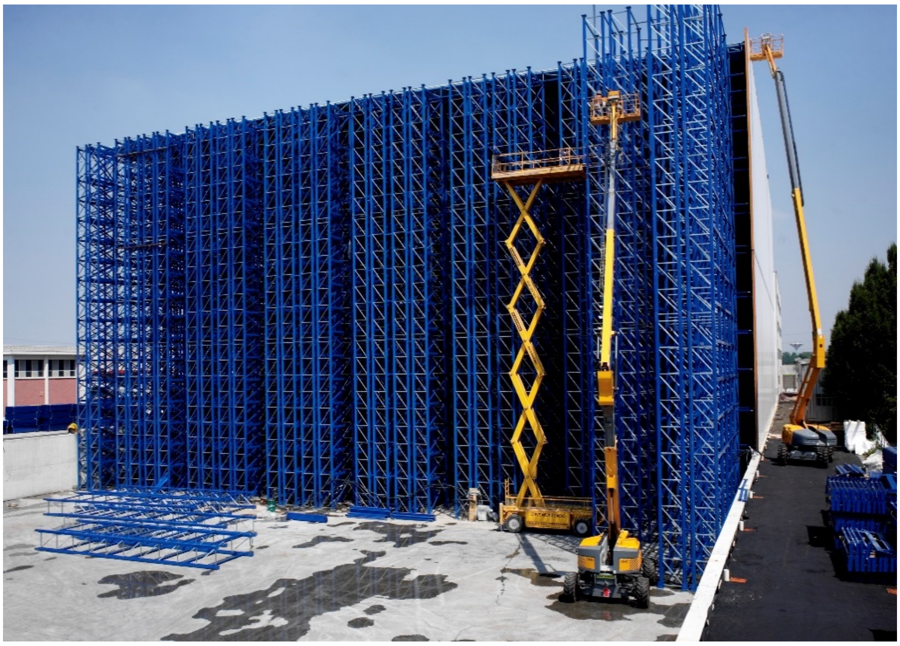

Figure 2.5: Example of a double-depth ARSW in the construction stage (photo courtesy of SACMA S.p.a.).

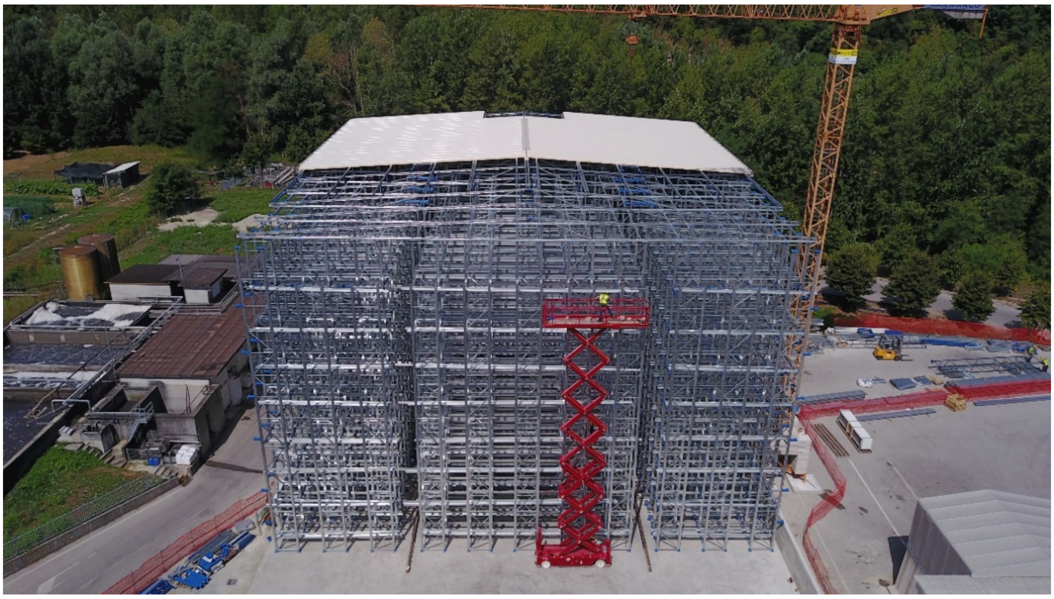

Figure 2.6: Example of a multi-depth ARSW in the construction stage (photo courtesy of SACMA S.p.a.).

Cantilever racks are used to easily store long products that typical pallet rack openings cannot handle, like steel profiles, steel or aluminum sheets, lumber, plywood, pipes etc. They employ a single upright that is perforated along the height to accommodate small cantilever beams, used to store the linear wares (Figure 2.8). The uprights are not made of open sections like in the other racking systems, but of rectangular hollow sections as no upright frame is formed in the cross-aisle direction. Instead, cross-aisle stability of the single upright acting as a cantilever is achieved solely by the moment-connection to a horizontal beam fixed to the foundation floor (FEM 10.2.09, 2013). On the down-aisle direction, a light bracing system is used, as the small horizontal elements that connect the uprights offer negligible moment-framing action.

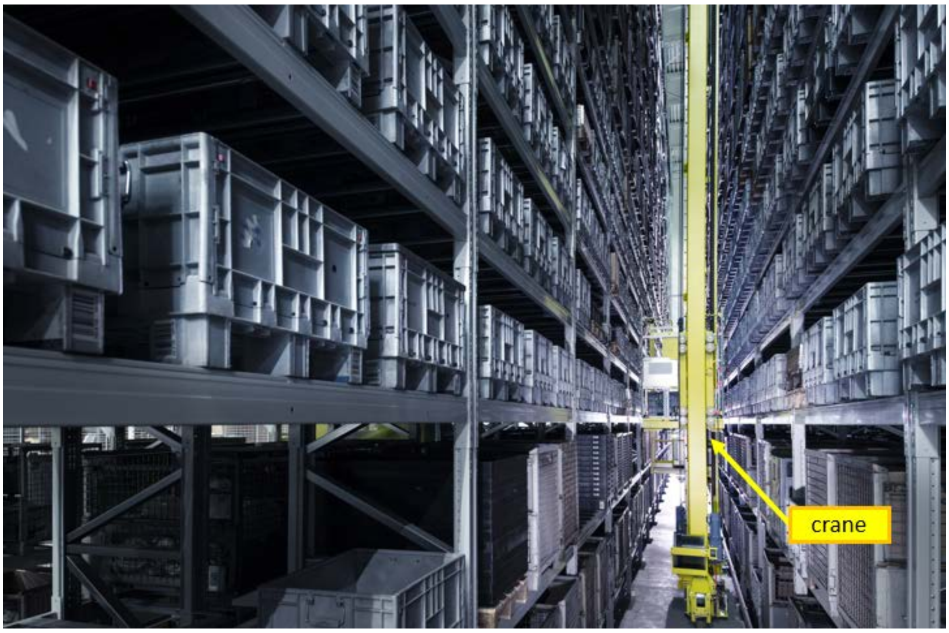

Figure 2.7: Example of a mini-load automated racking system (photo courtesy of Nedcon B.V.).

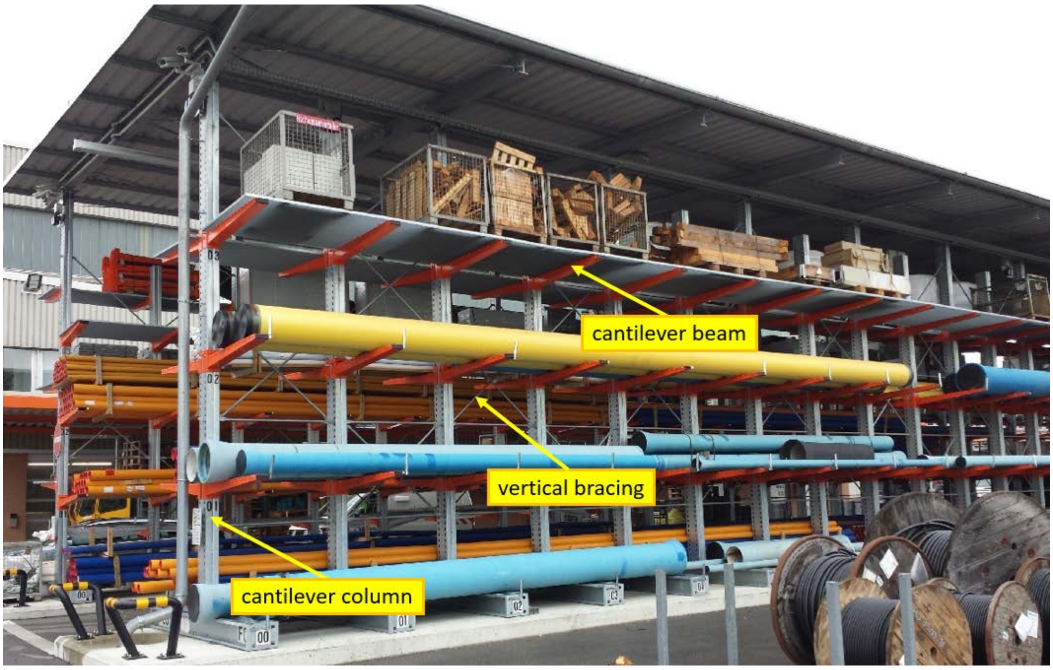

Figure 2.8: Example of a heavy-duty cantilever rack (photo courtesy of Modulblok).

A popular solution for domestic applications, libraries and superstores/markets open to the public is the light-duty hand-loaded shelving rack (Figure 2.9). It is used to store light-weight products on small boxes, trays or containers using hand-picking methods. The shelves that carry the unit-loads can be directly connected to the uprights by means of bolts and clips, or supported on beams (Bernuzzi et al., 2016a). Lateral stability in the down-aisle direction is provided by the semi-rigid moment connection between the beam-like edges of the shelf sheeting or by actual beams supporting said sheeting, if they are present. In the cross-aisle direction, one may employ (i) a bracing system forming lighter versions of the APR upright frames, (ii) a light moment-frame based on beam-like lacing members (Figure 2.10 left), or (iii) a combination of the two (Figure 2.10 right). Despite being low-rise structures carrying light goods, an abrupt collapse of a shelving rack might lead to loss of human life, apart from the economic impact due to damage on the stored wares.

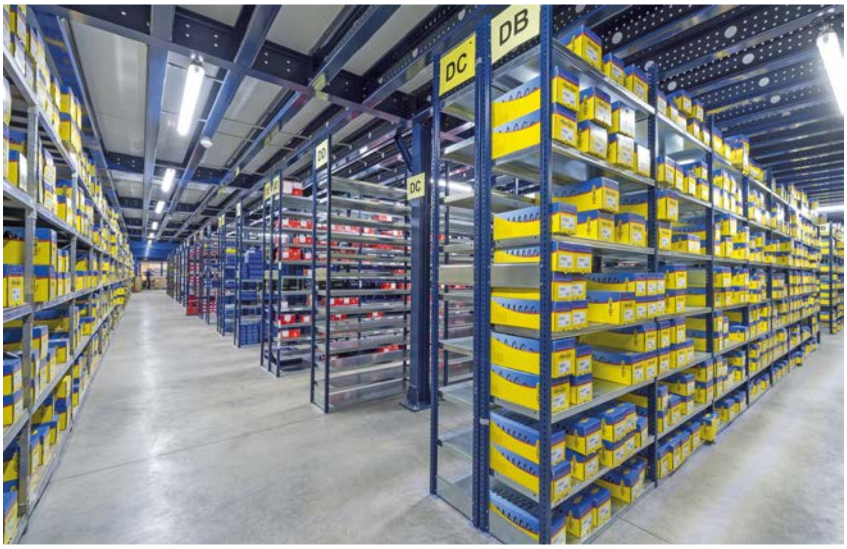

Figure 2.9: Example of a light-duty shelving rack (photo courtesy of MECALUX S.A.).

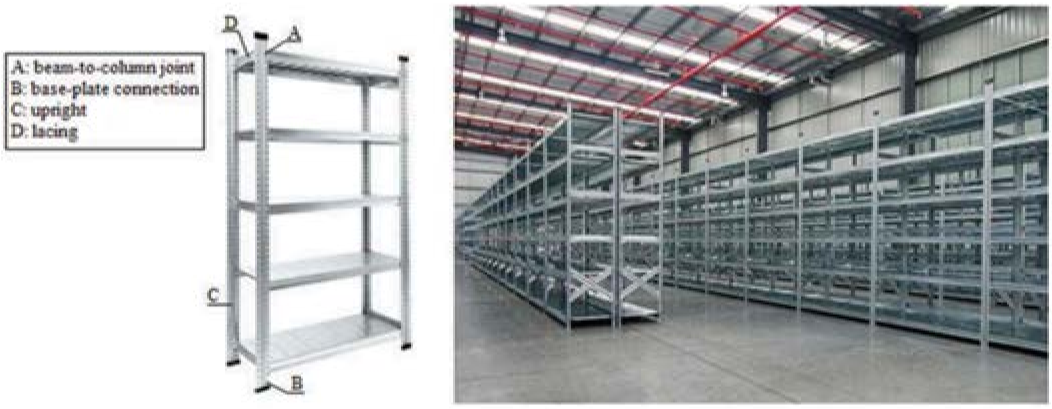

Figure 2.10: Typical shelving rack and key components (adopted from Bernuzzi et al., 2016a).

Finally, two niche rack typologies are the mobile and gravity flow racking systems. A mobile system comprises a series of independent APR or cantilever racks, without static aisles to separate them; instead, they are motorized and, guided by rails, they may move along the cross-aisle direction to open up an aisle where needed, (Figure 2.11). Thus, mobile systems maximize the exploitation of the available footprint as the individual racks move to create the only required aisle for withdrawal and retrieval. Gravity flow racking systems are structurally similar to the well-known APRs but employ a different logistic workflow: By sliding units along inclined rails (or surfaces), they take advantage of gravity to load, organize and retrieve. From a logistics point of view, gravity flow racks can be broken down to three sub-categories: The push-back (Figure 2.12), pallet-flow and carton-flow racking system.

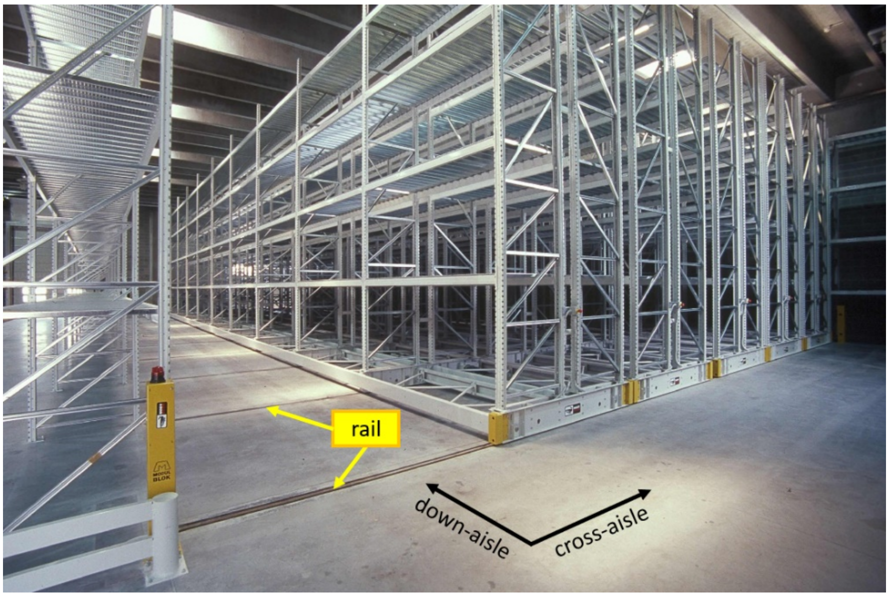

Figure 2.11: Example of a mobile racking system (photo courtesy of Modulblok).

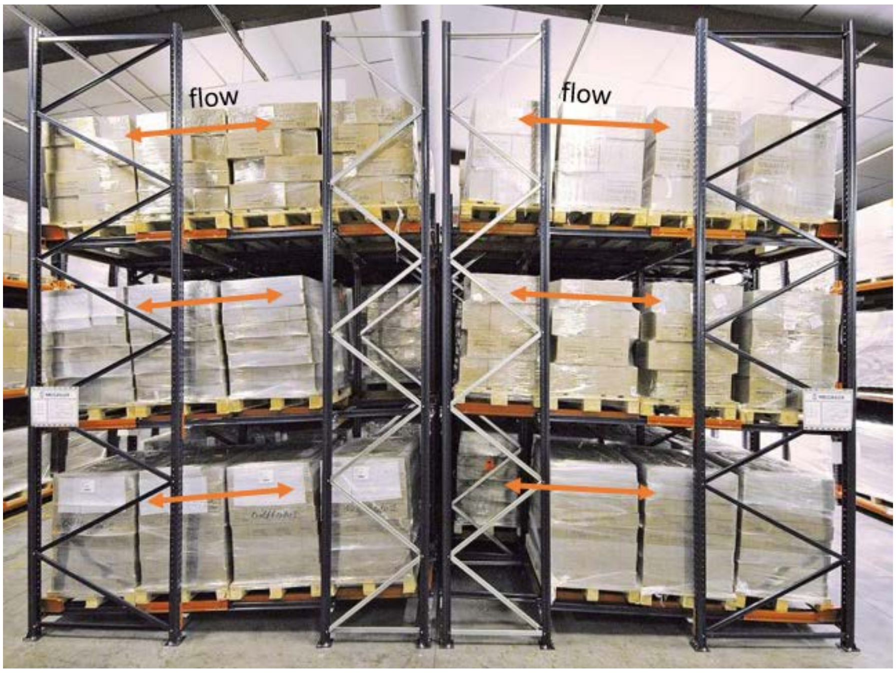

Figure 2.12: Example of a push-back gravity flow racking system (photo courtesy of MECALUX S.A.).

2.3 Seismic behaviour and design of racks

The design of steel racking systems is always accompanied by experimental tests, as they comprise thin-walled perforated members with semi-rigid connections whose actual strength and stiffness cannot be accurately calculated by analysis. The compression strength of the uprights is negatively influenced by the presence of holes and thus, lateral torsional buckling of the section is typically the dominant failure mode (Vayas et al., 2019). However, depending on the thickness-to-braced-length ratio, distortional buckling may also prevail, which can be identified either by means of experimental tests on full-scale upright frames or by numerical analyses (Elias et al., 2018; Miranda et al., 2018). In the cross-aisle direction, the shear stiffness of the upright frame is degraded by the axial deformation of the braces and their ends, as well as the slipping and bending of the bolts (Talebian et al., 2018). Structural engineers take this phenomenon into account in a conventional beam element model by applying a reduction, of the order of 95%, to the brace cross-sectional area according to shear tests on individual upright frames. Experimental calibration is also needed for the beam-to-column rack joints in order to determine the moment-rotation curve of the connection, whose hysteretic response is characterized by slippage, pinching and stiffness-degrading behaviour (Bernuzzi and Simoncelli, 2016b).

While the aforementioned local component tests are applicable to all types of racking systems, at the system level the focus of existing literature has been on the APR systems and for a good reason, as they comprise the most frequently used rack typology. Moreover, the logic of upright frames in the cross-aisle direction and MRFs in the down-aisle direction is also adopted in other systems, like the double- and multi-depth ARSWs. As a result, design codes are available almost solely for the adjustable racks and it is the designer’s responsibility to extend them to other systems. For instance, in USA, APRs are presently designed according to the Rack Manufacturer Institute (RMI) specification (2012), in Europe per EN 15512 (2009), while in Australia the AS 4084 (2012) standard is used.

Analysis and design become even more complicated when a storage rack is used in seismic areas where the structures have to withstand additional horizontal seismic forces. In most cases, the codes applicable to conventional buildings were employed, e.g., EN 1998-1 (2004) in Europe. Still, these are typically not sufficient to cover the seismic design of racking systems, thus additional provisions emerged. For example, the Federation Européenne De La Manutention (FEM) guideline 10.2.08 (2011) extended the provisions of Eurocode 8 with the introduction of additional elements specifically applicable to racks and governed the seismic design of racking systems in Europe from 2008 to 2016, until the introduction of EN 16681 (2016), which is now the de facto European seismic code for racking systems. In USA, RMI (2012) covers both seismic and non-seismic aspects.

Research done so far has demonstrated that typical APR systems offer limited ductility, which is reflected in the design codes by the adoption of low behaviour (or strength reduction) factors (e.g., 1.5 and 2.0 in the cross- and the down-aisle direction, respectively (EN 16681, 2016). In the cross-aisle direction, the horizontal seismic loads are balanced by a set of axial forces acting on the uprights, which are optimized to the maximum, leading to buckling failure modes before the bracing system enters the nonlinear range. Even if the uprights were capacity designed, special connection detailing would be mandatory for the braces in order to prevent bolt or bearing failure, a capacity check adopted in conventional steel buildings but seldomly in racks.

In the down-aisle direction, the flexible MRF relies on the hysteretic behaviour of the hooked beam-to-column joint to absorb plastic deformations (or dissipate energy in Eurocode parlance). Yin et al. (2016) conducted several monotonic and cyclic loading tests on beam-to-column connections and found that by introducing additional bolts and welds, the hysteretic response of the joint can be improved in terms of stiffness degradation and deformability. However, in high seismicity areas, the weak MRF is not always capable of resisting the increased horizontal forces and the contribution of the second-order effects becomes crucial. To alleviate this issue, designers typically install a vertical bracing system (Figure 2.13), also called spine bracing, that enhances the stiffness of the structure but not the ductility as the design codes do not mandate capacity design. Still, full-scale pushover tests (Castiglioni et al., 2014; Kanyilmaz et al., 2016a) demonstrated that higher behaviour factors can be achieved on braced racks by guaranteeing sufficient overstrength for the bracing connections to avoid a sudden brittle failure, such as bolt shear and bolt bending failures before brace yielding.

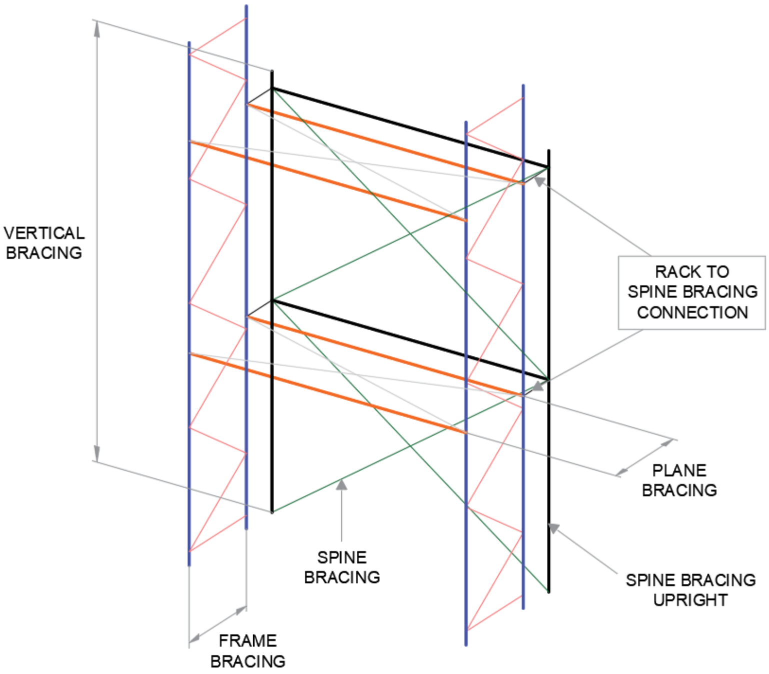

Figure 2.13: Spine bracing layout (adopted from FEM 10.2.08, 2011).

On the other hand, the design of drive-in racks in not well covered or documented in the literature. Gilbert et al. (2012; 2014) presented the structural behaviour of drive-in racks under static loading, in terms of experimental and analytical results. It was shown that the friction between pallet bases and rail beams provides additional horizontal bracing restraints on the system, however this contribution is relatively low in the overall design of the rack. Still, the work done focused on static loading conditions. A recent work by Shaheen and Rasmussen (2019) shed some light to the dynamic response of the drive-in racks along the cross-aisle direction by means of shaking table tests, concluding that the upright-to-diagonal connections experience severe local damage that led to brittle type of failures. For practical applications, the European Racking Federation design guideline FEM 10.2.07 (2012), which is perhaps the only widely available guideline specialized to drive-in racks, does not offer a seismic design procedure. If one extrapolates from APR system guidelines, a behaviour factor equal to 2.0 might seem appropriate in down-aisle direction but it is unclear whether this assumption is safe given that relevant research is lacking and there is higher flexibility in drive-in systems relative to APRs that may lead to earlier-than-expected failures.

Finally, there are racking systems whose structural behaviour is yet to be examined in detail, as research has not yet caught up to the rapid developments in racking technology. Some of these systems have many similarities with the well-known adjustable racks, with only some particular aspects remaining as a grey area. For instance, the recently introduced pallet shuttle system (Figure 2.4) resembles an APR but it also comprises horizontal grids of pallet and rail beams at each load level that can provide some beneficial diaphragm stiffness, which may or may not be accounted for in design, and may or may not act as additional overstrength in assessment. On the other hand, there are many widely used non-APR-like systems for which little experimental and analytical research is available, and design guides are either totally absent, or they only exist for non-seismic conditions (e.g., FEM 10.2.09 (2013) and FEM 10.2.06 (2012) for the cantilever (Figure 2.8) and shelving racks (Figure 2.10), respectively). Another example are the massive ARSWs (Figure 2.5 and Figure 2.6); such systems cannot always be treated as “very tall” APRs, among other reasons due to their high importance, the effect of pallet load distribution and automated pallet sorting algorithms, the high degree of optimization to minimize costs, and the subsequent razor-thin overstrength margins.

2.4 Proposed taxonomy

The sole purpose of a rack taxonomy is to describe and classify racks in a uniform manner as a key step towards assessing their risk to various hazards, such as seismic or extreme wind phenomena. While many taxonomies exist worldwide, such as the GEM (Brzev et al., 2013), EERI and IAEE World Housing Encyclopedia (Brzev and Greene, 2004), PAGER-STR (Jaiswal and Wald, 2008; USGS & WHE, 2008) and HAZUS (FEMA, 2003) taxonomy, they mainly target conventional buildings. For example, the Building Taxonomy adopted by the GEM Foundation comprises eight basic “Attributes” (or classes per other taxonomic systems) required to broadly characterize any building: (i) material of the lateral load resisting system, (ii) lateral load-resisting system (iii) roof, (iv) floor, (v) height, (vi) date of construction, (vii) structural irregularity, and (viii) occupancy. Each “Attribute” may be further broken down to several “Attribute Levels” delineating, e.g., the different available materials or types of lateral load-resisting systems, and then further discretized to several “Options” (or groups). Other proposed taxonomies may follow somewhat different terminology but overall similar patterns. Clearly, some customization for racks is in order. Herein five basic attributes are chosen to characterize racking systems: (i) structural typology, (ii) placement and cladding, (iii) height, (iv) storage system and (v) design code level, as illustrated in Table 2.1 and discussed in detail in the following sections.

Table 2.1: Proposed Rack taxonomy following the GEM breakdown to Attributes/Attribute-Levels/Options.

TaxT Attribute Group	**#**	**Attribute**	**Atrribute-Levels**	**Options**	
				Description	**ID**
Structural System	1	Structural typology	Gravity load-resisting system	Uprights+beams Uprights+rails Cantilever	GUB GUR GC
			Down-aisle lateral load-resisting system	Moment resisting frame Spine bracing Bracing tower	LMRF LSB LBT
			Steel type	Cold-formed Hot-rolled Mixed	CFS HRS MS
	2	Placement and cladding	Placement and cladding	Indoor racks Outdoor racks Clad-supporting racks	IDR ODR CLD
Rack Information	3	Height	Height	Low-rise [<8m] Medium-rise [8-12m] High-rise [12-20m] Very high-rise [>20m]	HL HM HH HVH
	4	Storage system	Unit load weight	Low [<200kg] Medium [200-1000kg] High [1000-2000kg]	WL WM WH
			Contact surface	Wood+Steel Plastic+Steel Steel+Steel Hanging goods	SURWS SURPS SURSS SURHG
			Material/goods handling	Manual Semi-automated Fully-automated	MA SA FA
	5	Design code level	Design code level	No-Code [Pre 1990 EU Pre 1976 USA] Mid-Code [1990-2008 EU 1976-1997 USA] High-Code [Post 2008 EU Post 1997 USA]	NC MC HC

2.4.1 Structural typology

The first Attribute, the structural typology, defines the racking system as a civil engineering structure that resists external loads and excitations. It is broken down to three Attribute-Levels that describe the gravity and lateral load-resisting systems, and the type of steel used for both. The gravity load-resisting system (GLRS) Attribute-Level, self-evidently describes the load path followed to transfer the gravity loads of the goods to the foundation. Three different Options are proposed, namely “uprights+beams”, “uprights+rails”, and “cantilever”. The majority of rack typologies belong to the “uprights+beams” group, meaning that the goods are carried by pallet beams semi-rigidly connected to the uprights (e.g., APR, pallet shuttle, ARSW, see Figure 2.14(a)). On the other hand, racks with no beams along the down-aisle direction belong to the “uprights+rails” group (e.g., drive-in, drive-through), where the goods are carried by continuous pallet rails that connect the individual upright frames along the cross-aisle direction (Figure 2.14(b)). Finally, the “cantilever” Option uses cantilever beams that are moment-connected to the uprights to accommodate the long products (Figure 2.14(c)).

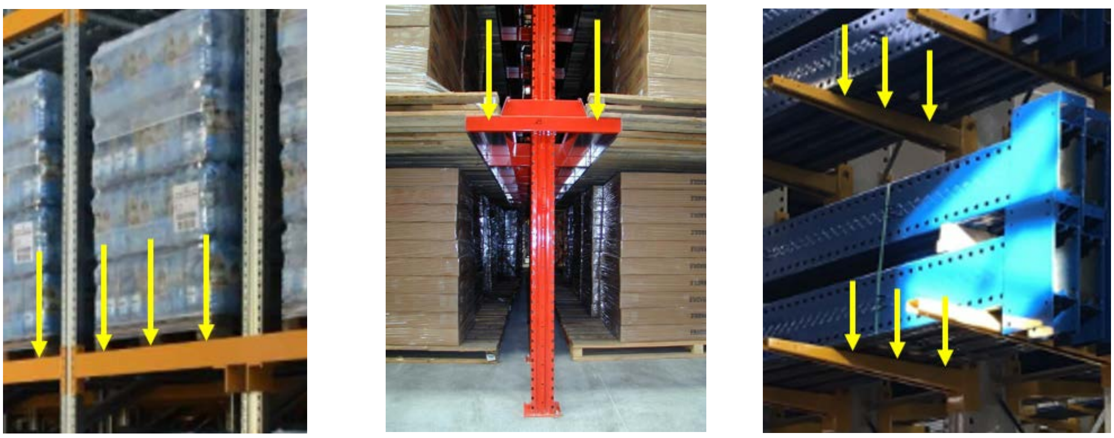
(a) (b) (c)

Figure 2.14: The GLRS Attribute-Level of the structural typology Attribute comprises three Options: (a) “uprights+beams”, (b) “uprights+rails” and (c) “cantilever”.

The second Attribute-Level is the lateral load-resisting system (LLRS) in the down-aisle direction, currently comprising the Options of MRF, spine bracing and bracing tower (Figure 2.15). It can be extended in the future to contain more load-bearing systems (e.g., base isolation, Simoncelli et al., 2020) as they evolve. In the cross-aisle direction no distinction was made, as the structural scheme always comprises upright frames, with the number of connected frames being the only variable. The only potential exception is the cantilever system, where the GLRS also fully describes the cross-aisle LLRS (which is simply that of a cantilevered upright), thus no further delineation is needed. Further extending the Attribute-Levels to consider the number of upright frames in the cross-aisle direction is a possibility, as for example note that the American codes (RMI, 2012) do consider the positive effect of multiple upright frames connected (e.g., in the pallet shuttle or the drive-in racks) by a so-called “redundancy factor”, assuming that a stress redistribution is possible when the most critical structural member fails. However, research so far has demonstrated that, especially in the cross-aisle direction, racks fail due to brittle failure modes and thus, a local failure will probably initiate a sudden global collapse. Hence, in the interest of simplicity, this further discretization of cross-aisle LLRS has not been introduced.

Finally, one may consider the type of steel used, which can be cold-formed, hot-rolled or mixed, e.g., as in having the uprights of the bracing towers hot-rolled while the rest cold-formed. The use of hot-rolled sections might imply a capacity design framework per conventional building seismic design, but this is the prerogative of the designer and not necessitated by rack-specific guidelines. Thus, the distinction between cold-formed and hot-rolled rack profiles does not necessarily imply an improved performance of the latter, but it was considered for completeness.

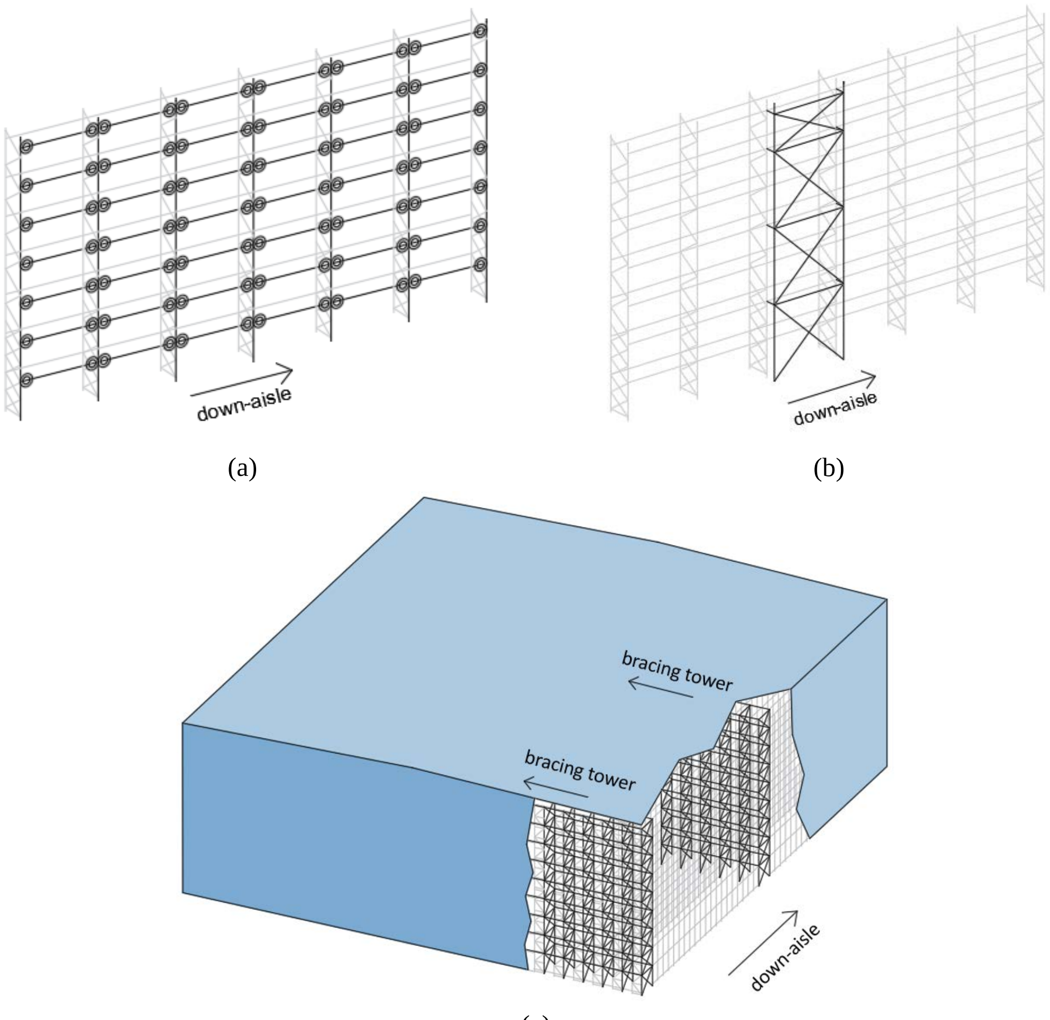

(a) (b)

(c)

Figure 2.15: The LLRS Attribute-Level of the structural typology Attribute comprises three Options: (a) MRF, (b) spine bracing and (c) bracing tower.

Two potential Attribute-Levels of the structural typology Attribute, not considered herein but may be added in the future, are related to the connection of the racking system with the ground. The first potential Attribute-Level is the type of foundation, which can be concrete slab, asphalt, tiles, suspended floors, etc. However, as the vast majority of racks are installed on concrete slabs, the classification according to the type of foundation was disregarded for reasons of simplicity. The second possible Attribute-Level is related to the behaviour of the base plates and the anchoring system. Indeed, the rotational stiffness and the hysteretic behaviour of the base plates can play a critical role on the seismic response of an unbraced rack along the down-aisle direction (Bernuzzi and Simoncelli, 2016b). They still comprise a structural component of the LLRS Attribute-Level, just like the beam-to-column joints or the spine braces. In this scope, as the APRs evolve to accommodate additional load levels with heavier unit loads, one could divide the MRF Option to weak-MRF and strong-MRF, indicating the use of flexible base plates and beam-to-column connections or not.

2.4.2 Placement and cladding

Placement and cladding, the second Attribute of the proposed rack taxonomy, comprises three Options, the indoor, outdoor, and clad-supporting racks. In terms of applicable natural hazards, while indoor racks (Figure 2.16(a)) are designed only for seismic actions, the other two groups are also exposed to wind and snow hazards. Outdoor racks share many structural characteristics (dimensions, sections, etc.) with indoor racks, however there is no external shell to protect them from the elements on all sides. Only a roof canopy may be installed at the top of the rack to partially shelter the stockpiled goods from rain and sun (Figure 2.16(b)).

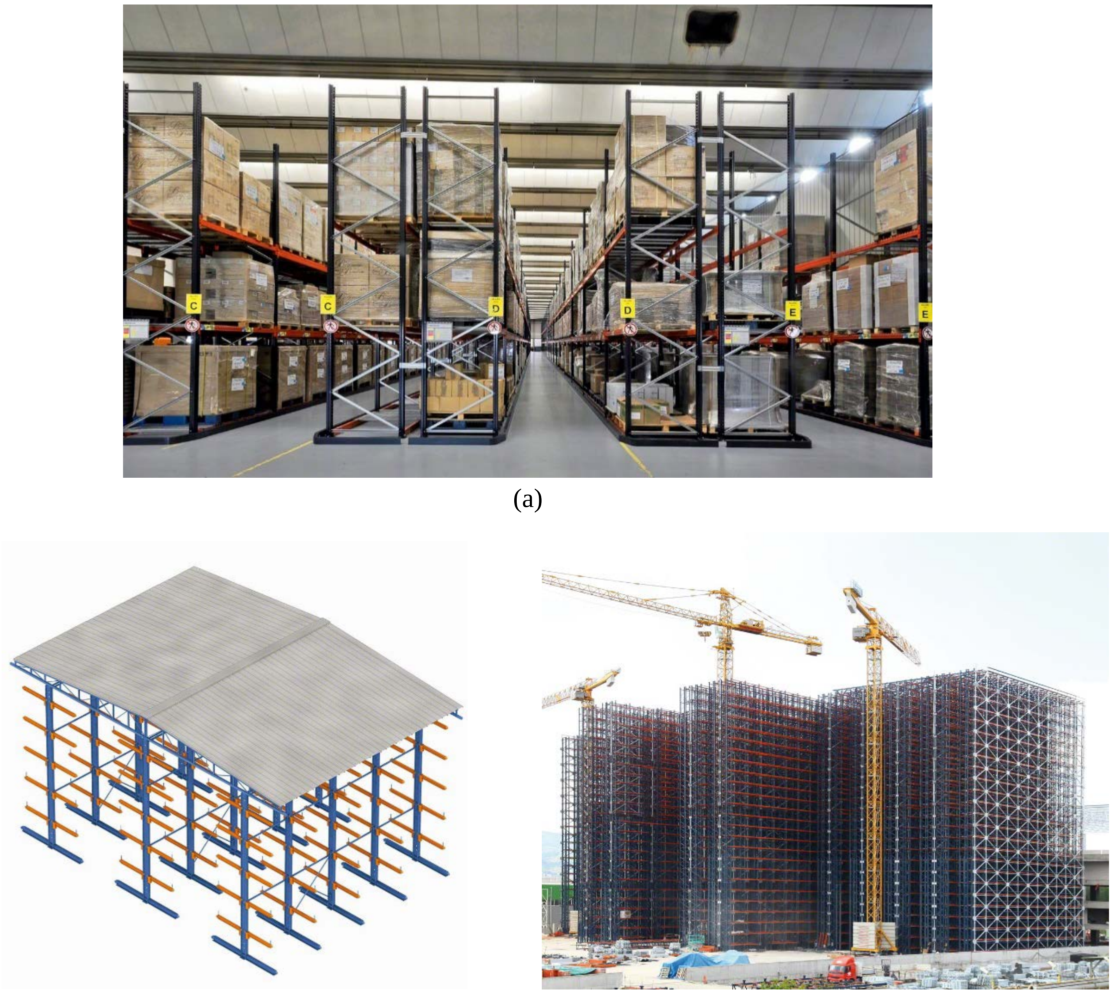
(a)

(b) (c)

Figure 2.16: The placement and cladding Attribute comprises three Options: (a) indoor, (b) outdoor and (c) clad-supporting racks (photos courtesy of MECALUX S.A.).

Clad-supporting racks (i.e., the rack supported warehouses (RSWs), Figure 2.16(c)) integrate the external envelope shell and the racking system into a compact structure. Typically, a shallow roof truss connects the upright frames in the cross-aisle direction, while horizontal bracing is employed to provide in-plane stiffness in the down-aisle direction. In general, the axially stiff roof truss can be expected to enforce equal displacements at the topmost level of the uprights in the cross-aisle direction, but a fully rigid diaphragm is not necessarily realized due to the limited horizontal bracing. RSWs are especially vulnerable to wind during the erection phase, where the lateral load resisting system (typically bracing towers) has not been fully installed.

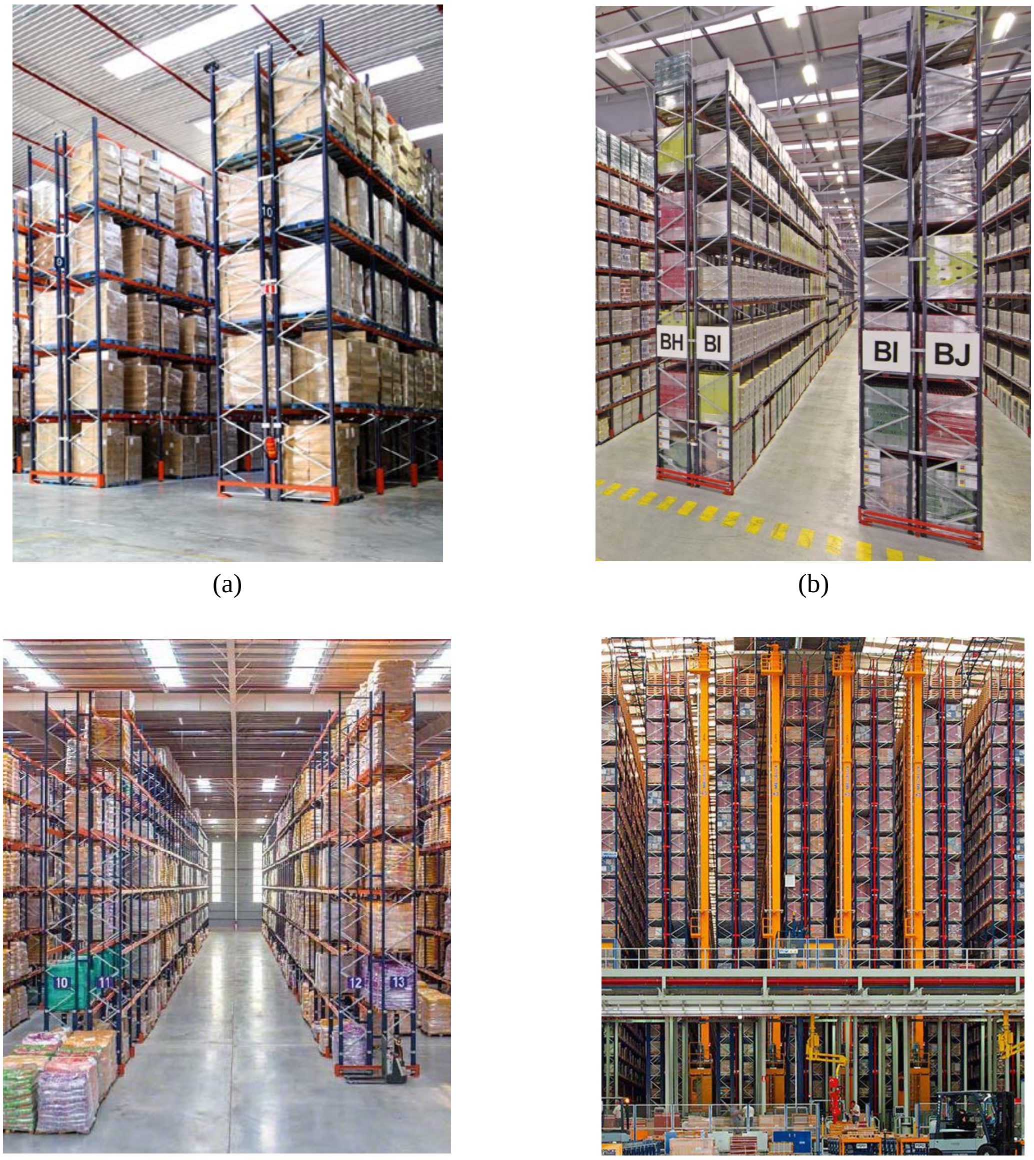

(a) (b)

(c) (d)

Figure 2.17: The height Attribute comprises four Options: (a) low-, (b) medium- (c) high- and (d) very high-rise racks (photos courtesy of MECALUX S.A.).

2.4.3 Height

The height of the racking system is adopted as the third Attribute. While for conventional buildings, the number of stories is often used as a proxy for height, the number of loading levels is not equally useful: The height of the load levels varies significantly among different warehouses, and even within the same structure, to serve different logistic demands. Conventionally, increased structural height is connected with augmented effects of higher modes, P-Δ, and of course larger member sections. Specifically for racks, increased height also acts as a multiplier on the consequences of goods falling off due to lateral displacement of the rack, increasing the impact energy as well as the probability of landing on an adjacent rack, thus becoming a source of damage spreading and potential progressive collapse.

Four Options were considered, which may not necessarily indicate a sharp difference in structural behaviour, but certainly correspond to different levels of engineering requirements: low-rise racks (below 8 meters), medium-rise (8 to 12 meters), high-rise (12 to 20 meters) and finally very high-rise (above 20 meters), as illustrated in Figure 2.17. The low-rise threshold may be chosen to be lower, at 6 meters, where it would mainly comprise shelving racks and few APR and drive-in systems. By increasing the value to 8 meters, the low-rise group becomes the most populated among the four, as it includes a large percentage of APR systems world-wide. However, APR systems tend to increase in height to better exploit the available footprint and it will not be surprising if the medium-rise becomes the "typical" group in a few years.

2.4.4 Storage system

The fourth Attribute is related to the functionality of a rack, the so-called storage system. It consists of three Attribute-Levels, namely the weight of the unit load, the contact surface and the handling system.

Regarding the first Attribute-Level, one may consider the number of unit loads per compartment instead of the weight of the unit load. Still, this can become ambiguous for the case of multi-depth racking systems (e.g., a pallet shuttle racking system with 6 upright frames and 14 pallet positions along the cross-aisle direction). Another rational choice would have been adopting the average weight of goods per square meter of load level, but racking technology seldomly uses this term, leading to ambiguity in subsequent discussions with professionals, leaving unit load weight as the best and most familiar concept.

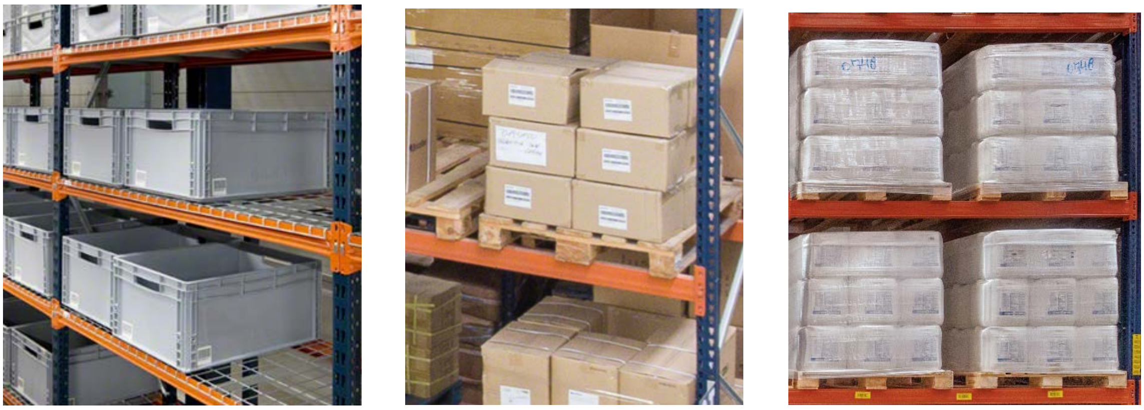

(a) (b) (c)

Figure 2.18: The weight of the unit load Attribute-Level of the storage system Attribute consists of three Options: (a) low-, (b) medium- and (c) high-weight (photos courtesy of MECALUX S.A.).

Three Options are proposed for the weight of the unit load: Low-weight (below 200 kg), medium-weight (200 to 1000 kg) and high-weight (1000 to 2000 kg), as illustrated in Figure 2.18. Unit loads heavier than 2000 kg are seldomly used as they demand special analysis and rack typology. The low-weight is the only Option related with hand-picking methods while in the medium- and high-weight groups the goods are usually palletized and require mechanical methods for their handling.

Unit loads can be stored using pallets, containers, boxes, trays or even be hung, with the pallets frequently related with heavier products. The engineering significance of such a variety of different storing methods can be summarized in terms of the “contact surface” between the goods and the rack as the second Attribute-Level. Goods may rest on top of beams/rails, or hung from them. In both cases, the apparent inertia of the rack is typically reduced during seismic excitations due to pendulum effects, for hanging goods, or sliding of goods-on-steel. Still, in the latter case, a low friction constant may lead to displacements of such magnitude that the products fall off and damage the adjacent racks, thus some differentiation of the materials in contact is required.

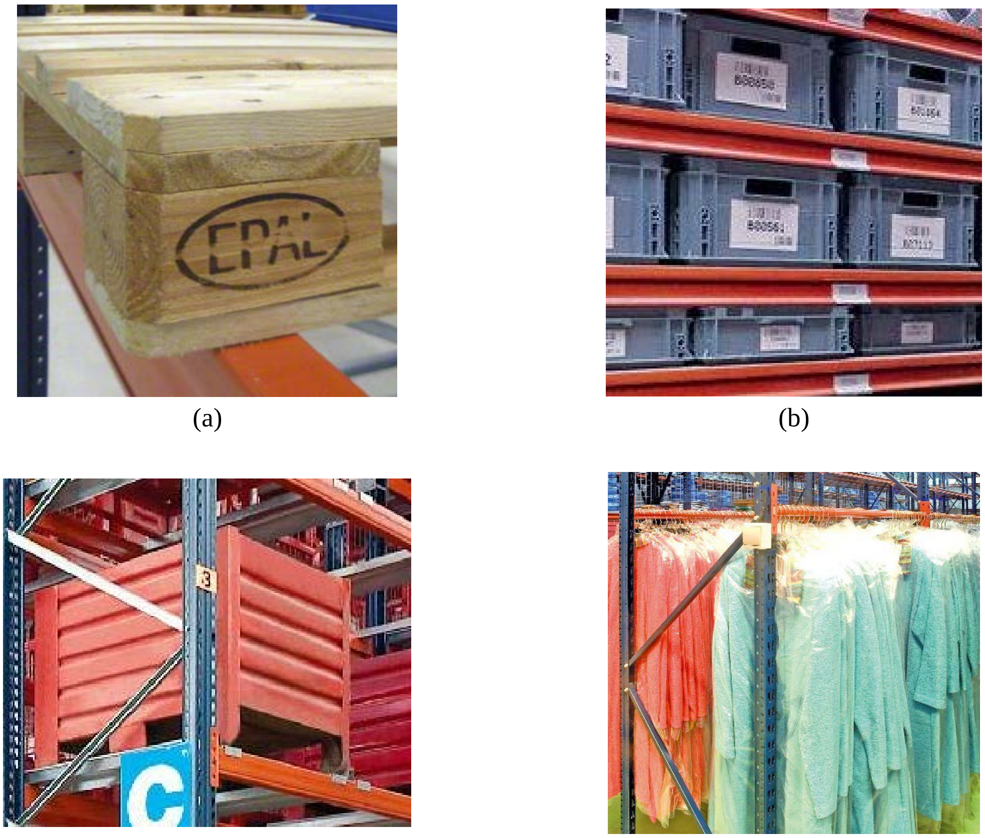

(a) (b)
(c) (d)

Figure 2.19: The contact surface Attribute-Level of the storage system Attribute consists of four Options: (a) wood+steel, (b) plastic+steel, (c) steel+steel and (d) hanging goods (photos courtesy of MECALUX S.A.).

Herein four Options are chosen, namely the “wood+steel”, “plastic+steel”, “steel+steel” and the “hanging goods”, as illustrated in Figure 2.19. The majority of racking systems fall into the “wood+steel” group, whereby wooden pallets are placed on steel beams. EN 16681 (2016) gives high reference values of the friction constant for the “wood+steel” group

($\mu = 0.37$) and lower for the “plastic+steel” and “steel+steel” group ($\mu = 0.15$). For the “hanging goods” little experimental or analytical data is available, however the inertia forces are relatively low in this kind of racking systems as they mainly store clothing products. Finally, there are cases that do not fall into any of the four Options (i.e., the cheese units in Figure 1.3(b)), but they are the exception, rather than the rule.

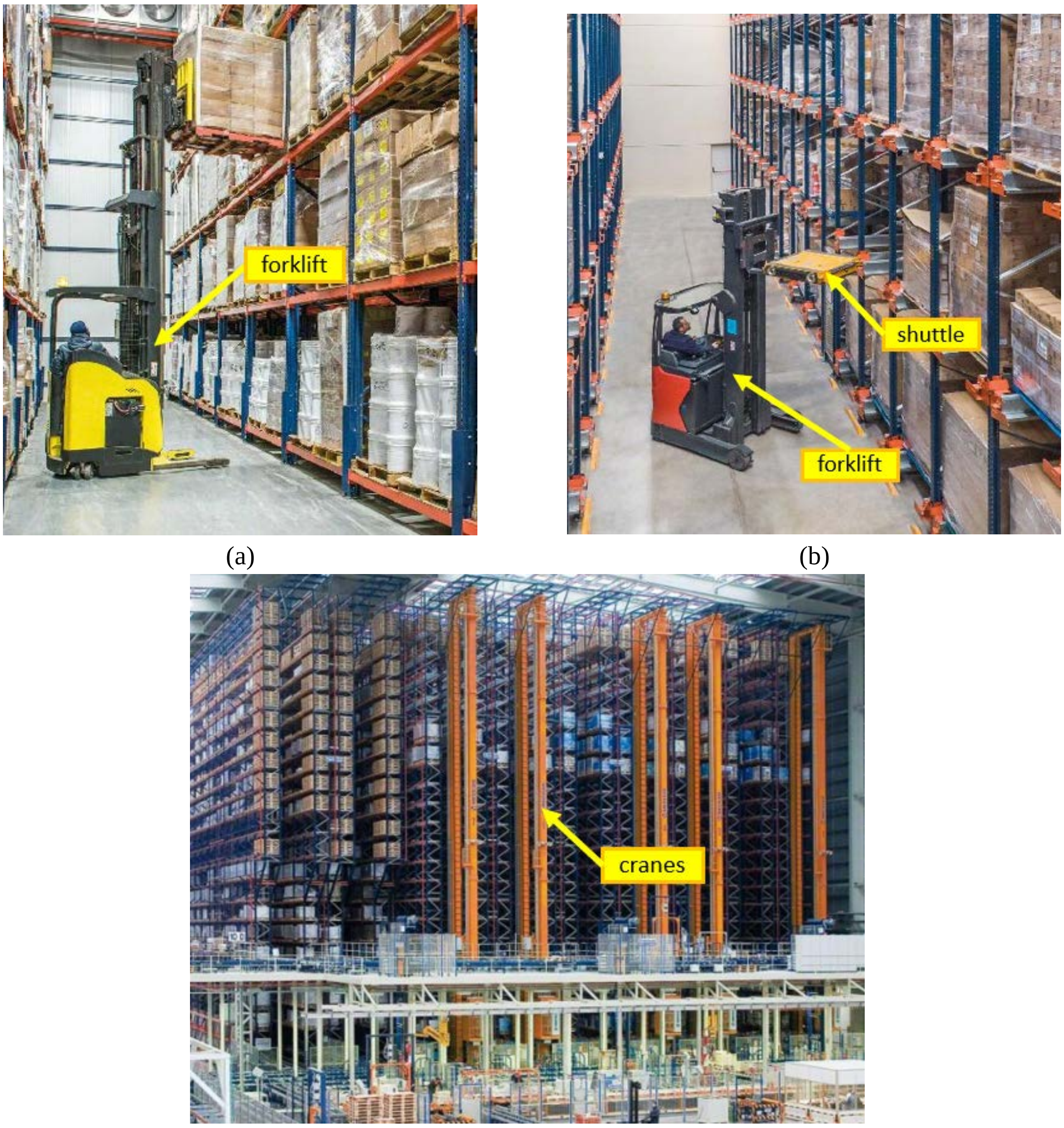

(a) (b)

(c)

Figure 2.20: Material/goods handling Attribute-Level of the storage system Attribute consists of three Options: (a) manual, (b) semi-automated, and (c) fully-automated (photos courtesy of MECALUX S.A.).

The third Attribute-Level is related to the handling system of the goods, consisting of three Options (Figure 2.20): Manual (forklift trucks or hand-picking), semi-automated (shuttles+forklift trucks) and fully-automated (shuttles+cranes). In the fully-automated systems, such as the ARSWs, there is no need for human intervention in the handling process, which minimizes the risk for human losses during an earthquake. However, as the goods are now handled only via robotic means with specific tolerances, it is often the case that after an earthquake event the shuttles will not be able to target correctly the pallets, as they have been displaced. In fact, repositioning of the pallets within system tolerances is a labor-intensive process, as a special team of workers has to climb inside the warehouse and adjust the position of all the goods, a procedure that may take weeks, or even a month, leading to the complete shut-down of the warehouse.

2.4.5 Design code level

Probably the most critical Attribute for the seismic assessment of steel racks, and civil engineering structures in general, is the design code level, which is closely correlated with the date of construction or retrofit. One may choose to maintain both pieces of information in the taxonomy as converting one to the other is not always straightforward. Herein, we shall attempt to provide a mapping of age to the seismic code, at least in EU and USA. Adding a separate "Date of construction or retrofit" Attribute can be easily done if needed as in GEM 3.1 Building Taxonomy. In general, seismic vulnerability is expected to increase with age, a universal trend that reflects the improvement of design and detailing standards for practically all countries, as well as due to the general upwards trend of design spectra. Specifically for racks, there are additional compounding reasons aggravating this phenomenon. First is the lack of knowledge; in contrast to the residential steel buildings, steel racks have only lately received the attention of the scientific community and standardization bodies. This is reflected in the delayed appearance of specialized seismic design codes for racks, in comparison to conventional buildings. For example, in USA, some of the earliest seismic design requirements for racks appeared circa 1974 (see Chen et al. (1980) for a detailed review), while for Europe the first draft of FEM 10.2.08 (2011) was published in 2003 and introduced in practice in 2008. Secondly, seismic design was/is not mandatory for racks in many countries, as they were/are considered as contents or equipment rather than civil engineering structures. For racks designed before the introduction of rack-specific codes, this led to a wide dispersion in the actually applied design standards, from cases where only gravity loads were employed for the design, up to some structures that received a full seismic design similar to conventional buildings. In fact, there remain many countries today where non-seismic-resistant indoor/outdoor racks (but not RSWs) may still be designed, and they are the standard go-to option to minimize the cost of the storage facility. Still, awareness of the seismic issues is spreading, leading to improved designs even where they are not mandated, especially in cases where the direct cost of the stored goods or the indirect cost of service disruption is far greater than the cost of the rack itself.

A comprehensive classification of racks according to their design code level is thus country-specific and largely depends on local design/construction practices and the date of actual code adoption, rather than the date of publication. Furthermore, most if not all guidelines concern APR systems, leaving some wide space for interpretation regarding other rack typologies. As an initial attempt, we propose classifying the racks into three groups with indicative cut-off dates of 1990 & 2008 for Europe and 1976 & 1997 for USA. Those constructed before the first cut-off date belong to the "no-code" group, meaning that the vast majority was not designed for seismic loads. The second group structures, namely "mid-code" racks, were built between the two cut-off dates (i.e., 1990-2008 for Europe and 1976-1997 for USA) using seismic design codes mostly meant for (or derived from) conventional steel structures, such as EN 1998 (2004), UBC (1997), or other relevant national codes. In general, for European racks this means that relatively high behaviour factors (e.g., 3.0 or greater) may have been employed, as recommended for conventional steel buildings, but without necessarily accounting for capacity design to ensure a ductile failure mechanism. For USA, the situation is more fragmented, as fairly conservative rules were employed early on, which were later relaxed (Chen et al., 1980), while at the same time subjected to changes in the design spectra. The third group comprises racks designed after 2008 for Europe, a milestone signifying the adoption of FEM 10.2.08 (2011) by EU industry, and post 1997 for USA, thanks to the introduction of updated RMI (2012) standards. Those "high-code" racks typically adopt low behaviour factors, at least compared to those of (superficially) similar conventional structures. For example, q = 1.5 to 2.0 is mandated for racks in EU (EN 16681, 2016), compared to 4.0 for buildings with concentric-braced frames and up to 6.5 for high-ductility moment-resisting frames per EN 1998-1 (2004). A direct comparison with USA practice is not necessarily informative due to other differences in the design process, but RMI (2012) considers R = 4 for braced directions of racks and up to R = 6 for high-ductility unbraced ones, compared to R = 6 for special concentric braced frames and R = 8 for special moment-resisting frames per ASCE7-16 (2017). Still, the improvement in performance is only due to this increased overstrength, as connections and members remain largely non-ductile.

2.4.6 Available literature per proposed taxonomy

To help populate and further substantiate the proposed taxonomy, we hereby classify several analytical and experimental publications that focus on the response of racking systems subjected to lateral loads according to the categorization of the racking structures studied. As we are interested in the characterization of racks from a global point of view, studies that investigated solely the behaviour of individual components, like the beam-to-column joint, were disregarded. The results appear in Table 2.2, showing the citation as well as the Attribute-Levels of each studied structure. Only the “Design code level” property is excluded, as design code is hard to determine for most case studies. In most cases, given the post-2006 date of publication and the general focus on improving design, it can be safely assumed that mid/high-code racks were studied.

Clearly, the majority of case studies comprised cold-formed, low-rise, indoor racks carrying medium-weight unit loads placed on pallets that are manually handled by forklift trucks; in essence, the literature so far has focused on the low-rise APR systems. On the other hand, the semi- and fully-automated systems, like the multi-depth pallet shuttle racks or the high-rise ARSWs have not yet received enough academic attention, despite being very popular systems in the market. Finally, only 2 out of 17 publications examined racks with bracing towers as the down-aisle LLRS, showing a reliance on data available for similar building-style LLRS, but potentially also a lack of knowledge for their idiosyncrasies when applied in the racking industry.

Table 2.2: Indicative publications related to the seismic performance of racks, categorized according to the proposed taxonomy.

Authors	Rack typology	GLRS	Down-aisle LLRS	Steel type	Placement and Cladding	Height (m)	UL weight (kg)	Contact surface	Goods handling
Kondratenko et al. (2022)	ARSW	Uprights+Beams	Bracing Tower	Mixed	Clad-supp.	VH[4] (22.0)	M (600-1000)	Wood+Steel	Fully-Autom.
Tsarpalis et al. (2021)	ARSW	Uprights+Beams	Bracing Tower	Mixed	Clad-supp.	VH (22.0-30.0)	M (600-1000)	Wood+Steel	Fully-Autom.
Caprili et al. (2018)	ARSW	Uprights+Beams	Spine Bracing	Mixed	Clad-supp.	VH (30.0)	M (1000)	Wood+Steel	Fully-Autom.
Franco et al. (2015)	Cantlilever	Cantilever	Spine Bracing	Cold-formed	Indoor	L[1] (7.0)	L (40)	Other	Manual
Shaheen et al. (2019)	Drive-in	Uprights+Rails	Spine Bracing	Cold-formed	Indoor	L (4.9)	N/A	Wood+Steel	Manual
Gilbert et al. (2012)	Drive-in	Uprights+Rails	Spine Bracing	Cold-formed	Indoor	L (5.0)	H (1200-2000)	Wood+Steel	Manual
Gabbianelli et al. (2020)	APR	Uprights+Beams	MRF	Cold-formed	Indoor	L (7.6)	M (295)	Wood+Steel	Manual
Bernuzzi et al. (2016b)	APR	Uprights+Beams	MRF	Cold-formed	Indoor	L (8.0)	M (800)	Wood+Steel	Manual
Gusella et al. (2018)	APR	Uprights+Beams	MRF	Cold-formed	Indoor	L (8.0)	M (800)	Wood+Steel	Manual
Filiatrault et al. (2006)	APR	Uprights+Beams	MRF	Cold-formed	Indoor	L (4.5)	M (500)	Wood+Steel	Manual
Kanyilmaz et al. (2016b)	APR	Uprights+Beams	MRF	Cold-formed	Indoor	M[2] (8.1-8.5)	M (800)	Wood+Steel	Manual
Maguire et al. (2020)	APR	Uprights+Beams	MRF	Cold-formed	Indoor	L (4.3)	M (800)	Wood+Steel	Manual
Yin et al. (2018)	APR	Uprights+Beams	Spine Bracing	Cold-formed	Indoor	H[3] (19.8)	M (450)	Wood+Steel	Manual
Avgerinou et al. (2019)	APR	Uprights+Beams	Spine Bracing	Cold-formed	Indoor	L (7.9)	M (800)	Wood+Steel	Manual
Kanyilmaz et al. (2016a)	APR	Uprights+Beams	Spine Bracing	Cold-formed	Indoor	L (8.0)	M (800)	Wood+Steel	Manual
Gabbianelli et al. (2020)	APR	Uprights+Beams	Spine Bracing	Cold-formed	Indoor	L (7.6)	M (295)	Wood+Steel	Manual
Bernuzzi et al. (2016a)	Shelving	Uprights+Beams	MRF	Cold-formed	Indoor	L (2.0)	L-M (100-300)	Steel+Steel	Manual

[1]L: Low, [2]M: Medium, [3]H: High, [4]VH: Very-high

2.5 Conclusions

A comprehensive review of the macro-characteristics of various racking typologies has been conducted in Chapter 2, focusing on their structural behaviour under lateral loading conditions. The proposed taxonomy follows the same terminology as the Building Taxonomy developed by the Global Earthquake Model, comprising five basic “Attributes” required to broadly characterize any racking system: (i) structural typology, (ii) placement and cladding, (iii) height, (iv) storage system and (v) design code level. Each “Attribute” is broken down to several “Attribute Levels” delineating, e.g., the different types of lateral load-resisting systems or handling methods, and then further discretized to several “Options” (or groups).

- In general, the vast majority of racks tend to conform to the low-rise APR type thus, for frugality, the taxonomy may be collapsed to examining archetypes of this type for no/mid/high code groups.
- Although the taxonomy is mainly developed for seismic conditions, it could also be adopted or modified for wind loads or other extreme hazards.
- It is designed to be extensible, meaning that it can easily accommodate new rack typologies and load-bearing mechanisms without changing the proposed five basic Attributes.
- It is user-friendly and intuitive, as the considered macro-characteristics can easily be identified by a non-expert, just by looking at pictures of the racking system.

2.6 References

AS 4084 (2012). *“Steel storage racking”*, Standard Australia.

ASCE 7-16 (2017). *“Minimum Design Loads and Associated Criteria for Buildings and Other Structures”*, American Society of Civil Engineers, Reston, Virginia.

Avgerinou S., Lignos X., Tsarpalis D., Vayas I. (2019). *“Full-scale tests on used steel storage racks.”*, Steel Construction Design and Research, **12**(3), 231-242. https://doi.org/10.1002/stco.201900009

Bernuzzi C., Gioia A., Gabbianelli G. (2016a). *“Pushover Analyses of Hand-Loaded Steel Storage Shelving Racks”*, Journal of Earthquake Engineering, **21**(8), 1256-1282. https://doi.org/10.1080/13632469.2016.1210063

Bernuzzi C., Simoncelli M. (2016b). *“An advanced design procedure for the safe use of steel storage pallet racks in seismic zones”*, Thin-Walled Structures, **109**, 73-87. https://doi.org/10.1016/j.tws.2016.09.010

Brzev S., Greene M. (2004). *“EERI World Housing Encyclopedia – Summary Publication”*, Earthquake Engineering Research Institute, 120 pp., Oakland, CA, USA.

Brzev S., Scawthorn C., Charleson A.W., Allen L., Greene M., Jaiswal K., and Silva V. (2013). *“GEM Building Taxonomy Version 2.0”*, GEM Technical Report 2013-02 V1.0.0, 188 pp., GEM Foundation, Pavia, Italy.

Caprili S., Morelli F., Salvatore W. Natali A. (2018). *"Design and Analysis of Automated Rack Supported Warehouses"*, The Open Civil Engineering Journal, **14**, 150-166. http://dx.doi.org/10.2174/1874149501812010150

Castiglioni C.A. et al. (2014). *"Seismic behavior of steel storage pallet racking systems (SEISRACKS2)"*, Final Report, RFSR-PR-03114, European Commission, DG Research, Brussels, Belgium.

Chen C.K., Scholl R.E., Blume J.A. (1980). *"Seismic Study of Industrial Steel Storage Racks"*, URS/John A. Blume & Associates, Engineers, San Francisco, California.

Cheng B., Wu Z. (2016). *"Simplified Method for Calculating the Laterial Stiffness of Drive-In Storage Racks"*, Practice Periodical on Structural Design and Construction, **21**(1). https://doi.org/10.1061/(ASCE)SC.1943-5576.0000266

Elias G.C., de Almeida Neiva L.H., Sarmanho A.M.C., Alves V.N., Barbosa e Castro A.F. (2018). *"Ultimate load of steel storage systems uprights"*, Engineering Structures, **170**, 53-62. https://doi.org/10.1016/j.engstruct.2018.05.078

EN 15512 (2009). *"Steel static storage systems - Adjustable pallet racking systems - Principles for structural design"*, European Committee for Standardization (CEN), Brussels, Belgium.

EN 16681 (2016). *"Steel static storage systems - Adjustable pallet racking systems - Principles for seismic design"*, European Committee for Standardization (CEN), Brussels, Belgium.

EN 1998-1 (2004). *"Eurocode 8: Design of structures for earthquake resistance - Part 1: General rules, seismic actions and rules for buildings"*, European Committee for Standardization, Brussels, Belgium.

FEM 10.2.06 (2012). *"The design of hand loaded low rise steel static shelving"*, FEM Racking & Shelving Product Group (European Racking Federation).

FEM 10.2.07 (2012). *"The design of drive-in and drive-through racking"*, FEM Racking & Shelving Product Group (European Racking Federation).

FEM 10.2.08 (2011). *"Recommendations for the design of static pallet racks in seismic conditions"*, FEM Racking & Shelving Product Group (European Racking Federation).

FEM 10.2.09 (2013). *"The design of cantilever racking"*, FEM Racking & Shelving Product Group (European Racking Federation).

FEMA (2003). *"HAZUS-MH MR4 Technical Manual"*, Federal Emergency Management Agency, Washington, D.C., USA.

Filiatrault A., Higgins P.S., Wanitkorkul A. (2006). *"Experimental Stiffness and Seismic Response of Pallet-Type Steel Storage Rack Connectors"*, Practice Periodical on Structural Design and Construction, **11**(3). https://doi.org/10.1061/(ASCE)1084-0680(2006)11:3(161)

Franco A., Massimiani S., Carfagni G.R. (2015). *"Passive Control of Steel Storage Racks for Parmigiano Reggiano Cheese under Seismic Accelerations"*, Journal of Earthquake Engineering, **19**(8), 1222-1259. https://doi.org/10.1080/13632469.2015.1049386

Gabbianelli G., Cavalieri F., Nascimbene R. (2020). *"Seismic vulnerability assessment of steel storage pallet racks"*, Ingegneria Sismica, **37**(2), 18-40.

GEM 3.1 Building Taxonomy (2021) repository: https://github.com/gem/gem_taxonomy

Gilbert B.P., Rasmussen K.J.R. (2012). *“Drive-in Steel Storage Racks I: Stiffness Tests and 3D Load-Transfer Mechanisms”*, Journal of Structural Engineering, **138**(2). https://doi.org/10.1061/(ASCE)ST.1943-541X.0000449

Gilbert B.P., Teh L.H., Badet R.X., Rasmussen K.J.R. (2014). *“Influence of pallets on behaviour and design of steel drive-in racks”*, Journal of Constructional Steel Research, **97**, 10-23. https://doi.org/10.1016/j.jcsr.2014.01.013

Gusella F., Orlando M., Spinelli P. (2018). *“Pinching in Steel Rack Joints: Numerical Modelling and Effects on Structural Response”*, International Journal of Steel Structures, **19**, 131-146. https://doi.org/10.1007/s13296-018-0095-x

Huang W., Zhou Z., Sun Q. (2012). *“Throughput Analysis of an Automated Warehouse with Pallet Shuttle”*, International Conference of Logistics Engineering and Management (ICLEM) 2010. https://doi.org/10.1061/41139(387)207

Jaiswal K.S., Wald D.J. (2008). *“Creating a Global Building Inventory for Earthquake Loss Assessment and Risk Management”*, U.S. Geological Survey Open-File Report 2008-1160, **103** pp.

Kanyilmaz A., Brambilla G., Chiarelli G.P., Castiglioni C.A. (2016a). *“Assessment of the seismic behaviour of braced steel storage racking systems by means of full-scale push over tests”*, Thin-Walled Structures, **107**, 138-156. https://doi.org/10.1016/j.tws.2016.06.004

Kanyilmaz A., Castiglioni C.A., Brambilla G., Chiarelli G.P. (2016b). *“Experimental assessment of the seismic behavior of unbraced steel storage pallet racks”*, Thin-Walled Structures, **108**, 391-405. https://doi.org/10.1016/j.tws.2016.09.001

Kondratenko A., Kanyilmaz A., Castiglioni C.A., Morelli F., Kohrangi M. (2022). *“Structural performance of automated multi-depth shuttle warehouses (AMSWs) under low-to-moderate seismic actions”*, Bulletin of Earthquake Engineering, **20**(2), 1247-1295. https://doi.org/10.1007/s10518-021-01193-y

Maguire J.R., Teh L.H., Clifton G.C., Tang Z.H., Lim J.B.P. (2020). *“Cross-aisle seismic performance of selective storage racks”*, Journal of Constructional Steel Research, **168**. https://doi.org/10.1016/j.jcsr.2020.105999

Miranda S., Melchionda D., Ungureanu V., Dubina D. (2018). *“A modified ECBL approach for cold-formed steel rack section members”*, Thin-Walled Structures, **130**, 47-56. https://doi.org/10.1016/j.tws.2018.05.012

RMI, ANSI MH16.1.12 (2012). *“Specification for the Design, Testing and Utilization for Industrial Steel Storage Racks”*, Rack Manufacturer’s Institute, Charlotte, NC.

Shaheen M.S.A., Rasmussen K.J.R. (2019). *“Seismic tests of drive-in steel storage racks in cross-aisle direction”*, Journal of Constructional Steel Research, **162**. https://doi.org/10.1016/j.jcsr.2019.105701

Simoncelli M., Tagliafierro B., Montuori R. (2020). *“Recent development on the seismic devices for steel storage structures”*, Thin-Walled Structures, **155**. https://doi.org/10.1016/j.tws.2020.106827

Talebian N., Benoit P.G., Baldassino N., Karampour H. (2018). *“Factors contributing to the transverse shear stiffness of bolted cold-formed steel storage rack upright frames with channel *bracing members”*, Thin-Walled Structures, **136**, 50-63. https://doi.org/10.1016/j.tws.2018.12.001

Tsarpalis D., Vamvatsikos D., Vayas I., Delladonna F. (2021). *“Simplified Modelling for the seismic Performance Assessment of Automated Rack-Supported Warehouses”*, Journal of Structural Engineering, **147**(11). https://doi.org/10.1061/(ASCE)ST.1943-541X.0003153

UBC (1997). *“Uniform Building Code”*, International Conference of Building Officials, Whitter, CA, USA.

USGS & WHE (2008). *“Listing of PAGER Construction Types and Comparison of Construction Types from Various Sources”*, A Joint Project of the USGS and the World Housing Encyclopedia (EERI).

Vayas I., Avgerinou S., Thanopoulos P. (2019). *“Failure of a steel pallet rack in Athens”*, Stahlbau, **87**(1), 30-37 (in German). https://doi.org/10.1002/stab.201810553

Yin L., Tang G., Zhang M., Wang B., Feng B. (2016). *“Monotonic and cyclic response of speed-lock connections with bolts in storage racks”*, Engineering Structures, **116**, 40-55. https://doi.org/10.1016/j.engstruct.2016.02.032

Yin L., Tang G., Li Z., Zhang M. (2018). *“Responses of cold-formed steel storage racks with spine bracings using speed-lock connections with bolts II: Nonlinear dynamic response history analysis”*, Thin-Walled Structures, **125**, 89-99. https://doi.org/10.1016/j.tws.2018.01.002

3 Seismic Assessment of Automated Rack Supported Warehouses

3.1 Introduction

The classification of several analytical and experimental publications performed in Chapter 2 and summarized in Table 2.2, highlights the lack of knowledge in many areas of the seismic behaviour of the high-rise automated rack supported warehouses (ARSWs), leaving several unanswered questions, such as (a) what q/R should be used along the cross- and down-aisle direction, (b) which are the most critical members/connections, (c) how to treat the second-order effects, and (d) is modal response spectrum analysis (MRSA) a sufficient method for the calculation of seismic loads/deformations?

Clearly there are no straightforward answers to any of the questions, as they require a lot of analytical and especially experimental work that is currently unavailable. As a first step towards the understanding of the seismic behaviour of ARSWs, five multi-depth case studies designed by professional engineers will be examined herein, using a set of 15 natural records selected to respect the hazard of the installation site. A series of linear response history analyses (RHAs) will be performed for each case study, to assess the applicability of the conventional MRSA for the design of ARSWs and to specify the most vulnerable members and connections of the structure, defining a *hierarchy of criticalities*.

3.2 Description of case studies

3.2.1 Structural configuration

All five case studies (CS1 to CS5) examined in this chapter comprise multi-depth ARSWs designed by professional engineers within the context of project STEELWAR (2017), according to EN 1993 (2005), EN 15512 (2009) and EN 16681 (2016) to be installed in the city of Van, Turkey, for a peak ground acceleration of $a_g = 0.3$ g. The overall plan dimensions vary from 64.84 to 65.05 m and 70.94 to 73.92 m in the cross- and down-aisle direction, respectively, while the peak height of the roof truss ranges from 25.31 to 26.71 m. The structural configurations of CS1 to CS5 are illustrated in Figure 3.1 to Figure 3.5, respectively. Each horizontal line in the plan views resembles a down-aisle frame (DA Frame), while each vertical a cross-aisle frame (CA Frame). CA Frames that are connected with beams and carry the pallets are the “Pallet” CA Frames, while those that belong to a bracing tower, the “Tower” CA Frames. For instance, CS1 (Figure 3.1) comprises 56 DA and 45 CA Frames; CA Frames 1, 2, 44, and 45 are “Tower”, while 3 to 43 are “Pallet”.

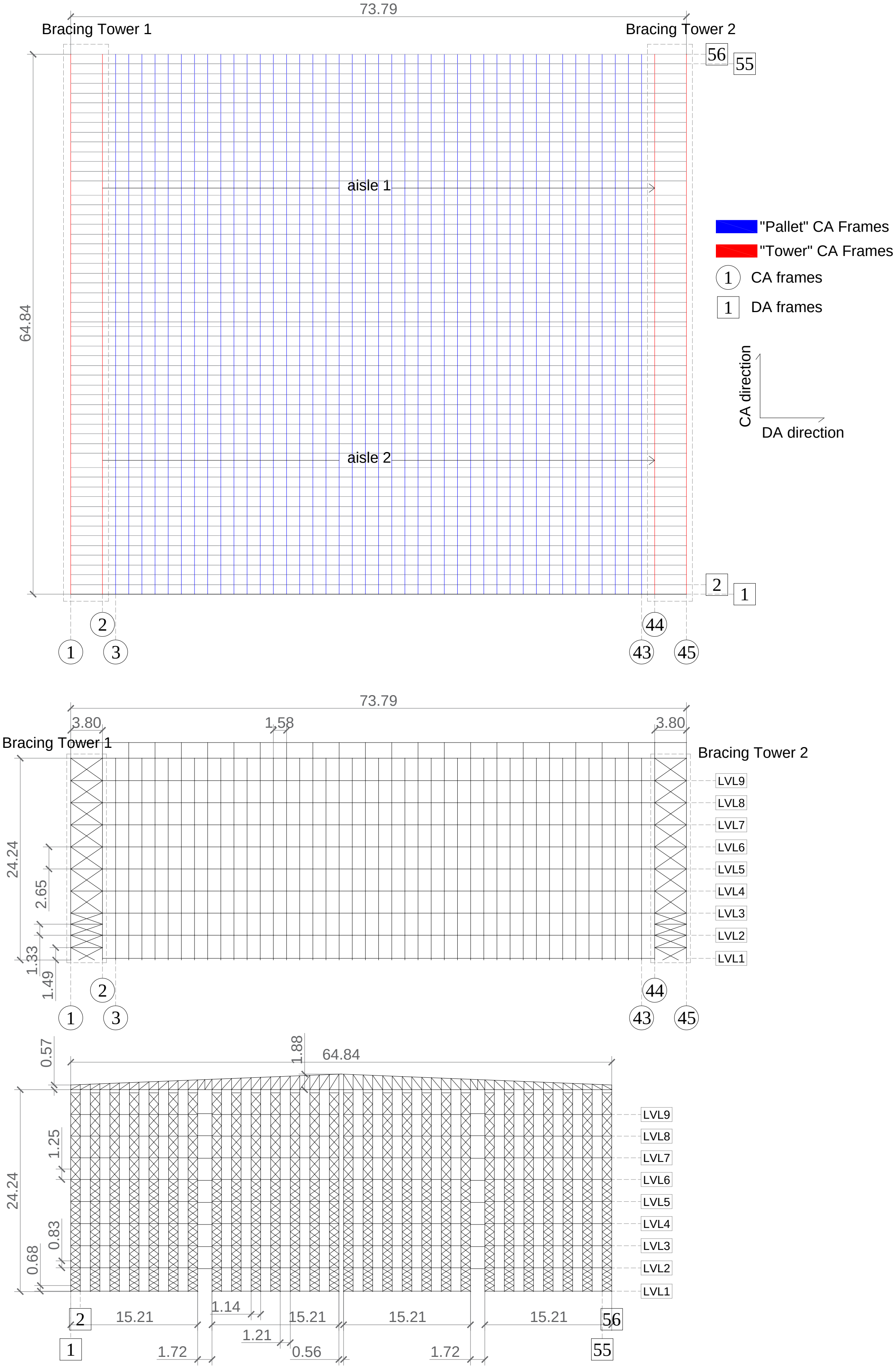
73.79
Bracing Tower 1
Bracing Tower 2
56
55
aisle 1
aisle 2
64.84
🟦 "Pallet" CA Frames
🟥 "Tower" CA Frames
① CA frames
1 DA frames
CA direction
DA direction
2
1
2
44
1
3
43
45
73.79
3.80
1.58
3.80
Bracing Tower 1
Bracing Tower 2
LVL9
LVL8
LVL7
LVL6
LVL5
LVL4
LVL3
LVL2
LVL1
24.24
2.65
1.33
1.49
2
44
1
3
43
45
0.57
1.88
64.84
24.24
1.25
0.83
0.68
LVL9
LVL8
LVL7
LVL6
LVL5
LVL4
LVL3
LVL2
LVL1
2
15.21
1.14
15.21
15.21
15.21
56
1
1.72
1.21
0.56
1.72
55

Figure 3.1: Structural configuration of CS1, showing plan, down- and cross-aisle views.

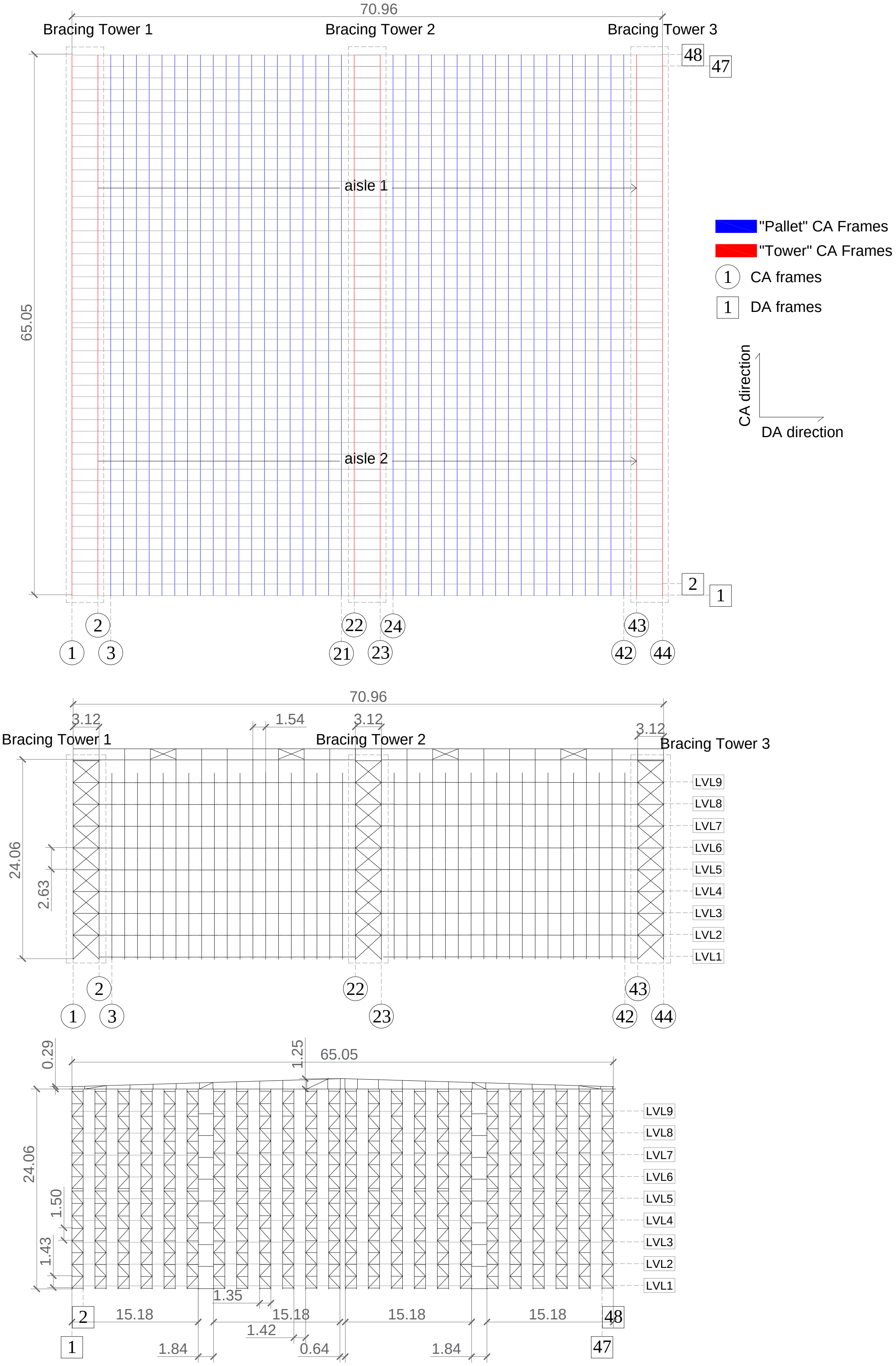
70.96
Bracing Tower 1
Bracing Tower 2
Bracing Tower 3
48
47
65.05
aisle 1
aisle 2
2
1
"Pallet" CA Frames
"Tower" CA Frames
1 CA frames
1 DA frames
CA direction
DA direction
2
22
24
43
1
3
21
23
42
44
70.96
3.12
1.54
3.12
3.12
24.06
2.63
LVL9
LVL8
LVL7
LVL6
LVL5
LVL4
LVL3
LVL2
LVL1
2
22
43
1
3
23
42
44
0.29
1.25
65.05
24.06
1.50
1.43
1.35
2
15.18
15.18
15.18
15.18
48
1.42
1
1.84
0.64
1.84
47

Figure 3.2: Structural configuration of CS2, showing plan, down- and cross-aisle views.

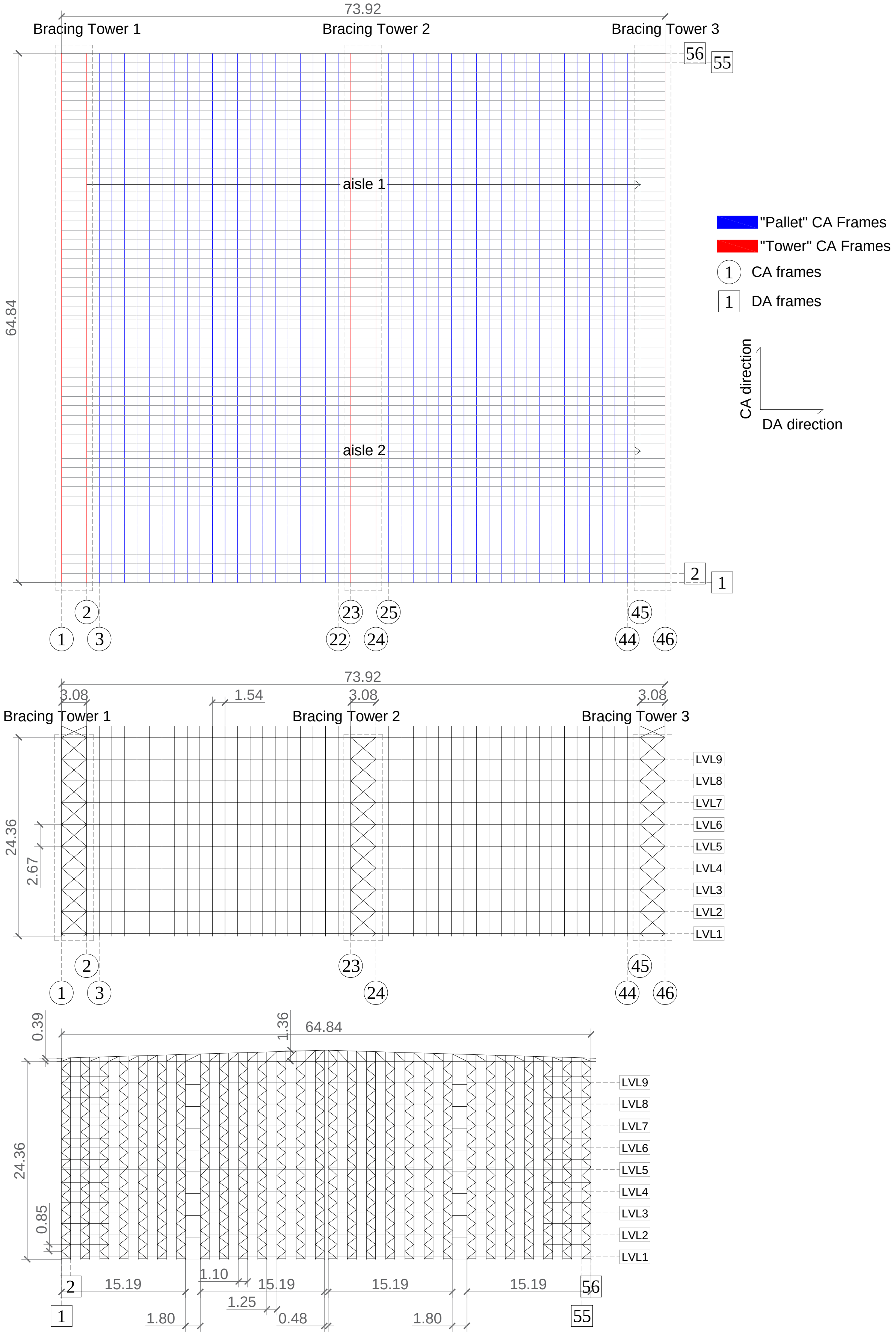
73.92
Bracing Tower 1
Bracing Tower 2
Bracing Tower 3
64.84
aisle 1
aisle 2
56
55
2
1
"Pallet" CA Frames
"Tower" CA Frames
1 CA frames
1 DA frames
CA direction
DA direction
1
2
3
22
23
24
25
44
45
46
3.08
1.54
24.36
2.67
LVL9
LVL8
LVL7
LVL6
LVL5
LVL4
LVL3
LVL2
LVL1
0.39
1.36
64.84
0.85
15.19
1.10
1.25
0.48
1.80

Figure 3.3: Structural configuration of CS3, showing plan, down- and cross-aisle views.

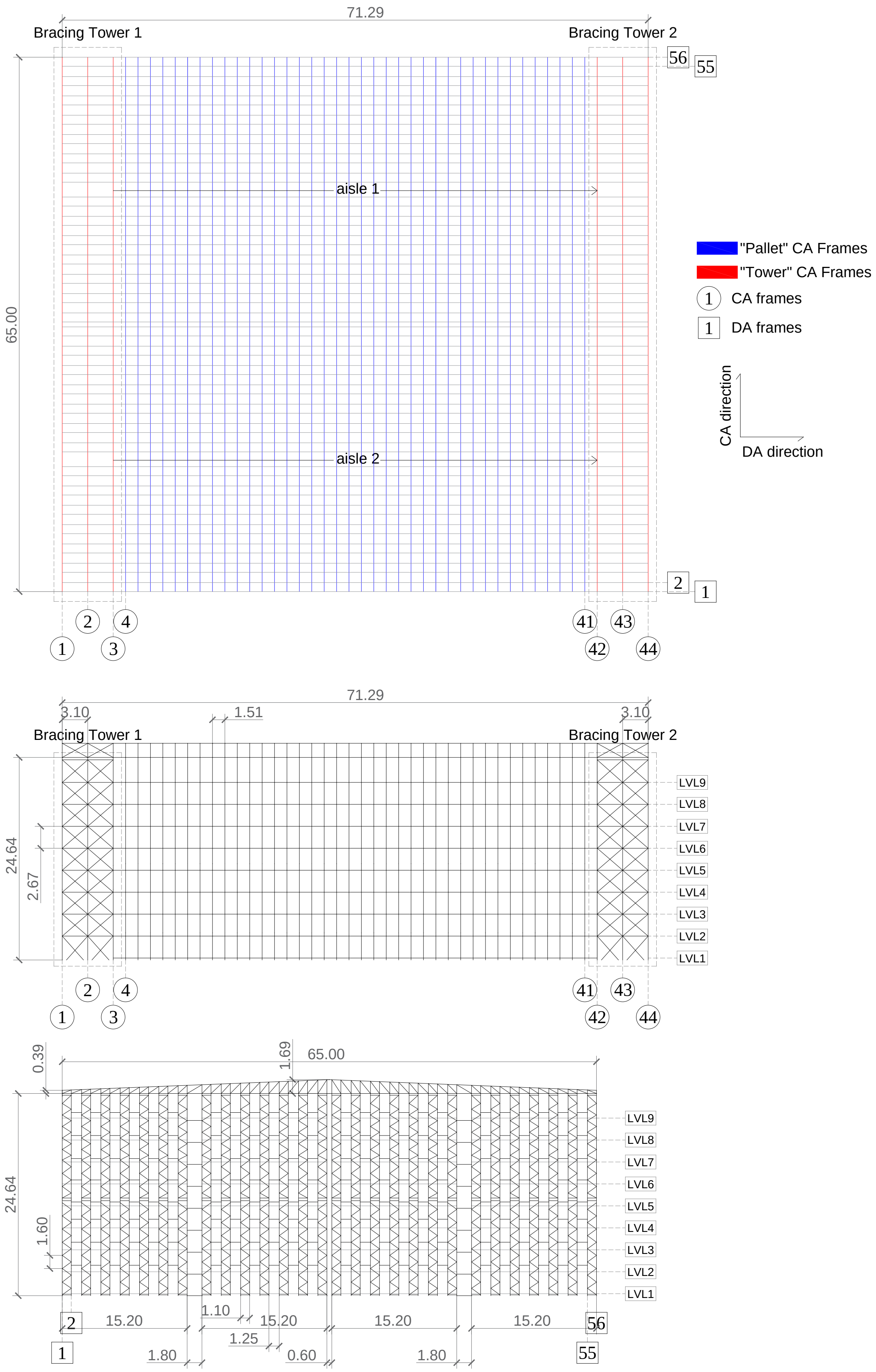
71.29
Bracing Tower 1
Bracing Tower 2
56
55
aisle 1
aisle 2
65.00
2
1
"Pallet" CA Frames
"Tower" CA Frames
1 CA frames
1 DA frames
CA direction
DA direction
1
2
3
4
41
42
43
44
71.29
3.10
1.51
3.10
Bracing Tower 1
Bracing Tower 2
24.64
2.67
LVL9
LVL8
LVL7
LVL6
LVL5
LVL4
LVL3
LVL2
LVL1
1
2
3
4
41
42
43
44
0.39
1.69
65.00
24.64
1.60
LVL9
LVL8
LVL7
LVL6
LVL5
LVL4
LVL3
LVL2
LVL1
2
1
15.20
1.10
15.20
15.20
15.20
1.25
1.80
0.60
1.80
56
55

Figure 3.4: Structural configuration of CS4, showing plan, down- and cross-aisle views.

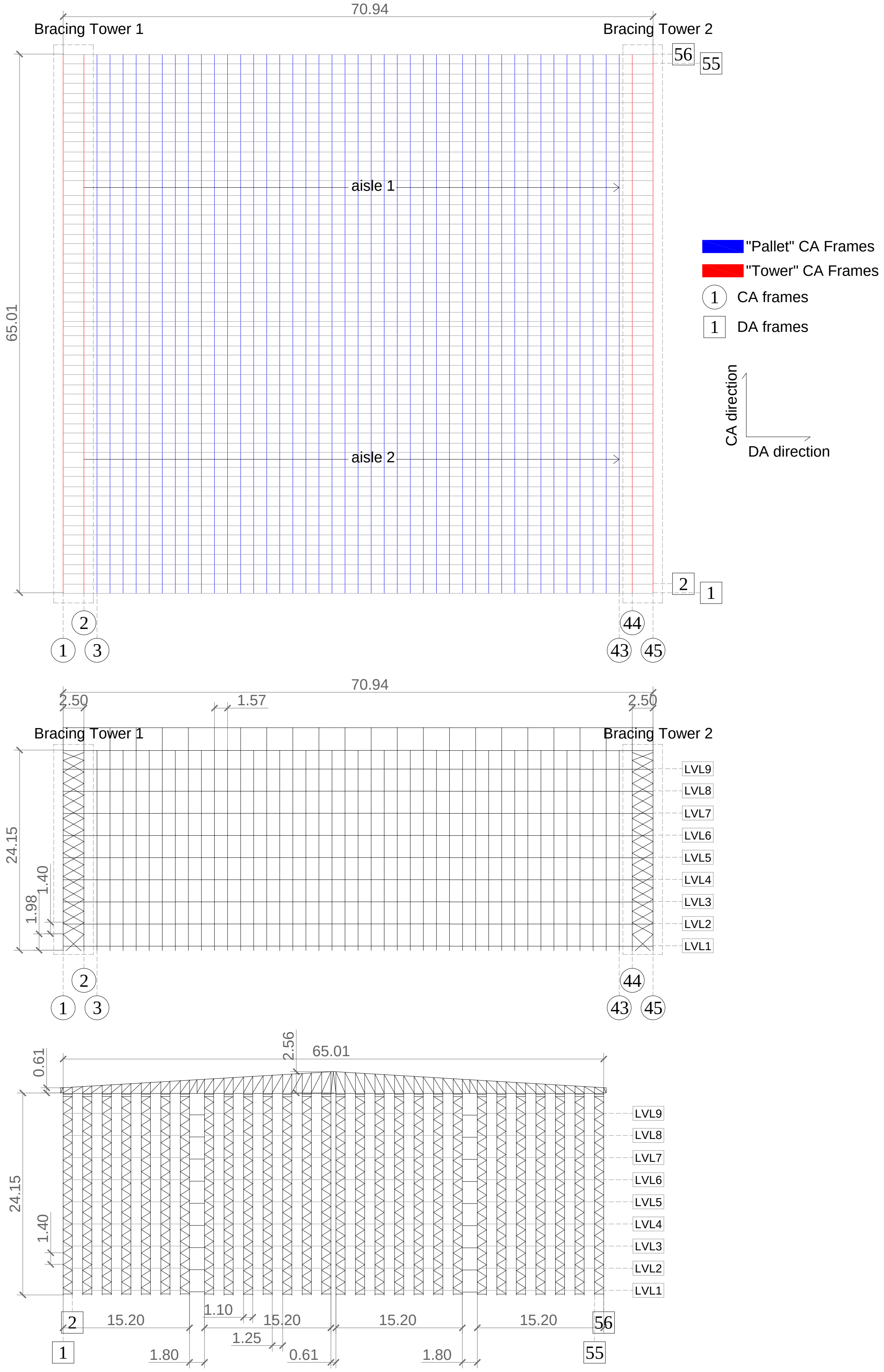
70.94
Bracing Tower 1
Bracing Tower 2
56
55
65.01
aisle 1
aisle 2
"Pallet" CA Frames
"Tower" CA Frames
1 CA frames
1 DA frames
CA direction
DA direction
2
1
2
1
3
44
43
45
70.94
2.50
1.57
2.50
Bracing Tower 1
Bracing Tower 2
24.15
1.40
1.98
LVL9
LVL8
LVL7
LVL6
LVL5
LVL4
LVL3
LVL2
LVL1
2
1
3
44
43
45
2.56
65.01
0.61
24.15
1.40
LVL9
LVL8
LVL7
LVL6
LVL5
LVL4
LVL3
LVL2
LVL1
2
15.20
1.10
15.20
15.20
15.20
56
1.25
1
1.80
0.61
1.80
55

Figure 3.5: Structural configuration of CS5, showing plan, down- and cross-aisle views.

The handling of the goods is fully-automated, using cranes and shuttles to withdraw and deposit the goods: Cranes are moving along the down-aisle direction using the two aisles of the warehouse to go to the desired "Pallet" CA Frame and then the shuttle moves along the cross-aisle direction, either inside the left or the right storage cell. Despite the small geometrical deviations among the case studies, they were all designed to carry 9 load levels with four storage cells of 13 unit-load capacity each, thus each "Pallet" CA Frame supports up to 468 pallets. Load levels 1 to 2 are for 1000 kg pallets, 3 to 5 for 800 kg, and 6 to 9 for 600 kg.

In the cross-aisle direction, all case study structures are composed of uprights, connected in pairs to form upright frames, and a roof truss that connects the individual upright frames at their topmost height. CS3, CS4, and CS5 use a "D-type" bracing pattern, while CS1 and CS2 an "X-type" and a "K-type", respectively. An important advantage of an "X-type" or "K-type" bracing pattern over a "D-type" is the shorter upright buckling length along the cross-aisle direction, with the obvious cost of adding more steel members. The roof truss varies from very shallow and flexible, like the one used in CS2, to highly-pitched and stiff in CS5.

Along the down-aisle direction, the seismic loads are carried almost solely by the stiff bracing towers, as the moment frame formed by the pallet uprights and beams is a way more flexible LLRS. CS1, CS4, and CS5 employ bracing towers at the two ends of the warehouse, while CS2 and CS3 have an additional in the middle, which interrupts the "Pallet" CA Frames but offers a more uniform distribution of the inertial forces. Horizontal braces are used in the bracing towers and the roof, which act as a horizontal diaphragm to the individual DA Frames. However, their structural behaviour and the effect of their distribution along the height of the warehouse is out of the scope of this investigation, as we focus on 2D analyses.

To minimize the weight of the steel used, designers tend to use lighter members at the higher levels of the ARSW, as the gravitational and seismic loads are lower. Depending on the structural philosophy of the designer, the cross- and down-aisle direction of an ARSW might be broken down to several vertical segments, but using more than three is considered to be insufficient, as it overcomplicates the installation process. This large variety of steel sections raises the demand for a component "tag" list of the most essential structural members/sections, which is given in Table 3.1 and shown graphically in Figure 3.6. Notably, only the first- and second-from-the-bottom structural components are included in the tag list, despite the fact that some case studies have three vertical segments (e.g., CS3 has three pallet upright sections). This decision was made to keep the tag list as short as possible, taking into account that typically the upper levels are less stressed than the lower ones.

Table 3.2 shows the section scheme and elevation of the considered structural components. Interestingly, the bottom uprights that belong to a "Tower" DA Frame (i.e., the "bu1" components) are always reinforced, as they have to withstand increased seismic forces coming from the vertical bracing system. CS1 and CS2 combine a standard Ω upright section with a U-profile that is continuously bolted to the upright, to create an Ω+U profile. CS4 and CS5 prefer to weld two standard Ω upright sections to create an Ω+Ω profile. On the other hand, CS3 employs a hot-rolled I-section for the "bu1" component, which enhances the seismic performance of the bracing towers but requires nonstandard details and connections.

Table 3.1: Tag list of structural components used for the seismic assessment of the five multi-depth ARSW case studies.

Component name	Tag	Description
Pallet Upright 1	pu1	The first-from-the-bottom upright section that belongs to a “Pallet” CA Frame.
Pallet Upright 2	pu2	The second-from-the-bottom upright section that belongs to a “Pallet” CA Frame.
Pallet Diagonal 1	pd1	The first-from-the-bottom diagonal section that belongs to a “Pallet” CA Frame.
Pallet Diagonal 2	pd2	The second-from-the-bottom diagonal section that belongs to a “Pallet” CA Frame.
Pallet Anchorage	panc	The anchorage system used to fix a pallet upright to the foundation concrete floor.
Pallet Beam 1	pb1	The first-from-the-bottom pallet beam section.
Pallet Beam 2	pb2	The second-from-the-bottom pallet beam section.
Bracing Upright 1	bu1	The first-from-the-bottom upright section that belongs to a “Tower” CA Frame.
Bracing Upright 2	bu2	The second-from-the-bottom upright section that belongs to a “Tower” CA Frame.
Bracing Diagonal 1	bd1	The first-from-the-bottom diagonal section that belongs to a “Tower” CA Frame.
Bracing Diagonal 2	bd2	The second-from-the-bottom diagonal section that belongs to a “Tower” CA Frame.
Bracing Upright Anchorage	buanc	The anchorage system used to fix a bracing upright to the foundation concrete floor.
Bracing Diagonal Anchorage	bdanc	The anchorage system used to fix a bracing diagonal to the foundation concrete floor.
Bracing Beam 1	bb1	The first-from-the-bottom bracing beam section.
Bracing Beam 2	bb2	The first-from-the-bottom bracing beam section.

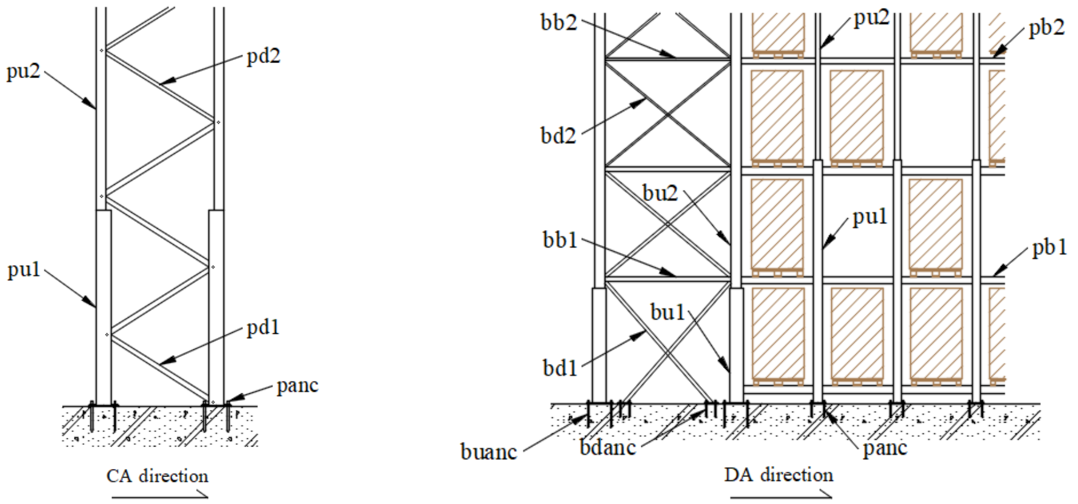

(a) (b)

Figure 3.6: Side views with the structural components considered in the tag list of Table 3.1, for the (a) cross-aisle, and (b) down-aisle direction.

Table 3.2: Section scheme and height of the structural components given in Table 3.1.

Tag		**CS1**	**CS2**	**CS3**	**CS4**	**CS5**
pu1	Height (m)	[0.00, 3.00]	[0.00, 12.00]	[0.00, 11.32]	[0.00, 3.25]	[0.00, 24.15]
	Section scheme	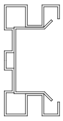	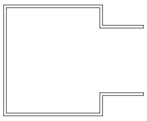	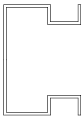	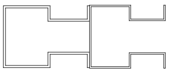 (50% scale)	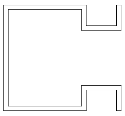
pu2	Height (m)	(3.00, 24.24]	(12.00, 24.06]	(11.32, 24.36]	(3.25, 11.5]	-
	Section scheme	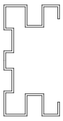	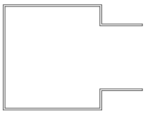	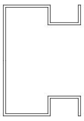	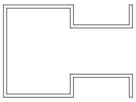	-
pd1	Height (m)	[0.00, 24.24]	[0.00, 11.85]	[0.00, 24.36]	[0.00, 10.45]	[0.00, 24.15]
	Section scheme	 A_{mult} = 0.125	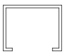 A_{mult} = 0.1	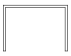 A_{mult} = 0.117	x2 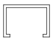 A_{mult} = 1.0	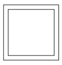 A_{mult} = 0.1
pd2	Height (m)	-	(11.85, 24.06]	-	(10.45, 13.95]	-
	Section scheme	-	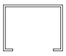 A_{mult} = 0.1	-	x2 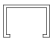 A_{mult} = 1.0	-
pb1	Height (m)	[0.00, 3.00]	[0.00, 24.06]	[0.00, 24.36]	[0.00, 2.92]	[0.00, 24.15]
	Section scheme	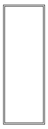	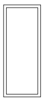	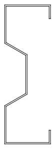	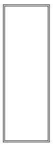	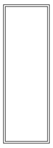
pb2	Height (m)	(3.00, 10.93]	-	-	(2.92, 10.92]	-
	Section scheme	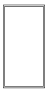	-	-	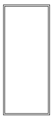	-
bu1	Height (m)	[0.00, 16.31]	[0.00, 5.85]	[0.00, 24.36]	[0.00, 8.60]	[0.00, 24.15]
	Section scheme	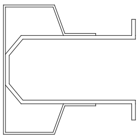	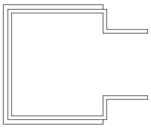	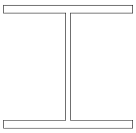	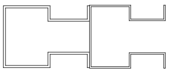 (50% scale)	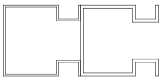 (50% scale)
bu2	Height (m)	(16.31, 24.24]	(5.85, 12.00]	-	(8.60, 11.50]	-
	Section scheme	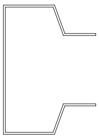	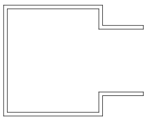	-	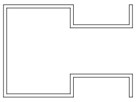	-
bd1	Height (m)	[0.00, 10.93]	[0.00, 13.40]	[0.00, 11.01]	[0.00, 8.25]	[0.00, 24.15]
	Section scheme	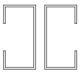	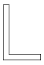	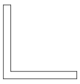	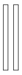	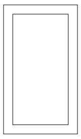
bd2	Height (m)	(10.93, 24.24]	(13.40, 24.06]	(11.01, 24.36]	(8.25, 24.64]	-
	Section scheme	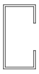	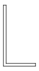	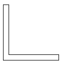	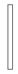	-

The transverse shear stiffness of the upright frame also has a significant impact on the behaviour of the rack structure in the cross-aisle direction. As pointed by Talebian et al. (2018) there are various factors influencing the transverse shear deformation of the frames, mostly related to the deformation of the braces and their ends, as well as slipping and bending of the bolts. In a beam-column element model this phenomenon was implicitly taken into account by using a cross-section area reduction multiplier (A_{mult}), as given in Table 3.2 for the pallet diagonals ("pd1", "pd2").

3.2.2 Seismic design assumptions

As the seismic design of ARSWs is not fully covered by current standards, designers are obliged to make assumptions for the definition of the design spectrum and the mass and load combinations, solely relying on their experience and on the behaviour of their steel profiles when used on conventional racks, like the APRs. Thus, despite the common installation site, same pallet-loading configuration, and similar geometry among the case studies, there is a variety of seismic design assumptions, as shown in Table 3.3 and described in the following sections.

Table 3.3: Seismic design assumptions adopted for each multi-depth ARSW case study.

	Direction	**CS1**	**CS2**	**CS3**	**CS4**	**CS5**
γ_I	both	0.8	0.8	0.8	0.8	0.8
E_{D1}	both	1.0	1.0	1.0	1.0	1.0
E_{D3}	both	0.8	0.8	0.8	0.8	1.0
q	cross-aisle	1.5	1.5	1.5	1.5	1.5
	down-aisle	2.0	1.5	2.0	2.0	1.5
Mass comb.	both	G + 0.64·Q	G + 0.8·Q	G + 0.8·Q	G + 0.8·Q	G + 0.8·Q
Load comb.	both	$G + Q$	$G + Q$	$G + Q$	$G + Q$	1.35·G + 1.5·Q

Importance factor

EN 16681 (2016) suggests to use the 20% in 50 years design spectrum for the design of fully-automated racks, which can be derived by multiplying the 10% in 50 years spectrum by an importance factor γ_I = 0.8. This simplified method to go from the 10% to the 20% in 50 years design spectrum, can be justified using the approximation of the site hazard curve as a straight line in log-log coordinates (Cornell et al, 2002):

$$\lambda(IM) = k_0 \cdot IM^{-k} \qquad \text{Eq. (3.1)}$$

where IM is the intensity measure (e.g., the spectral acceleration Sa), $\lambda(IM)$ is the hazard function which gives the mean annual frequency (MAF) of exceeding values of IM, and k is the (assumed) constant slope of the hazard curve in log-log coordinates. EN 1998-1 (2004) stipulates values of k = 2 – 4 for Europe, although a more accurate value can be estimated by fitting the actual hazard curve of the site at hand (Vamvatsikos, 2014). One can always map probabilities of p in N years to λ (i.e., MAF), by employing the exponential distribution of interarrival time implied by the Poisson assumption of seismic events:

$$\lambda = -\ln(1-p)/N \qquad \text{Eq. (3.2)}$$

Combining Eq. (3.1) and Eq. (3.2), we can define a relationship between the IMs that correspond to 10% and 20% in 50 years probability of exceedance, i.e., $IM_{10\%}$ and $IM_{20\%}$, respectively:

$$\left.\begin{aligned}\lambda(IM_{10\%}) &= k_0 \cdot IM_{10\%}^{-k}\\ \lambda(IM_{20\%}) &= k_0 \cdot IM_{20\%}^{-k}\end{aligned}\right\} \Rightarrow \frac{IM_{20\%}}{IM_{10\%}} = \left(\frac{\lambda(IM_{20\%})}{\lambda(IM_{10\%})}\right)^{-1/k} \approx \left(\frac{0.004453}{0.002105}\right)^{-1/3} \approx 0.78 \qquad \text{Eq. (3.3)}$$

where an average value of k = 3 was adopted. Using Sa as the IM, Eq. (3.3) suggests multiplying $Sa_{10\%}$ by 0.78 to get $Sa_{20\%}$, which is quite close to the 0.80 foreseen by

EN 16681 (2016). In the scope of optimizing the design, all case studies took advantage of this reduction of seismic loads and accepted a higher seismic risk, as γ_I = 0.8 corresponds to importance class I per EN 1998-1 (2004) parlance. In any case, while EN 16681 (2016) recommends some default values for the design lifetime and importance class of different racking systems, it states that the rack supplier is ultimately responsible for their selection.

Design spectrum modification factors

EN 16681 (2016) offers another source of seismic load reduction, the design spectrum modification factors E_{D1} and E_{D3}. Specifically, the design spectral acceleration is multiplied by a K_D factor, given as:

$$K_D = 1 - P_{E,prod}/P_E \cdot (1 - E_{D1} \cdot E_{D3}) \quad \text{Eq. (3.4)}$$

where P_E is the total weight of the rack in the seismic design situation (including dead weight, permanent weight, live load in the seismic situation and the store product weight) and $P_{E,prod}$ is the total product weight store on the rack, in the seismic design situation. A simplified form of Eq. (3.4) can be derived by assuming that $P_{E,prod}$ is greater or equal to 90% of P_E, which is the standard case for racking systems:

$$K_D = E_{D1} \cdot E_{D3} \quad \text{Eq. (3.5)}$$

The E_{D1} factor is related to the positive effect of pallet sliding that acts as a seismic isolation mechanism and reduces the apparent inertia of the rack. EN 16681 (2016) adopts the following formula:

$$E_{D1} = \max\{0.4,\ \mu/Sa(T_1) + 0.2\} \leq 1.0 \quad \text{Eq. (3.6)}$$

where μ is the reference value of the unit-load/beam friction coefficient, T_1 is the fundamental period of vibration of the racking structure in the considered direction, and $Sa(T_1)$ is the ordinate of the elastic spectrum defined in EN 1998-1 (2004), in units of g. Recently, Tsarpalis et al. (2021), based on a series of time-history analyses, proposed a new empirical formula of E_{D1} that largely removes the bias of Eq. (3.6). A detailed discussion of the content-structure-sliding-interaction (CSSI) problem is presented in Chapter 6.4 of this thesis. For all case studies, due to the low value of $Sa(T_1)$ relative to the μ, limited or no pallet sliding is foreseen and E_{D1} becomes 1.0, along both the cross- and down-aisle direction.

While E_{D1} is based on the physical mechanism of CSSI, E_{D3} is a somewhat-arbitrary reduction factor, having a constant value of 0.8. According to EN 16681 (2016), the E_{D3} factor is introduced to *“account for the dissipative phenomena typical of the dynamic behaviour of racking systems under seismic actions that are not included in the mathematical formulation presented in this European Standard, but that are observed on racks that have suffered earthquakes, and from tests performed on shaking tables”*. Unfortunately, the majority of racks tested on shaking tables or observed during post-earthquake surveys are not ARSWs, thus one has to be reluctant for the use of E_{D3} = 0.8 during the seismic design. Taking this into account, CS5 was chosen to be designed with E_{D3} equal to 1.0, while the other case studies went with the code-proposed value of 0.8.

Behaviour factors, mass and load combinations

The application of linear design procedures for seismic loading is based on the approximation of the nonlinear dynamic response of the structure via a linear model. To account for the beneficial effects of ductility, which allows trading off damage for lower design forces, EN 1998-1 (2004) adopts the behaviour (or q) factor to scale down the elastic design response spectrum. Many definitions of the q-factor have been proposed in the literature, which are based on experimental investigations (ECCS, 1986), nonlinear static analyses (Whittaker et al., 1999) or, more recently, risk-based procedures (Vamvatsikos et al., 2020). Despite the various methods of defining and evaluating the q-factor, it is always related to the overstrength Ω and ductility behaviour factor q_d of the system (Maheri and Akbari, 2003). As discussed in Chapter 2, experimental and analytical investigations demonstrated that typical racking systems offer limited ductility (i.e., low q_d), which is reflected in the design codes by the adoption of low q-factors.

All case studies used a q-factor of 1.5 along the cross-aisle direction, as proposed by EN 16681 (2016). Along the down-aisle direction, CS1, CS3 and CS4 used a q-factor of 2.0, while CS2 and CS5 of 1.5. Indeed, the codes allow to use a q-factor of 2.0 on a braced rack, as long as: (a) the members that contribute to the seismic resistance of the structure in compression or bending have a section classification 1, 2 or 3, (b) an “X-type” bracing configuration is used with horizontal compression elements and diagonals acting only in tension, and (c) in bolted shear connections, the shear strength of the bolts $F_{v,Rd}$ is 1.20 times higher the bearing resistance $F_{b,Rd}$ of the connected profiles. While the aforementioned rules (a) to (c) try to set a (limited) capacity design framework that justifies the use of q = 2, not enough scientific evidence exists to support it. During the SEISRACKS2 (2014) project, the performance of various braced APRs was tested by means of full-scale pushover tests and it was found that high q-factors can be achieved by guaranteeing sufficient overstrength for the bracing connections and allowing the diagonals to yield. Rules (a) to (c) do not enforce this type of overstrength. Moreover, while rule (c) prevents the bolts from failing in shear, it does not avoid the brittle net section rupture of the diagonal connections, which is in most cases the dominant failure mode.

Regarding the definition of the seismic mass, the following combination was used:

$$M_{E,tot} = M_{E,G} + \psi_2 \cdot M_{E,UL} \qquad \text{Eq. (3.7)}$$

where $M_{E,tot}$ is total seismic mass of the rack, $M_{E,G}$ is the mass coming from the self-weight of the steel members, $M_{E,UL}$ is the unit load mass, and ψ_2 is the combination coefficient of EN 1998-1 (2004). In conventional steel buildings ψ_2 is usually taken equal to 0.3, as during an extreme seismic event the live loads are expected to have way lower values than their design ones. On the other hand, EN 16681 (2016) does not consider ψ_2 (i.e., ψ_2 = 1.0), but instead introduces the following formula for the calculation of $M_{E,UL}$:

$$M_{E,UL} = R_F \cdot E_{D2} \cdot Q_{P,rated} \qquad \text{Eq. (3.8)}$$

where R_F is the rack filling grade reduction factor, E_{D2} is the unit load weight modification factor, and $Q_{P,rated}$ is the specified value of the weight of unit loads for the compartment. E_{D2} represents the effects of the interaction between the unit load and the racking structure and it was taken equal to 1.0. The R_F reduction factor is related to the occupancy of stored goods in the rack that can be assumed during the seismic event, essentially it acts as a ψ_2 factor. CS2, CS3, CS4, and CS5 assumed R_F = 0.8 and ψ_2 = 1.0, which led to a mass combination of G + 0.8·Q (G and Q represent the dead and the live/unit loads, respectively). Based on national codes, CS1 used R_F = 0.8 together with a ψ_2 = 0.8, resulting in a mass combination of G + 0.64·Q.

In contrast to the seismic mass, EN 16681 (2016) does not consider any reduction factors for the definition of the seismic vertical loads, i.e., R_F and ψ_2 should be equal to 1.0. Thus, the load combination G + Q was used in CS1, CS2, CS3, and CS4. Contrarily, CS5 assumed the overconservative 1.35·G + 1.5·Q load combination for the seismic design, which is conceptually equivalent to vertical loads during the Ultimate Limit State (EN 1990, 2002). While this difference between the definition of the masses and vertical loads is ambiguous, it still is on the safe side for the design of the steel members. However, it will be shown later that it is not safe for the design of the baseplates and anchors, as high vertical loads result in lower uplift forces.

3.2.3 Cumulative seismic load multiplier

The previous sections highlighted the large variety of seismic design assumptions among the five case studies, which emerged from the absence of a well-defined design standard specific for ARSWs. Consequently, each case study exploited different sources of seismic load reduction available by the codes, with the main being the γ_I, E_{D3}, q-factor, R_F, and ψ_2. The aforementioned reduction factors can be combined into a *cumulative seismic load multiplier*, given as:

$$R_{cum} = \gamma_I \cdot E_{D3} \cdot R_m \cdot R_q \qquad \text{Eq. (3.9)}$$

where R_m and R_q measure the reduction of the seismic loads due to R_F^* = ψ_2·R_F and q, respectively. R_m can be defined as the ratio between the design seismic loads subjected to a single degree of freedom (SDOF) system with mass m and stiffness k, and a SDOF with mass R_F^*·m and stiffness k:

$$R_m = \frac{(R_F^* \cdot m) \cdot Sa\left(T_{R_F^*}\right)}{m \cdot Sa(T)} = \frac{(R_F^* \cdot m) \cdot a_g \cdot S \cdot \eta \cdot 2.5 \cdot T_C/T_{R_F^*}}{m \cdot a_g \cdot S \cdot \eta \cdot 2.5 \cdot T_C/T} \Rightarrow$$
$$R_m = R_F^* \frac{T}{T_{R_F^*}} = R_F^* \frac{2\pi\sqrt{m/k}}{2\pi\sqrt{R_F^* \cdot m/k}} = \sqrt{R_F^*} = \sqrt{\psi_2 \cdot R_F} \qquad \text{Eq. (3.10)}$$

where a_g is the design peak ground acceleration, η is the damping correction factor, and T_C is the upper limit of the period of the constant spectral acceleration branch. In Eq. (3.10), the design spectral acceleration is calculated as $Sa(T) = a_g \cdot S \cdot \eta \cdot 2.5 \cdot T_C / T$ (see EN 1998-1, 2004), assuming that $T_C \leq T \leq T_D$, a condition that holds for the top modes of all case studies. While ARSWs are far from simple SDOF systems and the effect of higher modes is significant, Eq. (3.10) is still a good indicator of how a modification in the seismic mass affects the design seismic loads.

Following the same logic, R_q is defined as the ratio between the design seismic loads subjected to a structure with q = 1 and one with q > 1, $E_{q=1}$ and $E_{q>1}$, respectively. The q-factor has a dual behaviour during a seismic design, as on one hand it lowers the design spectral acceleration, but on other it increases the so-called interstory drift sensitivity coefficient θ (Black, 2011; Adam and Jäger, 2012). It essentially comprises a simplified method of accounting for P-Δ effects during MRSA for these flexible racks, by amplifying the seismic loads by $1/(1-\theta)$. Thus, R_q can be defined as:

$$R_q = \frac{E_{q>1}}{E_{q=1}} = \frac{1}{q} \cdot \frac{1-\theta_{q=1}}{1-\theta_{q>1}} \qquad \text{Eq. (3.11)}$$

EN 16681 (2016) offers a simplified formula for θ, which is commonly used for the seismic design of racks:

$$\theta = q_d \cdot \frac{P_E}{P_{cr,E}} = \frac{q_d}{a_{cr,E}} \qquad \text{Eq. (3.12)}$$

where P_E is the total gravity load of the rack in the seismic design situation, $P_{cr,E}$ is the Euler critical load, and $a_{cr,E} = P_{cr,E}/P_E$. Unless otherwise specified, the ductility behaviour factor q_d is taken equal to q, essentially neglecting overstrength. Using, Eq. (3.11) and Eq. (3.12), R_q can be given as:

$$R_q = \frac{1}{q} \cdot \frac{1-1/a_{cr,E}}{1-q/a_{cr,E}} = \frac{1}{q} \cdot \frac{a_{cr,E}-1}{a_{cr,E}-q} \qquad \text{Eq. (3.13)}$$

As expected, the effect of added flexibility due to a higher q decreases its capability to reduce the seismic loads, as $R_q > 1/q$ when $q > 1$. Table 3.4 presents the individual R_q and R_m reduction factors, together with the cumulative R_{cum}. Interestingly, R_{cum} ranges from 0.437 down to 0.307, which means that with a favorable selection of the design assumptions, one can decrease the seismic loads by almost 70%. As explained before, some of the terms involved in Eq. (3.9) are not based on comprehensive scientific research, but instead come from studies on the non-ARSW-like APRs and expert opinion. This means that R_{cum} inherits a significant amount of epistemic uncertainties which, combined with the aleatory randomness of the earthquake (Vamvatsikos and Fragiadakis, 2009), can lead to unsafe designs.

Table 3.4: Sensitivity factors and cumulative seismic load multipliers for each multi-depth ARSW case study.

	Direction	**CS1**	**CS2**	**CS3**	**CS4**	**CS5**
$a_{cr,E}$	cross-aisle	17.89	14.63	13.16	31.00	22.14
	down-aisle	16.06	16.68	10.57	15.05	21.47
θ	cross-aisle	0.084	0.103	0.114	0.048	0.068
	down-aisle	0.124	0.090	0.189	0.133	0.070
R_m	cross-aisle	0.894	0.894	0.894	0.894	0.800
	down-aisle	0.894	0.894	0.894	0.894	0.800
R_q	cross-aisle	0.687	0.692	0.695	0.678	0.683
	down-aisle	0.536	0.689	0.558	0.538	0.683
R_{cum}	cross-aisle	0.393	0.396	0.398	0.388	0.437
	down-aisle	0.307	0.394	0.319	0.308	0.437

3.3 Seismic hazard and record selection

To measure the effect of the record waveform in the performance of ARSWs, a series of 15 RHAs are conducted for each case study, using natural accelerograms that respect the hazard of Van in Turkey. The 15 records were selected from the NGA-West 2 database (Ancheta et al., 2013) to match the target conditional spectra (CS) (see Baker, 2010; Lin et al., 2013a; Lin et al., 2013b) at 2475 years return period, or equivalently an exceedance probability of 2% in 50 years. The selection procedure was based on the approximate method of CS (Lin et al., 2013a) using the geometric mean of spectral accelerations as the IM (Kohrangi et al., 2017). The Ground Motion Prediction Equations of Boore and Atkinson (2008) were used for all purposes of this work, from hazard analysis to record selection.

The use of the 2% instead of the 10% or 20% in 50 years hazard was chosen, as initially ARSWs were planned to be tested for the near collapse performance level (see FEMA 356, 2000). However, it was later understood that the brittle failure modes of the ARSWs render the conduction of RHAs at intensity levels higher than the design code ones meaningless. Thus, it would have been more rational to select records that match the 10% in 50 years CS. Nevertheless, as along as one scales the selected accelerograms to the intensity level of his choice and the numerical model is elastic, the difference between the two is of secondary importance.

3.3.1 Hazard analysis

A probabilistic seismic hazard analysis is performed in OpenQuake (Pagani et al., 2014), considering all sources within 150 km, using the area source model of SHARE (Giardini et al, 2013). A soil type C is considered, having a shear wave speed in the upper 30 m of $V_{S30} = 270\,\mathrm{m/s}$. The corresponding seismic hazard curve was computed for the IM of $AvgSa$ and is illustrated in Figure 3.7. $AvgSa$ (Cordova et al., 2001; Vamvatsikos and Cornell, 2005; Kazantzi and Vamvatsikos, 2015; Eads et al., 2015) is a modern IM that comprises the geometric mean of 5% damped spectral acceleration ordinates Sa at T_{Ri} ($i = 1,..,. n$) periods that characterize the archetype ARSW of interest:

$$AvgSa(T_{Ri}) = \left(\prod_{i=1}^{n} Sa(T_{Ri})\right)^{1/n} \qquad \text{Eq. (3.14)}$$

Each Sa value in Eq. (3.12) is actually the geometric mean of both horizontal components rather than an arbitrary selection of one of the two. Periods T_{Ri} were selected as linearly spaced within a range of $[T_L, T_H]$, where T_L is a low bound near the minimum second period of the investigated ARSWs, and T_H is a high bound that is near 1.5 times their fundamental period. Therefore, a single period range of [0.3 s, 3.0 s] was employed for all test cases, with T_{Ri}'s defined at an increment of 0.1 s.

Crossing the hazard curve of Van with horizontal lines at 10% and 20% in 50 years probability of exceedance, or at a MAF of 0.002105 and 0.004453 (Eq. (3.2)), respectively, one can calculate the ratio $AvgSa_{20\%}/AvgSa_{10\%} = 0.172/0.241 = 0.71$. Therefore, both $\gamma_I = 0.8$ suggested by EN 16681 (2016) and $\gamma_I = 0.78$ calculated by the approximation of the hazard curve by Eq. (3.1)), are safe reduction factors for the transformation from the 10% to the 20% in 50 years design spectrum. Of course, this is valid specifically for the city of Van and should not be extrapolated to other sites of installation with different hazard curves.

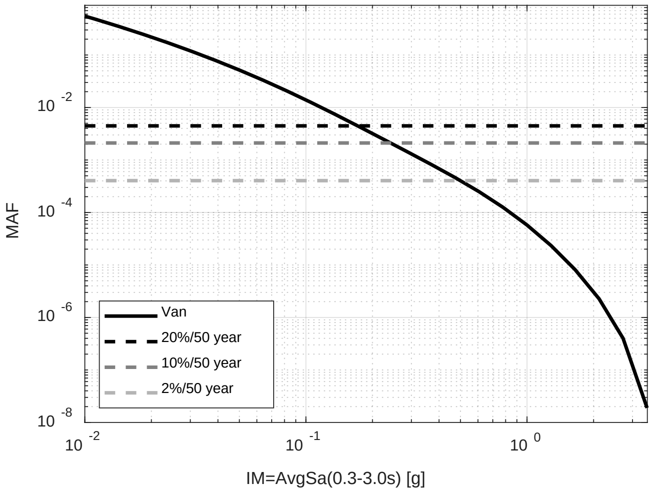

Figure 3.7: Hazard curve for the city of Van in Turkey, using $AvgSa$ as an IM.

3.3.2 Disaggregation analysis

Disaggregation analysis (Bazzuro and Cornell, 1999) was performed for a range of probabilities of exceedance, or equivalently for different levels of MAF. Specifically, the scenarios of exceedance probability equal to 60%, 30%, 10%, 5%, 2%, 1%, in 50 years were examined, as these correspond to return periods that are of engineering interest. For each MAF level, the value of $AvgSa$ was defined using the hazard curve of Figure 3.7 which was then used as input for the disaggregation analysis. The contribution from different magnitude (M), distance (R), and epsilon (ε) bins to the hazard are shown in detail in Figure 3.8(a)-(f). Epsilon (ε) shows the number of standard deviations from the logarithmic mean of the IM for a specific Ground Motion Prediction Equation (Baker and Cornell, 2006). The corresponding mean magnitude ($\overline{M}$), distance ($\overline{R}$), and epsilon ($\overline{\varepsilon}$) of all the scenarios are given in Table 3.5.

Table 3.5: IM value, mean magnitude, distance and epsilon obtained from disaggregation analysis for Van in terms of $AvgSa$ at nine selected return periods.

p% in 50 years	**MAF of exceeding**	**Return period**	$AvgSa$ **(g)**	$\overline{M}$	$\overline{R}$	$\overline{\varepsilon}$
60	1.83E-02	55	0.087	6.67	51.84	1.09
30	7.13E-03	140	0.138	6.78	36.49	1.17
10	2.11E-03	475	0.241	6.90	19.30	1.19
5	1.03E-03	975	0.334	6.97	11.78	1.21
2	4.04E-04	2475	0.499	7.07	6.25	1.31
1	2.01E-04	4975	0.656	7.14	4.39	1.45
0.6	1.20E-04	8303	0.789	7.20	3.68	1.59
0.2	4.00E-05	24975	1.106	7.29	2.99	1.89
0.1	2.00E-05	49975	1.333	7.35	2.76	2.04

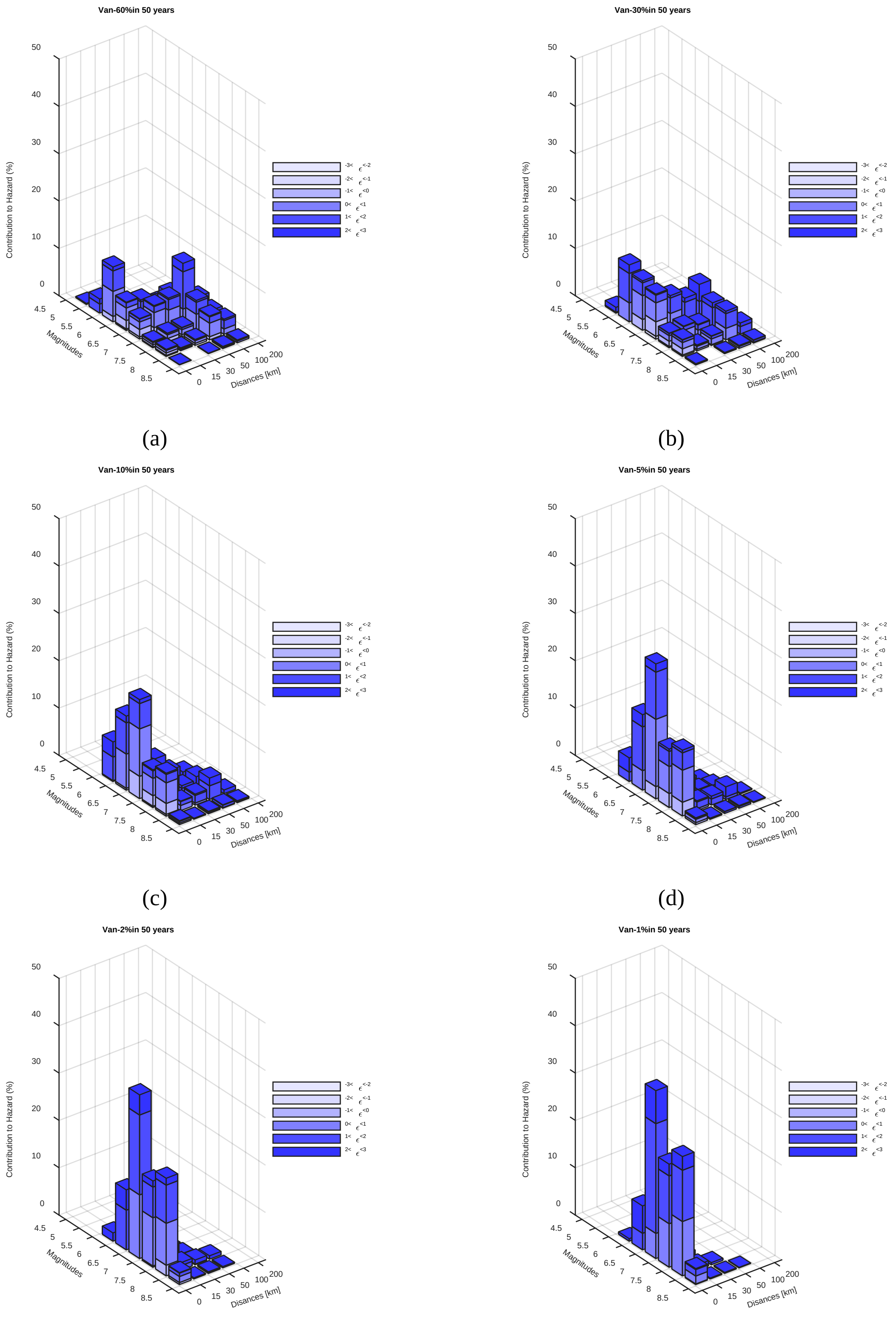

(a) (b)

(c) (d)

(e) (f)

Figure 3.8: Disaggregation analysis for 60% to 1% in 50 years probability of exceedance for the city of Van in Turkey, using $AvgSa$ as an IM.

3.3.3 Record selection

Finally, a set of 15 records was produced based on CS($AvgSa$) (Kohrangi et al., 2017), using the mean scenarios in terms of mean magnitude ($\overline{M}$) and mean distance from rupture ($\overline{R}$).

The records were selected from the NGA-West2 database (Ancheta et al., 2013), without distinguishing between pulse-like and non-pulse-like or considering limitations for causal parameters (M, R and V_{S30}). Thus, it is assumed that the spectral shape can explain all the characteristics of the site's hazard and there is no need to specifically select the records that match with certain bins of M, R and V_{S30} or pulse/non-pulse earthquakes observed in the site of interest (for more details see Tarbali and Bredley, 2016). Figure 3.9 shows the selected records and the 2.5/50/97.5th percentiles of the CS target spectra at 2475 years return period for Van. The set is available at Kohrangi et al. (2018), together with the scale factors for the 2475 years return period CS.

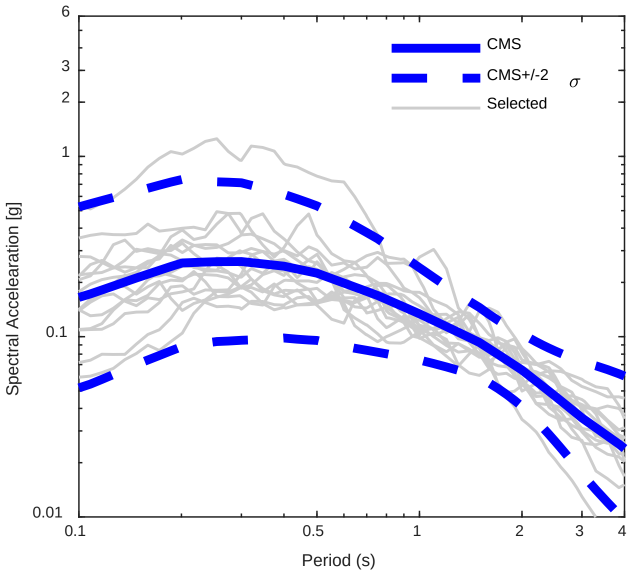

Figure 3.9: Set of 15 records and 2.5/50/97.5th percentiles of the CS at 2475 years return period, for the city of Van in Turkey, using $AvgSa$ as the conditioning IM.

3.4 Response History Analyses

3.4.1 Modelling and analysis parameters

All case studies were realized using SAP2000 structural analysis program, employing two 2D models for the simulation of the cross- and down-aisle direction, respectively. The models incorporated geometric nonlinearities via P-Δ formulation, and Rayleigh damping (Bathe, 2014) with viscous damping ratio of 3%. The ductility behaviour factor q_d was taken equal to 1.0, as brittle failure modes typically precede more ductile behaviours. Thus, the overstrength Ω of the system is the only component that contributes to the q-factor, i.e., q = Ω. Still, ARSWs are characterized by a high degree of optimization to minimize costs, leaving razor-thin overstrength margins. This means that even the selection of q = Ω = 1.5 should be in question. In this scope, all RHAs conducted herein used a q-factor of 1.0, meaning that the material behaviour of all elements and connections was assumed to be elastic and the verification checks do not account for any overstrength factors.

In contrast to the seismic design process, where different combinations were used for the seismic masses and seismic vertical loads, herein a common $G + 0.8{\cdot}Q$ was assumed. Moreover, while the 20% in 50 years design spectrum was used for design, here the records were scaled for an $AvgSa$ = 0.241 g, which corresponds to 10% in 50 years probability of exceedance (Table 3.5). Along the down-aisle direction, the section area of the bracing diagonals was reduced to 50%, as they are very slender and behave as tension-only members, except for CS5 where RHS braces were used. Finally, Table 3.6 contains the periods and mass participation factors for the first five modes of each structure. The geometric stiffness matrix was used for the modal analysis, accounting for the reduced stiffness of the structure due to P-Δ effects (Yang and McGuire, 1986). Evidently, all case studies share similar modal properties, having a relatively low mass participation factor on the first mode and thus, the contribution of higher modes is expected to be significant.

Table 3.6: Periods and mass participation factors for the five multi-depth ARSW case studies.

Dir.	Mode #	CS1		CS2		CS3		CS4		CS5	
		Period (sec)	**Mass Part.**	**Period (sec)**	**Mass Part.**	**Period (sec)**	**Mass Part.**	**Period (sec)**	**Mass Part.**	**Period (sec)**	**Mass Part.**
CA	1	1.63	63%	1.76	68%	2.00	64%	1.12	53%	0.97	62%
	2	0.49	17%	0.58	16%	0.61	19%	0.28	18%	0.23	18%
	3	0.26	5.4%	0.31	4.5%	0.32	5.3%	0.12	9.4%	0.11	8.6%
	4	0.18	1.8%	0.22	1.8%	0.22	1.7%	0.08	4.9%	0.08	3.8%
	5	0.15	0.7%	0.16	0.9%	0.18	0.7%	0.06	2.2%	0.06	1.9%
DA	1	1.39	60%	1.40	56%	1.06	57%	0.94	57%	1.43	55%
	2	0.49	19%	0.47	22%	0.30	23%	0.39	19%	0.35	17%
	3	0.32	4.0%	0.27	4.8%	0.18	5.9%	0.29	4.4%	0.28	5.4%
	4	0.27	1.3%	0.21	2.8%	0.15	2.0%	0.26	2.2%	0.21	6.7%
	5	0.23	0.5%	0.17	0.8%	0.14	0.6%	0.23	1.5%	0.18	0.9%

3.4.2 Verification checks and resistances

The seismic assessment of the ARSWs is conducted in the base of verification checks, by examining the time-history of utilization factors of the most important structural members and connections, which are illustrated in Table 3.1 and Figure 3.6. Specifically, the steel elements are checked according to EN 1993-1-1 (2005), EN 1993-1-3 (2006), and EN 15512 (2009), the steel bolted connections using EN 1993-1-8 (2005), and the base plates with bonded anchors using EN 1992-4 (2018). The individual verification checks for each structural component are summarized in Table 3.7.

Figure 3.10(a)-(j) show, for each case study, bar charts with the normalized member/connection axial resistances along the cross-aisle direction. On average, the buckling resistance ($N_{b,Rd}$) of the pallet uprights ("pu1" and "pu2" components) is equal to 55% of their tensile resistance ($N_{t,Rd}$) or, equivalently, the buckling reduction factor (χ_{min}) of "pu1" and "pu2" has a mean value of 0.55. The uplift resistance ($N_{anc,Rd}$) of the pallet anchorage ("panc") is on average equal to 19% of the $N_{t,Rd}$ of "pu1", with a coefficient of variance (CoV) of 0.51. This significant deviation on the resistance of the "panc" components, comes from the differences on the definition of the seismic mass and load combinations assumed among the case studies (Table 3.3). Moreover, as no special detailing is considered in the bolted connections of the pallet diagonals (i.e., the "pd1" and "pd2" components), their plastic resistance ($N_{pl,Rd}$) is always greater than the bolt shear resistance ($F_{v,Rd}$) or bearing failure resistance ($F_{b,Rd}$). Therefore, the pallet diagonals will not be able to develop a stable plastic failure mechanism during a seismic event. No specific trend holds for the failure mechanism of "pd1" and "pd2"; in some cases, flexural buckling is the dominant failure mode, in others the brittle bolt shear failure or the plastic ovalization of bolt's hole. An alternative design approach that utilizes the plastic ovalization mechanism of pallet diagonals' bolted connections is discussed in Chapter 4.

Likewise, Figure 3.11(a)-(j) contain bar charts with the dimensionless axial resistances for the down-aisle direction. The bracing uprights ("bu1" and "bu2" components) show similar behaviour to "pu1" and pu2", having a mean value of χ_{min} equal to 0.63. The bracing upright anchorage ("buanc") has a mean resistance equal to 11% the $N_{t,Rd}$ of "bu1" and a CoV of 0.41. The pallet beams ("pb1" and "pb2"), which are responsible for transferring the inertial loads from the "Pallet" to the "Bracing" CA Frames, have a mean $N_{b,Rd}$ equal to 20% the $N_{t,Rd}$ of "bu1". Finally, the bracing diagonals ("bd1" and "bd2") do not have a certain failure mode; net section rupture, bolt shear failure or plastic ovalization might be the dominant failure mechanism. Similarly to "pd1" and "pd2", the $N_{pl,Rd}$ of "bd1" and "bd2" is always greater than the connection resistances. It should be highlighted that the $N_{b,Rd}$ of the RHS bracing diagonals used in CS5 is greater than $F_{v,Rd}$, thus both compression and tension elements were kept in the analysis.

Table 3.7: Element/connection verification checks conducted during the seismic assessment of the five multi-depth ARSW case studies.

Component	**Checks**
Uprights (pu1, pu2, bu1, bu2)	Shear Tension Compression (A_{eff} was used) Bending Tension + Bending Compression + Bending Buckling (flexural, torsional, flexural torsional, distortional) Buckling + Bending
Diagonals (pd1, pd2, bd1, bd2)	Tension Compression (excluded for tension-only members) Buckling (excluded for tension-only members) Bolt shear failure Net section rupture Bearing failure of weakest steel plate involved in the connection
Beams (pb1, pb2, bb1, bb2)	Shear Tension Compression Bending Tension + Bending Compression + Bending Buckling (flexural) Buckling + Bending Hooked end-connection bending (excluded for pinned beams)
Anchors (panc, buanc, bdanc)	Tension steel failure Tension concrete breakout Tension combined pullout and concrete breakout Tension splitting failure Shear steel failure Shear concrete edge breakout Shear pryout failure

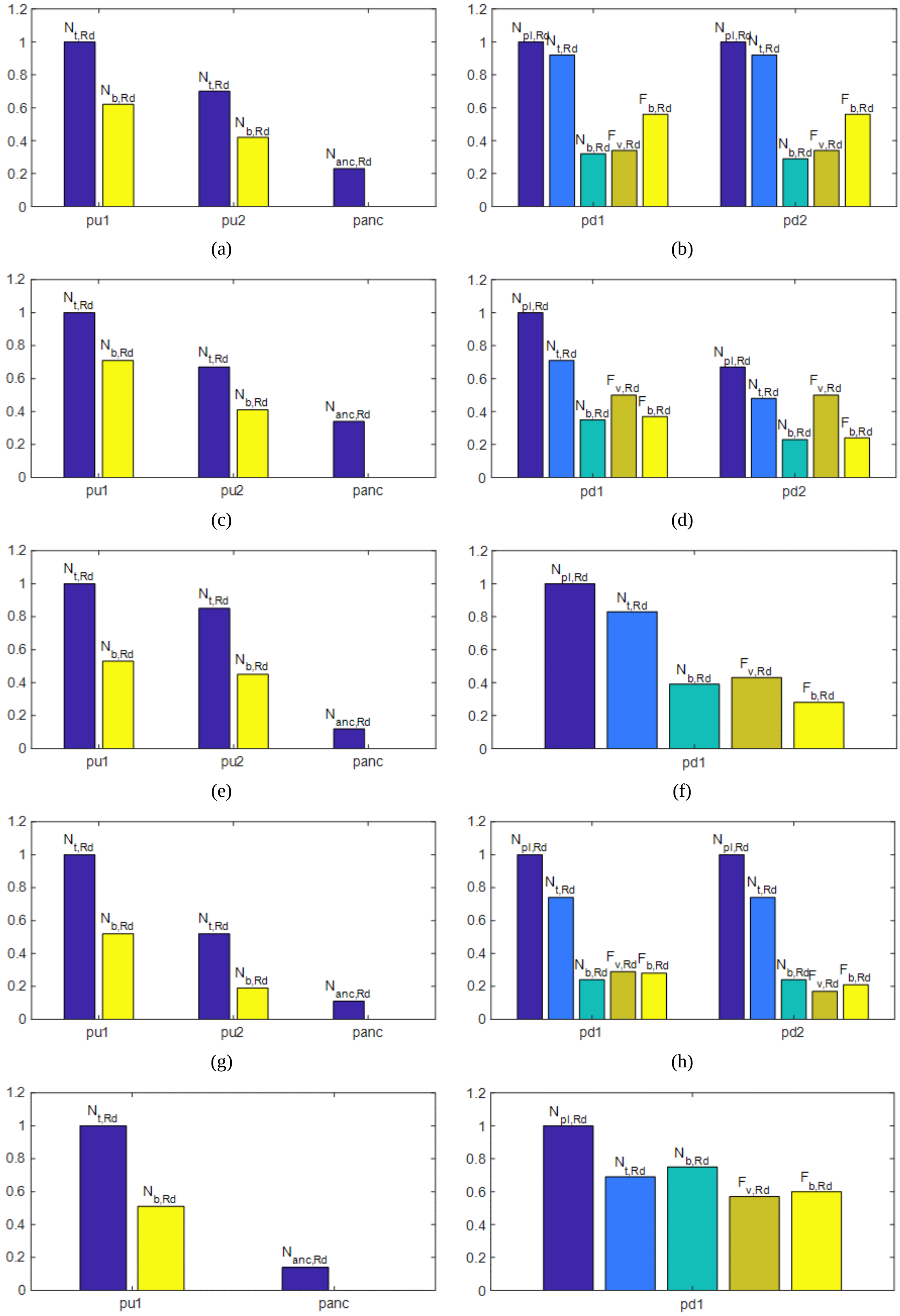

(a) (b)

(c) (d)

(e) (f)

(g) (h)

(i) (j)

Figure 3.10: Normalized member and connection resistances for the cross-aisle direction: (a)+(b), (c)+(d), (e)+(f), (g)+(h), and (i)+(f) are for CS1, CS2, CS3, CS4, and CS5 multi-depth ARSWs, respectively (see Table 3.1 for the description of the tag of each structural component).

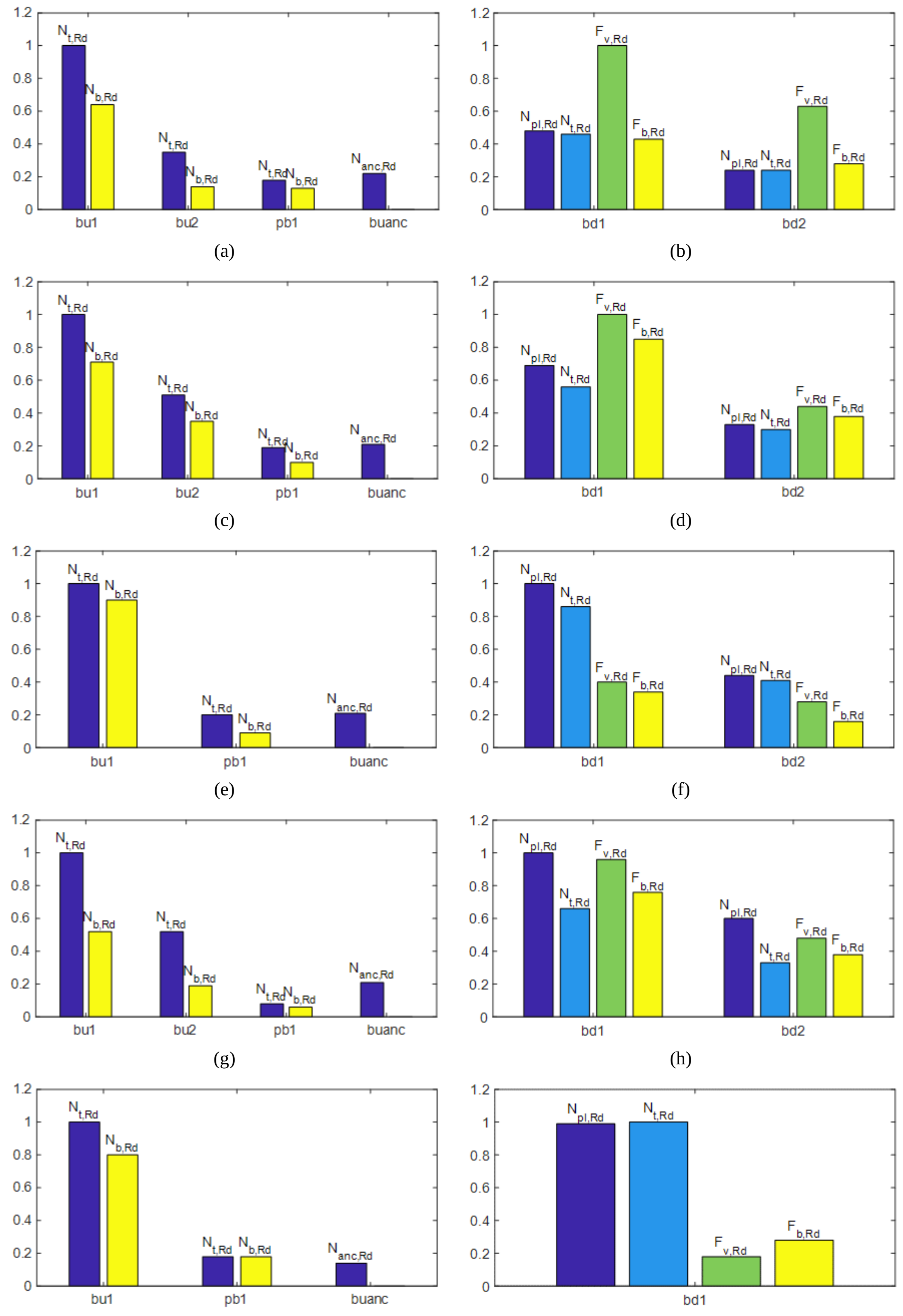

(a) (b)

(c) (d)

(e) (f)

(g) (h)

(i) (j)

Figure 3.11: Normalized member and connection resistances for the down-aisle direction: (a)+(b), (c)+(d), (e)+(f), (g)+(h), and (i)+(f) are for CS1, CS2, CS3, CS4, and CS5 multi-depth ARSWs, respectively (see Table 3.1 for the description of the tag of each structural component).

3.4.3 Hierarchy of criticalities

For each record, the time-history of stress resultants (i.e., forces and moments) and base reactions was used as input for the execution of the verification checks of Table 3.7. Figure 3.12(a)-(e) show boxplots with the utilization factors (UFs) of the most critical structural components along the cross-aisle direction, excluding the roofing elements. On average, the weakest component is the anchorage system of the pallet uprights (“panc”), having a mean UF of 2.45 and CoV of 0.53. The large deviation on the UFs of the “panc” components, highlights the potential risk of a seismic design based on MRSA, taking also into account that the anchors are typically designed with minimum overstrength tolerances. The next criticality is related to the pallet uprights (“pu1” and “pu2”), having a mean UF of 1.44 and CoV of 0.28. The least stressed components are the pallet diagonals (“pd1” and “pd2”) and their bolted connections, having an average UF equal to 1.05 and CoV equal to 0.32. This “overstrength” of the diagonals over the other components comes from a rule foreseen by EN 16681 (2016), which states that the diagonals and their connections should be designed by multiplying their design axial forces with the q-factor. As a result, even if “pd1” and “pd2” were capacity designed so that $N_{pl,Rd}$ was lower than the connection resistances, they would never have been able to exploit their plastic behaviour, as the brittle concrete cone failure and upright buckling come first in the hierarchy of criticalities.

Figure 3.13(a)-(e) show boxplots with the UFs of the most important structural elements and connections along the down-aisle direction. Again, the weakest component is the anchorage system of the bracing uprights (“buanc”), having a mean UF of 3.24 and CoV of 0.55. CS5 has exceptionally high UFs on the “buanc” components, due to the very low base uplift forces calculated by the seismic design. Recalling Table 3.3, CS5 was designed by adopting a seismic vertical load combination of $1.35 \cdot G + 1.5 \cdot Q$, which resulted in high gravitational loads on the bases of the uprights. Thus, the calculated uplift forces were deemed to be lower than expected. As a remedy, we suggest to use multiple vertical load combinations (e.g., $G + Q$ and $G + 0.8 \cdot Q$) during the seismic design, in order to create an envelope of UFs both for the structural elements and the base connections. Next in the hierarchy come the bracing diagonals (“bd1” and “bd2”), with their connections typically being more vulnerable than the members themselves, and the bracing uprights (“bu1” and “bu2”). The least critical components shown in the figures are the pallet beams (“pb1”). The bracing beams (“bb1” and “bb2”) were not shown, as they were typically under-stressed.

3.4.4 Effect of seismic design assumptions

The mean values of the UFs presented in Figure 3.12(a)-(e) and Figure 3.13(a)-(e), typically exceed the safety threshold 1.0. This is due to the fact that the RHAs did not consider all the favorable assumptions adopted in the MRSA, which are summarized in the cumulative seismic load multiplier factor, R_{cum} (see Eq. (3.9)). In the absence of experimental and analytical evidence that prove the applicability of such seismic design assumptions on the ARSWs, one should be cautious on accepting them all.

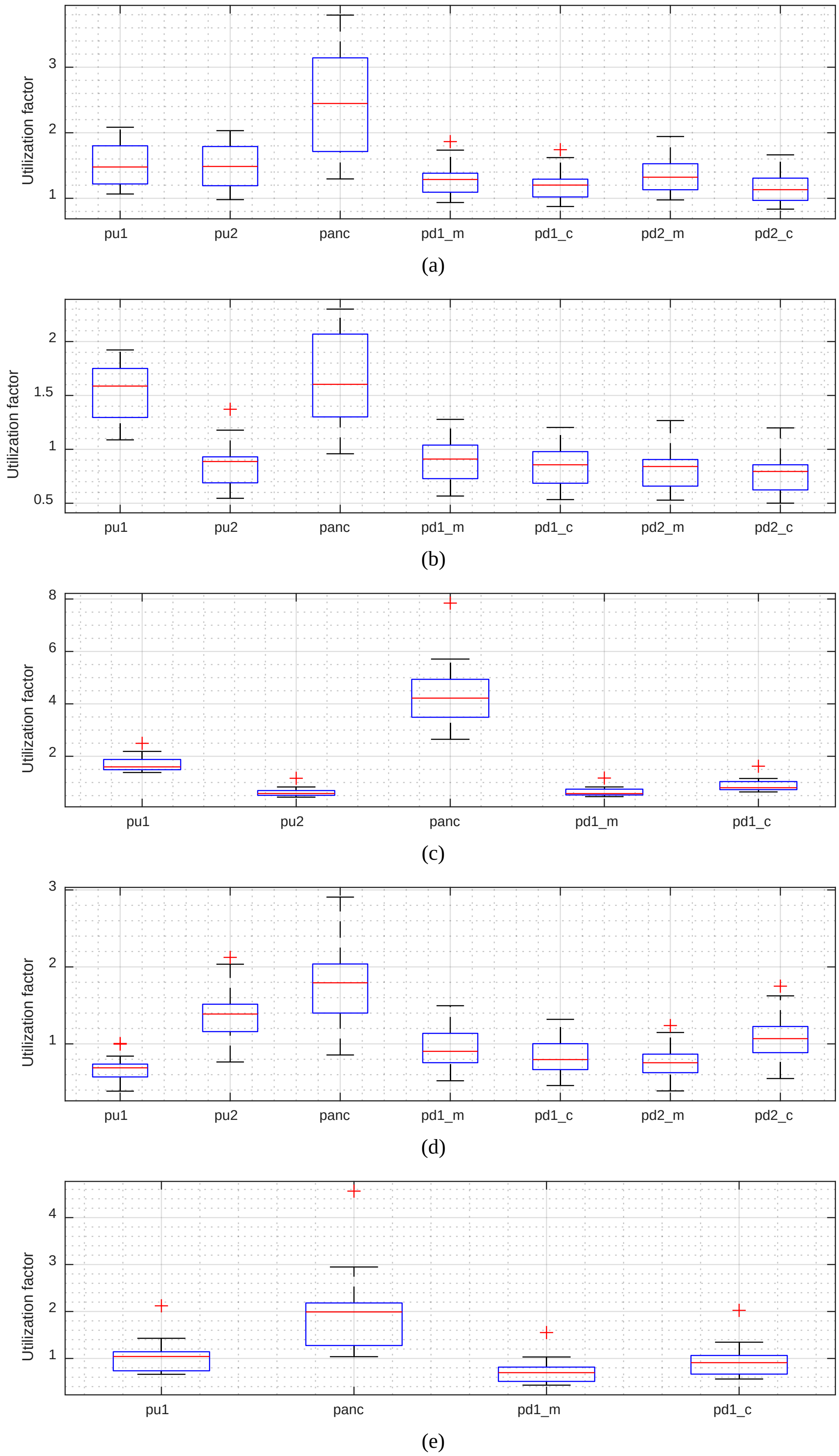

Figure 3.12: Boxplots with the utilization factors of the critical structural components along the cross-aisle direction for 15 RHAs scaled to IM that corresponds 10% in 50 years probability of exceedance, showing the: (a) CS1, (b) CS2, (c) CS3, (d) CS4, and (e) CS5 multi-depth ARSW (the suffixes “_m” and “_c” indicate member and connection resistances, respectively).

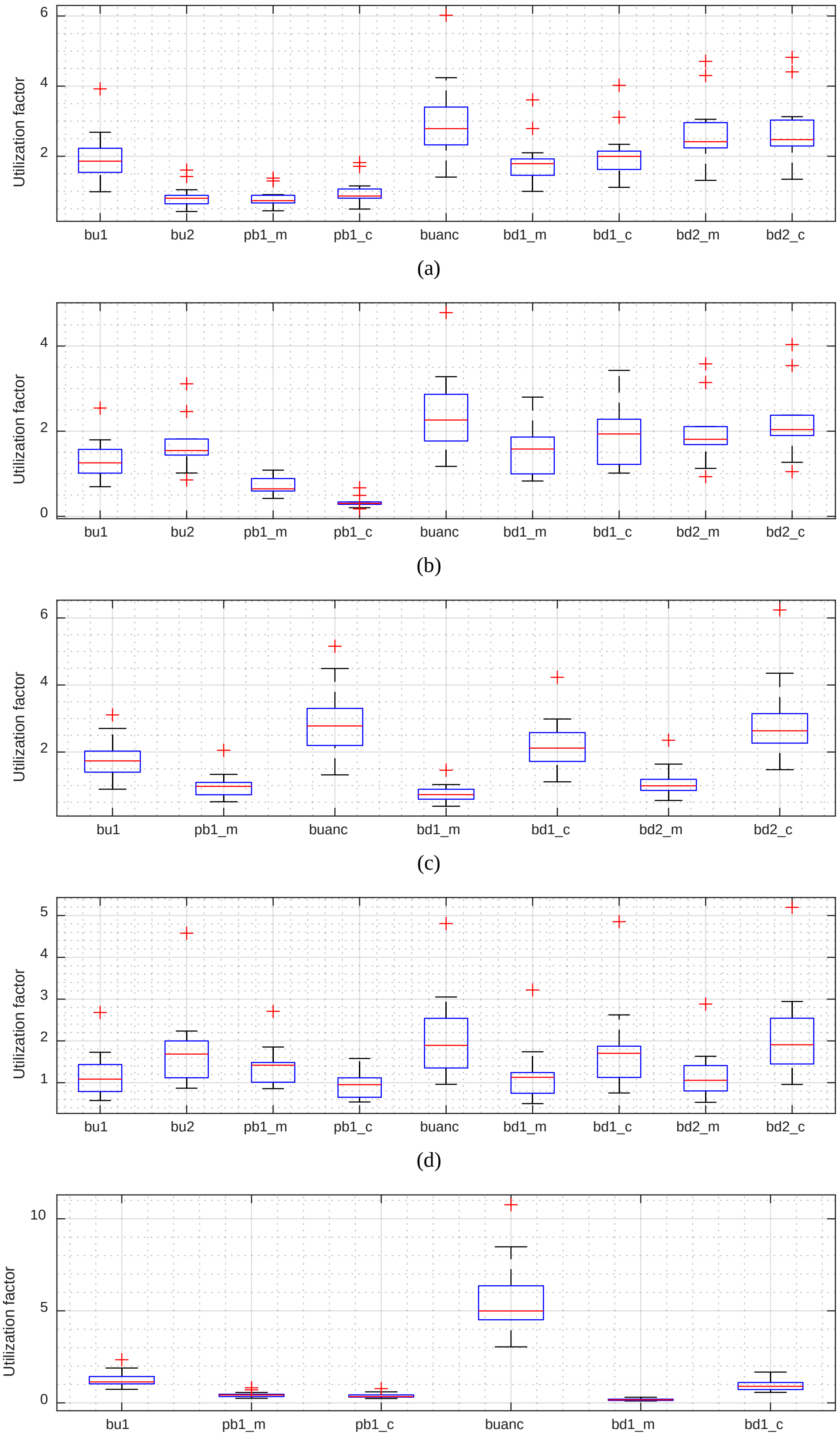

(a)

(b)

(c)

(d)

(e)

Figure 3.13: Boxplots with the utilization factors of the critical structural components along the down-aisle direction for 15 RHAs scaled to IM that corresponds 10% in 50 years probability of exceedance, showing the: (a) CS1, (b) CS2, (c) CS3, (d) CS4, and (e) CS5 multi-depth ARSW (the suffixes “_m” and “_c” indicate member and connection resistances, respectively).

To assess the effect of R_{cum} and its components, we realized a series of scenarios for each case study, where each scenario exploited a certain level of seismic load reduction. By progressively multiplying the UFs of the RHAs with the components of R_{cum} (i.e., γ_I, E_{D3}, R_m, R_q), we can derive what-if scenarios where, e.g., E_{D3} worked, but R_q did not. The effect of the E_{D1} factor on the UFs was not examined, as it was equal to 1.0 for all case studies. It should be noted that by directly multiplying the UFs of the RHAs with the seismic load reduction factors, one also decreases the part of the UFs coming from the gravitational loads. Thus, if UF_{G+Q} is the part of the UF coming from the vertical loads and the UF_E from the seismic loads, one should only reduce the latter part. Finally, the following five scenarios were considered:

- RHA: no seismic design assumption was made. Essentially, this is the basic scenario used to derive the UFs for the hierarchy of criticalities in the previous section. The UFs are calculated as $UF = UF_{G+Q} + UF_E$.
- RHA(γ_I): the γ_I factor was used. The UFs are calculated as $UF = UF_{G+Q} + \gamma_I \cdot UF_E$.
- RHA(γ_I, E_{D3}): the γ_I and E_{D3} factors were used. The UFs are calculated as $UF = UF_{G+Q} + (\gamma_I \cdot E_{D3}) \cdot UF_E$.
- RHA(γ_I, E_{D3}, R_m): the γ_I, E_{D3}, and R_m factors were used. The UFs are calculated as $UF = UF_{G+Q} + (\gamma_I \cdot E_{D3} \cdot R_m) \cdot UF_E$. Recalling Eq. (3.10), R_m is a factor of (a) the rack filling grade reduction factor, R_F, and (b) the combination coefficient, ψ_2. However, as the same R_F = 0.80 was used both in the MRSAs and the RHAs, R_m should not consider it twice, i.e., $R_m = \sqrt{\psi_2}$.
- RHA(γ_I, E_{D3}, R_m, R_q): the γ_I, E_{D3}, R_m, and R_q factors were used. The UFs are calculated as $UF = UF_{G+Q} + (\gamma_I \cdot E_{D3} \cdot R_m \cdot R_q) \cdot UF_E$. Regarding R_m, the same comment applies as in the previous case.

Figure 3.14(a)-(f) show boxplots with the UFs of the six most critical structural components in both directions, for each of the five scenarios described above. For brevity, we combined the results of all five case studies and 15 RHAs per case study, thus each boxplot resembles a 5·15 = 75 set of UFs. The mean (μ_{UF}), standard deviation (σ_{UF}), minimum, and maximum values of the boxplots are summarized in Table 3.8. A simple rule was used to assess the performance of each scenario: if the mean UF of a component does not exceed 1.0, i.e., $\mu_{UF} < 1.0$, then the scenario is characterized as safe for this specific component (see Table 3.8 for the “scenario-checks”). Theoretically, one should opt for a higher percentile (say 75-90%) of the UF value to be lower than 1.0 for added confidence, but this consideration will not be discussed further. As expected, in the first scenario (RHA) none of the six structural components passes the $\mu_{UF} < 1.0$ check. In the second scenario, the RHA(γ_I), the pallet diagonals (“pd1” and “pd2”) pass the check, but the rest five components do not. The third (RHA(γ_I, E_{D3})) and fourth (RHA(γ_I, E_{D3}, R_m)) scenarios show the same behaviour as the second, only being safe for the pallet diagonals. In the fifth scenario (RHA(γ_I, E_{D3}, R_m, R_q)), the pallet uprights (“pu1” and “pu2”), the bracing uprights (“bu1” and “bu2”), the bracing diagonals (“bd1” and “bd2”), and the pallet diagonals pass the check, but the anchorage systems (“panc” and “buanc”) do not.

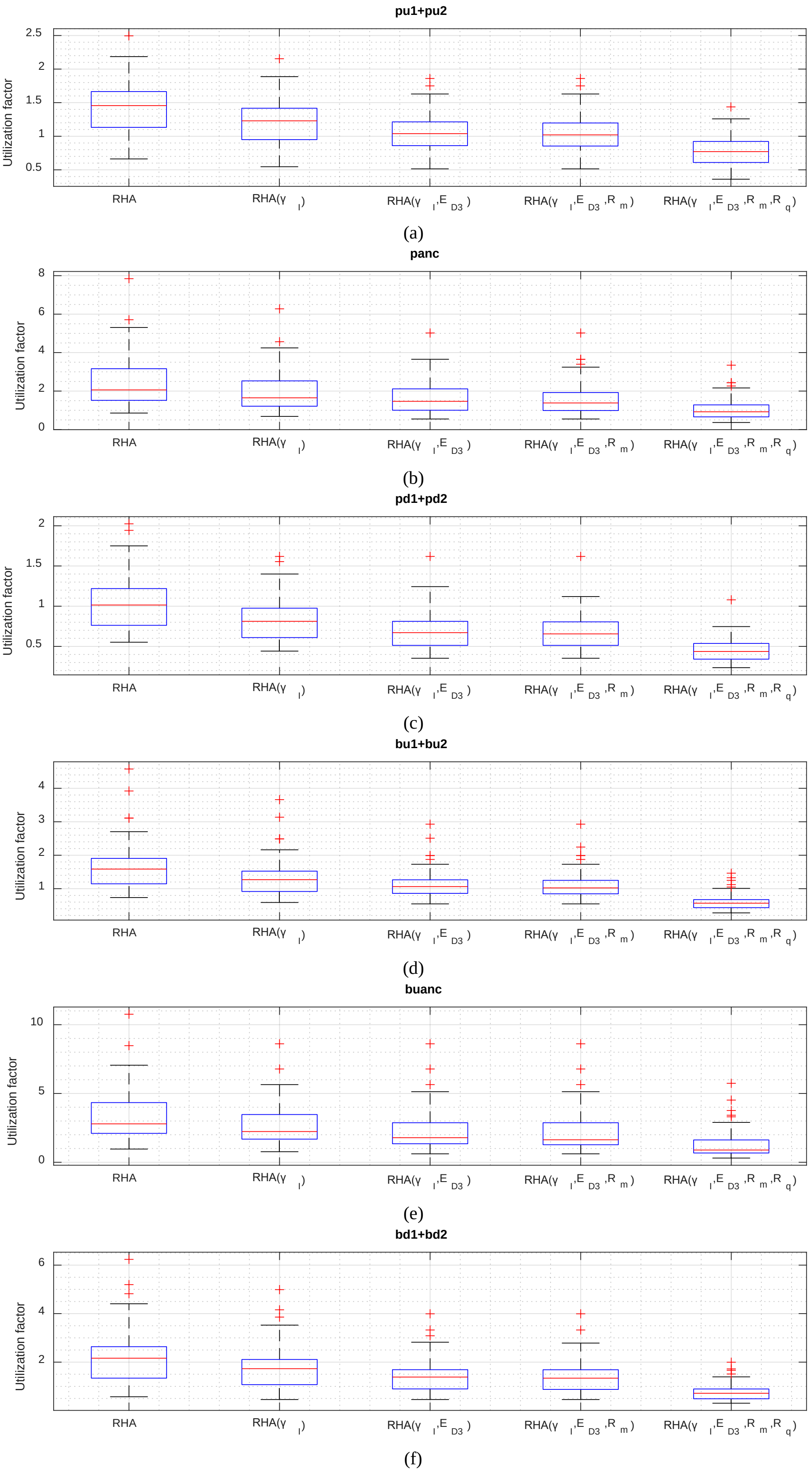

(f)

Figure 3.14: Boxplots with the utilization factors of the five scenarios of accepted seismic design assumptions, for the: (a) “pu1” and “pu2”, (b) “panc”, (c) “pd1” and “pd2”, (d) “bu1” and “bu2”, (e) “buanc”, and (f) “bd1” and “bd2” structural components (each boxplot has a size of 75 UFs, containing the results of all 5 case studies and 15 RHAs per case study).

Table 3.8: Statistics for the utilization factors displayed in Figure 3.14(a)-(f) and scenario checks.

Component	**Statistic**	**RHA**	**RHA(γ_I)**	**RHA(γ_I, E_{D3})**	**RHA(γ_I, , E_{D3}, R_m)**	**RHA(γ_I, E_{D3}, R_m, R_q)**
pu1+pu2	μ_{UF}	1.44	1.21	1.05	1.03	0.76
	σ_{UF}	0.40	0.35	0.29	0.28	0.22
	min(UF)	0.66	0.55	0.51	0.51	0.36
	max(UF)	2.50	2.15	1.86	1.86	1.43
	Check	✗	✗	✗	✗	✓
panc	μ_{UF}	2.45	1.96	1.63	1.60	1.06
	σ_{UF}	1.30	1.04	0.84	0.84	0.56
	min(UF)	0.86	0.68	0.55	0.55	0.37
	max(UF)	7.88	6.28	5.02	5.02	3.35
	Check	✗	✗	✗	✗	✗
pd1+pd2	μ_{UF}	1.05	0.84	0.70	0.68	0.45
	σ_{UF}	0.34	0.27	0.23	0.22	0.15
	min(UF)	0.55	0.44	0.35	0.35	0.24
	max(UF)	2.02	1.62	1.62	1.62	1.08
	Check	✗	✓	✓	✓	✓
bu1+bu2	μ_{UF}	1.69	1.35	1.12	1.09	0.61
	σ_{UF}	0.69	0.56	0.43	0.42	0.24
	min(UF)	0.74	0.59	0.55	0.55	0.28
	max(UF)	4.58	3.66	2.93	2.93	1.46
	Check	✗	✗	✗	✗	✓
buanc	μ_{UF}	3.24	2.59	2.26	2.22	1.31
	σ_{UF}	1.79	1.44	1.49	1.50	1.05
	min(UF)	0.96	0.77	0.62	0.62	0.31
	max(UF)	10.76	8.61	8.61	8.61	5.74
	Check	✗	✗	✗	✗	✗
bd1+bd2	μ_{UF}	2.18	1.74	1.43	1.39	0.76
	σ_{UF}	1.13	0.90	0.69	0.67	0.34
	min(UF)	0.57	0.46	0.46	0.46	0.30
	max(UF)	6.24	4.99	3.99	3.99	2.00
	Check	✗	✗	✗	✗	✓

Summing up the above, even if (a) the structural designer accepts a higher seismic risk by using the 20% in 50 years design spectrum, (b) the E_{D3} seismic reduction factor (which has not yet been proved experimentally for the ARSWs) works, and (c) the seismic mass that was assumed in the design is present during the earthquake event (i.e., the RHA(γ_I, E_{D3}, R_m) scenario), the designed ARSW will still be unsafe, as 5 out of its 6 critical components have $\mu_{UF} > 1.0$. Along with the (a), (b), and (c) conditions, the structure must also demonstrate a non-negligible overstrength Ω, which is reflected in the R_q reduction factor ($q = \Omega$, as there is no ductility in the systems). Indeed, by employing a q-factor between 1.5 and 2.0 (i.e., the RHA(γ_I, E_{D3}, R_m, R_q) scenario) the pallet and bracing uprights and diagonals have μ_{UF} values lower than 1.0. However, as stated before, the ARSWs are highly optimized structures, leaving razor-thin overstrength margins; the actual Ω of the structures may be lower than 1.5. Moreover, even in the most favorable scenario where all the assumptions worked properly, the pallet and bracing anchorage systems are still unsafe, having $\mu_{UF} = 1.06$ and $\mu_{UF} = 1.31$, respectively. Previous experience with structures exposed to high uplift forces due to earthquake excitations, has demonstrated that the anchors accumulate a significant amount of structural damage. For instance, the post-earthquake assessment of wine storage tanks after the 2013 New Zealand earthquake, has shown that 47% of the tanks sustained damage to their anchorage system (Yazdanian et al., 2020). A capacity design framework that increases the redundancy of the base connections by using the elastic uplift forces is proposed in Chapter 4.

3.5 Conclusions

A comprehensive study on the seismic performance of five multi-depth ARSWs has been conducted in Chapter 3. The case studies were designed by professional engineers according to the European standards EN 1993 (2005), EN 15512 (2009), and EN 16681 (2016), to be installed in the city of Van, Turkey. Despite the common installation site, same pallet-loading configuration and similar geometry, each case study adopted different seismic design assumptions (Table 3.3), due to the absence of a design standard specific for ARSWs. These design assumptions were combined into a so-called *cumulative seismic load multiplier*, R_{cum} (Eq. (3.9)), which majorly affects the design of ARSWs by decreasing the design seismic loads by almost 70%. However, some components of R_{cum} are not based on comprehensive scientific research, but instead come from limited studies on APRs and expert opinion.

To assess the seismic behaviour of the ARSW case studies, a series of 15 RHAs was conducted in each of their principal axes, using natural accelerograms that respect the hazard of Van in Turkey. Prior to the execution of the RHAs, the resistance of each structural component was determined. It was found that all case studies were vulnerable to brittle connection failures and abrupt member buckling modes, which prevent the structure from exploiting any ductility. In this sense, the RHAs were conducted without considering any material nonlinearities. Finally, the time-history of stress resultants and base reactions was used as input for the execution of the verification checks (Table 3.7), and a *hierarchy of criticalities* was defined in each direction.

Along the cross-aisle direction, the weakest component was typically the anchorage system of the pallet uprights. The UFs of the anchors were also characterized by a significant dispersion, which highlights the potential risk of a seismic design based solely on MRSA. The next criticality was related to the pallet uprights, being prone to local and global buckling failure. The least stressed components were the pallet diagonals and their bolted connections, as they had overstrength with respect to the other components. Along the down-aisle direction, again the anchorage system of the bracing uprights was first in the hierarchy of criticalities. Next come the bracing diagonals, with their connections typically being more vulnerable than the members themselves, and the bracing uprights. The least critical components were the pallet and bracing beams.

Finally, the effect of R_{cum} was investigated by realizing a series of scenarios for each case study, where each scenario exploited a certain level of seismic load reduction. It was found that, even if (a) the structural designer accepts a higher seismic risk, (b) the, somewhat-arbitrary, E_{D3} seismic reduction factor works, and (c) the seismic mass assumed in the design is present during the earthquake event, the designed ARSW was still unsafe, as most of its components had mean UFs greater than 1.0. By also employing a $q = \Omega > 1$, the UFs of the pallet and bracing uprights and diagonals fell under the 1.0 safety threshold. However, the ARSWs are highly optimized structures, leaving razor-thin overstrength margins; their actual Ω might be way lower than e.g., 1.5. Moreover, even in the most favorable scenario where all the assumptions worked properly, the pallet and bracing anchorage systems had mean UFs greater than 1.0. Concluding, while the size of the $5 \cdot 15 = 75$ RHA set was not big enough to draw general conclusions, still the results are indicative of the underlying risk in the design of ARSWs when using codes meant for conventional racks.

3.6 References

Adam C., Jäger C. (2012). *“Simplified collapse capacity assessment of earthquake excited regular frame structures vulnerable to P-delta”*, Engineering Structures, **44**, 159-173. https://doi.org/10.1016/j.engstruct.2012.05.036

Ancheta T.D., Darragh R.B., Stewart J.P., Seyhan E., Silva W.J., Chiou B.S.J., Wooddell K.E., Graves R.W., Kottke A.R., Boore D.M., Kishida T., Donahue J.L. (2013). *“PEER NGA-West2 Database”*, Technical Report PEER 2013/03. Pacific Earthquake Engineering Research Center, Berkeley, CA.

Baker J.W., Cornell C.A. (2006). *“Spectral shape, epsilon and record selection”*, **35**(9), 1077-1095. https://doi.org/10.1002/eqe.571

Baker J.W. (2010). *“Conditional Mean Spectrum: Tool for Ground-Motion Selection”*, Journal of Structural Engineering, **137**(3). https://doi.org/10.1061/(ASCE)ST.1943-541X.0000215

Bathe K.J. (2014). *“Finite Element Procedures”*, Klaus-Jürgen Bathe, second edition. ISBN-10: 0979004950

Bazzurro P., Cornell C.A. (1999). *“Disaggregation of seismic hazard”*, Bulletin of the Seismological Society of America, **89**(2), 501-520. https://doi.org/10.1785/BSSA0890020501

Black E.F. (2011). *“Use of stability coefficients for evaluating the $P-\Delta$ effect in regular steel moment resisting frames”*, Engineering Structures, **33**(4), 1205-1216. https://doi.org/10.1016/j.engstruct.2010.12.042

Boore D.M., Atkinson G.M. (2008). *“Ground-Motion Prediction Equations for the Average Horizontal Component of PGA, PGV, and 5%-Damped PSA at Spectral Periods between 0.01s and 10.0s”*, Earthquake Spectra, **24**(1). http://dx.doi.org/10.1193/1.2830434

Castiglioni C.A., Bernuzzi C., Hoffmeister B. (2014). *“Seismic behavior of steel storage pallet racking systems (SEISRACKS2).”*, Final Report, RFSR-PR-03114, European Commission, DG Research, Brussels, Belgium.

Cordova P., Deierlein G., Mehanny S.S.F., Cornell C.A. (2001). *“Development of a two-parameter seismic intensity measure and probabilistic assessment procedure”*, Journal of Engineering and Applied Sciences, **51**.

Cornell C.A., Jalayer F., Hamburger R.O. (2002). *“Probabilistic Basis for 2000 SAC Federal Emergency Management Agency Steel Moment Frame Guidelines”*, Journal of Structural Engineering, **128**(4). https://doi.org/10.1061/(ASCE)0733-9445(2002)128:4(526)

Eads L., Miranda E., Lignos D.G. (2015). *“Average spectral acceleration as an intensity measure for collapse risk assessment”*, Earthquake Engineering and Structural Dynamics, **137**(12), 2057-2073. https://doi.org/10.1002/eqe.2575

ECCS - European Convention for Constructional Steelwork, Technical Committee 1, Technical Working Group 1.3 (1986). *“Recommended testing procedure for assessing the behaviour of structural steel elements under cyclic loads”*, ECCS General Secretariat, Brussels, Belgium.

EN 15512 (2009). *“Steel static storage systems - Adjustable pallet racking systems - Principles for structural design”*, European Committee for Standardization (CEN), Brussels, Belgium.

EN 16681 (2016). *"Steel static storage systems - Adjustable pallet racking systems - Principles for seismic design"*, European Committee for Standardization (CEN), Brussels, Belgium.

EN 1990 (2002). *"Eurocode - Basis of structural design"*, European Committee for Standardization, Brussels, Belgium.

EN 1992-4 (2018). *"Eurocode 2: Design of concrete structures - Part 4: Design of fastenings for use in concrete"*, European Committee for Standardization, Brussels, Belgium.

EN 1993 (2005). *"Eurocode 3: Design of Steel Structures"*, European Committee for Standardization, Brussels, Belgium.

EN 1993-1-1 (2005). *"Eurocode 3: Design of Steel Structures - Part 1-1: General rules and rules for buildings"*, European Committee for Standardization, Brussels, Belgium.

EN 1993-1-3 (2006). *"Eurocode 3: Design of Steel Structures - Part 1-3: General rules - Supplementary rules for cord-formed members and sheeting"*, European Committee for Standardization, Brussels, Belgium.

EN 1993-1-8 (2005). *"Eurocode 3: Design of Steel Structures - Part 1-8: Design of joints"*, European Committee for Standardization, Brussels, Belgium.

EN 1998-1 (2004). *"Eurocode 8: Design of structures for earthquake resistance - Part 1: General rules, seismic actions and rules for buildings"*, European Committee for Standardization, Brussels, Belgium.

FEMA 356 (2000). *"FEMA 356, Prestandard and Commentary for The Seismic Rehabilitation of Buildings"*, Federal Emergency Management Agency, Washington, USA.

Giardini D., Woessner J., Danciu L., Crowley H., Cotton F., Grünthal G., Pinho R., Valensise G., Akkar S., Arvidsson R., Basili R. (2013). *"Seismic Hazard Harmonization in Europe (SHARE)"*. Online data resource, Swiss Seismological Service: ETH Zurich, Zurich, Switzerland, [Available at: http://www.efehr.org].

Kazantzi A., Vamvatsikos D. (2015). *"Intensity measure selection for vulnerability studies of building classes"*, Earthquake Engineering and Structural Dynamics, **44**(15), 2677-2694. https://doi.org/10.1002/eqe.2603

Kohrangi M., Bazzurro P., Vamvatsikos D., Spillatura A. (2017). *"Conditional spectrum-based ground motion record selection using average spectral acceleration"*, Earthquake Engineering and Structural Dynamics, **46**(10), 1667-1685. https://doi.org/10.1002/eqe.2876

Kohrangi M., Tsarpalis D., Vamvatsikos D. (2018). *"CS(AvgSA) consistent Records and Hazard curves for Van and Montopoli"*. STEELWAR Project. Link: http://users.ntua.gr/divamva/resources/SteelWAR_MontopoliVanRecords_2in50.rar

Lin T., Haselton C.B., Baker J.W. (2013a). *"Conditional spectrum-based ground motion selection. Part I: Hazard consistency for risk-based assessments"*, Earthquake Engineering and Structural Dynamics, **42**(12), 1847-1865. https://doi.org/10.1002/eqe.2301

Lin T., Haselton C.B., Baker J.W. (2013b). *"Conditional spectrum-based ground motion selection. Part II: Intensity-based assessments and evaluation of alternative target spectra"*, Earthquake Engineering and Structural Dynamics, **42**(12), 1867-1884. https://doi.org/10.1002/eqe.2303

Maheri M.R., Akbari R. (2003). *"Seismic behaviour factor, R, for steel X-braced and knee-braced RC buildings"*, **25**(12), 1505-1513. https://doi.org/10.1016/S0141-0296(03)00117-2

Pagani M., Monelli D., Weatherill G., Danciu L., Crowley H., Silva V., Henshaw P., Butler L., Nastasi M., Panzeri L., Simionato M., Vigano D. (2014). *"OpenQuake Engine: An Open Hazard (and Risk) Software for the Global Earthquake Model"*, Seismological Research Letters, **85**(3), 692-702. https://doi.org/10.1785/0220130087

SAP2000, CSI, Computers and Structures Inc., homepage: https://www.csiamerica.com

STEELWAR (2017). *"Advanced structural solutions for automated STEELrack supported WARehouses"*, The Steelwar Project Consortium, Pisa, Italy. https://www.unipi.it/index.php/risultati-e-prodotti/item/10663-steelwar

Talebian N., Benoit P.G., Baldassino N., Karampour H. (2018). *"Factors contributing to the transverse shear stiffness of bolted cold-formed steel storage rack upright frames with channel bracing members"*, Thin-Walled Structures, **136**, 50-63. https://doi.org/10.1016/j.tws.2018.12.001

Tarbali K., Bradley B.A. (2016). *"The effect of causal parameter bounds in PSHA-based ground motion selection"*, Earthquake Engineering and Structural Dynamics, **45**(9), 1515-1535. https://doi.org/10.1002/eqe.2721

Tsarpalis D., Vamvatsikos D., Vayas I. (2021). *"Seismic assessment approaches for mass-dominant sliding contents: The case of storage racks"*, Earthquake Engineering and Structural Dynamics, **51**(4), 812-831. https://doi.org/10.1002/eqe.3592

Vamvatsikos D., Cornell C.A. (2005). *"Developing efficient scalar and vector intensity measures for IDA capacity estimation by incorporating elastic spectral shape information"*, Earthquake Engineering and Structural Dynamics, **34**(13), 1573-1600. https://doi.org/10.1002/eqe.496

Vamvatsikos D., Fragiadakis M. (2009). *"Incremental dynamic analysis for estimating seismic performance sensitivity and uncertainty"*, Earthquake Engineering and Structural Dynamics, **39**(2), 141-163. https://doi.org/10.1002/eqe.935

Vamvatsikos D. (2014). *"Accurate Application and Second-Order Improvement of SAC/FEMA Probabilistic Formats for Seismic Performance Assessment"*, Journal of Structural Engineering, **140**(2). https://doi.org/10.1061/(ASCE)ST.1943-541X.0000774

Vamvatsikos D., Bakalis K., Kohrangi M., Pyrza S., Castiglioni C.A., Kanyilmaz A., Morelli F., Stratan A., D' Aniello M., Calado L., Proença J.M., Degee H., Hoffmeister B., Pinkawa M., Thanopoulos P., Vayas I. (2020). *"A risk-consistent approach to determine EN1998 behaviour factors for lateral load resisting systems"*, Soil Dynamics and Earthquake Engineering, **131**. https://doi.org/10.1016/j.soildyn.2019.106008

Whittaker A., Hart G., Rojahn C. (1999). *"Seismic Response Modification Factors"*, Journal of Structural Engineering, **125**(4). https://doi.org/10.1061/(ASCE)0733-9445(1999)125:4(438)

Yang Y.B., McGuire W. (1986). *"Stiffness Matrix for Geometric Nonlinear Analysis"*, Journal of Structural Engineering, **112**(4). https://doi.org/10.1061/(ASCE)0733-9445(1986)112:4(853)

Yazdanian M., Ingham J.M., Kahanek C., Dizhur D. (2020). *"Damage to flat-based wine storage tanks in the 2013 and 2016 New Zealand earthquakes"*, Journal of Constructional Steel Research, **168**. https://doi.org/10.1016/j.jcsr.2020.105983

4 Plastic Ovalization Strategy

4.1 Introduction

The high importance of warehousing facilities to the logistics sector raises the demand for racking structures that are resilient to extreme hazards. A disruption to the supply chain, or even worse, a destruction of stockpiled goods, might lead to economic losses that are far greater than the initial cost of the supporting rack. This is true especially for the innovative ARSWs, as they play a dual role in the warehousing process, supporting the wares and at the same time offering protection from the external environment. In this sense, the owners of high-rise ARSWs may be willing to pay for a slightly more expensive, yet less vulnerable structure, in order to mitigate the risk of a temporary shutdown or complete loss of their property.

One straightforward option to decrease the seismic risk, is a brute increase of strength by using heavier, and thus stronger, steel sections. This can be done either by increasing the design seismic forces (e.g., by using the 10% in 50 years design spectrum instead of the 20% in 50 years), or by tasking inherent overstrength to increase the safety margin, rather than employing it to reduce section size (e.g., use a $q = \Omega = 1.0$). While such approaches can help an ARSW safely resist somewhat higher hazards, they do not guard against disproportionate impact due to local brittle failures, and as such they can be problematic for rare events with higher return periods. Indeed, modern seismic design codes like EN 1998-1 (2004), do not recommend adopting a low-dissipative approach when designing steel structures in high seismicity areas, as the lack of load redistribution means that a local failure of a component can initiate the complete collapse of the structure.

A more agile approach to this problem is to increase the ductility of the rack, by exploiting the plastic behaviour of certain components, while keeping the rest of the structure in the elastic zone (Tsarpalis et al., 2020). However, such a new design strategy should respect the philosophy of the rack industry, which demands thin-walled steel sections with very simple bolted/hooked connections, minimizing the effort during the installation and disassembly process.

To enhance the seismic behaviour of the ARSWs along the down-aisle direction, an intuitive solution is to reinforce the bracing towers, by adopting capacity design rules similar to those of braced frames in typical steel buildings (Brandonisio et al., 2012). As found in Chapter 3, the bracing towers accumulate most of the seismic loads. This comes very handy for the development of a reliable plastic failure mechanism, as one may apply the costly rules of capacity design only on few parts of the structure, herein the bracing towers. For instance, heavy upright sections and complicated bracing connections can be adopted in the stiff bracing towers, while the typical profiles can be used for the more flexible pallet uprights and beams, as they only serve as a medium to carry gravity loads and transfer the inertial forces to the stiff braces.

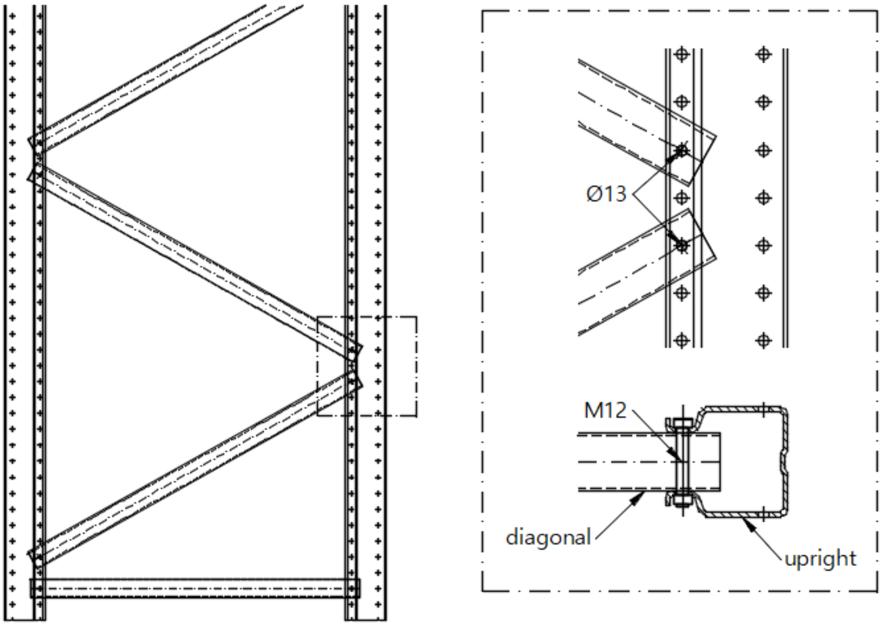

Figure 4.1: Typical diagonal-to-upright bolted connection, using an M12 bolt with two shear planes.

On the other hand, the achievement of a plastic mechanism along the cross-aisle direction is a more tedious task, as the seismic loads are distributed almost evenly along the individual upright frames. This means that one has to increase the ductility of all upright frames in order to develop a global ductile behaviour. As the upright frames are basically braced frames, a potential source of ductility are the diagonals (“pd1” and “pd2” components in Figure 3.6(a)). However, the diagonal-to-upright bolted connection is typically realized with only one M10 or M12 bolt, potentially with two shear planes to increase the connection resistance, as illustrated in Figure 4.1. As a result, the resistance of the connection is not sufficiently high to allow the diagonal member to yield and enter the nonlinear zone. This is illustrated in the right column of Figure 3.10, which shows that the plastic resistance of the diagonals ($N_{pl,Rd}$) is always greater than the bearing strength ($F_{b,Rd}$) and the bolt shear resistance ($F_{v,Rd}$) of the connection.

The creation of an over-resistant diagonal-to-upright connection that would resolve the aforementioned capacity-design incompatibility is one of the most interesting outcomes of the STEELWAR (2017) European project. Still, per the author’s experience in racking technology, it requires the introduction of additional bolts, plates, or even welds, which complicate the installation process. Moreover, “X-type” bracing has to be adopted in the upright frames, as in the more common “D-type”, if the diagonal under compression buckles, there is no diagonal under tension to arrest the formation of a weak/soft level. Herein, we will investigate a humbler solution of seismic improvement, the so-called plastic ovalization strategy (POS), which relies on the plastic ovalization of the diagonal bolt holes to keep all brittle failure mechanisms at bay.

POS is expected to increase the overall ductility of the upright frames only by a certain amount, without aiming to achieve the high q-factors, e.g., 4.0 (Brandonisio et al., 2012), typical of steel braced frames. On the positive side, it does not require an over-resistant diagonal-to-upright connection, while less-demanding capacity design rules can be employed. Moreover, as the diagonals do not buckle, the typical “D-type” of bracing can be used, allowing designers and manufactures to stay within their comfort zone in terms of design and construction practices. Two case studies will be examined in this chapter, one double- and one multi-depth ARSW. Their cross-aisle direction will be re-designed according to the new capacity design rules proposed for the POS, and a comprehensive seismic assessment will be performed to compare the performance of the POS with the standard design approaches.

4.2 Theoretical concept and design rules

4.2.1 Failure modes of a shear bolted connection

Steel bolted joints, which comprise one of the most efficient methods of connecting steel members onsite, are characterized by the interaction between their constituent bolts and steel plates. Six distinct modes of failure can be identified in a shear bolted connection (Draganić et al., 2014): (I) end failure, which is further discretized to (Ia) shear, or (Ib) tearing end failure, (II) bearing failure, (III) net section failure, (IV) bolt failure, (V) block tear out failure, and (VI) bolt pull-through failure (Figure 4.2). From all six modes, Mode (II), the bearing failure, is considered to be the most ductile. Indeed, pure bearing failure involves the plastic ovalization of the bolt holes, allowing for large deformations of the connection, to as much as the bolt diameter before material rupture (Kiymaz, 2009). However, excessive hole elongations might lead to impractical displacements and, thus, they need to be controlled under the service loads (Kiymaz, 2009).

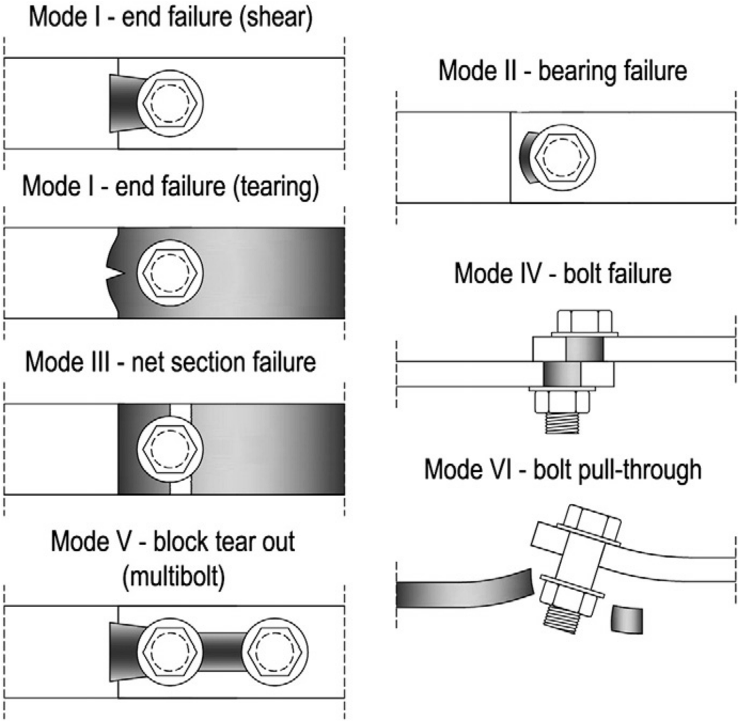
Mode I - end failure (shear)
Mode I - end failure (tearing)
Mode III - net section failure
Mode V - block tear out (multibolt)
Mode II - bearing failure
Mode IV - bolt failure
Mode VI - bolt pull-through

Figure 4.2: Failure modes on a shear bolted connection (Draganić et al., 2014).

On the other hand, the current European (EN 1993-1-8, 2005) and American (AISC, 2005) specifications, aggregate the six failure modes of a shear bolted connection to only four mechanisms: (1) block tear out failure, (2) bearing failure, (3) net section failure, and (4) bolt shear failure. Essentially, they combine Modes (Ia) and (V) into mechanism (1), while Modes (Ib) and (VI) are considered to be covered by the resistance of mechanism (2), the bearing failure (Draganić et al., 2014; Može and Bek, 2014). Specifically in Europe, EN 1993-1-8 (2005) offers the following equation for the calculation of block tear out resistance (i.e., mechanism (1)) under concentric loading:

$$V_{eff,1,Rd} = \frac{A_{nt} \cdot f_u}{\gamma_{M2}} + \frac{A_{nv} \cdot f_y}{\sqrt{3} \cdot \gamma_{M0}} \qquad \text{Eq. (4.1)}$$

where $V_{eff,1,Rd}$ is the design block tear out resistance, f_u is the nominal ultimate tensile strength of the steel plate, f_y is the yield stress, A_{nt} is the net area subjected to tension, A_{nv} is the net area subjected to shear, and γ_{M2} and γ_{M0} are partial safety factors equal to 1.25 and 1.0, respectively.

The bearing resistance of a steel plate (i.e., mechanism (2)) is influenced mostly by the proximity of the plate hole to the plate boundaries and the additional restraint provided by the nut and bolt head (Kiymaz, 2009). EN 1993-1-8 (2005) uses the following expression for the calculation of the design bearing resistance per bolt and shear plane:

$$F_{b,Rd} = \frac{k_1 \cdot a_b \cdot f_u \cdot d \cdot t}{\gamma_{M2}} \qquad \text{Eq. (4.2)}$$

where $F_{b,Rd}$ is the design bearing resistance of the plate per bolt and shear plane, d is the bolt diameter, and t is the thickness of the steel plate. The coefficients a_b and k_1 are defined as follows:

- Parallel to the direction of load transfer

$$a_b = \min\left\{a_d,\ \frac{f_{ub}}{f_u},\ 1\right\} \qquad \text{Eq. (4.3)}$$

$$a_d = \frac{e_1}{3 \cdot d_0} \quad \text{, for end bolts} \qquad \text{Eq. (4.4)}$$

$$a_d = \frac{p_1}{3 \cdot d_0} - \frac{1}{4} \quad \text{, for inner bolts} \qquad \text{Eq. (4.5)}$$

- Perpendicular to the direction of load transfer

$$k_1 = \min\left\{2.8 \cdot \frac{e_2}{d_0} - 1.7,\ 1.4 \cdot \frac{p_2}{d_0} - 1.7,\ 2.5\right\} \quad \text{, for end bolts} \qquad \text{Eq. (4.6)}$$

$$k_1 = min\left\{1.4 \cdot \frac{p_2}{d_0} - 1.7,\ 2.5\right\} \quad \text{, for inner bolts} \qquad \text{Eq. (4.7)}$$

where f_{ub} is the nominal ultimate tensile strength of the bolt, d_0 is the diameter of the hole, e_1, p_1, e_2, and p_2 are the edge and inner distances of the bolts, as shown in Figure 4.3. Notably, EN 1993-1-3 (2006) offers a slightly modified formula of $F_{b,Rd}$ that is applicable only on thin-walled cold formed members, but it will not be discussed herein for brevity.

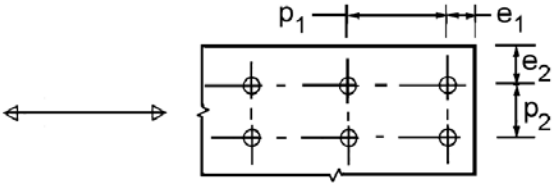

Figure 4.3: Edge and inner distances of a bolt layout according to EN 1993-1-8 (2005).

The net cross-section resistance (i.e., mechanism (3)) entails the fracture limit of a plate with holes in tension. According to EN 1993-1-1 (2005), it is calculated as:

$$N_{u,Rd} = \frac{0.9 \cdot A_{net} \cdot f_u}{\gamma_{M2}} \qquad \text{Eq. (4.8)}$$

where $N_{u,Rd}$ is the design ultimate resistance of the net cross-section of the plate and A_{net} is the net area of the plate section.

Finally, in mechanism (4) the resistance is given as:

$$F_{v,Rd} = \frac{a_v \cdot f_{ub} \cdot A}{\gamma_{M2}} \qquad \text{Eq. (4.9)}$$

where $F_{v,Rd}$ is the design shear resistance per bolt and shear plane. When the shear plane passes through the unthreaded portion of the bolt, A is taken equal to the gross cross section of the bolt and a_v is equal to 0.6. When the shear plane passes through the threaded portion, A is taken equal to the tensile stress area of the bolt (A_s) and a_v depends on the class of the bolt; for classes 4.6, 5.6, and 8.8, a_v is equal to 0.6, while for 4.8, 5.8, 6.8, and 10.9 equal to 0.5. Notably, in the rack industry it is quite common to have bolts working in the threaded part in a diagonal-to-upright bolted connection. Finally, if for each bolt $F_{v,Rd} \geq F_{b,Rd}$ holds, then the bolted connection is characterized as ductile, and the total bearing resistance is equal to the sum of the bearing resistances of the individual bolts.

Even though bearing failure is considered to be ductile on static loading conditions, its cyclic behaviour has not been investigated thoroughly yet. One of the main reasons is that on typical steel structures the bolted connections are designed with overstrength, so that during a seismic event, yielding and buckling of the diagonal braces occurs before any connection failure (EN 1998-1, 2004). According to the author’s knowledge, the only available data on the seismic behaviour of bolted connections subject to bearing failure are related to steel corrugated shear wall systems (e.g., Stojadinovic and Tipping 2007; Vigh et al., 2013; Vigh et al., 2014). It was observed that the failure mechanism was initiated by ovalization of the sheet holes, followed by screw tilt and ultimately pull out, resulting in a pinched hysteretic behaviour.

4.2.2 Proposed capacity design rules

The proposed plastic ovalization strategy (POS) relies on the plastic deformation of the diagonal-to-upright bolted connection, mainly due to the elongation of the bolt hole. As mentioned previously, an over-resistant diagonal-to-upright connection may come at odds with the philosophy of the racking structures that prefers simple connections without any additional plates and welds. As a remedy, POS exploits the ductility of the bearing failure mechanism by employing capacity design rules both in the connections and the members of the upright frame, which are presented in the next paragraphs.

Diagonals and diagonal-to-upright connections

The design of the diagonals and the diagonal-to-upright connections shall ensure the occurrence of bearing failure before any other failure mechanism of the diagonal, by adopting the following rules (all resistances below are expressed as the total resistance of the connection, i.e., if a connection has one bolt with two shear planes, $F_{v,Rd}$ is two times the resistance of the bolt in each shear plane):

- **POS 1**: The bolt shear resistance ($F_{v,Rd}$) should be 1.20 times greater than the bearing resistance of the diagonal's hole ($F_{b,d,Rd}$):

$$F_{v,Rd} \geq 1.20 \cdot F_{b,d,Rd}$$

- **POS 2**: The bearing resistance of the upright's hole ($F_{b,u,Rd}$) should be 1.20 times greater than the bearing resistance of the diagonal's hole ($F_{b,d,Rd}$):

$$F_{b,u,Rd} \geq 1.20 \cdot F_{b,d,Rd}$$

- **POS 3**: The net section resistance of the diagonal ($N_{u,Rd}$) should be 1.20 times greater than the member's bearing resistance ($F_{b,d,Rd}$):

$$N_{u,Rd} \geq 1.20 \cdot F_{b,d,Rd}$$

- **POS 4**: The buckling resistance of the diagonal ($N_{b,Rd}$) should be 1.20 times greater than the member's bearing resistance ($F_{b,d,Rd}$):

$$N_{b,Rd} \geq 1.20 \cdot F_{b,d,Rd}$$

- **POS 5**: The bearing resistance of the diagonal in tension and in compression, $F_{b,d,Rd}^{+}$ and $F_{b,d,Rd}^{-}$, respectively, should not differ by more than 10%. This can be achieved with the introduction of an empty hole in the direction of the load that is adjacent to the bolt hole and away from the member end.
- **POS 6**: Rule 8.1.6e of EN 16681 (2016) that governs the design of the diagonals and their connections by multiplying the seismic forces by the behavior factor of q, should be discarded.
- **POS 7**: The overstrength factor 1.20 employed in rules POS 1 to POS 4, may be reduced by appropriate testing that ensures the occurrence of bearing strength failure before any other failure mechanism of the diagonal and its connection.

Rules POS 1 and POS 3 are introduced to prevent the brittle bolt shear failure and net section rupture, respectively. Rule POS 2 is meant to ensure that the bolt hole elongation only occurs on the easily replaceable diagonal and does not unduly impact the section of the upright, potentially damaging its buckling capacity. POS 4 protects the diagonal member from abrupt buckling and thus allows designers to employ bracing patterns with diagonals working both in tension and in compression, like the typical "D-type" bracing. On the other hand, rule POS 5 is employed to achieve a symmetric cyclic behaviour of the connection, while rule POS 6 aims to reduce diagonals' overstrength with respect to the connected uprights. Finally, POS 7 is introduced to “reward” structural designers that employ experimental tests to reliably calculate the resistances of the involved members and connections.

Non-dissipative elements

The uprights, the horizontal braces, and the roof truss (i.e., the non-dissipative elements) shall be designed to remain in the elastic region under the design seismic loads. This can be achieved by employing the following capacity design rules:

- **POS 8**: The uprights should be designed by computing the design axial forces (N_{Ed}), shear forces (V_{Ed}), and bending moments (M_{Ed}) as following:

$$N_{Ed} = N_{Ed,G} + 1.1 \cdot \gamma_{ov} \cdot \Omega_{min} \cdot N_{Ed,E}$$

$$M_{Ed} = M_{Ed,G} + 1.1 \cdot \gamma_{ov} \cdot \Omega_{min} \cdot M_{Ed,E}$$

$$V_{Ed} = V_{Ed,G} + 1.1 \cdot \gamma_{ov} \cdot \Omega_{min} \cdot V_{Ed,E}$$

where:

$N_{Ed,G}$, $M_{Ed,G}$, and $V_{Ed,G}$ are the compression force, bending moment, and shear force in the upright due to the non-seismic actions included in the combination of actions for the seismic design situation;

$N_{Ed,E}$, $M_{Ed,E}$, and $V_{Ed,E}$ are the compression force, bending moment, and shear force in the upright due to the seismic actions;

γ_{ov} is the overstrength factor equal to 1.25;

Ω_{min} = max{$\Omega_{min,L}$, $\Omega_{min,U}$}, and $\Omega_{min,L}$ and $\Omega_{min,U}$ are the minimum overstrengths of the braces connected to the lower and the upper half of upright frame’s height, respectively. In other words, first we divide the upright frames into two equal vertical segments and we compute the utilization factor for each diagonal. Then we take the maximum utilization factor of the lower and the upper part ($UF_{max,L}$ and $UF_{max,U}$, respectively), and we compute the $\Omega_{min,L}$ = $1/UF_{max,L}$ and $\Omega_{min,U}$ = $1/UF_{max,U}$.

One may notice that, contrarily to the capacity design rules for typical steel columns, Ω_{min} has a constant value along the height of the upright frame. In its classical form, the Ω factor is calculated for each diagonal, and it is used to increase the seismic forces and moments of the column element it intersects with. However, this would have required to continuously modify the bearing resistance of the diagonals (e.g., by adjusting the distance of the bolt hole to the member end, or the e_1 parameter), to achieve a uniform distribution of Ωs. To keep things simple, we decided to adopt the $\Omega_{min,L}$ & $\Omega_{min,U}$ concept, but it should be stressed that it is a first-guess capacity rule; if the re-assessment of the case studies reveals weaknesses in the uprights, stricter rules will be proposed.

- **POS 9**: The horizontal braces and the roof truss should be designed by computing the design forces and moments as follows:

$$N_{Ed} = N_{Ed,G} + 1.1 \cdot \gamma_{ov} \cdot \Omega_{min} \cdot N_{Ed,E}$$

$$M_{Ed} = M_{Ed,G} + M_{Ed,E}$$

$$V_{Ed} = V_{Ed,G} + V_{Ed,E}$$

In contrast to rule POS 8, rule POS 9 does not multiply the design seismic moments and shear forces by the factor of $1.1 \cdot \gamma_{ov} \cdot \Omega_{min}$, as the horizontal braces and the roof elements are usually (a) simulated as truss elements that work only axially and (b) under-stressed with respect to the uprights and diagonals.

Base connections

The connection of the upright frames to the concrete slab comprises the weakest component of the ARSWs along the CA direction (see Chapter 3). Specifically, the anchorage system was the only component with a mean UF greater than 1.0, even in the scenario where all favourable assumptions were made (Table 3.8). To decrease the vulnerability of the base connections to high uplift seismic loads, the following rule is proposed:

- **POS 10**: The base connections should be designed by multiplying the design base reactions by the q-factor used in the seismic design analysis. Additionally, they shall be verified using two load scenarios for the gravitational loads: $G + 0.8 \cdot Q$ and $G + Q$ (G and Q represent the dead and the unit loads, respectively).

4.3 Numerical study on the behaviour of the diagonal bolt hole in bearing

4.3.1 Existing analytical expressions

The POS approach relies on the ductility of the diagonal-to-upright connection for the development of a reliable plastic failure mechanism. Thus, an accurate determination of the force and displacement capacity of this connection is of high importance. Lately, experimental and analytical studies have showed that the well-known formula of EN 1993-1-8 (2005), as given in Eq. (4.2), underestimates the bearing resistance of a bolted connection (Može et al., 2021). Indeed, the revised prEN 1993-1-8:2021 (2021) proposes a new formula for the bearing resistance that depends on the relative end-distance e_1 / d_0 or the spacing between the bolts p_1 / d_0, while it is independent of the distance perpendicular to the bearing force:

$$F_{b,Rd}^{(2021)} = \frac{k_m \cdot a_b^{(2021)} \cdot f_u \cdot d \cdot t}{\gamma_{M2}} \qquad \text{Eq. (4.10)}$$

where $F_{b,Rd}^{(2021)}$ is the design bearing resistance per prEN 1993-1-8:2021 (2021), k_m is 1 except for steel grades equal to or greater than S460, for which k_m is 0.9. The coefficient $a_b^{(2021)}$ is given as:

$$a_b^{(2021)} = \begin{cases} \min\left(\frac{e_1}{d_0},\ 3 \cdot \frac{f_{ub}}{f_u},\ 3\right) & \text{, for end bolt} \\ \min\left(\frac{p_1}{d_0} - \frac{1}{2},\ 3 \cdot \frac{f_{ub}}{f_u},\ 3\right) & \text{, for inner bolt} \end{cases} \qquad \text{Eq. (4.11)}$$

The new formula of the bearing resistance in Eq. (4.10) does not account for distances e_2 and p_2, which are assumed to be sufficiently high to prevent fracture in the net area in tension. Otherwise, the design resistance of the connection is indirectly controlled by the design for block tear out (Eq. (4.1)) or the net cross-section resistance (Eq. (4.8)).

Regarding the displacement capacity of the connection, experimental results have demonstrated that the bearing deformation of the bolt hole can be of magnitude of one bolt diameter, d (Kiymaz, 2009). Draft prEN 1993-1-8:2021 (2021) provides a method for the calculation of the bearing deformation at bolt holes at or before yielding:

$$\bar{\sigma}_b = \frac{126 \cdot u/d}{\left(1 + \sqrt{30 \cdot u/d}\right)^2} \qquad \text{Eq. (4.12)}$$

where $\bar{\sigma}_b$ is the normalized bearing stress, u is the embedding of the bolt that causes a local yielding at the edge of the bolt hole, i.e., the bearing deformation. The embedding u is carried out up to 80% of the maximum bearing resistance for grades up to S460 and up to full bearing resistance for S460 and higher grades, as shown in Figure 4.4. Afterwards, the stress-deformation relationship is linear (hardening for grades up to S460, perfectly plastic for higher ones) until the achievement of the bolt hole ultimate deformation given by (Može et al., 2021):

$$u_{Xd} = \min\left(\frac{k_m \cdot a_b^{(2021)}}{3}, k_m^2\right) \cdot d \qquad \text{Eq. (4.13)}$$

Given the normalized bearing stress, $\bar{\sigma}_b$, the bearing force per bolt can be calculated as:

$$F_b(u) = \bar{\sigma}_b(u) \cdot d \cdot t \cdot f_u \qquad \text{Eq. (4.14)}$$

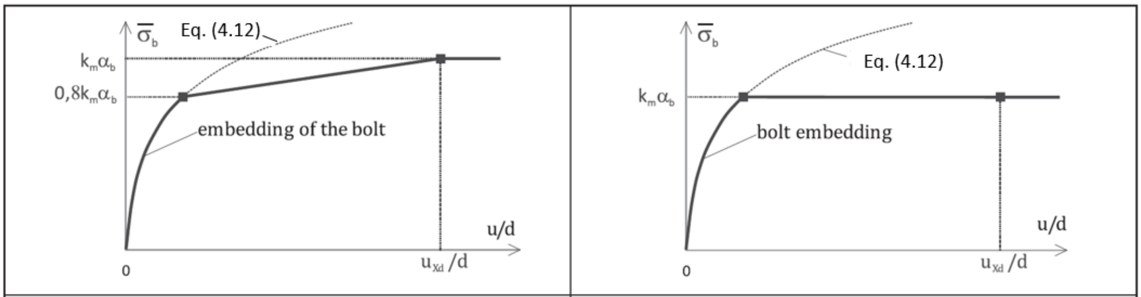

a) Steel grades up to S460 ($k_m = 1$)

b) Steel grades equal to and greater than S460 ($k_m = 0.9$)

Figure 4.4: Bearing deformation behaviour (adopted from Može et al., 2021).

4.3.2 Numerical simulation of tension/compression quasi-static tests

Combining Eq. (4.13) and Eq. (4.14), one may derive an analytical expression for the nonlinear force-displacement curve of the diagonal-to-upright connection, which can later be used to define a zero-length material (or axial spring) to represent the connection behaviour at the ends of each diagonal. However, the aforementioned equations are based on experimental and analytical studies on steel plates thicker than the typical diagonal of an upright frame. As a result, the plastic or hardening post-yield behaviour shown in Figure 4.4 might not be realized on a thin-walled diagonal element. To shed light to this issue, a series of parametric numerical analyses was conducted, simulating quasi-static tension and compression tests on a universal testing machine (UTM), as shown in Figure 4.5.

The test setup was designed to prevent all failure modes except bearing of the diagonal hole. It consists of one diagonal element made of steel S355MC with 500 mm length, that is bolted to two thick end plates (S235JR, t = 15 mm), using M12 10.9 bolts. Each end of the diagonal has two holes, one bolt hole with end distance e_1 = 40 mm and one empty hole at p_1 = 49 mm. The empty hole is used to satisfy capacity design rule POS 5, i.e., to have “equal” bearing resistance in tension and in compression. To achieve this, the hole-to-hole distance p_1 was calculated by taking the equality of the right parts of Eq. (4.4) and Eq. (4.5) Finally, one end plate is fixed, while the other one is attached to the (virtual) UTM actuator that imposes positive or negative displacement increments until failure of the test specimen.

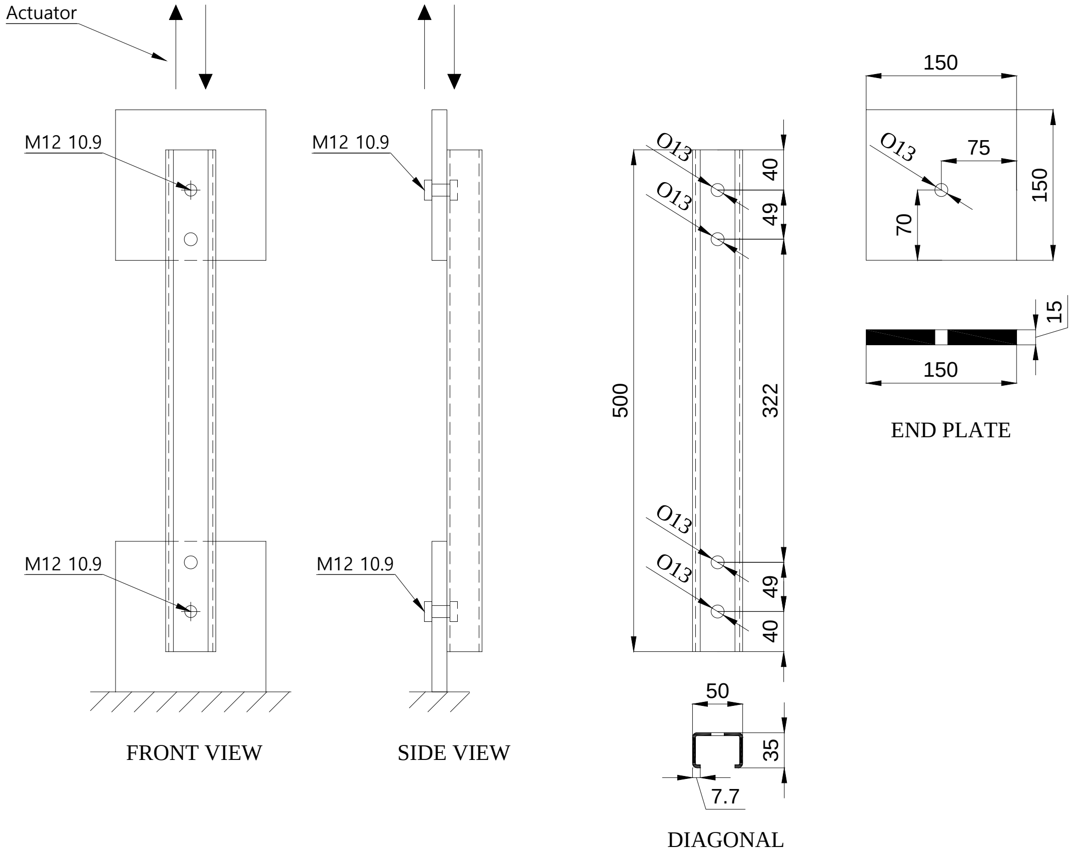

Figure 4.5: Test setup of quasi-static tension/compression numerical tests on a UTM.

The numerical models were realized using the finite element software ABAQUS v6.14 (2014). All components were modelled as deformable homogeneous solids and meshed by linear brick finite elements with eight nodes, reduced integration, and hourglass control (C3D8R). Due to symmetry, only the upper half of the test assembly was considered (Figure 4.6(a)), while symmetric boundary conditions were adopted at the symmetry plane. Moreover, a relatively simple numerical model of the M12 10.9 bolt was built, in order to simplify the modelling and reduce the computational load (Figure 4.6(d)). A “hard” surface-to-surface contact formulation in the normal direction was defined between the bolt, the steel plate, and the diagonal. In the tangential direction, a friction coefficient of 0.1 was adopted between all components, together with a minor pretension of the bolt equal to 5 kN, to improve the stability of the numerical model. An elastic-plastic behaviour was adopted for all structural steel materials. The elastic behaviour was defined by Young's modulus and Poisson's ratio of E = 210,000 MPa and ν = 0.3, respectively. The von Mises yield surface was used to define isotropic yielding. The true stress and strain of each steel material were evaluated to match the results of tensile tests found in the literature. The nominal values of the yield and ultimate stresses were considered; for S235JR f_y = 235 MPa and f_u = 360 MPa, while for S355MC f_y = 355 MPa and f_u = 510 MPa.

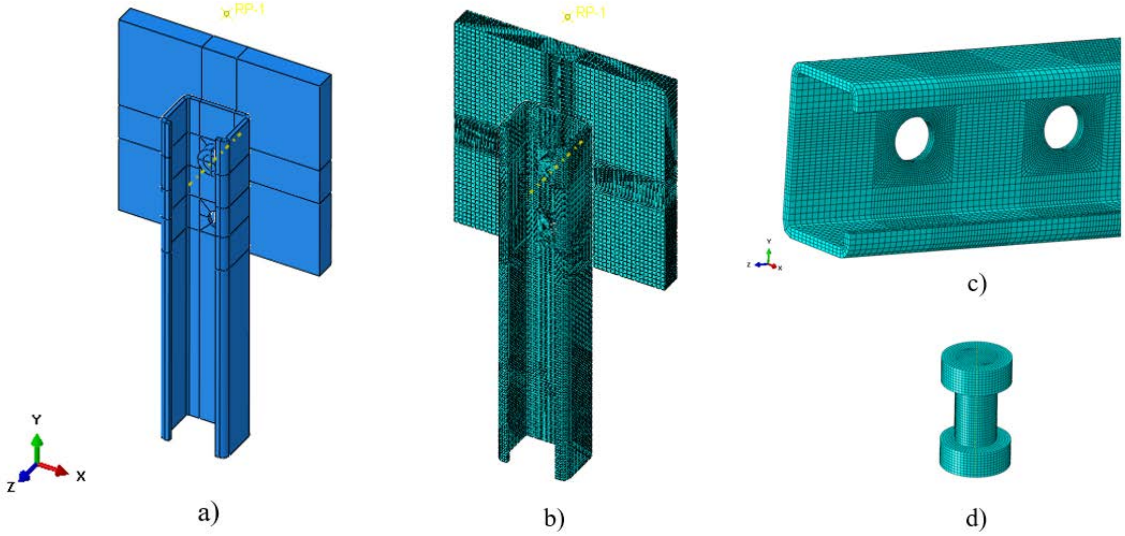

Figure 4.6: Numerical model of the UTM numerical tests: a) model assembly, b) model mesh, c) mesh refinement near the holes, and d) bolt mesh.

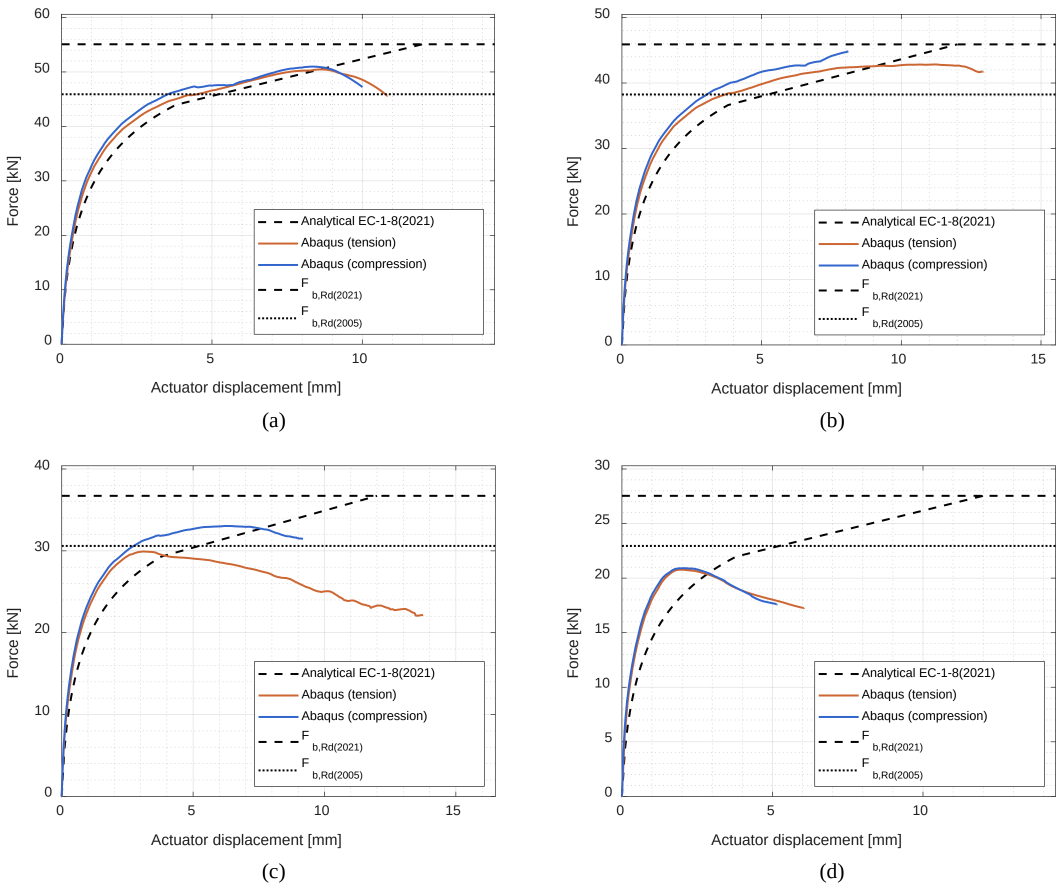

(a)

(b)

(c)

(d)

Figure 4.7: Analytical (EN 1993-1-8:2005 and 2021) versus numerical (ABAQUS) force-displacement curves of the quasi-static compression/tension tests, for diagonals of (a) 3 mm, (b) 2.5 mm, (c) 2 mm, and (d) 1.5 mm thickness.

The parametric study considered four diagonal thicknesses that are typically used in the rack industry, namely 3.0 / 2.5 / 2.0 / 1.5 mm. For each realization, one tension and one compression numerical test was conducted and compared to the bearing resistance calculated by Eq. (4.2) of EN 1993-1-8 (2005), as well as the force-displacement curve of prEN 1993-1-8:2021 (2021) using Eq. (4.13) and Eq. (4.14). The results can be found in Figure 4.7(a)-(d).

Interestingly, the analytical expressions of prEN 1993-1-8:2021 (2021) accurately predict the development of plastic ovalization for diagonals with 3 and 2.5 mm thickness, both in terms of stiffness deterioration and ultimate bearing resistance. Moreover, for these thicknesses the connection demonstrated adequate ductility, as the displacement capacity was almost equal to one bolt diameter. One the other hand, prEN 1993-1-8:2021 (2021) poorly predicted the numerical results for the diagonals with 2 and 1.5 mm thickness, indicating that the analytical formulae of Eq. (4.13) and Eq. (4.14) are mainly applicable for thicker steel plates. Especially for the 1.5 mm diagonal, the finite element models failed to converge due to excessive local deformations at about 6 mm of actuator displacement. Furthermore, the connection reached its peak capacity at 2 mm, far earlier than thicker diagonals, entering a negative stiffness descending branch, rather than a ductile or hardening plateau. The 2 mm thick diagonal was only marginally better, especially in compression.

An explanation of this significant difference between the behaviour of the 3 mm and the 1.5 mm diagonal, can be found in Figure 4.8, which compares their deformed shapes at a displacement increment where the thin diagonal started losing its capacity. While the failure mode of the thick diagonal was pure bearing, the thin one was characterized by a combination of bearing failure and local buckling of the diagonal’s web in the proximity of the bolt hole. This local buckling was initiated after the steel material near the bolt hole entered the plastic zone, which, combined with the low thickness of the diagonal’s section, led to an early loss of strength.

This negative stiffness behaviour is not necessarily detrimental for the ductility of the member or the structure, as it seems fairly stable and it extends at with low slope to non-negligible displacement. Still, it introduces uncertainties regarding the estimation of the ultimate strength and displacement, which are not conducive to a safe design without considerable investigation. Therefore, in order to avoid over-complicating the POS approach, one may aim to avoid it.

While the numerical analyses offered are not enough in number to draw general conclusions, they still indicate that the thickness of the diagonal or, more conveniently, the normalized ratio d/t may majorly affect the bearing failure mechanism if local buckling occurs. Another factor that may exacerbate this phenomenon is the width of the diagonal’s web (b); assuming a uniform distribution of normal stresses along the section of the diagonal, a long web is more prone to local buckling than a short one. To test the sensitivity of the diagonal-to-upright connection to the b/d ratio, an additional series of four numerical analyses was conducted, this time by adjusting b, from 70 mm down to 40 mm. The parametric study used the 1.5 mm thickness diagonal, as, based on the previous analyses, it ensures that for b = 50 mm (i.e., the base case of Figure 4.5) the web will buckle locally.

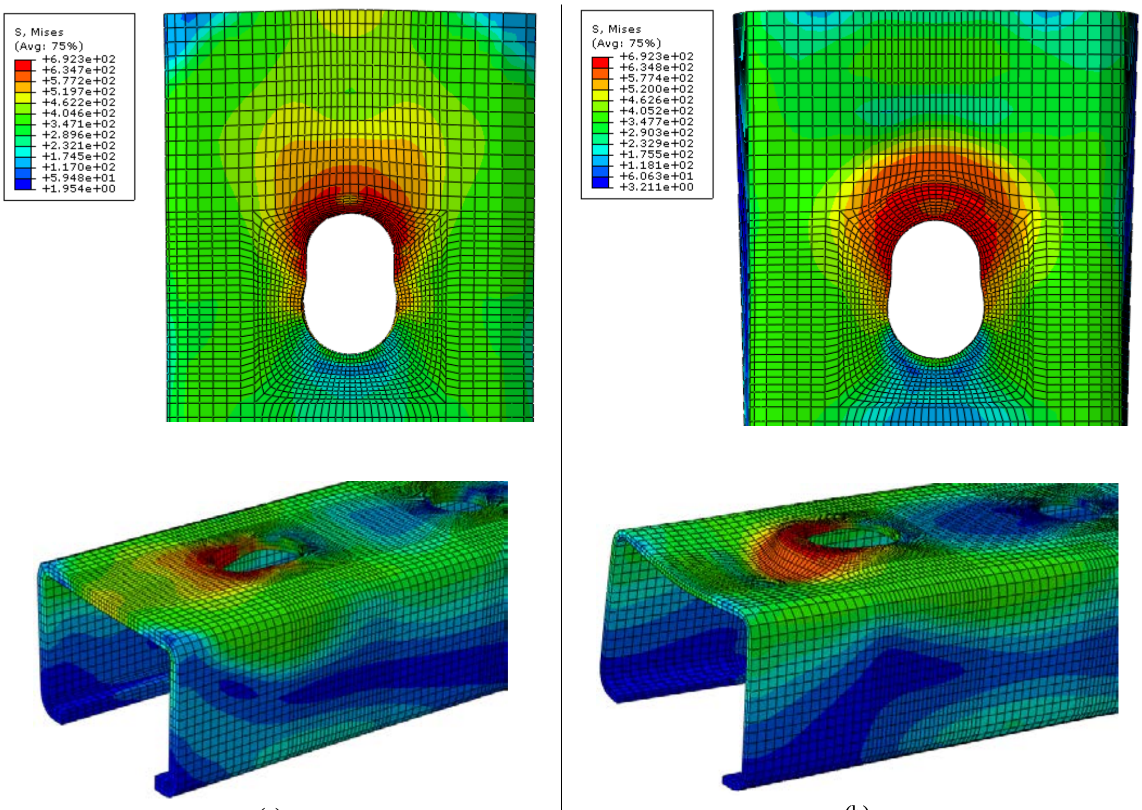
S, Mises
(Avg: 75%)
+6.923e+02
+6.347e+02
+5.772e+02
+5.197e+02
+4.622e+02
+4.046e+02
+3.471e+02
+2.896e+02
+2.321e+02
+1.745e+02
+1.170e+02
+5.948e+01
+1.954e+00
S, Mises
(Avg: 75%)
+6.923e+02
+6.348e+02
+5.774e+02
+5.200e+02
+4.626e+02
+4.052e+02
+3.477e+02
+2.903e+02
+2.329e+02
+1.755e+02
+1.181e+02
+6.063e+01
+3.211e+00

(a) (b)

Figure 4.8: Deformed shapes and stress fields near the bolt hole for the (a) 3 mm and (b) the 1.5 mm diagonal thickness.

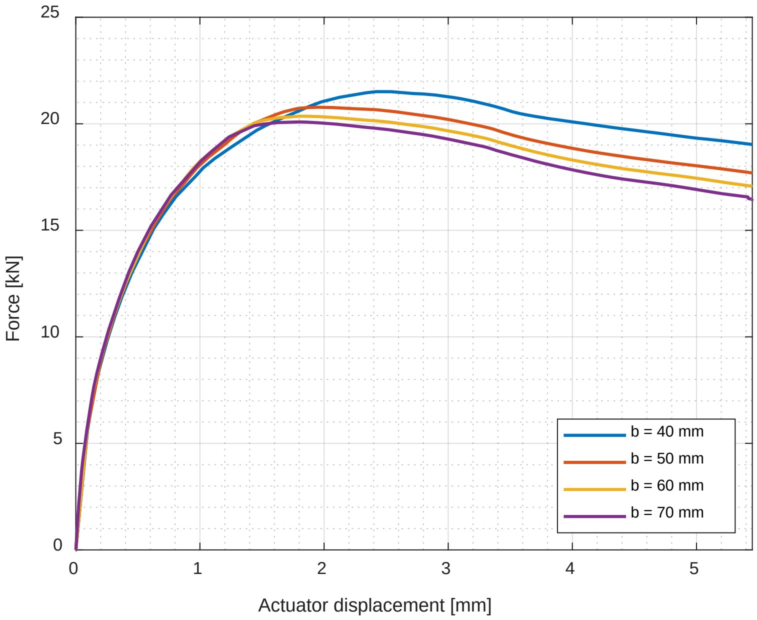

Figure 4.9: Numerical force-displacement curves of the (virtual) UTM tension tests, for the 40 mm, 50 mm, 60 mm, and 70 mm width of the diagonal's web.

Figure 4.9 illustrates the force-displacement curves for the four test specimens. Evidently, the web width has a minor effect on the behaviour of the connection, with the shorter webs leading to only slightly improved ultimate resistance. This independence of the failure mode from the b/d ratio can be explained by examining the deformed shapes and stress fields of the diagonals in Figure 4.10. As high plastic strains are localized in the proximity of the bolt hole, only a small part of the diagonal participates in the failure mechanism and, therefore, d/t dominates the behaviour of the connection rather than b/d. Based on the limited results presented, a limit of $d/t < 5$ seems like a reasonable constraint that ensures reaching the prEN 1993-1-8:2021 estimate of the bearing strength while maintaining adequate ductility.

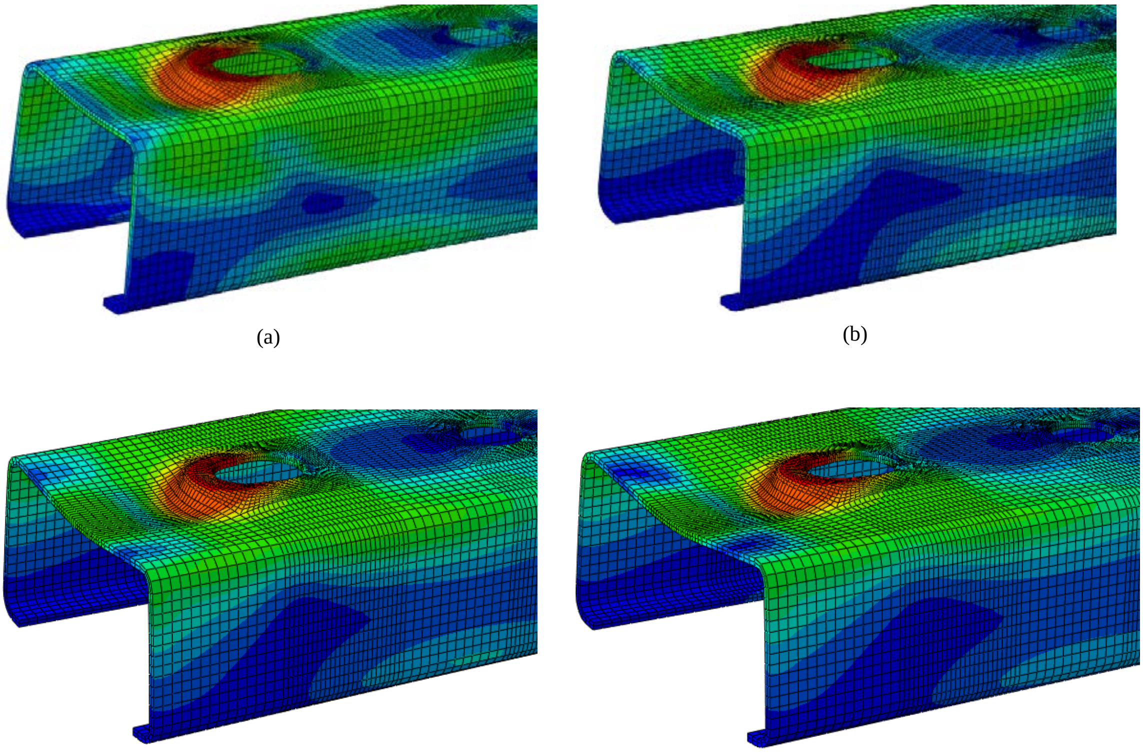
(a) (b)

(c) (d)

Figure 4.10: Deformed shapes and stress fields near the bolt hole at 5 mm of (virtual) actuator displacement for the (a) 40 mm, (b) 50 mm, (c) 60 mm, and (d) 70 mm width of the diagonal's web.

4.4 Response History Analyses

4.4.1 Description of case studies

To assess the performance of the POS, the cross-aisle frames of one double-depth (DD) and one multi-depth (MD) ARSW will be examined. Case study DD has four "macro-columns" of 25.56 m height and 2.35 m width (Figure 4.11), where each "macro-column" comprises two upright frames with mirrored bracing patterns, connected with spacers along their height. Regarding the down-aisle direction (which is not shown here for brevity), the pallet beams are designed to carry two pallets per bay, thus each upright carries approximately one pallet per load level. Automated cranes are used for goods handling, operating in 14 load levels: Load level 1 to 3 are for 1000 kg pallets, 4 to 11 for 800 kg, and 12 to 14 for 600 kg.

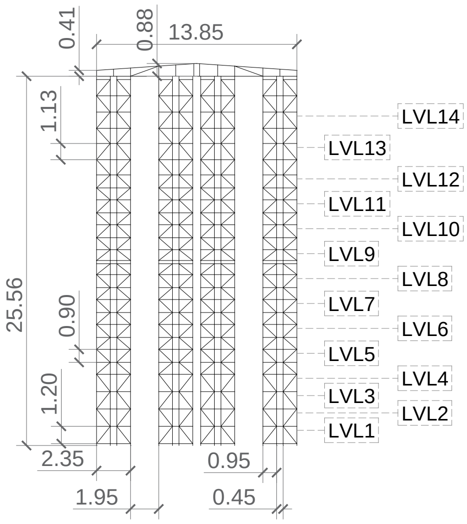
0.41
0.88
13.85
1.13
25.56
0.90
1.20
2.35
1.95
0.95
0.45
LVL14
LVL13
LVL12
LVL11
LVL10
LVL9
LVL8
LVL7
LVL6
LVL5
LVL4
LVL3
LVL2
LVL1

Figure 4.11: Cross-aisle view of case study DD (dimensions in m).

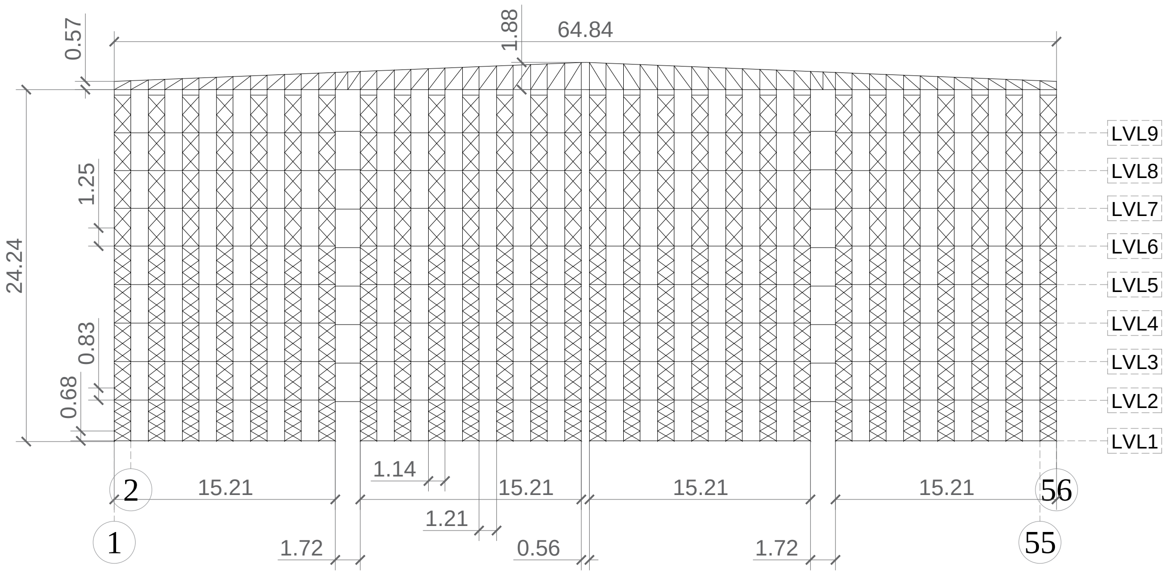
0.57
1.88
64.84
1.25
24.24
0.83
0.68
LVL9
LVL8
LVL7
LVL6
LVL5
LVL4
LVL3
LVL2
LVL1
2
15.21
1.14
15.21
15.21
15.21
56
1.21
1
1.72
0.56
1.72
55

Figure 4.12: Cross-aisle view of case study MD (dimensions in m).

On the other hand, the cross-aisle direction of case study MD comprises 28 “X-type” upright frames of 24.24 m height and 1.14 m width (Figure 4.12). MD is designed to carry 9 load levels with four storage cells of 13 unit-load capacity each. Load levels 1 to 2 are for 1000 kg pallets, 3 to 5 for 800 kg, and 6 to 9 for 600 kg. The handling process is again fully automated, using cranes and shuttles to deposit and withdraw the pallets.

Each case study was designed twice by a professional engineer expert in rack structures. First, a “standard” non-ductile design was performed using EN 1993 (2005), EN 15512 (2009) and EN 16681 (2016), using a behaviour factor of $q = 1.5$. Then, the case studies were re-designed according to the new rules POS 1 to POS 10, employing a factor of $q = 1.8$; this value is a preliminary recommendation pending a more accurate evaluation involving numerous experimental and numerical analyses. The following mass combinations were used for the POS: $G + Q$ for the double-depth, and $G + 0.8 \cdot Q$ for the multi-depth case study. On the other hand, the importance and spectrum modification factors were not modified. All the seismic design assumptions are summarized in Table 4.1, where “STD” corresponds to the standard, and “POS” to the plastic ovalization design.

Table 4.1: Seismic design assumptions adopted in case studies DD and MD according to the standard design (STD), and the POS re-design (POS).

	DD-STD	**DD-POS**	**MD-STD**	**MD-POS**
γ_I	0.8	0.8	0.8	0.8
E_{D1}	1.0	1.0	1.0	1.0
E_{D3}	0.8	0.8	0.8	0.8
q	1.5	1.8	1.5	1.8
Mass comb.	$G + Q$	$G + Q$	$G + 0.64 \cdot Q$	$G + 0.8 \cdot Q$
Load comb.	$G + Q$	$G + Q$ $G + 0.8 \cdot Q$ *	$G + Q$	$G + Q$ $G + 0.8 \cdot Q$ *

* only for the design of the base connections, see rule POS 10.

Due to the introduction of capacity design rules POS 1 to POS 10, some members and connections of the upright frames had to be modified during the re-design. Table 4.2 summarizes the major changes in the cross-sections and the bolted connections of case study DD. One may observe that lighter diagonals (30% less material) were used during the POS re-design, basically due to rule POS 6, which disregards the code-recommended multiplication of the seismic forces by the q-factor. Moreover, while not imposed by the new design rules, the designer chose to use a single diagonal section in the lower half of the structure and a lighter one for the upper half. Each half was further separated into quarters by modifying the e_1 parameter. This smooth reduction of the diagonal’s resistance along the height of the upright frame is expected to enhance the seismic behaviour of the rack. On the other hand, the uprights were not modified during the POS design. While rule POS 8 aims to create over-resistant uprights, it is based on a “relaxed” version of the overstrength factor of EN 1998-1 (2004) and the designer was able to satisfy the capacity checks without increasing the upright section. As a result, the POS design used less steel material with respect to the standard approach. Regarding the base connections, rule POS 10 led to a stronger anchorage system with greater anchor diameter and embedment depth.

The effects of the POS rules in case study MD are illustrated in Table 4.3. Contrarily to the DD example, herein heavier diagonals (+25% more material) were employed during the POS re-design, even though rule POS 6 led to lower design seismic forces. Indeed, in the standard design, the diagonals had slender circular hollow sections (with folded ends to achieve a thickness of 3 mm at the connection), which do not satisfy rule POS 4, i.e., the buckling resistance being greater than the bearing resistance. Thus, in the POS re-design, channel sections with lips were used for the diagonals, with different e_1 parameters at the lower and the upper half of the structure. Concerning the uprights, heavier profiles were employed at the POS re-design, but only for the first 2.98 m from the ground. Again, the design rules did not lead to major changes in the uprights, as the designer was able to optimize the diagonals instead. Note, that in all cases, the resulting diagonals did not respect the $d/t < 5$ condition. This leaves some questions regarding the actually achieved ductility, which nevertheless is not out of proportion with respect to the low behaviour factor employed. Finally, the resistance of the anchors was increased during the POS re-design, having greater diameter and embedment depth.

Table 4.2: Member and connection properties of case study DD according to the standard design (STD), and the POS re-design (POS). Section areas are given normalized to the bottommost elements of the STD design.

Member	Height (m)	STD	POS
Uprights	[0.00, 3.73]	Ω+U [*]: $A = A_1$	Ω+U: $A = A_1$
	(3.73, 12.58]	Ω [**]: $A = 0.5 \cdot A_1$	Ω: $A = 0.5 \cdot A_1$
	(12.58, 25.56]	Ω: $A = 0.32 \cdot A_1$	Ω: $A = 0.32 \cdot A_1$
Diagonals	[0.00, 6.65]	C [***]: $A = A_2$ t = 3 mm, e_1 = 24 mm 1M12 8.8 (2 shear planes)	C: $A = 0.7 \cdot A_2$ t = 2 mm, e_1 = 29 mm 1M12 8.8 (2 shear planes)
	(6.65, 12.80]	C: $A = A_2$ t = 3 mm, e_1 = 24 mm 1M12 8.8 (2 shear planes)	C: $A = 0.7 \cdot A_2$ t = 2 mm, e_1 = 22 mm 1M12 8.8 (2 shear planes)
	(12.80, 18.73]	C: $A = 0.7 \cdot A_2$ t = 2 mm, e_1 = 24 mm 1M12 8.8 (2 shear planes)	C: $A = 0.5 \cdot A_2$ t = 1.5 mm, e_1 = 23 mm 1M12 8.8 (2 shear planes)
	(18.73, 25.56]	C: $A = 0.7 \cdot A_2$ t = 2 mm, e_1 = 24 mm 1M12 8.8 (2 shear planes)	C: $A = 0.5 \cdot A_2$ t = 1.5 mm, e_1 = 15 mm 1M12 8.8 (2 shear planes)
Anchorage system	-	4M20 8.8 embedment depth: 400 mm	4M24 8.8 Embedment depth: 500 mm

[*] Ω+U: Ω-type upright section reinforced with a U-type section; [**] Ω: Ω-type upright section; [***] C: channel section with lips.

Table 4.3: Member and connection properties of case study MD according to the standard design (STD), and the POS re-design (POS). Section areas are given normalized to the bottommost elements of the STD design.

Member	Height (m)	STD	POS
Uprights	[0.00, 2.98]	Ω+U [a]: $A = A_1$	Ω+U: $A = 1.79 \cdot A_1$
	(2.98, 13.32]	Ω+U: $A = A_1$	Ω+U: $A = A_1$
	(13.32, 24.24]	Ω [b]: $A = 0.68 \cdot A_1$	Ω: $A = 0.68 \cdot A_1$
Diagonals	[0.00, 10.81]	CHS [c]: $A = A_2$ t = 3 mm, e_1 = 18 mm 1M8 8.8 (1 shear plane)	C [d]: $A = 1.25 \cdot A_2$ t = 1.5 mm, e_1 = 20 mm 1M12 8.8 (1 shear plane)
	(10.81, 24.24]	CHS: $A = A_2$ t = 3 mm, e_1 = 18 mm 1M8 8.8 (1 shear plane)	C: $A = 1.25 \cdot A_2$ t = 1.5 mm, e_1 = 15 mm 1M12 8.8 (1 shear plane)
Anchorage system	-	2M16 8.8 embedment depth: 250 mm	2M20 8.8 Embedment depth: 350 mm

[a] Ω+U: Ω-type upright section reinforced with a U-type section; [b] Ω: Ω-type upright section; [c] CHS: circular hollow section; [d] C: channel section with lips.

4.4.2 Numerical modelling

The four structures were realized using the OpenSees (McKenna et al., 2000) open-source software. To reduce the number of elements and degrees of freedom, we simplified the models using the methodology described in Tsarpalis et al. (2021) (see also Chapter 6). Specifically, in the DD example we substituted the full cross-aisle frame with a pair of connected upright frames (i.e., one “macro-column”) with calibrated horizontal springs at the top level, to simulate the stiffness of the roof. Similarly, in the MD case study we used a single upright frame instead of the 28 of the full model. A Rayleigh damping formulation was employed, using a viscous damping ratio of 3% for the first and second eigenperiods, and a $G + 0.8 \cdot Q$ combination for mass and gravity loads. The periods and mass participation factors of the four structures can be found in Table 4.4. The effect of pallet sliding was not considered in the analyses.

Table 4.4: Periods and mass participation factors for the case studies DD and MD according to the standard design (STD), and the POS re-design (POS).

Mode #	DD-STD		DD-POS		MD-STD		MD-POS	
	Period (sec)	**Mass Part.**	**Period (sec)**	**Mass Part.**	**Period (sec)**	**Mass Part.**	**Period (sec)**	**Mass Part.**
1	2.60	68%	2.46	69%	1.58	63%	1.31	63%
2	0.97	11%	0.85	17%	0.51	17%	0.42	19%
3	0.53	5%	0.45	6%	0.26	5.4%	0.21	5.6%
4	0.35	3%	0.30	2.8%	0.18	1.8%	0.15	1.4%
5	0.25	1.2%	0.21	1.3%	0.14	0.7%	0.11	1.0%

The uprights were simulated as elastic beam elements with a P-Δ formulation to account for the effect of geometric nonlinearities. In the standard design, material nonlinearities were not considered, as the elements and their connections are prone to brittle failure modes, which, if simulated, would have caused the analysis to stop at the very first steps. In the POS re-design, the only source of material nonlinearity was that of plastic ovalization of the diagonal bolt hole. The opening of the bolt hole was simulated using a zero-length element with an elastic-perfectly-plastic gap material, as illustrated in Figure 4.13.

During loading (Points 1 to 3), the material behaves elastically with an elastic tangent E_0, until it reaches the yield force F_y; from this point onwards, it continues with a post-elastic (hardening) tangent E_1. The gap opens by the amount of plastic deformation the material accumulates during the post-elastic phase (Points 2 to 3). Then, in the unloading branch, the material first unloads elastically to zero force (Points 3 to 4), and then it returns to its initial position with zero stiffness (Points 4 to 5) due to the gap opening. If load reversal occurs (Points 5 to 7), the same elastic-perfectly-plastic response is observed, and the gap opens also in the other direction of loading. From this point on, the material can bounce freely between Points 8 to 9 without developing any reaction force; it has to be subjected to a greater yield force (Point 10) to encounter any resistance while enlarging the gap. This flag-shaped force-deformation diagram is characterized by significant pinching, which downgrades the amount of plastic energy the connection is capable of absorbing during a seismic excitation.

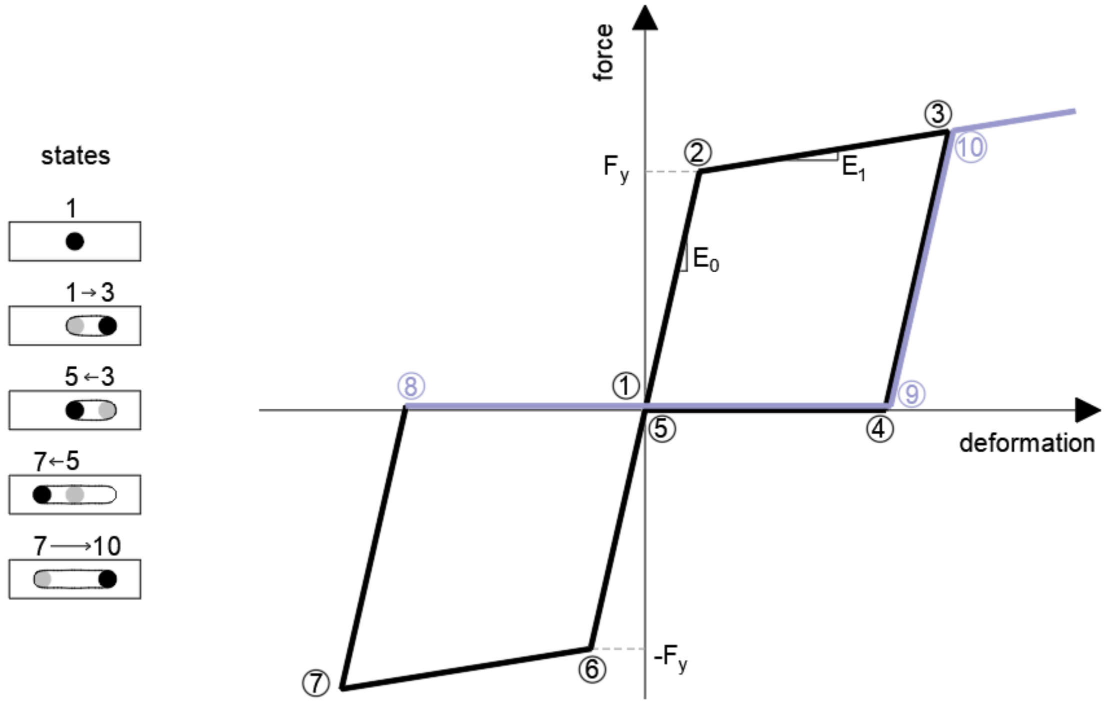

Figure 4.13: Simulating the plastic ovalization of a bolt hole under cyclic loading, using the elastic-perfectly-plastic gap material of OpenSees (McKenna et al., 2000). F_y is the yield force, E_0 is the elastic tangent, and E_1 is the hardening tangent. The gap opens by the amount of plastic strain the material accumulates at each excursion. In the left side of the figure, the loading, unloading, and reloading states of the bolt hole are shown schematically, along with the numbered points corresponding to the right diagram (the gray and black circles indicate the initial and final position of the bolt, respectively).

To determine the three parameters of the elastic-perfectly-plastic gap material (F_y, E_0, and E_1), a fitting procedure is followed. Recalling Figure 4.4(a), the bearing deformation of a steel material lower than S460 (which is typical for diagonals on racking systems) follows a nonlinear path until it reaches 80% of the maximum bearing resistance, i.e., up to point ($u_{80\%}$, $0.8{\cdot}F_{bR}$) in Figure 4.14. It then continues with a constant slope up to full bearing resistance, i.e., point (u_{xd}, F_{bR}). From this point we assume that it continues with zero stiffness until the bearing deformation is equal to one bolt diameter, d. The overall fitting procedure is as follows (see Figure 4.14):

(a) Find the elastic tangent of the gap material as: $E_0 = 0.8{\cdot}F_{bR} / u_{80\%}$.

(b) Find the optimal F_y so that the hatched areas below and under the bilinear fit in Figure 4.14 are approximately equal.

(c) Find the hardening tangent of the gap material as: $E_1 = (F_{bR} - F_y) / (d - F_y / E_0)$.

Note that the above fitting procedure assumes that the force-deformation curve of prEN 1993-1-8:2021 (2021) is valid. As found by previous numerical analyses and illustrated in Figure 4.7, the failure mode of diagonals with thicknesses 2 and 1.5 mm, or, more generally, of diagonals with $d/\mathrm{t} > 5$, is a combination of plastic ovalization and local buckling of the web, with the resulting force-deformation curve deviating from the expected per prEN 1993-1-8:2021 (2021). Unfortunately, the finite element analyses of Subsection 4.3.2 were executed after the POS re-design by the racking experts, and the limitations on the diagonal's thickness were not considered in rules POS 1 to POS 10. Nevertheless, for the purposes of seismic assessment we neglect this inconsistency, and we model the diagonals as if they were thick enough to avoid local buckling of the web. The experimental campaign that (at the time of writing) is under way in the context of the European project STEELWAR (2017) is expected to shed more light to this issue.

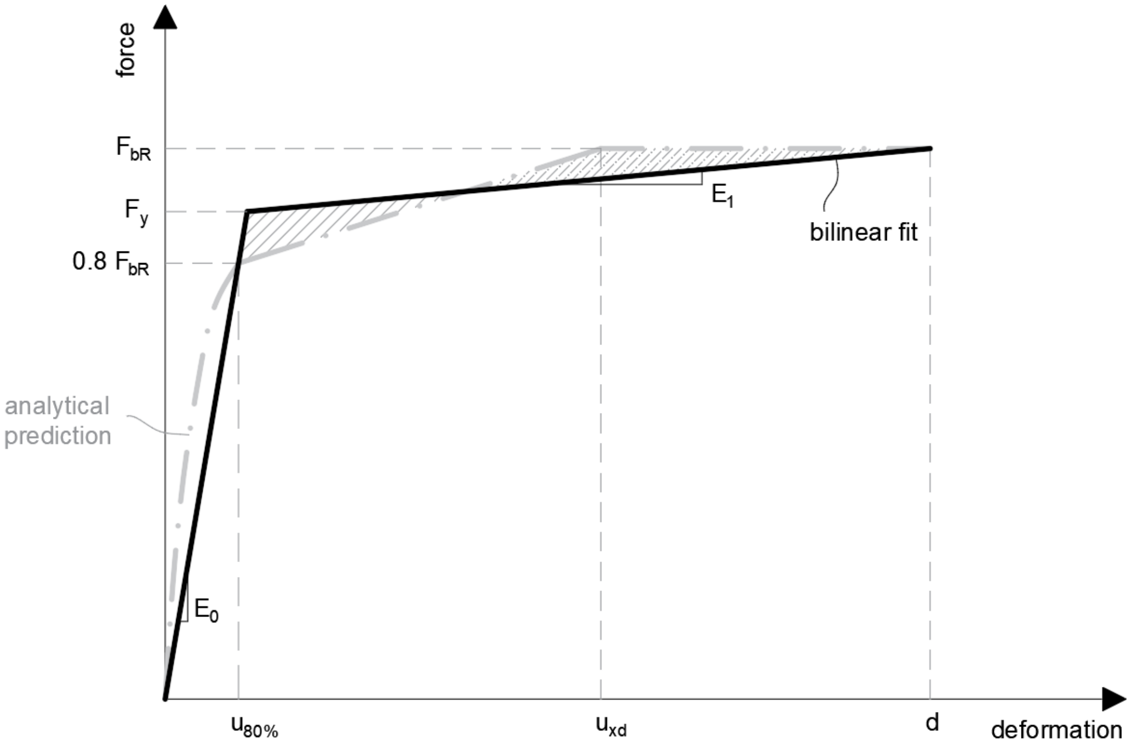

Figure 4.14: Fitting the parameters F_y, E_0, and E_1 of the elastic-perfectly-plastic gap material, to match the analytical predictions of Eq. (4.12), Eq. (4.13), and Eq. (4.14). F_y is calculated so that the hatched areas below and under the bilinear fit are approximately equal.

After the determination of F_y, E_0, and E_1, the diagonal and its bolted ends can be simulated by a macroelement that comprises (a) a zero-length element with an elastic-perfectly-plastic gap material, and (b) an elastic beam element, as shown in Figure 4.15. Instead of using two zero-length elements, one for each end of the diagonal, it is more efficient to use one and multiply the elastic and hardening tangents by 0.5, i.e., $0.5 \cdot E_0$ and $0.5 \cdot E_1$, respectively. F_y is not modified as the two ends are springs in series.

A final modelling detail is related to the initial shear stiffness of the upright frame, which is significantly reduced due to the deformation of the braces and their ends, as well as the slipping and bending of the bolts (Talebian et al., 2018). This phenomenon is typically taken into account in a beam-column element model by employing an axial spring in series with the diagonal. This spring has a stiffness of K_{tot}, calibrated by experimental shear tests. One may break down K_{tot} into two springs in series, one is the aforementioned elastic-perfectly-plastic gap element that accounts for the bearing deformation and has elastic stiffness $0.5 \cdot E_0$, and the other should account for all the other factors that contribute to the shear stiffness of the upright frame. Thus, this second spring should have an axial stiffness of $(K_{tot} \cdot 0.5 \cdot E_0) / (K_{tot} - 0.5 \cdot E_0)$. Instead of using these two springs, we found that it was more efficient to use only the one that accounts for the bearing deformation, and implicitly consider the other by reducing numerically the cross-section area of the diagonal element to a value of A'(see Figure 4.15).

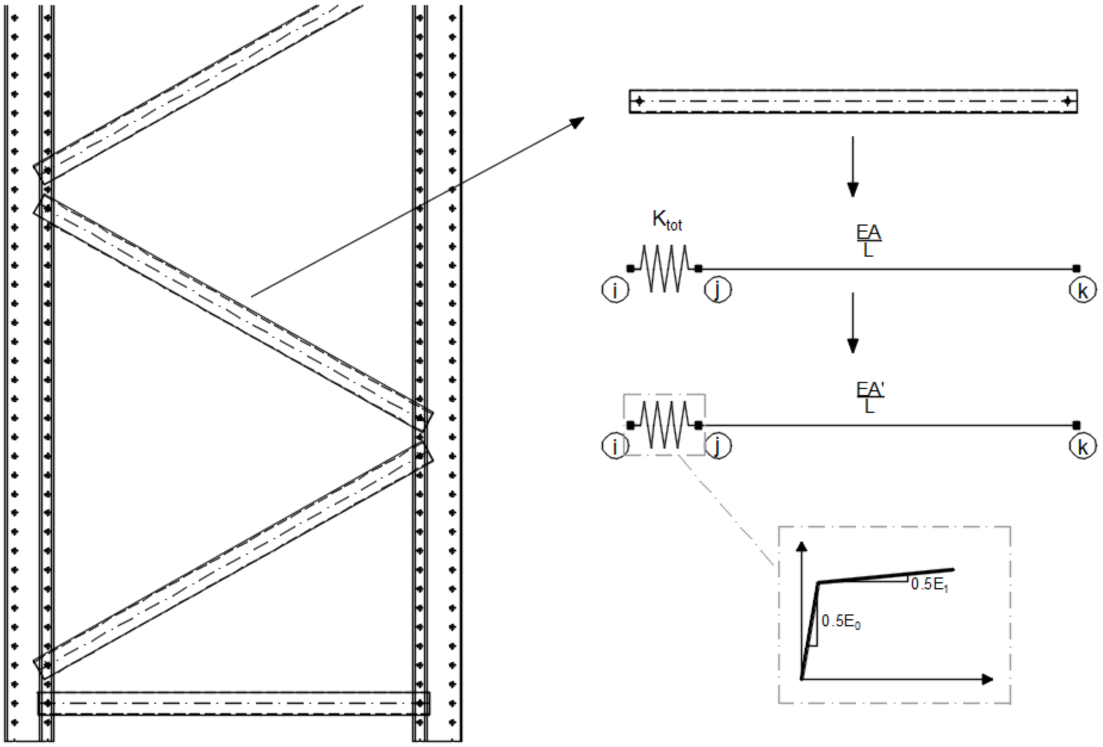

Figure 4.15: Numerical modelling of a diagonal element with bearing failure behaviour in OpenSees (McKenna et al., 2000). Nodes i and j are connected by a zero-length element with an elastic-perfectly-plastic gap material, and nodes j and k by an elastic beam element with stiffness EA'/L. The cross-section area of the beam element is numerically reduced to A', to achieve the elastic shear stiffness of the upright frame taken from experimental shear tests.

4.4.3 Comparison of design approaches

To compare the two design approaches, a multi stripe analysis (Jalayer and Cornell, 2009) was performed for each case study, employing 30 natural records that match the conditional spectrum (Baker, 2010; Lin et al., 2013a; Lin et al., 2013b; Kohrangi et al., 2017) of Van in Turkey, using $AvgSa$ (Eq. (3.14)) as the intensity measure (IM). The set is available at Kohrangi et al. (2018). The records were scaled to six IM levels that correspond to 60%, 30%, 20%, 10%, 5%, and 3% in 50 years probability of exceedance. Additionally, all records were pre-multiplied by the design spectrum modification factor E_{D3}. E_{D3} is suggested by EN 16681 (2016) to “*account for the dissipative phenomena that are observed on racks that have suffered earthquakes or tested experimentally, but cannot be described in a mathematical formulation*”. While one may be reluctant regarding the actual value of E_{D3}, to achieve a fair assessment of the designs at the design-level intensity (i.e., the 20% in 50 years stripe), we considered a uniform value of E_{D3} = 0.8 (see Table 4.1).

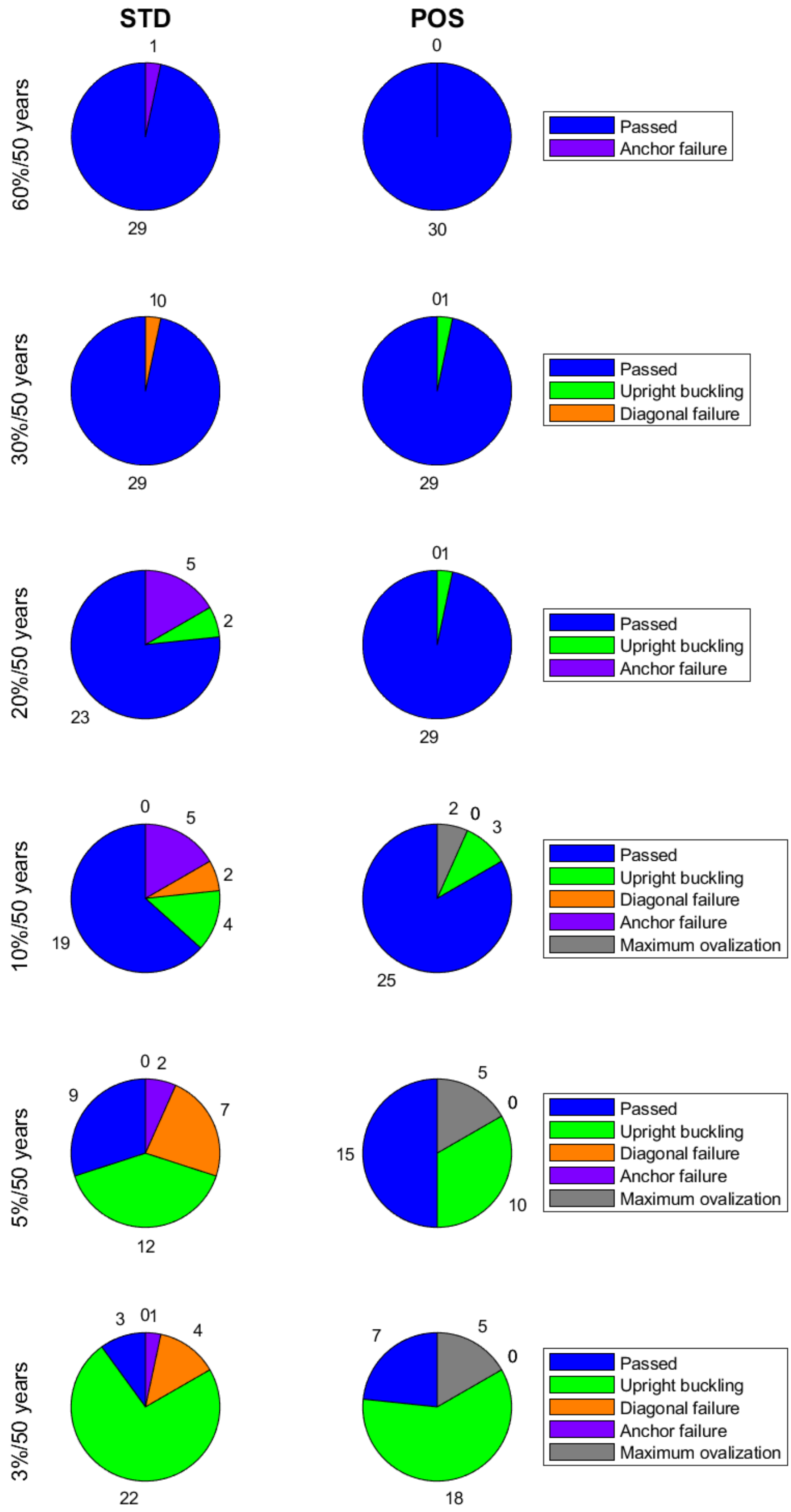

Figure 4.16: Multi stripe analysis for double-depth case study DD, using a set of 30 records scaled to six IM levels. Two pie charts are given per stripe, showing the number of times a failure mode was observed on the standard (left) and the POS (right) design. If multiple failure modes were observed on a single record, the one with the highest utilization factor is considered.

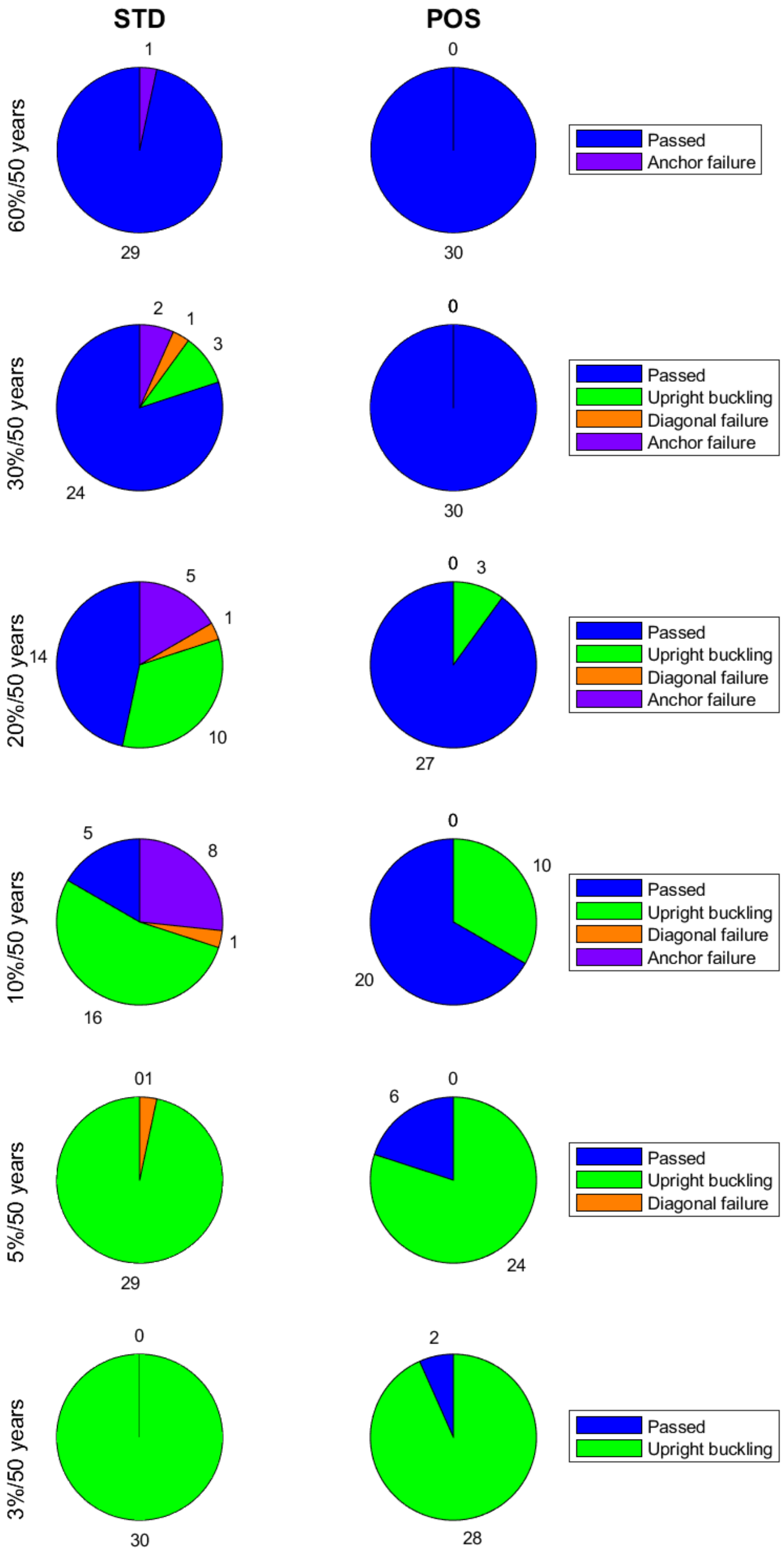

Figure 4.17: Multi stripe analysis for multi-depth case study MD, using a set of 30 records scaled to six IM levels. Two pie charts are given per stripe, showing the number of times a failure mode was observed on the standard (left) and the POS (right) design. If multiple failure modes were observed on a single record, the one with the highest utilization factor is considered.

In the numerical models of the standard design, we followed a post-processing procedure to derive the utilization factors of the most critical members and connections, using the verification checks given in Table 3.7. All design resistances were multiplied by a factor of 1.1, which roughly approximates the available overstrength of the structure (i.e., a mapping between design and expected values). Due to the prevalence of brittle failure modes, we assume that the failure of any member/connection (i.e., when a utilization factor exceeds the threshold value of 1.0) leads to a global collapse of the structure.

In the "POS" numerical models, the diagonal-to-upright connection was modelled using the nonlinear zero-length element of Figure 4.15. While deriving its force-deformation curve (Figure 4.14), F_{bR} was calculated by omitting the safety factor γ_{M2} in Eq. (4.10). An additional global collapse rule was considered: if the gap displacement of the zero-length element exceeds the value of $1.1 \cdot d_0$, then we assume that the deformation of the connection is so large that the upright frame loses its global stability. The rest structural components were modelled and verified similarly to the standard design.

Figure 4.16 summarizes the results of the multi stripe analysis for case study DD, using pie charts to compare the two designs. The pie charts show the number of times a failure mode was observed in each stripe of analyses; if multiple failure modes were observed for a single record, the one with the highest utilization factor is considered. As expected, both designs performed excellently at the two lowest scales, with very few records leading to a component failure. At the design level (i.e., the 20% in 50 years stripe), 7 and 1 out of the 30 records had a component failure in the standard and the POS models, respectively, showing a clear advantage of the latter. The difference between the two designs is also pronounced at probabilities of exceedance lower (i.e., higher intensities) than the design level. For instance, at the 10% in 50 years stripe, which is the design level for regular steel buildings, POS achieved a 32% increase of "passing" records. Still, at the highest IM scales, the utilization factors on the uprights exceeded the threshold value of 1.0 even in the POS design, despite the reduction of seismic forces due to the ovalization of the diagonal bolt hole.

Accordingly, Figure 4.17 shows the results of the multi stripe analysis for case study MD. POS was again capable of completely preventing the diagonals and the anchorage system from failing and scored better results for all IM levels. At the design-level stripe, 16 and 3 out of the 30 records led to a component failure in the standard and the POS models, respectively, highlighting a remarkable improvement in the seismic performance of the upright frames. However, upright buckling was still prevalent at high IMs, which indicates that rule POS 8 only partially creates over-resistant columns. In this sense, stricter capacity design rules could be used on the uprights, similar to those of EN 1998-1 (2004), with the obvious drawback of increasing the overall cost of the racking structure.

Finally, one may observe that the MD example demonstrated an inferior seismic performance with respect to the DD, in both standard and POS designs. This was attributed to the different assumptions adopted during their seismic design and to the fact that DD employed a more uniform distribution of Ω factors on the diagonals, by dividing them into four groups along the vertical direction. While this smooth reduction of the diagonals' resistance was not explicitly imposed by the capacity design rules POS 1 to POS 10, it potentially leads to a more uniform exploitation of structural ductility, and thus, to an improved seismic behaviour.

4.5 Conclusions

Chapter 4 proposes a state-of-the-art seismic design of racking systems along their cross-aisle direction, the so-called plastic ovalization strategy (POS). POS aims to enhance the ductility of the upright frames, and at the same time respects the philosophy of the rack industry that demands simple bolted connections and light steel members. It relies on the bearing deformation of the diagonal bolt hole to absorb seismic deformation, while the rest structural components are designed to be over-resistant, by employing ten capacity design rules, POS 1 to POS 10. A parametric study using three-dimensional finite element models has demonstrated that a ductile behaviour of the connection can be achieved, as long as local buckling of the diagonal's web is prevented. To assess the performance of POS, the cross-aisle frames of one double-depth and one multi-depth ARSW were examined. Each case study was designed twice by an expert, once using conventional design standards, and then by employing the proposed capacity design rules. Finally, a multi stripe analysis was conducted, using 30 records and six IM levels. A distinct advantage of the POS design was observed, especially for IMs that exceed the design level. Moreover, POS does not necessarily increase the cost of the racking system: the cross-sections of the uprights were slightly modified, while in some cases lighter diagonals were employed by removing a redundant requirement of EN 16681 (2016). Overall, POS promises to increase the resilience of high-rise racking systems in an economic and efficient way and sets the ground for a performance-based earthquake design of racks, in tandem with the current trends in the earthquake engineering community.

4.6 References

ABAQUS v6.14 (2014). *"ABAQUS Documentation (6.14)"*, Dassault Systèmes Simulia Corp., Providence, RI, USA.

American Institute of Steel Construction (AISC) (2005). *"AISC 360-05, specification for structural steel buildings"*, Chicago, Illinois, USA.

Baker J.W. (2010). *"Conditional Mean Spectrum: Tool for Ground-Motion Selection"*, Journal of Structural Engineering, **137**(3). https://doi.org/10.1061/(ASCE)ST.1943-541X.0000215

Brandonisio G., Toreno M., Grande E., Mele E., De Luca A. (2012). *"Seismic design of concentric braced frames"*, Journal of Constructional Steel Research, **78**, 22-37. https://doi.org/10.1016/j.jcsr.2012.06.003

Draganić H., Dokšanović T., Markulak D. (2014). *"Investigation of bearing failure in steel single bolt lap connections"*, Journal of Constructional Steel Research, **98**, 59-72. https://doi.org/10.1016/j.jcsr.2014.02.011

EN 15512 (2009). *"Steel static storage systems - Adjustable pallet racking systems - Principles for structural design"*, European Committee for Standardization (CEN), Brussels, Belgium.

EN 16681 (2016). *"Steel static storage systems - Adjustable pallet racking systems - Principles for seismic design"*, European Committee for Standardization (CEN), Brussels, Belgium.

EN 1993-1-1 (2005). *"Eurocode 3: Design of Steel Structures - Part 1-1: General rules and rules for buildings"*, European Committee for Standardization, Brussels, Belgium.

EN 1993-1-3 (2006). *"Eurocode 3: Design of Steel Structures - Part 1-3: General rules - Supplementary rules for cord-formed members and sheeting"*, European Committee for Standardization, Brussels, Belgium.

EN 1993-1-8 (2005). *"Eurocode 3: Design of Steel Structures - Part 1-8: Design of joints"*, European Committee for Standardization, Brussels, Belgium.

EN 1998-1 (2004). *"Eurocode 8: Design of structures for earthquake resistance - Part 1: General rules, seismic actions and rules for buildings"*, European Committee for Standardization, Brussels, Belgium.

Jalayer F., Cornell C.A. (2009). *"Alternative non-linear demand estimation methods for probability-based seismic assessments"*, Earthquake Engineering and Structural Dynamics **38**(8), 951-972. https://doi.org/10.1002/eqe.876

Kiymaz G. (2009). *"Investigations on the bearing strength of stainless steel bolted plates under in-plane tension"*, Steel and Composite Structures, **9**(2), 173-189. 10.12989/scs.2009.9.2.173

Kohrangi M., Bazzurro P., Vamvatsikos D., Spillatura A. (2017). *"Conditional spectrum-based ground motion record selection using average spectral acceleration"*, Earthquake Engineering and Structural Dynamics, **46**(10), 1667-1685. https://doi.org/10.1002/eqe.2876

Kohrangi M., Tsarpalis D., Vamvatsikos D. (2018). *"CS(AvgSA) consistent Records and Hazard curves for Van and Montopoli"*. STEELWAR Project. Link: http://users.ntua.gr/divamva/resources/Van_set_10_50yrs.rar

Lin T., Haselton C.B., Baker J.W. (2013a). *"Conditional spectrum-based ground motion selection. Part I: Hazard consistency for risk-based assessments"*, Earthquake Engineering and Structural Dynamics, **42**(12), 1847-1865. https://doi.org/10.1002/eqe.2301

Lin T., Haselton C.B., Baker J.W. (2013b). *"Conditional spectrum-based ground motion selection. Part II: Intensity-based assessments and evaluation of alternative target spectra"*, Earthquake Engineering and Structural Dynamics, **42**(12), 1867-1884. https://doi.org/10.1002/eqe.2303

McKenna F., Fenves G.L., Scott M.H., Jeremic B. (2000). *"Open System for Earthquake Engineering Simulation (OpenSees)"*, Pacific Earthquake Engineering Research Center, University of California, Berkeley, CA.

Može P., Beg. D. (2014). *"A complete study of bearing stress in single bolt connections"*, Journal of Constructional Steel Research, **95**, 126-140. https://doi.org/10.1016/j.jcsr.2013.12.002

Može P., Yang. F., Veljkovic M. (2021). *"Validation and application of bearing and block tearing resistance; background to prEN1993-1-8:2021"*, Journal of Constructional Steel Research, **187**. https://doi.org/10.1016/j.jcsr.2021.106985

prEN 1993-1-8 (2021). *"Eurocode 3: Design of Steel Structures - Part 1-8: Design of joints"*, European Committee for Standardization, Brussels, Belgium.

STEELWAR (2017). *"Advanced structural solutions for automated STEELrack supported WARehouses"*, The Steelwar Project Consortium, Pisa, Italy. https://www.unipi.it/index.php/risultati-e-prodotti/item/10663-steelwar

Stojadinovic B., Tipping S. (2007). *"Structural testing of corrugated sheet steel shear walls"*, Research report, Berkeley, University of California.

Talebian N., Benoit P.G., Baldassino N., Karampour H. (2018). *"Factors contributing to the transverse shear stiffness of bolted cold-formed steel storage rack upright frames with channel bracing members"*, Thin-Walled Structures, **136**, 50-63. https://doi.org/10.1016/j.tws.2018.12.001

Tsarpalis D., Vamvatsikos D., Vayas I. (2021). *"Seismic assessment approaches for mass-dominant sliding contents: The case of storage racks"*, Earthquake Engineering and Structural Dynamics, **51**(4), 812-831. https://doi.org/10.1002/eqe.3592

Tsarpalis P., Bakalis K., Thanopoulos P., Vayas I., Vamvatsikos D. (2020). *"Pre-normative assessment of behaviour factor for lateral load resisting system FUSEIS pin-link"*, Bulletin of Earthquake Engineering, **18**, 2681-2698. 10.1007/s10518-020-00799-y

Vigh L.G., Deierlein G.G., Miranda E., Liel A.B., Tipping S. (2013). *"Seismic performance assessment of steel corrugated shear wall system using non-linear analysis"*, Journal of Constructional Steel Research, **45**, 48-59. http://dx.doi.org/10.1016/j.jcsr.2013.02.008

Vigh L.G., Liel A.B., Deierlein G.G., Miranda E., Tipping S. (2014). *"Component model calibration for cyclic behavior of a corrugated shear wall"*, Thin-Walled Structures, **75**, 53-62. https://doi.org/10.1016/j.tws.2013.10.011

5 Simplified Modelling of Automated Rack Supported Warehouses[2]

5.1 Introduction

Despite their differences in terms of dimensions and structural behaviour, automated rack supported warehouses (ARSWs) are typically built with the same thin-walled cold-formed profiles used in the most-common adjustable pallet racking systems (APRs). In addition, there is no official document worldwide specific for their seismic design, forcing the structural engineers to use EN 16681 (2016) and other APR standards, without any modifications to respect their structural idiosyncrasies and nonconventional geometry. All these uncertainties render ARSWs vulnerable to extreme hazards, such as high wind speeds and vigorous seismic motions. This was also highlighted during the Emilia-Romagna earthquake (Figure 1.4), where several ARSWs experienced severe damages or even collapsed. Given the above observations, there is presently significant interest in improving the seismic behaviour of ARSWs installed in high-seismicity areas, by forming at least a limited plastic failure mechanism (see for example the new design approach presented in Chapter 4).

Nowadays, seismic performance assessment (EN 1998-3, 2005; ASCE 41-13, 2014) is based on comprehensive numerical analyses via nonlinear static or dynamic approaches. However, a detailed nonlinear simulation of a modern ARSW is practically infeasible even for academic purposes, as a full 3D model may comprise hundreds of thousands of nodes and elements with almost a million of degrees of freedom (DOFs). Even during elastic design, simplifications are accepted in terms of accuracy by using only a part of the structure or relying on 2D models, as performing all verification checks on the complete 3D model can take days or even weeks. Herein, a simplified modelling approach is presented that is based on the substitution of the truss columns (i.e., upright frames) with equivalent Timoshenko/link elements. The methodology is applied on two ARSW case studies, using 2D/3D linear and nonlinear analyses to compare the different simulation approaches.

5.2 Proposed simplified model

The idea of substituting truss beams and columns with equivalent elastic elements has found good use in literature. For example, a methodology for simplified seismic design of industrial buildings has been proposed by Belleri et al. (2017), which employed equivalent beam elements in tandem with elastic springs. On the other hand, Kalochairetis and Gantes (2012) introduced elastic Timoshenko beam-column elements to determine the buckling capacity of laced built-up columns and to perform rapid parametric analyses on the effect of imperfections. Building upon such ideas, we propose a linear Timoshenko beam model to substitute the truss members of a racking system when material inelasticity is not considered, as well as a nonlinear link element model to capture the material nonlinearity of more ductile designs. In the latter case, novel nonlinear Timoshenko beam elements can offer alternative modelling solutions (Amir et al., 2020a; 2020b). The target is to offer a flexible approach for quantifying the seismic performance of racking systems, especially of multi- and double-depth ARSWs. Then the simplified methodology continues with the aggregation of several upright frames to a single equivalent element, in order to further reduce the number of DOFs.

---

[2] This work contains material from “Tsarpalis D., Vamvatsikos D., Deladonna F., Vayas I. (2021). *Simplified Modelling for the Seismic Performance Assessment of Automated Rack-Supported Warehouses*, Journal of Structural Engineering. https://doi.org/10.1061/(ASCE)ST.1943-541X.0003153”, reproduced here with permission.

To substitute a single upright frame with an equivalent beam-column or link element, one has first to transform it into a Timoshenko-beam. Considering an upright frame that comprises N upright members, each having A_i cross-section area and d_i distance from the mass centre, the equivalent area (A_{eq}) and moment of inertia (I_{eq}) of the Timoshenko-beam will be equal to:

$$A_{eq} = \sum_{i=1}^{N} A_i \qquad \text{Eq. (5.1)}$$

$$I_{eq} = \sum_{i=1}^{N} A_i d_i^2 \qquad \text{Eq. (5.2)}$$

Table 5.1: Cross-section shear area for bracing patterns D, Z, K, and X per EN 1993-1-1 (2005).

D-bracing	**Z-bracing**	**K-bracing**	**X-bracing**
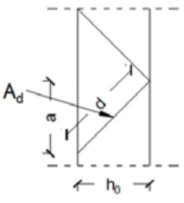	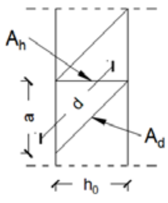	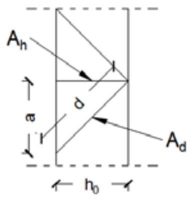	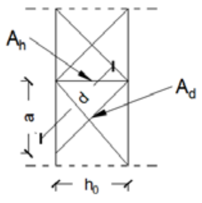
$A_s = \frac{EA_d}{G}\frac{h_0^2 a}{d^3}$	$A_s = \frac{\frac{EA_d}{G}\frac{h_0^2 a}{d^3}}{1+\frac{h_0^3}{d^3}\frac{A_d}{A_h}}$	$A_s = \frac{EA_d}{G}\frac{h_0^2 a}{d^3}$	$A_s = 2\frac{EA_d}{G}\frac{h_0^2 a}{d^3}$

While only A_{eq} and I_{eq} are required to simulate the bending of a 2D Euler-Bernoulli-beam, the equivalent shear area $A_{s,eq}$ is also needed to capture the shear deformability of Timoshenko-beams. Essentially, $A_{s,eq}$ accounts for the deformation of the bracing elements and their connections and thus depends on the geometry and typology of the bracing system. For common bracing patterns with constant cross-sections and geometry along the height, closed-form formulae can be defined by enforcing static equilibrium on a small portion of the truss member. For example, expressions for patterns D, Z, K, and X are already available in the literature (EN 1993-1-1, 2005), as shown in Table 5.1. To account for the additional factors that govern the shear stiffness of the upright frames (Talebian et al., 2018), an axial release with stiffness $K_{p.release}$ is typically introduced at one end of the diagonal, calibrated by experimental shear tests (EN 15512, 2009). Considering that the diagonal and its connection act as springs in series, one can avoid using the axial release and instead reduce numerically the cross-section area of the diagonal as:

$$\frac{EA_{d,red}}{L} = \frac{K_d K_{p.release}}{K_d + K_{p.release}} \qquad \text{Eq. (5.3)}$$

where $K_d = EA_d/L$, while A_d and $A_{d,red}$ are the actual and the reduced cross-sectional area of the diagonal, respectively. Subsequently, the shear area of the equivalent column is calculated using the formulae of Table 5.1 with A_d replaced by $A_{d,eq}$.

For systems with non-constant bracing sections one can divide the upright frame into several vertical segments and compute $A_{s,eq}$ separately for each part. However, when the spacing of the diagonals also varies along the height, an approximate procedure can be followed, which significantly reduces the size of the numerical model:

1. Separate the considered upright frame and calculate its A_{eq} and I_{eq} from Eq. (5.1) and Eq. (5.2), respectively

2. Perform a cantilever test by applying pinned releases to the nodes at the bottom and concentrated loads on the top. The sum of nodal loads P_{tot} and corresponding top-height displacement δ_{tot} are related as:

$$P_{tot} = \frac{12}{4+\Phi}\frac{EI_{eq}}{L^3}\delta_{tot} \qquad \text{Eq. (5.4)}$$

where $\Phi = 12EI_{eq}/G\overline{A}_{s,eq}L^2$ and L the length of the upright frame.

3. Solving Eq. (5.4) for the approximated $\overline{A}_{s,eq}$ results in:

$$\overline{A}_{s,eq} = \frac{E}{G}\frac{P_{tot}(3I_{eq})L}{(3EI_{eq})\delta_{tot} - P_{tot}L^3} \qquad \text{Eq. (5.5)}$$

When examining models that incorporate only linear elastic materials, the above information is adequate for transforming the upright frame to an equivalent beam-column element. However, for nonlinear designs where the diagonals and the uprights may buckle or yield, the elastic Timoshenko element is not sufficient for simulating the in-cycle stiffness and strength degradation.

Herein, we propose a further transformation of the derived Timoshenko beam to a two-node link element that can simulate accurately the inelastic bending, shear, and axial response of the upright frame. It connects its two end nodes by distinct, typically non-interacting, uniaxial springs, one for each mode of relative deformation. In two dimensions, the two-node link element of OpenSees (e.g., McKenna et al, 2000) comprises three springs that capture the axial, shear, and rotational DOFs (Figure 5.1). In the elastic region, the link element should have the same elastic stiffness matrix as the equivalent Euler/Timoshenko beam it substitutes. In Annex A an analytical procedure is described, for the calculation of the elastic springs' stiffnesses in the two dimensions, while the extension in 3D is straightforward.

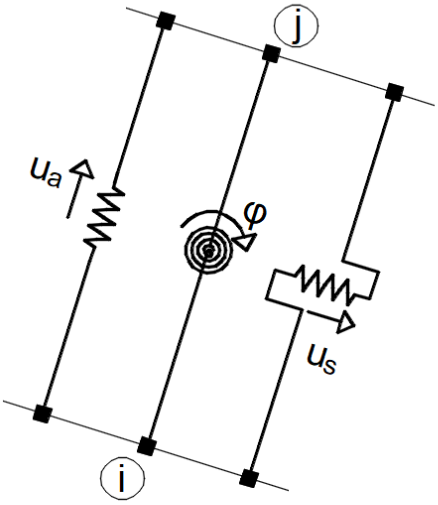

Figure 5.1: OpenSees' two-node link element for 2D analysis (McKenna et al., 2000). Nodes i and j are connected via three independent uniaxial springs to capture the axial, shear and rotational DOFs.

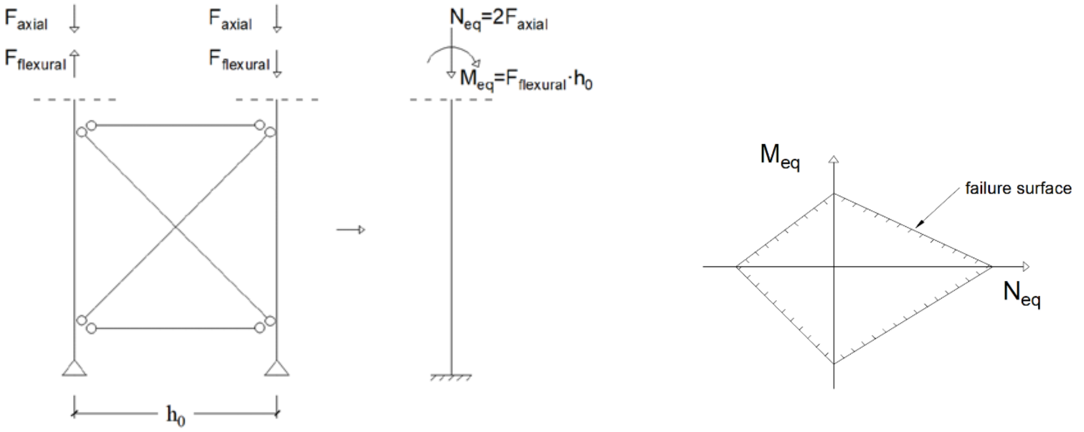

(a) (b)

Figure 5.2: Transformation of member uprights' axial forces to stress resultants on the equivalent column, showing (a) a numerical example of an upright frame comprising two columns, and (b) the interaction between bending moment and axial force and the corresponding failure surface.

Considering inelastic response, the equivalent element axial force N_{eq} and bending moment M_{eq} for a frame comprising two uprights are related to pairs of axial forces of same and opposite direction, respectively, on the individual uprights (Figure 5.2(a)). Thus, failure occurs when the resulting axial force in any of the uprights exceeds the corresponding compressive or tensile strength, $N_{u,Rd}$, with compression being typically the governing situation:

Regarding nonlinear behaviour, Figure 5.2(a) shows that if N_{eq} and M_{eq} are the axial force and bending moment of the equivalent element that simulates a two-uprights frame, respectively, these correspond to pairs of axial forces of same and opposite direction on the individual uprights, respectively. As a result, the equivalent link element should fail axially when the total axial force in any of the two uprights exceeds the compressive or tensile strength, $N_{u,Rd}$, with compression commonly being more critical:

$$N_{u,Rd} = \frac{N_{eq}}{2} + \frac{M_{eq}}{h_0} \qquad \text{Eq. (5.6)}$$

where h_0 is the horizontal distance between the uprights' center lines. From Eq. (5.6) it is evident that an interaction between the axial and rotational springs is required to determine failure (Figure 5.2(b)). However, due to the low stiffness of the roof truss connecting the upright frames, the shear lag between frames is of such magnitude that essentially the individual frames do not interact in developing appreciable global overturning resistance. Therefore, seismic forces do not influence N_{eq}, but only M_{eq}. As a result, N_{eq} can be considered to be constant as calculated from the gravity load analysis and decoupled axial/rotational springs can be employed. Thus Eq. (5.6) is solved for $M_{eq} = M_{eq,Rd}$, representing the maximum moment that the rotational spring can bear:

$$M_{eq,Rd} = h_0 \left(N_{u,Rd} - \frac{N_{eq}}{2} \right) \qquad \text{Eq. (5.7)}$$

As upright buckling is an unstable failure mechanism, an abrupt drop to near-zero strength was employed for the post-buckling behaviour of the rotational spring. While Eq. (5.7) holds for upright frames with two uprights, it can straightforwardly be extended to the case of three equidistant uprights as $M_{eq,Rd} = 2h_0(N_{u,Rd} - N_{eq}/3)$. As the above simplifications assume no shear lag between adjacent uprights, extension to more than three is not recommended without care. Instead, one can combine multiple two- or three-member upright frames into one link element by summing their springs' stiffness, assuming negligible shear stiffness of the connecting roof truss (an assumption that introduces a small error as it will be seen later), the "100% shear lag" (Figure 5.4). This simplification procedure can be exploited to considerably reduce the complexity of the model, given the high level of commonality among the upright frames, with the associated penalties in considering spatial differences in the mass distribution and in the resolution of the analysis results.

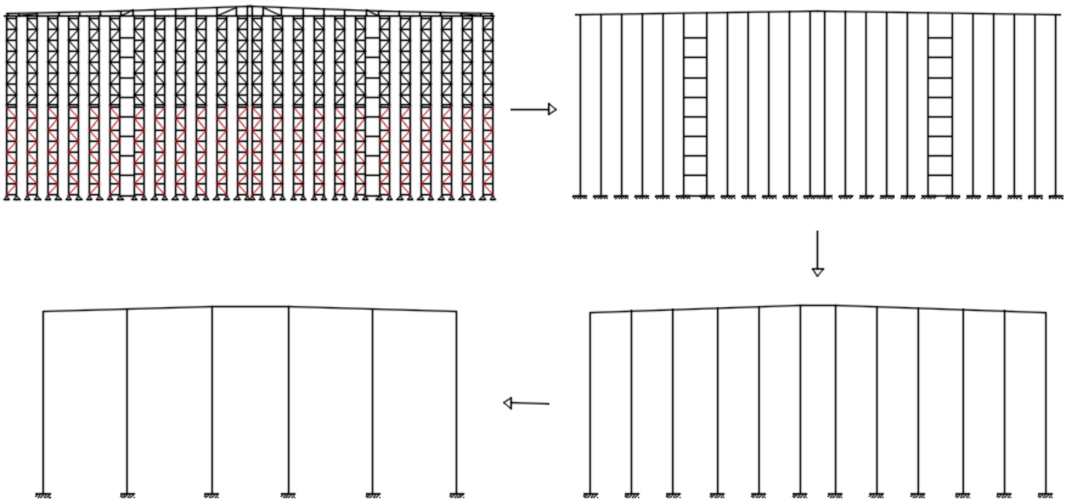

Figure 5.3: Simplification stages for a multi-depth cross-aisle frame; assuming negligible shear stiffness of the roof truss, multiple two- or three- member upright frames can be substituted by a single link element.

Regarding the shear spring's nonlinear material law, a more sophisticated procedure was followed. A portion of the upright frame was isolated and tested under shear loading (Figure

5.4). Pinned supports were employed at the bottom nodes of the tested segment while rollers at the top ones. To account for the stiffness contribution of the adjacent (upper and lower) uprights, rotational springs were employed at the restrained nodes. The stiffness value of these springs cannot be derived analytically, but values between $EI/(4L)$ and $EI/(8L)$ (I and L the moment of inertia and the length of the adjacent upright, respectively) were adequately accurate. The horizontal and diagonal braces were simulated by force-based fiber elements with a corotational geometric transformation and a bow-type initial imperfection. The derived force-displacement curve was fitted by a piece-wise linear backbone, suitable for use with the OpenSees Pinching4 material to represent each shear spring.

The force-deformation response of the shear spring under cyclic loading can be derived by performing a quasi-static analysis on the same test segment used for the backbone fit (Figure 5.4). A total of 10 cycles is performed, where the displacement increment is increased by 50% in each cycle. Figure 5.5 illustrates the “loading protocol” and the corresponding force-deformation curve of a test segment comprising 2 uprights. The hysteretic behaviour is characterized by significant pinching, due to the slenderness of the braces (typically allowed to be much higher than for conventional buildings), as also observed during experimental tests on concentrically-braced-frame specimens (Kanyilmaz, 2015). To decrease the work load, this quasi-static test was performed once and the same hysteretic properties were used for all the shear springs, assuming a similar cyclic behaviour.

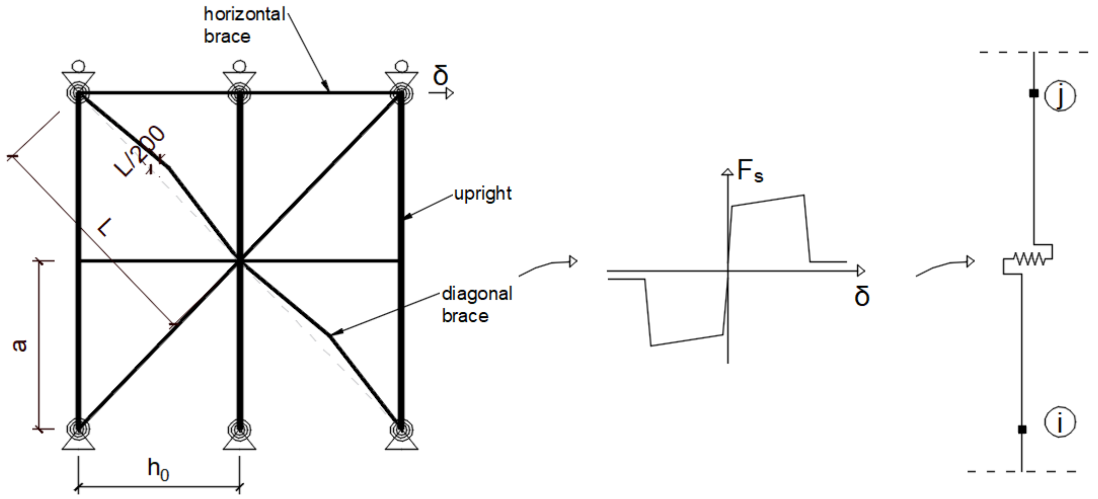

Figure 5.4: Numerical shear testing of a triple-upright segment. Bow-type imperfections of $L/200$ are applied to the diagonals, while rotational springs stiffen the pin/roll end supports. The derived force-displacement curve is employed to define the shear spring of the link element.

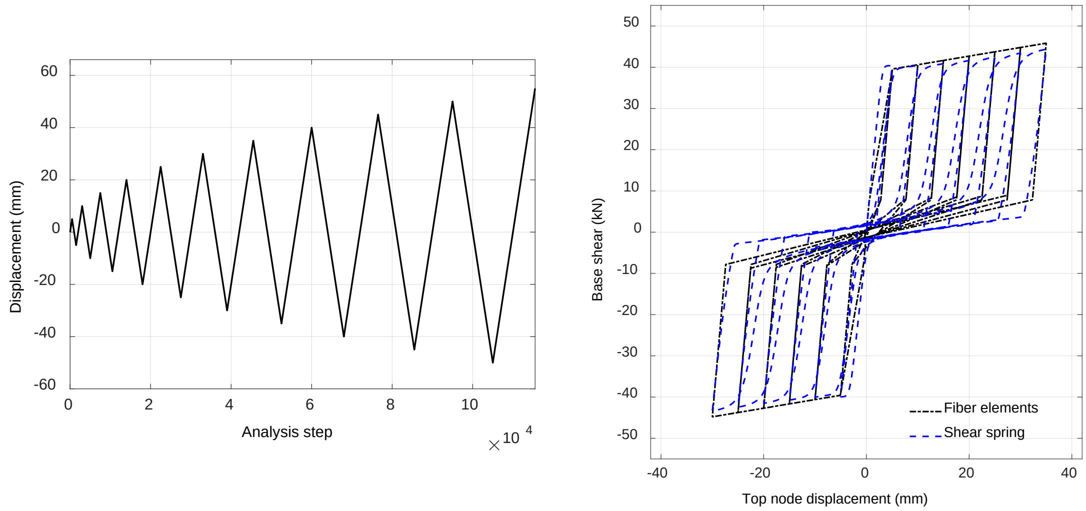

Figure 5.5: Cycle shear testing of the upright frame segment showing, the loading protocol (left) and the calibrated force-deformation response of the shear spring (right).

Another important attribute that has to be discussed is the contribution of second-order effects. Elastic Timoshenko elements can easily consider geometric nonlinearities by employing a so-called P-Δ stiffness matrix, modified to account for shear deformations (see for instance, the standard beam element of SAP2000). On the other hand, a closed-form P-Δ matrix does not exist for a link element. As a remedy, OpenSees offers the ability to implicitly take into account the P-Δ effects, by introducing two “P-Delta moment contribution ratios”, namely μ_1 and μ_2. Essentially these ratios increase the shear forces by $V_{P-\Delta}$ and bending moments by $M_{1,P-\Delta}$ and $M_{2,P-\Delta}$ on the connected nodes by a multiple of N/L, where N the axial force acting on the link element and L the length of the element. This is expressed in the following equations (dv is the nodal relative displacement, perpendicular to the axis of the element):

$$V_{P-\Delta} = (1 - \mu_1 - \mu_2) \cdot \frac{N}{L} \qquad \text{Eq. (5.8)}$$

$$M_{1,P-\Delta} = \mu_1 \cdot \frac{N \cdot dv}{L} \qquad \text{Eq. (5.9)}$$

$$M_{2,P-\Delta} = \mu_2 \cdot \frac{N \cdot dv}{L} \qquad \text{Eq. (5.10)}$$

Deriving a general analytical solution would require accounting for the effect of different bracing patterns, as well as different yielding mechanisms within the built-up column. Rather than attempting this approach, it is easier to perform the shear test (Figure 5.4) twice. The first time, the standard shear test is performed and the material law of the shear spring is derived. The second time, axial forces are assigned at the top nodes of the tested segment and the “P-Delta moment contribution ratios” of the link element are calibrated to match the corresponding force-displacement curve. The axial forces may assume the value of the gravity loads acting on the segment. Of course, then it becomes a question of whether the derived contribution factors depend on the magnitude of said forces. Our tests so far indicate that the contribution factors are largely insensitive to the magnitude of the axial forces, with the N/L term sufficiently capturing the effect of the different axial forces and the contribution factors characterizing the bracing configuration characteristics, as long as the yielding progression within the built-up column is not altered, e.g., the uprights do not buckle due to increased axial force before the braces yield in tension. This is indeed the general case for our case study and it considerably simplifies the modeling effort. For the case at hand, $\mu_1 = \mu_2 = 0.20$ to 0.25 were found to be sufficient for all built-up column segments.

After the transformation of the upright frames, one may follow the same strategy for the simplification of the roof, but without the need of link elements, as the roof members are typically under-stressed and, thus, remain elastic. Essentially, one can substitute the entire roof truss by elastic Timoshenko elements, using the average vertical distance between the lower and upper chord, as it varies due to the inclination. Finally, rigid offsets are used at the two ends of each equivalent roof beam, to account for the difference between its clear span and its centreline length, as shown in Figure 5.6.

Finally, a structural detail that is worth mentioning is the grid formed by the rail and pallet beams in the multi-depth systems. This horizontal system affects the stiffness of the warehouse both in the cross- and the down-aisle direction (especially in the former) and it can only be captured by a 3D analysis. While the elastic properties of the equivalent uprights and pallet beams can be derived analytically, there is no closed-form solution for the equivalent rail beam. Thus, to consider the effect of the grid in the simplified model, a calibration procedure is followed. A small part of the ARSW is isolated both in the full and the simplified model, as shown in Figure 5.7. It was chosen to maintain the initial elastic length of the rail beam, by introducing rigid offsets and calibrating the torsional constant of the pallet beam until the first few modes of vibration of the simplified model match those of the full model. This procedure produces rapid results, as only a part of the full 3D model is considered.

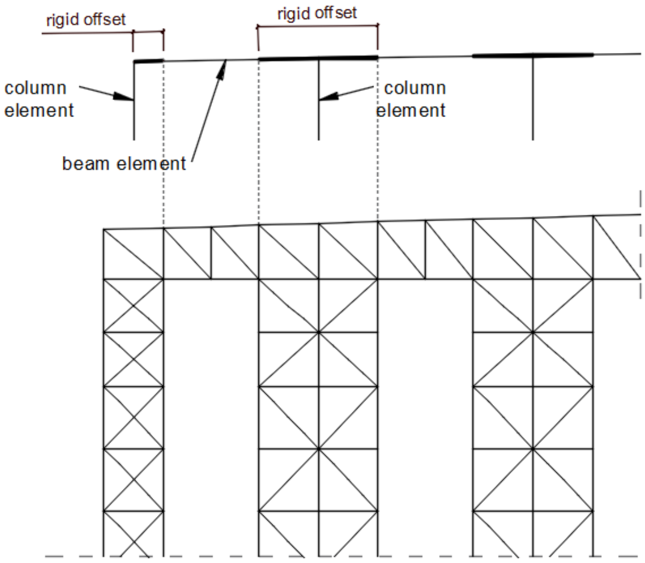

Figure 5.6: Each roof beam element comprises two rigid parts at the two ends and one elastic in the middle, as its clear span is significantly different from the centreline length.

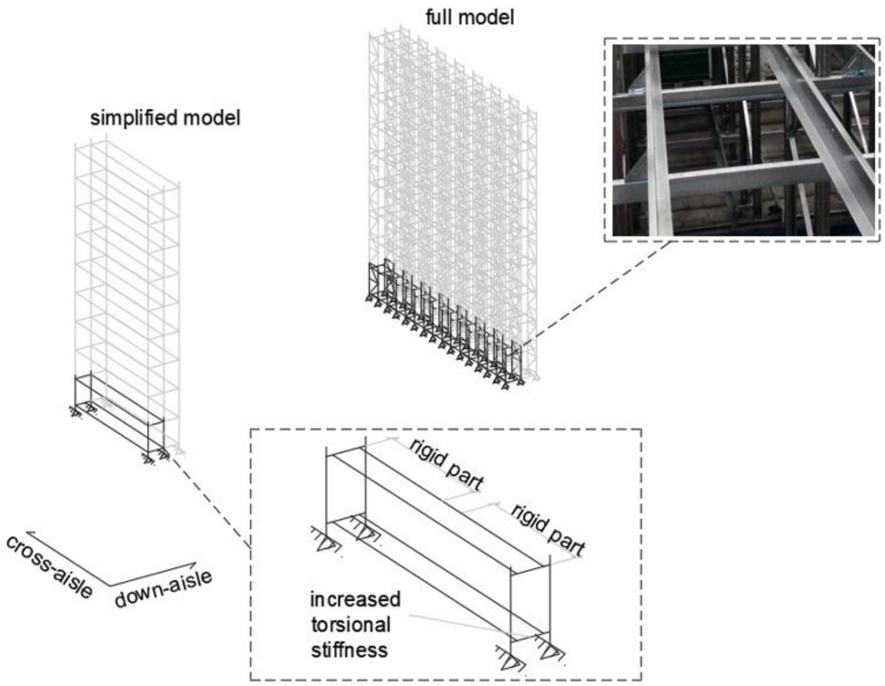

Figure 5.7: Calibration procedure for the grid formed by the rail and pallet beams in multi-depth systems. A small part of the rack is considered (the black lines in the figure) and the torsional constant of the equivalent pallet beam is calibrated until the first few modes of vibration of the simplified model match those of the full model.

5.3 Elastic model validation on single upright frames

The proposed simplification methodology was first validated by performing elastic modal analysis on the two upright frames of Figure 5.8. Both examples comprise two uprights of 16.0 m length each, separated by 1.2 m centroid distance, and connected by an “X-type” bracing pattern with 1.0 m stride. The first case study, the “uniform” Upright Frame 1, employs constant upright and diagonal sections, while the unit load weight is uniformly equal to 5 kN. On the other hand, the “nonuniform” Upright Frame 2 is divided into four vertical segments, where each segment has different steel members and pallet weight. Table 5.2 contains the cross-sectional properties of the full and the simplified models for the two case studies. The equivalent properties of the simplified Timoshenko beam were calculated according to Eq. (5.1), Eq. (5.2), and Table 5.1.

The numerical models were realized using SAP2000 structural analysis software. In both case studies the uprights were pinned at the bottom, which corresponds to fix supports in the simplified models. In the “nonuniform” Upright Frame 2, additional pinned supports were employed at the topmost height of the structure, which can simulate a stiff roof of an ARSW. The first three modes are illustrated in Figure 5.9 and Figure 5.10 for the first and the second case study, respectively. Evidently, the simplified models excellently predicted both the modal shapes (i.e., the eigenvectors) and the actual period values (i.e., the eigenvalues).

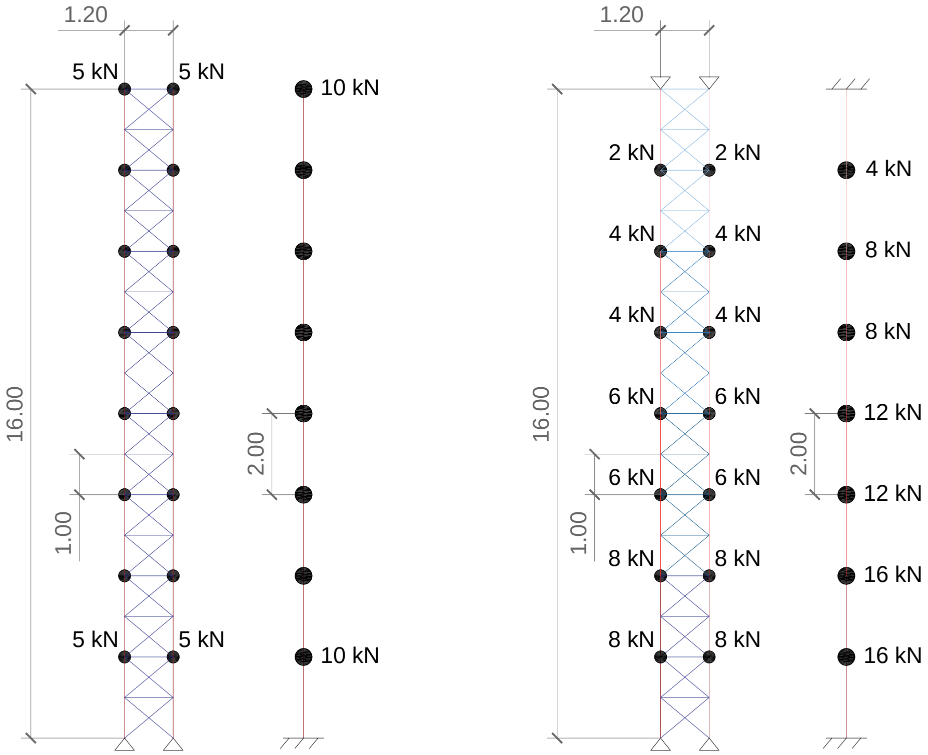
1.20
5 kN
5 kN
10 kN
16.00
1.00
2.00
5 kN
5 kN
10 kN
1.20
2 kN
2 kN
4 kN
4 kN
4 kN
4 kN
6 kN
6 kN
6 kN
6 kN
8 kN
8 kN
8 kN
8 kN
16.00
1.00
4 kN
8 kN
8 kN
12 kN
12 kN
16 kN
16 kN
2.00

(a) (b)

Figure 5.8: Full and simplified models of (a) “uniform” Upright Frame 1 and (b) “nonuniform” Upright Frame 2.

Table 5.2: Unit load weight and cross-sectional properties of “uniform” Upright Frame 1 and “nonuniform” Upright Frame 2.

	Upright Frame 1		**Upright Frame 2**	
Height (m)	Full model	Simplified model	Full model	Simplified model
[0.00, 4.00]	A_c [a] = 1164 mm^2 A_d [b] = 231 mm^2 UL [c] = 5 kN	A_{eq} [d] = 2328 mm^2 I_{eq} [e] = 8.4e+8 mm^4 $A_{s,eq}$ [f] = 454 kN	A_c = 1404 mm^2 A_d = 291 mm^2 UL = 8 kN	A_{eq} = 2808 mm^2 I_{eq} = 1.0e+9 mm^4 $A_{s,eq}$ = 571 mm^2
(4.00, 8.00]			A_c = 1164 mm^2 A_d = 231 mm^2 UL = 6 kN	A_{eq} = 2328 mm^2 I_{eq} = 8.4e+8 mm^4 $A_{s,eq}$ = 454 mm^2
(8.00, 12.00]			A_c = 875 mm^2 A_d = 156 mm^2 UL = 4 kN	A_{eq} = 1750 mm^2 I_{eq} = 6.3e+8 mm^4 $A_{s,eq}$ = 306 mm^2
(12.00, 16.00]			A_c = 624 mm^2 A_d = 116 mm^2 UL = 2 kN	A_{eq} = 1248 mm^2 I_{eq} = 4.5e+8 mm^4 $A_{s,eq}$ = 228 mm^2

[a] A_c: upright cross-section area; [b] A_d: diagonal cross-section area; [c] UL: unit load weight; [d] A_{eq}: equivalent cross-section area; [e] I_{eq}: equivalent moment of inertia; [f] $A_{s,eq}$: equivalent shear area.

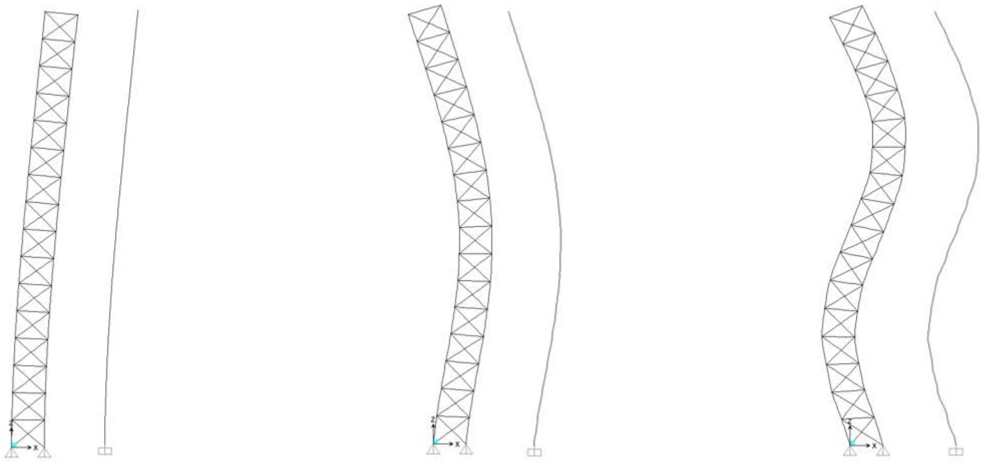

(a) (b) (c)

Figure 5.9: Modes of vibration of “uniform” Upright Frame 1, showing (a) the first mode: T_1^{full} = 1.025 sec, T_1^{simpl} = 1.024 sec, (b) the second mode: T_2^{full} = 0.198 sec, T_2^{simpl} = 0.197 sec, and (c) the third mode: T_3^{full} = 0.087 sec, T_3^{simpl} = 0.087 sec.

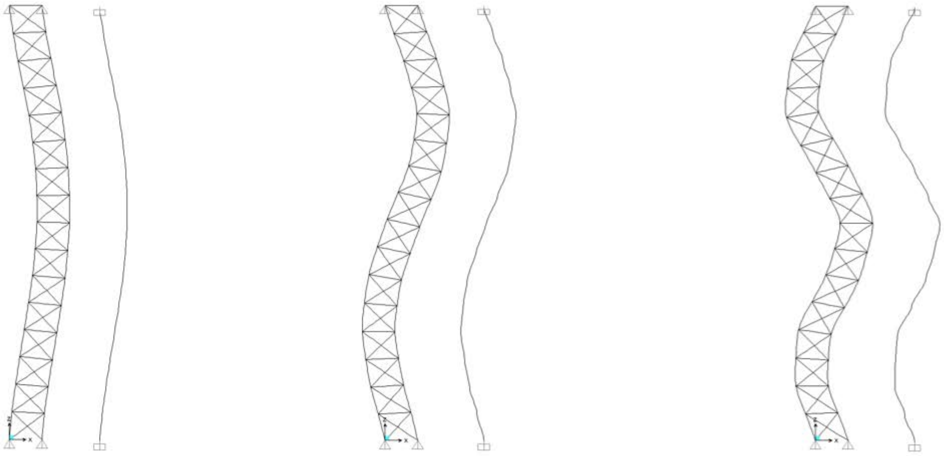

(a) (b) (c)

Figure 5.10: Modes of vibration of “nonuniform” Upright Frame 2, showing (a) the first mode: T_1^{full} = 0.195 sec, T_1^{simpl} = 0.195 sec, (b) the second mode: T_2^{full} = 0.088 sec, T_2^{simpl} = 0.088 sec, and (c) the third mode: T_3^{full} = 0.056 sec, T_3^{simpl} = 0.055 sec.

5.4 Case study A: Elastic model of a multi-depth ARSW

5.4.1 Structure and model description

To illustrate the application of the proposed simplified model, a multi-depth ARSW is studied. It has been designed by professional engineers according to EN 1993 (2005), EN 15512 (2009) and EN 16681 (2016) for a peak ground acceleration of a_g = 0.3 g and assuming a behaviour (or strength reduction) factor of q = 1.5. Despite being higher than 1.0, this value of q does not imply the presence of any appreciable ductility or capability for load redistribution in the structure, but only some inherent overstrength. Thus, a linear-elastic material model with geometric nonlinearities is suitable for full range assessment. The overall plan dimensions are 65.80 m × 71.50 m in the cross- and down-aisle direction, respectively, while the total height is about 25.60 m. Due to the high seismicity, three bracing towers are required along the down-aisle direction, placed at the two ends and the middle of the total length. Therefore, in the down-aisle direction 44 cross-aisle frames (Figure 5.11) are foreseen, comprising 38 “pallet frames” and 6 “tower frames”. The latter are connected in pairs by X-braces to form three concentrically braced towers that support the structure down-aisle.

Each cross-aisle frame is composed of 48 uprights, connected in pairs to form 24 “K-type” upright frames of 1.35 m width (Figure 5.12). “Tower” and “pallet” cross-aisle frames have similar geometry and bracing pattern, but the former ones use heavier sections. In both cases, their elements are cold-formed, with the uprights having Ω sections (Figure 5.13) and the K-braces channel sections. To optimize the design of the warehouse, profiles of lower thickness are used for the upper part of each upright frame. In the down-aisle direction, the pallet beams have a constant cross-section (with the exception of only a few that do not affect the stiffness of the structure) and are hooked to the uprights, creating semi-rigid connections (Figure 5.13). As for the bracing towers, reinforced Ω+U uprights are introduced up until the second load level, to withstand the increased axial forces arising from the seismic actions.

Table 5.3 contains the cross-sectional characteristics of the main structural components. Based on experimental shear tests on upright frames with similar geometric configuration and steel profiles, the cross-section areas of all diagonals were numerically multiplied by a factor of 0.1, to consider for the flexibility of diagonal-to-upright bolted connections (Talebian et al., 2018). Each pallet frame can support up to 468 pallets; there are nine load levels in total, each storing pallets at four storage cells of 13 unit-load capacity each cell (Figure 5.12). Load levels 1 to 2 are designed for 10 kN unit-load weight, while 3 to 5 for 8 kN, and 6 to 9 for 6 kN.

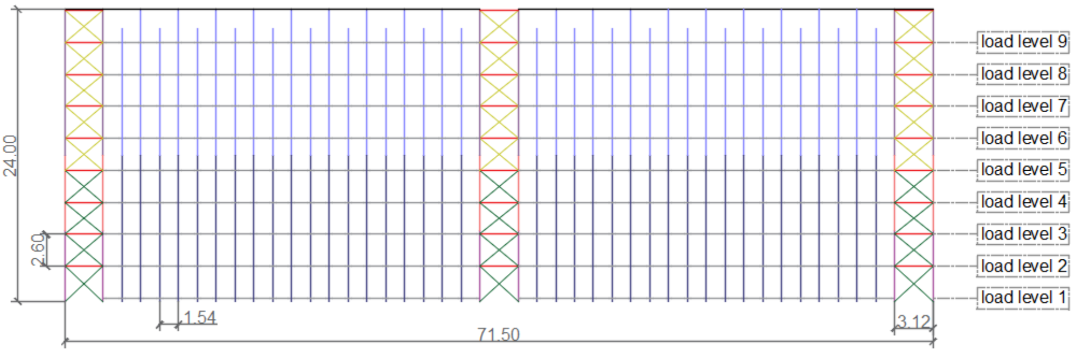

Figure 5.11: Down-aisle view of the multi-depth 3D Case Study A. Each of the 44 vertical lines represents a single cross-aisle frame running perpendicularly to this figure. The 6 column-lines connected by X-braces correspond to heavy “tower” frames, while the remaining 38 are lighter “pallet” frames (units in meters).

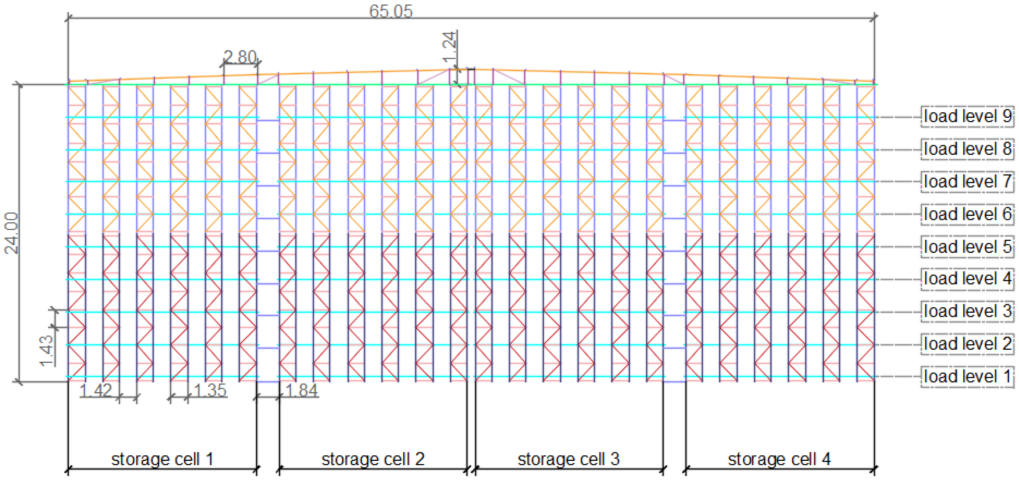
65.05
2.80
1.24
24.00
1.43
1.42
1.35
1.84
load level 9
load level 8
load level 7
load level 6
load level 5
load level 4
load level 3
load level 2
load level 1
storage cell 1
storage cell 2
storage cell 3
storage cell 4

Figure 5.12: Cross-aisle view of the multi-depth 3D Case Study A, comprising 24 “K-type” upright frames and a connecting shallow roof truss (units in meters). Along the vertical there are 9 load levels, while along the horizonal direction, four storage cells are distinguished comprising 6 upright frames each.

Table 5.3: Cross-section properties of structural members (multi-depth, Case Study A). Cross-section areas are rounded to the third digit while moments of inertia to the fifth.

Member	**Section**	A **(mm^2)**	I_y [a] **(mm^4)**	I_z [b] **(mm^4)**	I_t **(mm^4)**
Lower bracing upright (reinforced)	Ω+U [c]	3500	9000000	6800000	24000
Lower bracing upright	Ω [d]	1700	3900000	3800000	9000
Upper bracing upright	Ω	1100	2500000	2400000	2000
Lower pallet upright	Ω	1300	3000000	2900000	4000
Upper pallet upright	Ω	900	2000000	1900000	1000
Lower upright frame diagonal	C [e]	500	150000	110000	500
Upper upright frame diagonal	C	300	340000	230000	500
Lower vertical bracing (floor-5th level)	L [f]	600	70000	200000	7000
Lower vertical bracing (6th level-top)	L	300	120000	20000	1000

[a] I_y: cross-aisle moment of inertia; [b] I_z: down-aisle moment of inertia; [c] Ω+U = Ω-type upright section reinforced with a U-type section; [d] Ω: Ω-type upright section; [e] C: channel section with lips; [f] L: angle section.

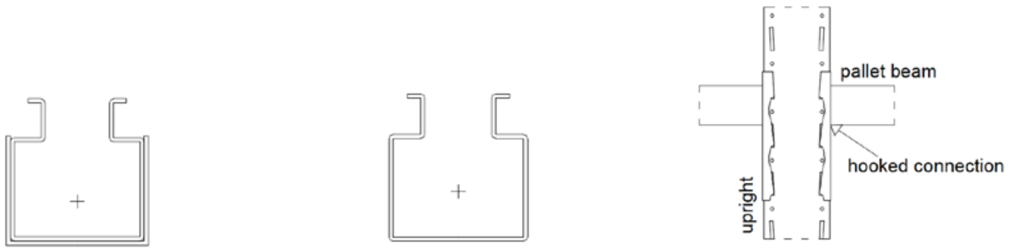
pallet beam
hooked connection
upright

(a) (b) (c)

Figure 5.13: Detail drawings for multi-depth Case Study A, showing (a): a reinforced upright Ω+U section, (b): a standard upright Ω section and (c): an upright-to-beam hooked connection.

5.4.2 Model validation

Modal analysis is performed as an initial benchmark test, to check both the eigenvalues and the eigenmodes of the full versus the reduced model. The high commonality among the adjacent upright frames and the low shear stiffness of the roof truss enables the substitution of one to four upright frames (i.e., built-up columns) by a single equivalent “macro-column”, and thus each cross-aisle frame may be simplified to comprise only six such “macro-columns”. Both numerical models were realized using SAP2000. Along the down-aisle direction, half of the vertical braces than belong to the bracing towers were deleted, as they behave as tension-only elements due to their high slenderness. The full model (Figure 5.14(a)), which captures all the structural details of the warehouse, requires approximately 647,000 DOFs and 200,000 Euler-Bernoulli beam elements, making the pre- and post-processing extremely cumbersome. On the other hand, the simplified model with the six “macro-columns” (Figure 5.14(b)), comprises 17,000 DOFs and 7,500 Timoshenko beam elements, leading to a reduction of 97.4%. Finally, Figure 5.15 illustrates the modes of vibration for both models.

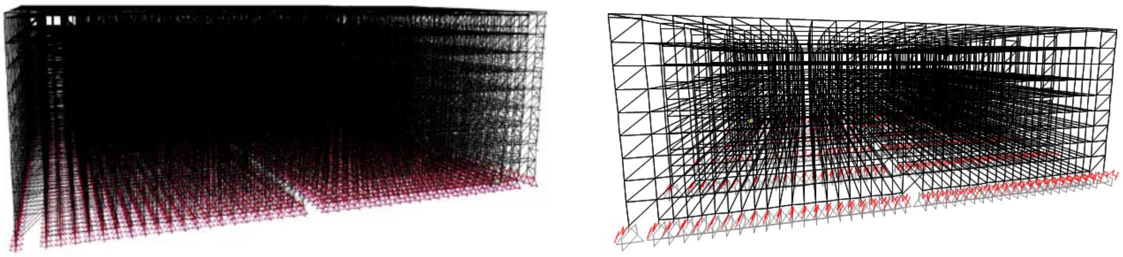

(a) (b)

Figure 5.14: Numerical models of the multi-depth Case Study A, showing (a) the full 3D beam-column model (647,000 DOFs), and (b) the simplified 3D Timoshenko-beam model (17,000 DOFs)

As observed, some modes along the cross-aisle direction have sinusoidal shapes (i.e., diaphragm shearing), arising from the absence of a stiff roof that would act as a diaphragm. In the context of a modal response spectrum analysis (MRSA), an assumption of uniform spatial distribution of mass, and consequently seismic loading, would mean that such eigenmodes correspond to nearly zero modal participation factors, as typically estimated for the roof deformation. This can be shown by assuming N cross-aisle frames of m total mass each, moving in a sinusoidal pattern along the cross-aisle direction:

$$\begin{aligned}\Gamma_i &= \frac{L_i}{\widehat{m}_i} = \frac{\varphi_i^T[M]\vec{r}}{\widehat{m}_i} = \frac{\varphi_i^T[M]\vec{r}}{\widehat{m}_i} \\ &= \frac{m\sum_{j=1}^{N} sin\big(2\pi i(j-1)/(N-1)\big)\,\vec{r}}{\widehat{m}_i} \approx \frac{m\left(\int_0^1 sin(2\pi i x)\,dx\right)\vec{r}}{\widehat{m}_i} = 0\end{aligned} \qquad \text{Eq. (5.11)}$$

where $i \geq 1$, φ_i the eigenvector, $\widehat{m}_i$ the modal mass, Γ_i the modal participation factor of mode i, and $\vec{r}$ the influence vector (Chopra, 1996). In practice, though, minor asymmetries in the mass and/or stiffness distribution will typically result to small, non-zero values of Γ_i. As a result, the typical 90% mass participation is difficult to achieve, as it requires the addition of many such modes, leading to prohibitive time and storage costs. More worrisome is the fact that, despite their near-zero contribution to the roof deformation (where Γ_i and effective masses practically refer to), diaphragm-shearing modes have non-negligible contribution to local deformations and moments/forces on each frame. In other words, the missing 10% from a 90% effective mass inclusion may have significant consequences for some members. This highlights the potential for large errors at the local level when seismic design is based only on MRSA with modes selected according to their roof-level participation (Chopra, 1996).

Full model Simplified model

Cross-aisle, T = 1.53 sec Cross-aisle, T = 1.52 sec

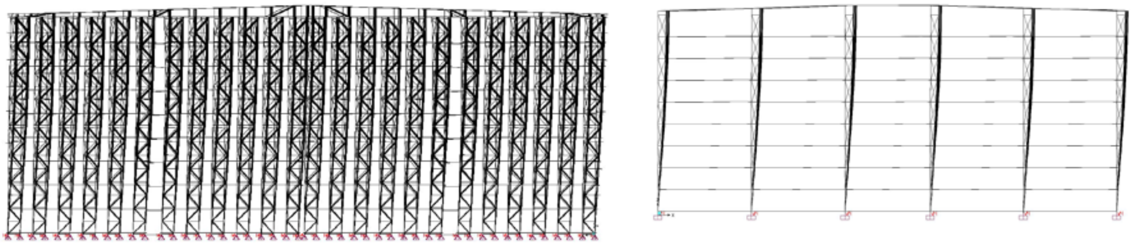

Diaphragm shearing, T = 1.50 sec Diaphragm shearing, T = 1.51 sec

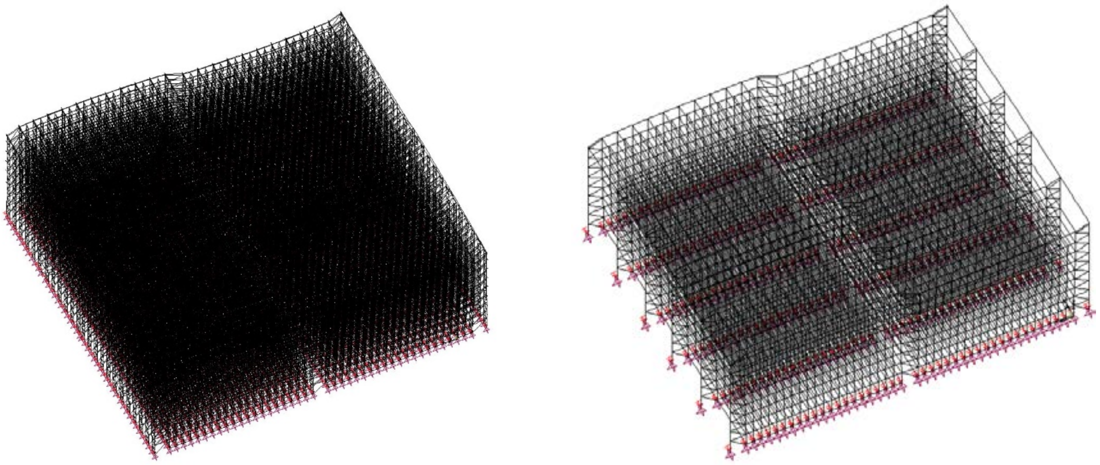

Down-aisle, T = 1.33 sec Down-aisle, T = 1.25 sec

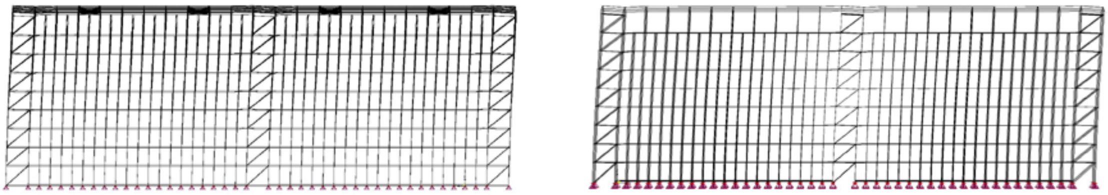

Figure 5.15: Modal analysis results of the 3D multi-depth Case Study A showing the dominant modes along the cross- and down-aisle direction as well as diaphragm shearing for the full model (left) and the simplified one (right).

Further to modal analysis, time-history analysis was conducted as a second benchmark test using a single 2D cross-aisle frame. The North-South component of the ChiChi 1999 event at Station CHY026 was selected from the PEER NGA database (Ancheta et al., 2013). To demonstrate the progressive order (and resolution) reduction, four models were considered, namely the “full” model (4863 DOFs), the “24 macro-columns” model (900 DOFs), the “12 macro-columns” model (396 DOFs) and finally the “6 macro-columns” (198 DOFs), as shown in Figure 5.3. All models incorporated geometric nonlinearities via P-Δ formulation and Rayleigh damping with viscous damping ratio of 3%. The maximum interstory drift profiles are shown in Figure 5.16, along with the relative error of each model. The “24 macro-columns” model showed excellent performance as it overestimated the maximum interstory drift only by 2%, while using 18.5% the DOFs of the full one. The other two models were less accurate which is attributed to the order reduction and to the assumption of “100% shear lag” during the combination of multiple upright frames. However, this may be a valid compromise as the complexity of the problem is reduced by orders of magnitude. Depending on numerical difficulty and the nature of the problem, one can choose the desired level of fidelity or even combine different simplified approaches in the context of a multi-fidelity analysis.

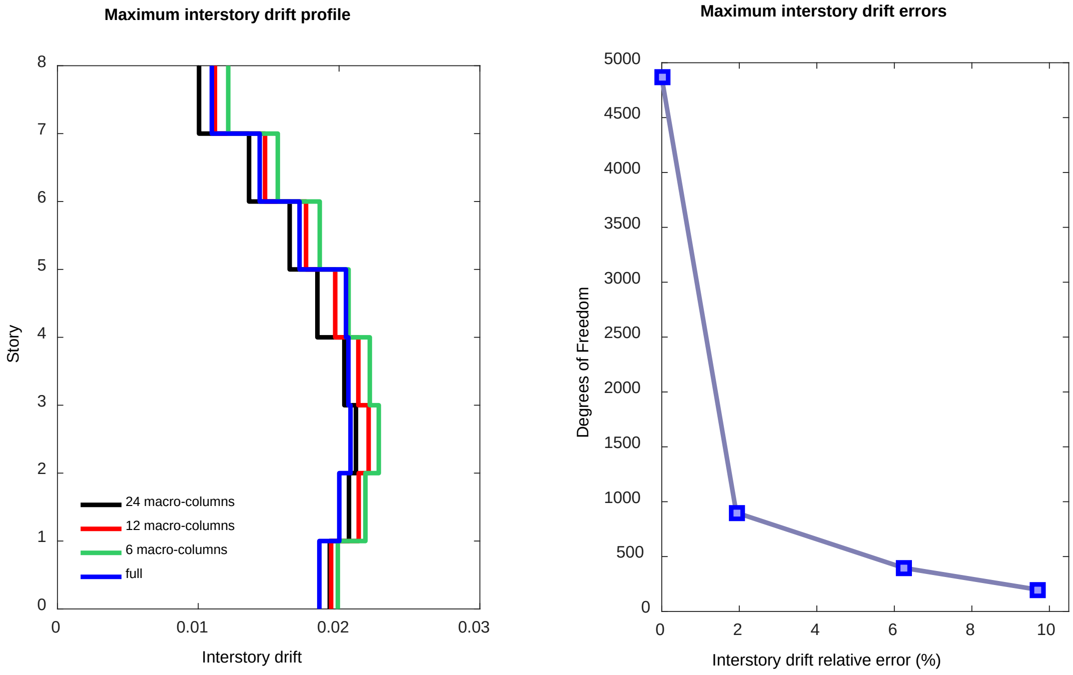

Figure 5.16: Response history results for the 2D cross-aisle frame of Case Study A, showing the peak interstory drift profiles for the four models (left) and the relative error of the maximum (over all stories) interstory drifts versus the DOFs of each model (right).

5.4.3 Fragility assessment

A set of 30 records is employed for conducting response history analyses. This has been selected to be consistent with the hazard at an intensity level corresponding to a 2%/50 years probability of exceedance in high seismicity European sites (Tsarpalis et al., 2020). The record set is available at Kohrangi and Vamvatsikos (2016). To reduce the computational demands, a multi stripe analysis is performed (Jalayer and Cornell, 2009) by scaling said records to three intensity levels, approximately corresponding to exceedance probabilities of 50%, 10%, and 2% in 50 years. As intensity measure (IM) we employed the geometric mean of spectral acceleration from both horizontal components, $Sa(\overline{T})$, estimated at a mean period of $\overline{T}$ = 0.5·(T_x+T_y), where T_x and T_y are the dominant modes along the cross- and down-aisle direction, respectively. The three intensity levels thus become [0.5, 1.0, 1.5]·$Sa_d(\overline{T})$, where $Sa_d(\overline{T})$ is the 10% in 50 years value typically used in design.

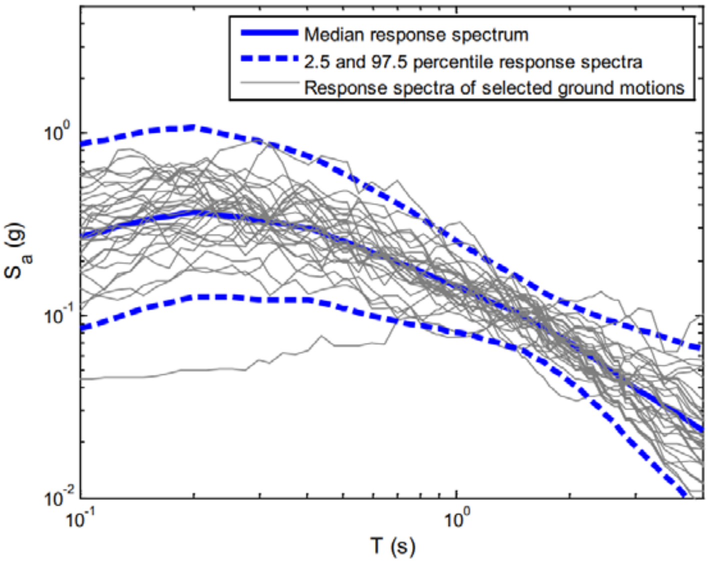

Figure 5.17: Response spectra of selected ground motions for high seismicity European sites, scaled at 2% in 50 years level (Kohrangi and Vamvatsikos, 2016).

The maximum interstory drift was adopted as the engineering demand parameter (EDP). Rayleigh damping was employed with a viscous damping ratio of 3% (per design specifications) assigned to periods 1.5 s and 1.0 s, due to the high concentration of multiple locally-important modes within this range, as a consequence of having no rigid diaphragm. To account for global geometric nonlinearity effects, a P-Δ formulation was used in all beam-column elements. As a result of the introduced geometric nonlinearity, and despite the otherwise elastic model, a direct integration scheme was adopted, increasing the numerical effort for each time-history analysis. However, the simplified model was able to provide robustness, fast convergence and therefore significant time savings.

Figure 5.18 illustrates the results of the multi stripe analysis, highlighting the significant impact of the second-order effects, as the seismic response of the structure is highly nonlinear despite the absence of material nonlinearity. For illustrative purposes three indicative limit states are employed. They are defined by means of maximum interstory drift thresholds, namely Light Damage at 1%, Moderate Damage at 2% and Collapse Prevention at 4%. Non-simulated modes of failure were included in post-processing by checking for local member brittle failures (e.g., buckling of uprights, connection failure, etc.), which are assumed to rapidly propagate to global collapse due to the lack of any meaningful force redistribution capability. Fragilities were derived by fitting the three stripes via the 5-parameter model of Jalayer and Cornell (2009), comprising a lognormal distribution to capture collapse points (either from simulated or non-simulated modes), together with a power-law relationship (Cornell et al., 2002) to model the conditional distribution of EDP given IM for non-collapse points. From Figure 5.18 it is evident that the derived Moderate Damage and Collapse Prevention fragility curves are almost identical, with the former having a probability of exceedance at the design level equal to 18% and the latter 16%. This confirms our intuition, i.e., the ARSWs designed according to current professional practice are optimized to the maximum, delivering the desired performance for design level intensities but not being able to extend into the beyond-design range with any confidence.

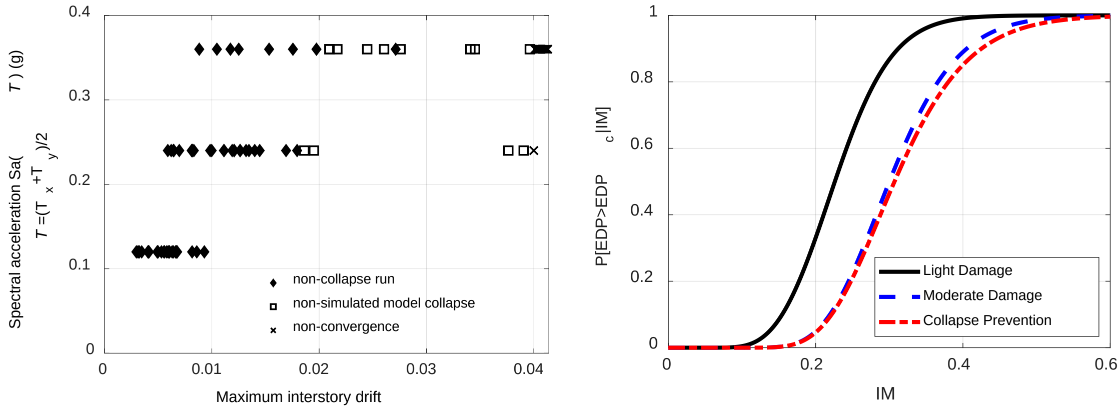

Figure 5.18: Multi stripe analysis for the multi-depth Case Study A, showing the IM-EDP stripes for the three intensity levels (left), and the fragility curves for the three examined limit states (right).

5.5 Case study B: Nonlinear model of a double-depth ARSW

5.5.1 Structure and model description

The ARSW double-depth frame under consideration was adopted from Caprili et al. (2018), who designed it according to EN 1993 (2005) and EN 1998-1 (2004) for a peak ground acceleration of $a_g = 0.163$ g and assuming a behaviour (or strength reduction) factor of $q = 2$. It consists of 19 loading levels (“stories”), each with two exterior double-upright frames and four interior triple-upright frames (Figure 5.19(a)). Exterior frames can carry one pallet of 1000 kg at each level, while interior frames carry two. This is a proof-of-concept design that does not follow current industry norms. It adopts a design approach more akin to conventional ductile concentric-braced frame buildings, where plasticity is concentrated in the bracing system while the uprights remain elastic. Thus, compact hot-rolled sections are employed for the uprights (class 1 per EN 1993 (2005), see Table 5.4), while capacity design is employed to ensure that no connections fail and tension braces yield before global or local buckling of uprights occurs.

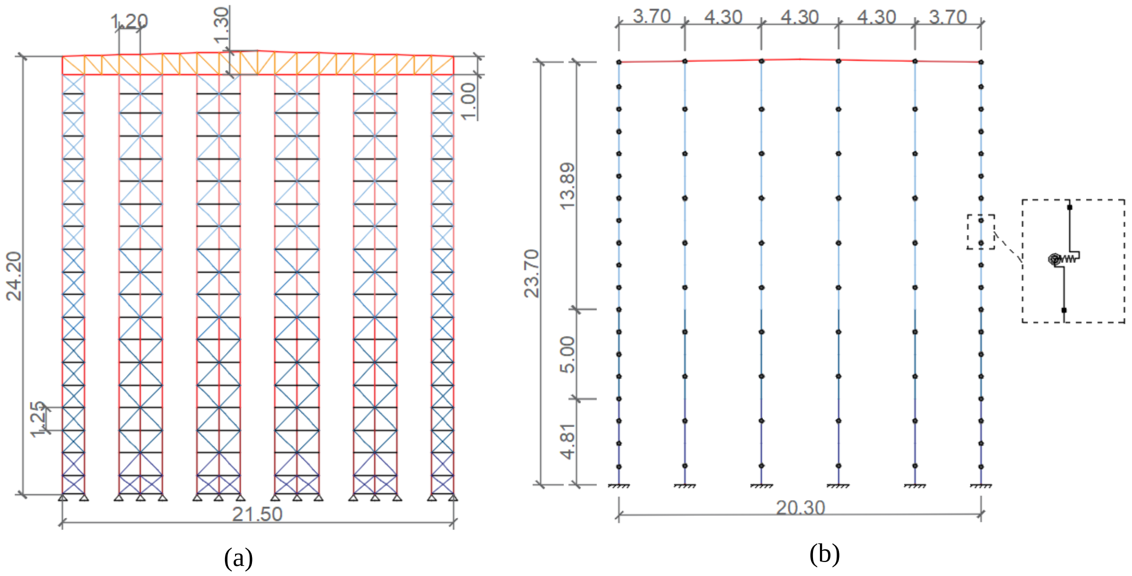

(a) (b)

Figure 5.19: The cross-aisle view of the ARSW double-depth frame of Caprili et al. (2018), showing (a) the full model, and (b) the reduced-order one (units in meters).

Three numerical models of decreasing complexity were realized in OpenSees. A Rayleigh damping formulation was employed in all three, assigning a viscous damping ratio of 3% to the first and second eigenperiods of 1.03 and 0.41 s, respectively. Firstly, a “fiber model” (4758 elements, 3738 DOFs) was defined, where all structural members were simulated as force-based distributed-plasticity beam-column elements with fiber sections at three integration points. The Steel02 material of OpenSees (McKenna et al., 2000) was chosen with 0.5% strain-hardening and 10% fracture strain, representing the well-established Giuffré-Menegotto-Pinto model (Giuffrè and Pinto, 1970). To account for flexural buckling, an imperfection equal to $L/200$ was introduced at mid-span of the diagonal braces. End releases were employed at the ends of the hinged diagonals and horizontals. As the fiber elements are computationally demanding, a “truss model” (1134 elements, 1086 DOFs) was also considered by substituting the distributed plasticity diagonal braces with lumped-plasticity nonlinear truss elements. The material law was derived from a uniaxial compression-tension numerical test of each diagonal, as shown in Figure 5.20. Clearly this is a conscious choice to ensure maximum compatibility and a fair comparison basis between the fiber and the truss model; in practice one could directly determine the truss member backbone, e.g., as per ASCE 41-13 (2014). Considering the force-deformation response under cycle loading, the Pinching4 material of OpenSees was again used, calibrated in a same fashion as for the case of the shear spring of the link element (Figure 5.5). Only in-cycle degradation was incorporated in the trusses, neglecting any cyclic degradation effects. Finally, in the “link model” (252 elements, 234 DOFs), each square segment of an interior or exterior upright frame, measuring 2.5 m and 1.25 m high, respectively, is replaced by an equivalent two-node link element, while linear elastic Timoshenko beam elements are used for the truss roof (Figure 5.19(b)).

Table 5.4: Structural member cross-sections and steel grade for interior and exterior upright frames (Case B). Per EN 1993 (2005), steel grade Sxxx has a characteristic yield strength of xxx MPa.

Height (m)	**Uprights (both)**	**Diagonal (exterior)**	**Diagonal (interior)**	**Horizontal (both)**
[0.0, 2.3)	RHS * (S355) 120x80x10	L + (S355) 40x40x5	L (S355) 40x40x5	DC ++ (S355) 80x50x3
[2.3, 4.8)	RHS (S355) 120x80x10	L (S275) 40x40x4	RHS (S355) 30x30x2.5	DC (S355) 80x50x3
[4.8, 9.8)	RHS (S355) 120x80x6	L (S275) 40x40x4	RHS (S355) 30x30x2.5	DC (S355) 80x50x3
[9.8, 13.6)	RHS (S355) 120x80x4	L (S275) 35x35x4	RHS (S275) 30x30x2.5	DC (S355) 80x50x3
[13.6, 23.2]	RHS (S355) 120x80x4	L (S235) 30x30x4	RHS (S235) 30x30x2	DC (S355) 80x50x3

* RHS: Rectangular hollow section; + L: angle section; ++ DC: double-channel Section.

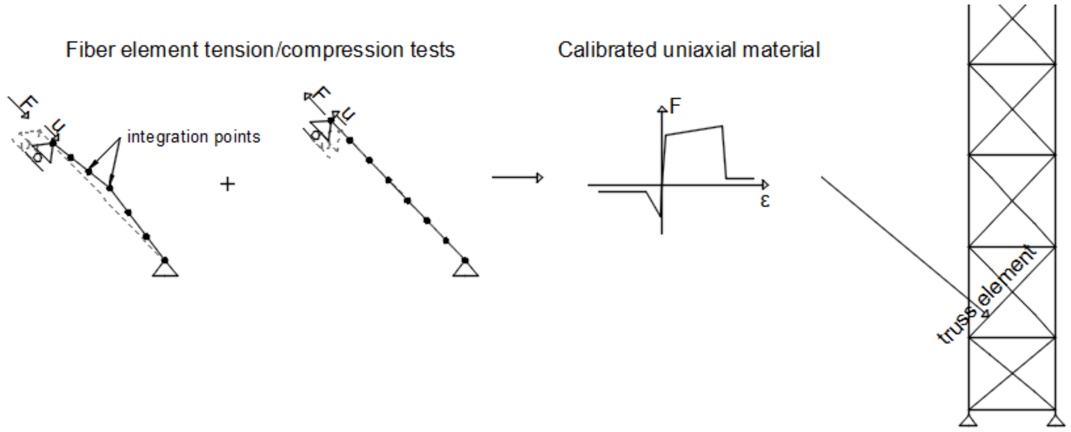
Fiber element tension/compression tests
F
u
integration points
+
F
u
Calibrated uniaxial material
F
ε
truss element

Figure 5.20: Axial compression-tension numerical test for a distributed plasticity beam-column representation of diagonal brace. The derived force-deformation curve is employed to characterize the equivalent nonlinear truss element.

5.5.2 Model validation

Static pushover (SPO) analysis was conducted to verify the suitability of the proposed models in the inelastic region. A first-mode-like triangular load distribution was adopted and the displacement of the roof was monitored up until 4.0% interstory drift was achieved. Figure 5.21 illustrates the capacity curves for the three models under consideration, signifying the ability of the frugal link model to produce accurate results even for large inelastic deformations.

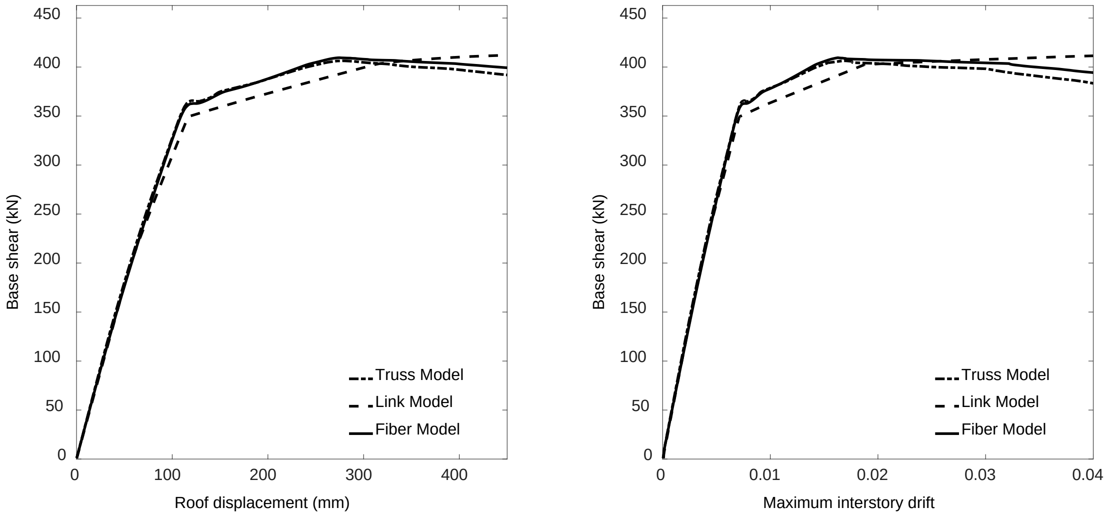

Figure 5.21: Capacity curves for the three numerical models of Case Study B, showing the base shear versus the roof displacement (left), and versus the maximum interstory drift (right).

For further verification a series of nonlinear response history analyses was performed using the same ground motion record as for the Case Study A (ChiChi 1999, Station CHY026 (Ancheta et al., 2013)). Four levels of intensity were employed, at scale factors of 0.89, 1.00, 2.41 and 4.44 to show progressive levels of damage.

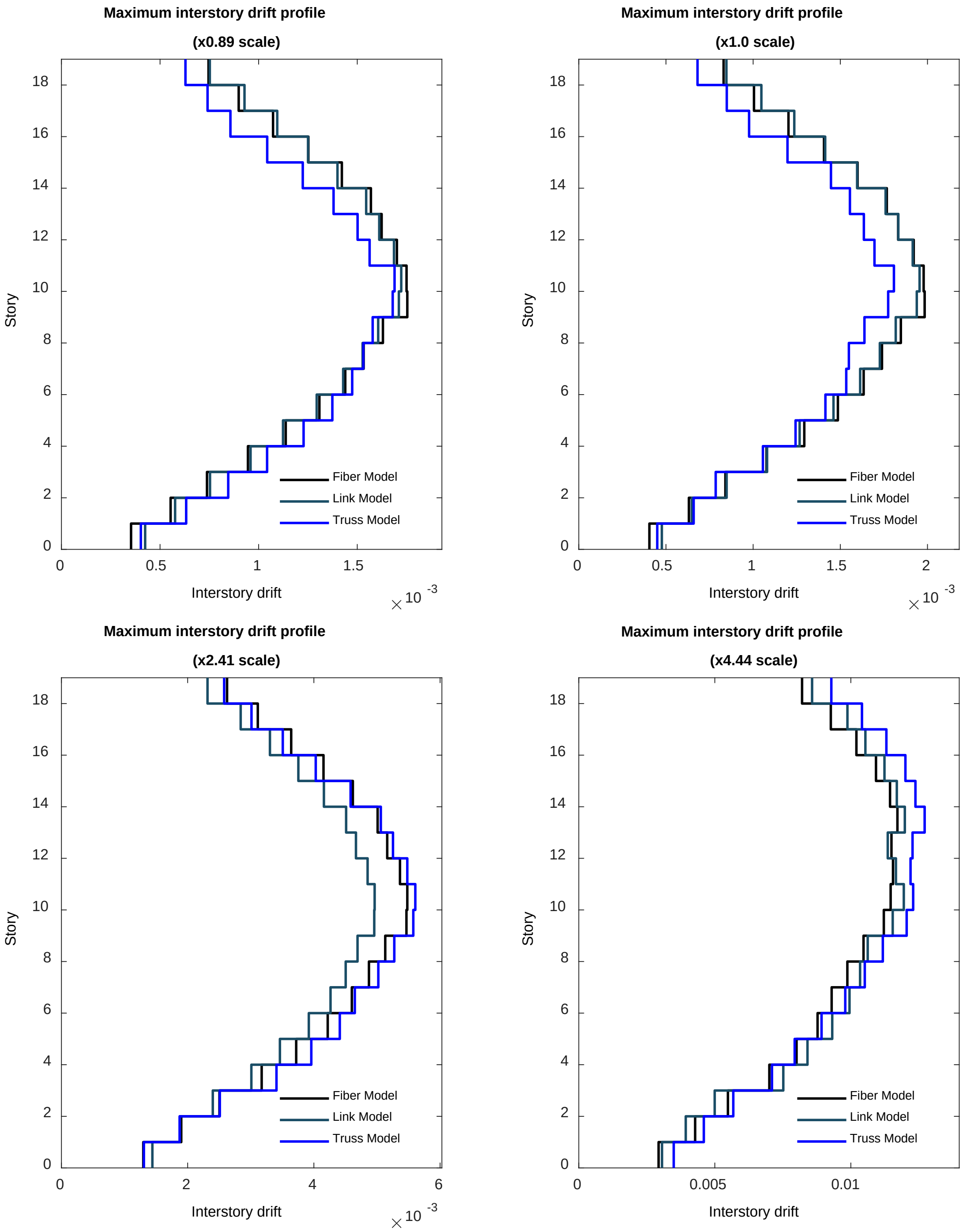

Figure 5.22: Maximum inter-story drift profile for the three numerical models of Case Study B (full, truss and link model). Four record scales were considered corresponding scale factors of 0.89, 1.00, 2.41 and 4.44.

Figure 5.22 illustrates the maximum drift profiles for each record scale, showing a good correspondance among the three numerical models. At the third scaling level, where the highest divergence was found, the link model predicted a maximum interstory drift equal to 0.50% vis-à-vis 0.55% of the fiber, showing a 10% underestimation. However, this relative difference is not consistent, as the link model sometimes overestimates and others times understimates the maximum interstory drift, depending on the record employed. Thus, it is more akin to random error (i.e., noise) rather than bias, and it could thus be treated by increasing the dispersion of the predicted response to account for modelling uncertainty

(FEMA P-58-1, 2018). Still, its magnitude is negligible vis-à-vis the 30% to 40% dispersion due to record-to-record variability, allowing us to safely disregard it. Finally, considering performance gains, each time-history analysis requires approximately 30 seconds for the link model, 60 minutes for the truss model and the 90 minutes for the fiber model on an Intel i5 3.40 GHz desktop. These time-savings are expected to be even greater for the case of multi-depth ARSWs (as the number of upright frames is increased) or for the obvious case of three-dimensional analyses.

5.5.3 Fragility assessment

Offering a detailed view of demand at each IM level, incremental dynamic analysis (IDA) (Vamvatsikos and Cornell, 2002) is adopted to conduct fragility assessment. Due to their propensity for numerical instabilities in the post-yield region and the prohibitive computational time required, models that comprise fiber elements (i.e., both the “fiber” and the “truss” models) were not considered; instead, the “link” model allowed us to perform the analysis within only 2-3 hours on an Intel i5 3.40 GHz desktop. The same set of 30 records (Kohrangi and Vamvatsikos, 2016) employed for Case Study A is also used here. The maximum interstory drift was adopted as the EDP and the 5%-damped first-mode spectral acceleration as the IM.

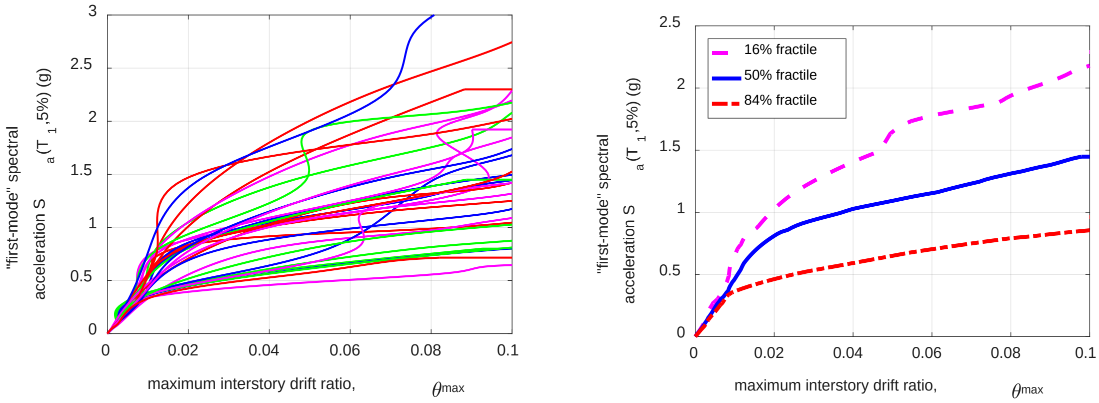

(a) (b)

Figure 5.23: IDA analysis results for the link model of Case Study B, showing (a) the individual IDA curves of each record, and (b) the corresponding 16%, 50% and 84% fractiles.

Figure 5.23(a)-(b) present the IDA curves and the 16%, 50%, 84% fractiles, respectively, highlighting the significant record-to-record variability, easily eclipsing the much lower modeling uncertainty. The IDA curves indicate the presence of considerable ductility, thanks to the capacity design rules employed. As already mentioned, this is atypical of actual ARSW structures, yet highly indicative of the seismic performance gains realized by adopting ductile design standards. Fragility curves corresponding to an exceedance of 1%, 2% and 4% maximum interstory drift, akin to a Light Damage, Moderate Damage and Collapse Prevention limit-states, respectively, are illustrated in Figure 5.24. The resulting median value of spectral acceleration is 1.0 g, whereas the design value is only 0.26 g, showing excellent performance. Actually, at the design level acceleration there is practically a zero probability of limit-state exceedance, compared to the 17% probability derived for Case Study A. Still, such performance gains come at a substantial cost of material, employing hot-rolled rather than cold-formed members, together with stronger connections, making this a difficult choice.

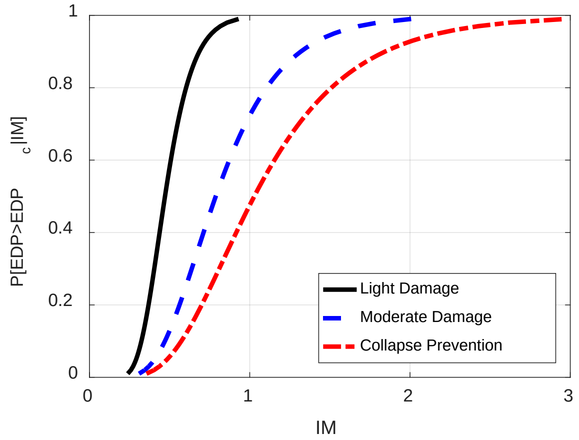

Figure 5.24: Fragility curves for Light Damage, Moderate Damage and Collapse Prevention limit states of Case Study B.

5.6 Conclusions

A reduced-order modelling approach for the seismic analysis of ARSWs has been presented in Chapter 5. It is based on the well-established substitution of built-up columns and truss beams with equivalent Timoshenko beam elements, reducing the size of the numerical problem by orders of magnitude. The proposed simplified model goes one step beyond by providing the ability for inelastic static and dynamic simulations with negligible loss of accuracy. This is achieved with the use of link elements that can capture the shear, axial and rotational stiffness degradation of the substituted upright frames. As the evaluation of ARSWs' seismic behaviour is an on-going research process, the proposed simplified model can suitably fit in the context of performance-based assessment and design, where low complexity without loss of fidelity is a primary goal.

5.7 References

Amir M., Papakonstantinou K.G., Warn G.P. (2020a). *"Hysteretic Beam Finite-Element Model Including Multiaxial Yield/Capacity Surface Evolution with Degradations"*, Journal of Engineering Mechanics **146**(9). https://doi.org/10.1061/(ASCE)EM.1943-7889.0001767

Amir M., Papakonstantinou K.G., Warn, G.P. (2020b). *"A consistent Timoshenko hysteretic beam finite element model"*, International Journal of Non-Linear Mechanics, **119**, 103218.

Ancheta T.D., Darragh R.B., Stewart J.P., Seyhan E., Silva W.J., Chiou B.S.J., Wooddell K.E., Graves R.W., Kottke A.R., Boore D.M., Kishida T., Donahue J.L. (2013). *"PEER NGA-West2 Database"*, Technical Report PEER 2013/03. Pacific Earthquake Engineering Research Center, Berkeley, CA.

ASCE 41-13 (2014). *"Seismic Evaluation and Retrofit of Existing Buildings"*, ASCE/SEI 41-13, American Society of Civil Engineers, Reston, VA.

Belleri A., Torquati M., Marini A., Riva P. (2017). *"Simplified building models as advanced seismic screening tools for steel industrial buildings"*, Journal of Constructional Steel Research, **138**, 51-64. https://doi.org/10.1016/j.jcsr.2017.06.027

Caprili S., Morelli F., Salvatore W. Natali A. (2018). *“Design and Analysis of Automated Rack Supported Warehouses”*, The Open Civil Engineering Journal, **14**, 150-166. http://dx.doi.org/10.2174/1874149501812010150

Chopra A.K. (1996). *“Modal Analysis of Linear Dynamic Systems: Physical Interpretation”*, Journal of Structural Engineering **122**(5). https://doi.org/10.1061/(ASCE)0733-9445(1996)122:5(517)

Cornell C.A., Jalayer F., Hamburger R., Foutch D. (2002). *“Probabilistic Basis for 2000 SAC Federal Emergency Management Agency Steel Moment Frame Guidelines”*, Journal of Structural Engineering **128**(4). https://doi.org/10.1061/(ASCE)0733-9445(2002)128:4(526)

EN 15512 (2009). *“Steel static storage systems - Adjustable pallet racking systems - Principles for structural design”*, European Committee for Standardization (CEN), Brussels, Belgium.

EN 16681 (2016). *“Steel static storage systems - Adjustable pallet racking systems - Principles for seismic design”*, European Committee for Standardization (CEN), Brussels, Belgium.

EN 1998-1 (2004). *“Eurocode 8: Design of structures for earthquake resistance - Part 1: General rules, seismic actions and rules for buildings”*, European Committee for Standardization, Brussels, Belgium.

EN 1998-3 (2005). *“Eurocode 8: Design of structures for earthquake resistance - Part 3: Assessment and retrofitting of buildings”*, European Committee for Standardization, Brussels, Belgium.

EN 1993 (2005). *“Eurocode 3: Design of Steel Structures”*, European Committee for Standardization, Brussels, Belgium.

EN 1993-1-1 (2005). *“Eurocode 3: Design of Steel Structures - Part 1-1: General rules and rules for buildings”*, European Committee for Standardization, Brussels, Belgium.

FEMA P-58-1 (2018). *“Seismic Performance Assessment of Buildings, Volume 1 – Methodology”*, The Federal Emergency Management Agency.

Giuffrè A., Pinto P.E. (1970). *“Il comportamento del cemento armato per sollecitazioni cicliche di forte intensità”*, Giornale del Genio Civile.

Jalayer F., Cornell C.A. (2009). *“Alternative non-linear demand estimation methods for probability-based seismic assessments”*, Earthquake Engineering and Structural Dynamics **38**(8), 951-972. https://doi.org/10.1002/eqe.876

Kalochairetis K. Gantes C.J. (2012). *“Axially and transversely loaded Timoshenko and laced built-up columns with arbitrary supports”*, Journal of Constructional Steel Research, **77**, 95-106. https://doi.org/10.1016/j.jcsr.2012.05.004

Kanyilmaz A. (2015). “*Validation of Fiber-Based Distributed Plasticity Approach for Steel Bracing Models*”, Civil Engineering Journal, **1**, 1-13. 10.28991/cej-2015-00000005

Kohrangi M., Vamvatsikos D. (2016). *“INNOSEIS ground motion set for high seismicity European sites”*. INNOSEIS Project. Link: http://innoseis.ntua.gr/high_record_set.rar

McKenna F., Fenves G.L., Scott M.H., Jeremic B. (2000). *“Open System for Earthquake Engineering Simulation (OpenSees)”*, Pacific Earthquake Engineering Research Center, University of California, Berkeley, CA.

SAP2000, CSI, Computers and Structures Inc., homepage: https://www.csiamerica.com

Talebian N., Benoit P.G., Baldassino N., Karampour H. (2018). *“Factors contributing to the transverse shear stiffness of bolted cold-formed steel storage rack upright frames with channel* *bracing members"*, Thin-Walled Structures, **136**, 50-63. https://doi.org/10.1016/j.tws.2018.12.001

Tsarpalis P., Bakalis K., Thanopoulos P., Vayas I., Vamvatsikos D. (2020). *"Pre-normative assessment of behaviour factor for lateral load resisting system FUSEIS pin-link"*, Bulletin of Earthquake Engineering, **18**, 2681-2698. 10.1007/s10518-020-00799-y

Vamvatsikos D., Cornell C.A. (2002). *"Incremental dynamic analysis"*, Earthquake Engineering and Structural Dynamics **31**(3), 491-514. https://doi.org/10.1002/eqe.141

6 Seismic Assessment Approaches for Sliding Contents in Storage Racks[3]

6.1 Introduction

Steel pallet racking systems are civil engineering structures used to store goods and materials before their distribution to the public. They comprise thin-walled cold-formed members that carry high live loads, by far greater than their self-weight. Contents are not mechanically connected to the racking system, but are placed on pallets, boxes, containers or even hanged (Tsarpalis et al., 2022). As a result, the seismic response of racks is characterized by a content-structure-sliding interaction (CSSI) that typically does not appear in conventional buildings. Specifically, during seismic excitation, inertia forces are initially transferred from the goods to the rack by means of static friction forces acting on the surface between, e.g., the pallet and the supporting beams in case of an adjustable pallet racking (APR) system. Depending on the applied excitation, this stabilizing mechanism may not be adequate to restrain the contents, which can then *slide* relative to the rack. CSSI is multi-faceted, offering both detrimental and beneficial effects. Before the onset of sliding, the transfer of forces between adjacent pallet beams or rails and the immobile pallets themselves offers a horizontal diaphragm effect (Gilbert et al., 2013; 2014). Additionally, after content sliding is initiated, sliding friction sets an upper boundary to the inertia forces transferred to the racking system, effectively reducing the horizontal mass of the contents that needs to be accounted for deriving the seismic forces. This reduction of the apparent inertia of the rack due to sliding of the goods is akin to a *seismic isolation mechanism* and henceforth it will be referred to as such.

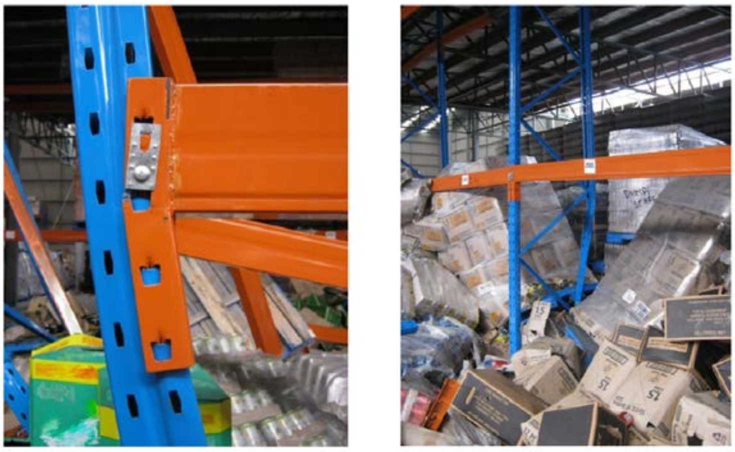

Figure 6.1: Partial collapse of an adjustable steel rack due to pallet falling during the Christchurch earthquake of 2011 (Clifton et al., 2011).

On the other hand, excessive content sliding can lead to localized damages due to impacts on structural components or even global collapse due to contents falling off (Figure 6.1) and crushing adjacent frames. The first phenomenon is prevalent in the down-aisle direction where the uprights can arrest excessive pallet displacements. Content fall-off is especially critical in the cross-aisle direction, as there are no uprights to prevent the goods from sliding off. It is also noted that even moderate levels of sliding may result to long downtimes in automated rack warehouses. Therein, robotic systems store and retrieve the pallets, thus, whenever a unit load slides beyond the systems' tolerances, operation ceases until manual re-adjustment of pallets takes place. There are even more aspects to CSSI that cannot be fully discussed herein. For example, Adamakos et al. (2018) found that, contrary to current code assumptions, e.g., EN 16681 (2016), the friction force is unequally distributed between the two edges of a pallet resting on supporting beams, with higher forces appearing on the leading edge in the direction of sliding.

---

[3] This work contains material from “Tsarpalis D., Vamvatsikos D., Vayas I. (2021). *Seismic assessment approaches for mass-dominant contents: The case of storage racks*, Earthquake Engineering and Structural Dynamics. https://doi.org/10.1002/eqe.3592”, reproduced here with permission.

Of particular interest in accounting for CSSI in design and assessment are (i) the beneficial effect of reduced horizontal inertial mass for estimating lateral loads, and (ii) the estimation of sliding displacements to avoid fall-off and/or impact. Current seismic codes do not offer a tool to predict the latter, as it is related to absolute floor (or *load level*, in rack parlance) accelerations, for which a conventional modal response spectrum analysis (MRSA) is not able to provide any information (for alternatives see Taghavi and Miranda (2005), Moschen et al. (2016), Pozzi and Der Kiureghian (2015)). On the other hand, they incorporate the positive effect of sliding isolation using the inertial mass reduction factors.

For example, in USA, the Rack Manufacturer Institute, RMI (2012), specification accounts for sliding by applying a multiplication factor of 0.67 to reduce the seismic mass of contents, regardless of the friction coefficient of the contact surface or the seismic intensity. On the other hand, in Europe, EN 16681 (2016) adopts an E_{D1} factor to modify the design spectrum in the context of MRSA, given as (recalling Eq. (3.6)):

$$E_{D1} = \max\{0.4,\ \mu/Sa(T_1) + 0.2\} \leq 1.0 \qquad \text{Eq. (6.1)}$$

where μ is the reference value of the unit-load/beam friction coefficient, T_1 is the fundamental period of vibration of the racking structure in the considered direction, and $Sa(T_1)$ is the ordinate of the elastic spectrum defined in EN 1998-1 (2004), in units of g.

Eq. (6.1) is based on a limited study from the SEISRACKS (Rosin et al., 2007) European project. Elastic time-history analyses were performed on a low-rise APR system along the down-aisle direction, using 3 loading situations, 3 levels of spectral acceleration and 7 artificial accelerograms. It was found that the 0.67 mass reduction factor suggested by RMI is close to the average value of the inertial reduction predicted by the time-history analyses, however it can be unconservative for moderate seismicity levels, where seismic intensities are not high enough to overcome friction and initiate sliding. While the E_{D1} factor given by EN 16681 (2016) is a conceptually better approach over the seismic-intensity-independent 0.67 mass reduction suggested by RMI, it is still questionable whether it can safely be applied for designing along the cross-aisle direction or for high-rise racking systems, where the contribution of higher modes is increased.

To address such issues in CSSI, we shall offer three comprehensive solutions for accounting for CSSI in rack systems:

(i) Nonlinear RHA for MDOF structures, employing realistic friction sliders under nonlinear response-history analysis,

(ii) Linear RHA for MDOF models, employing increased viscous damping to account for sliding “isolation” of pallets,

(iii) MRSA of elastic models, using reduced seismic loads to account for the effect of sliding.

To fully explain the differences among the three approaches, and understand their capabilities, let us first delve into the simplest of CSSI problems and the available methods to treat them.

6.2 RHA for SDOF systems

6.2.1 Newmark’s sliding block analysis

Newmark’s sliding block analysis (NSBA) was first introduced to calculate the permanent displacement of soil slopes during seismic loading (Newmark, 1965). It uses the time history of accelerations that exceed friction to derive sliding displacement via a double integration. Let us consider a body with mass m (i.e., the pallet) resting on a platform (i.e., the racking system), as illustrated in Figure 6.2. Assuming a Coulomb friction model (Coulomb, 1776) the contact surface between the body and the platform is characterized by a friction constant μ, which linearly relates the developed friction F_T with the normal force acting on the body N, i.e., $F_T = \mu \cdot N$. Whenever the external/inertial forces acting on the body exceed T (in absolute value), the body starts moving relatively to the platform and Newton’s third law of motion gives:

$$\begin{aligned} &\Sigma F = ma_{rel} \Rightarrow ma_{plat} - F_T = ma_{rel} \Rightarrow ma_{plat} - \mu m g = ma_{rel} \Rightarrow \\ &a_{rel} = a_{plat} - \mu g \Rightarrow a_{rel} = a_{plat} - a_y \end{aligned} \qquad \text{Eq. (6.2)}$$

where a_{rel} is the relative-to-the-platform acceleration of the body, a_{plat} is the absolute acceleration of the platform, and $a_y = \mu g$ is the *yield* (or sliding-onset) acceleration, which determines whether the body starts sliding on the platform or “re-sticks” to it. The term ma_{plat} is introduced because we are examining the motion of the body relatively to the platform, which is a non-inertial frame of reference.

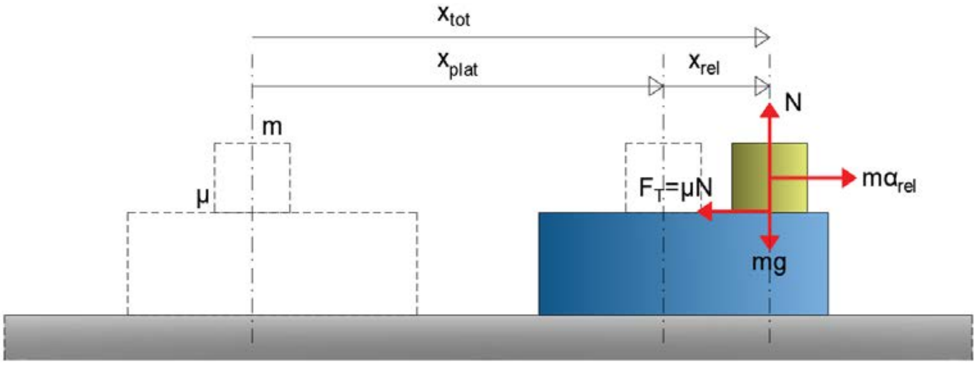

Figure 6.2: Idealized model of a body with mass m sliding with a friction constant μ on a moving rigid platform.

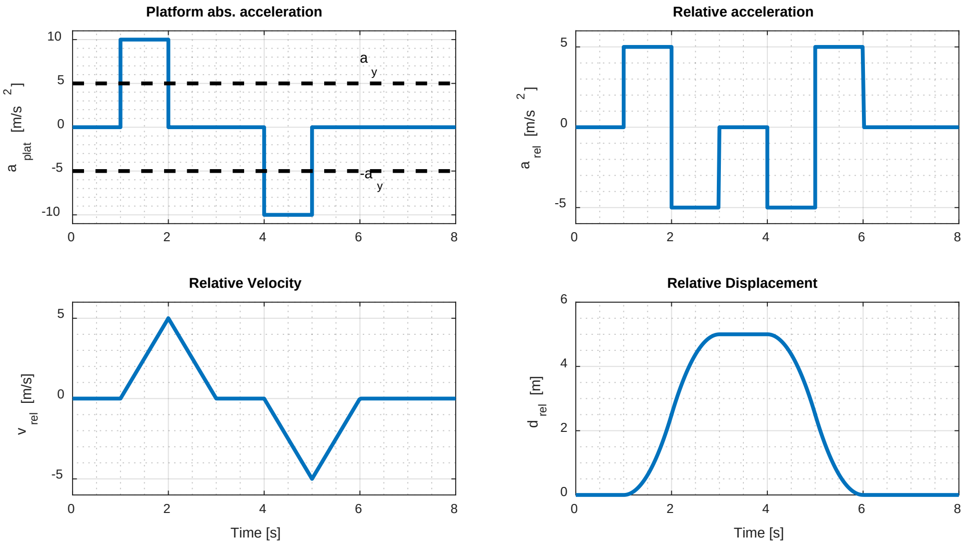

Figure 6.3: NSBA of an idealized body sliding with a_y = 5 m/s^2 on top of a rigid platform that is subjected to two rectangular pulses.

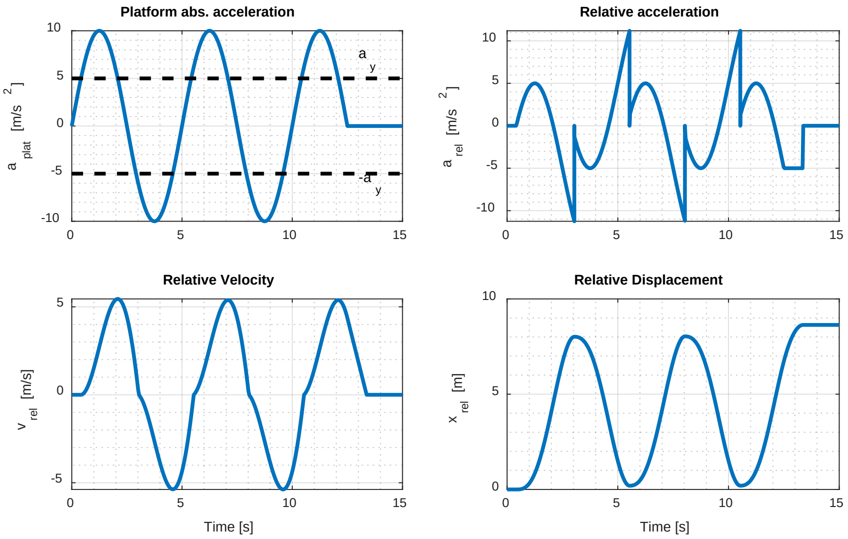

Figure 6.4: NSBA of an idealized body sliding with a_y = 5 m/s^2 on top of a rigid platform that is subjected to two-and-a-half sinusoidal pulses.

In Annex B one may find a numerical implementation of NSBA that is written in MATLAB (MATLAB, 2020) and employs an explicit time-integration scheme. The user has to provide three inputs: the yield acceleration (a_y), a vector with the timesteps, and a vector containing the a_{plat} values for each timestep. The function then returns three outputs: the relative acceleration (a_{rel}), relative velocity (v_{rel}), and relative displacement/sliding (x_{rel}) of the moving body. The algorithm was first verified by subjecting the platform to the simple pulse excitations of Figure 6.3. A yield acceleration of $a_y = 5$ m/s^2 was considered, which corresponds to a friction constant of $\mu \approx 0.5$. At $t = 1$ sec, the platform is subjected to a rectangular pulse of 1 sec duration and a constant absolute acceleration of 10 m/s^2. As a_{plat} exceeds a_y, the body starts sliding with a_{rel} = 5 m/s^2 (Eq. (6.2)). At t = 2 sec the pulse ends and Eq. (6.2) yields $a_{rel} = -a_y = -5$ m/s^2. The body continues to decelerate until t = 3 sec, where v_{rel} becomes zero and the relative motions stops. Integrating twice a_{rel} for the interval [0, 3] sec yields a sliding displacement of $x_{rel} = 5$ m. Then, at $t = 4$ sec the platform is subjected to a second rectangular pulse of the same duration and magnitude as the first one, but with opposite direction. As it was expected, the opposite relative motion occurs, and the body returns to its initial-to-the-platform position. While rectangular pulses are easy to be solved analytically, in most cases a numerical integration is required, as even in the simple example of the sinusoidal pulses of Figure 6.4, the relative motion of the body can be quite complex.

6.2.2 CSSI for SDOF structures

Instead of employing NSBA to calculate the relative motion of the body in post-processing of the structural analysis results, one may directly employ "flat slider" finite elements that explicitly consider the effect of sliding and friction, such as the flatSliderBearing element of OpenSees (McKenna et al., 2000) coupled with a Coulomb friction model. Let us consider a sliding body on top of a single-degree-of-freedom (SDOF) cantilever, essentially a two-degree-of-freedom (2DOF) slider-on-cantilever model with a total mass of M at the top, comprising three nodes (Figure 6.5(a)): Node 1 that has a fix support and nodes 2 and 3 that have the vertical and the rotational DOFs restrained. Nodes 1 and 2 are connected by a beam-column element of EI stiffness, while nodes 2 and 3 by a flat slider with friction constant μ. By assigning a very high value of EI, i.e., a 2DOF system with $T = 0$ sec, one can recover the simpler model of a body sliding on the ground (or on a platform rigidly connected to the ground) resembling Figure 6.2. An example of such a system appears in Figure 6.6, illustrating the absolute acceleration and sliding graphs for a seismic excitation with a PGA that exceeds the yield acceleration of $a_y = 3\ \mathrm{m/s^2}$. Notably, the absolute acceleration diagram of the model with the flat slider is bounded between [–3, +3] $\mathrm{m/s^2}$, while the one employed with NSBA is by definition identical to the imposed ground motion, as the 2DOF system has a period of vibration $T = 0$ sec. As expected, the analytical model can achieve almost perfect results without the need of a more expensive numerical integration.

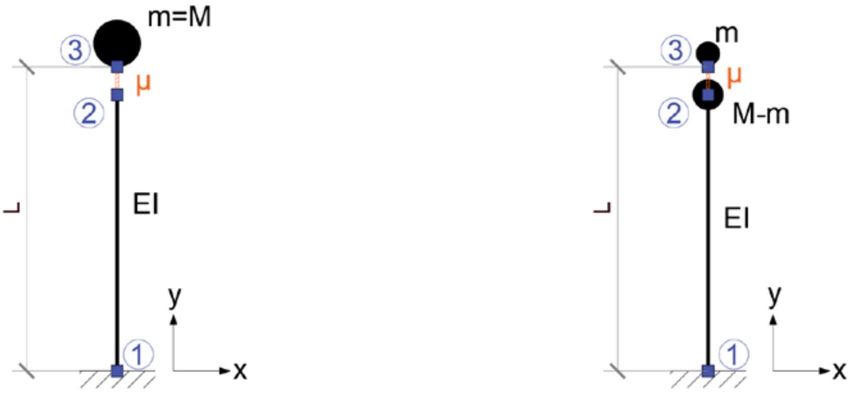

(a) (b)

Figure 6.5: Numerical model of a 2DOF system of a cantilever beam with a flat slider at the top, showing (a) a case where the whole mass can slide ($m = M$), and (b) a case where only a portion m of the total mass M can slide, while $M - m$ is attached to the beam.

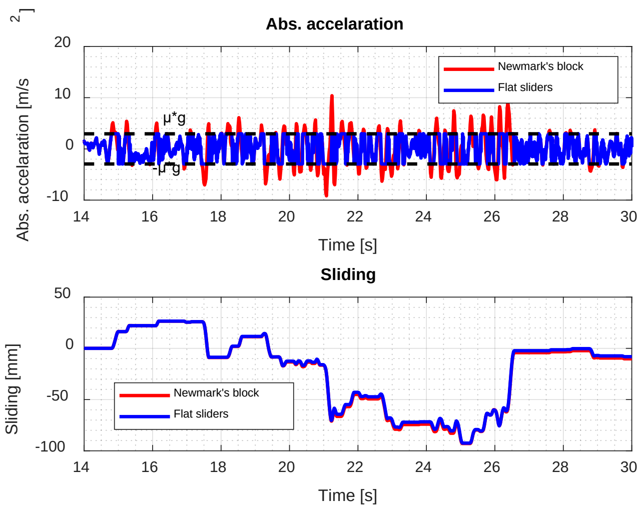

Figure 6.6: Absolute acceleration and sliding diagrams of a mass sliding with friction coefficient $\mu = 0.3$ on top of a rigid platform (period $T = 0$ sec), comparing the predictions of NSBA (SDOF system with rigidly connected mass, where sliding is estimated in post-processing) against the 2DOF flat slider model of Figure 6.5(a) (Landers 1992, Station BAKER FIRE, PEER NGA2 (Ancheta et al., 2013), scaled by 3.28).

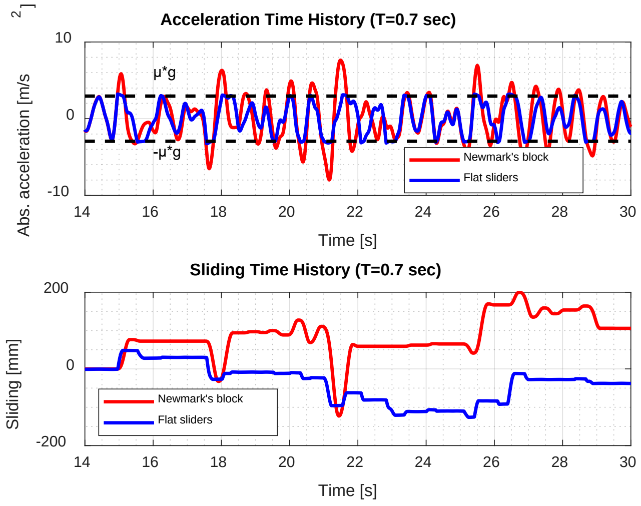

Figure 6.7: Absolute acceleration and sliding diagrams of a 2DOF system with period $T = 0.7$ sec, $\mu = 0.3$, and $m = M$ (100% of mass can slide) comparing the predictions of NSBA (SDOF system with rigidly connected mass, where sliding is estimated in post-processing) against the 2DOF flat slider model of Figure 6.5(a) (Landers 1992, Station BAKER FIRE, PEER NGA2 (Ancheta et al., 2013), scaled by 3.28).

While NSBA performs excellently when analyzing the motion of a body that slides on top of a rigid platform, its accuracy is harshly decreased when examining flexible structures/platforms, i.e., 2DOF systems with $T > 0$ sec. To demonstrate this issue, the excitation used in the previous example of Figure 6.6 was employed again, but this time the stiffness of the cantilever beam was adjusted to achieve a $T = 0.7$ sec. In the “flat slider” analysis, nodes 2 and 3 were connected by a flat slider element with $\mu = 0.3$ (Figure 6.5(a)), supporting a sliding mass of $M = 10{,}000$ kg. Then, in the “NSBA” analysis, nodes 2 and 3 were rigidly connected and NSBA was performed at post-processing, using the time-history of absolute accelerations at node 3. Comparing the two approaches in Figure 6.7, one may observe that NSBA overpredicted the sliding displacement almost by two times, while the difference is even greater for the residual displacements. An intuitive explanation can be found by comparing the time-history of absolute accelerations of the two models: NSBA does not consider the interaction between the flexible platform and the sliding content (i.e, CSSI), and, thus, is based on the full mass and inertia of the system. On the other hand, the "flat slider" model changes its inertia from 10,000 to 0 kg when the mass slides, and thus the seismic action has a lower impact on the structure.

While NSBA is not suitable for cases where the entire system mass can slide, it can still be quite accurate for typical buildings, where the mass of the contents is a small portion of the total. This can be demonstrated by modifying the slider-on-cantilever model of Figure 6.5(a), to a model with a sliding mass m on node 3 and a non-sliding mass $M - m$ on node 2, as shown in Figure 6.5(b). Figure 6.8 compares NSBA with the flat slider in terms of predicted sliding, using a set of 30 ordinary records selected and scaled to be hazard-consistent at the intensity with a 10% in 50 years probability of exceedance for Van, Turkey (Kohrangi et al., 2018), and m/M ranging within 1% to 100%. For values of $m/M < 0.05$, NSBA gives near perfect results, as CSSI has a minor effect. Values of $0.05 < m/M < 0.8$ lead to an unbiased median, yet a steadily increasing standard deviation, either on the low side (16%) or the high side (84%). In other words, NSBA would not be an accurate, or even safe alternative (for $m/M > 0.3$), despite being unbiased. On the other hand, for high $m/M > 0.8$ the sliding overestimation grows exponentially, starting from a mean value of 110% (median of 100%) for $m/M = 0.8$, up to 170% for $m/M = 1.0$. Still, how this translates to a multi-degree-of-freedom (MDOF) racking system with multiple load levels and modes of vibration is not apparent.

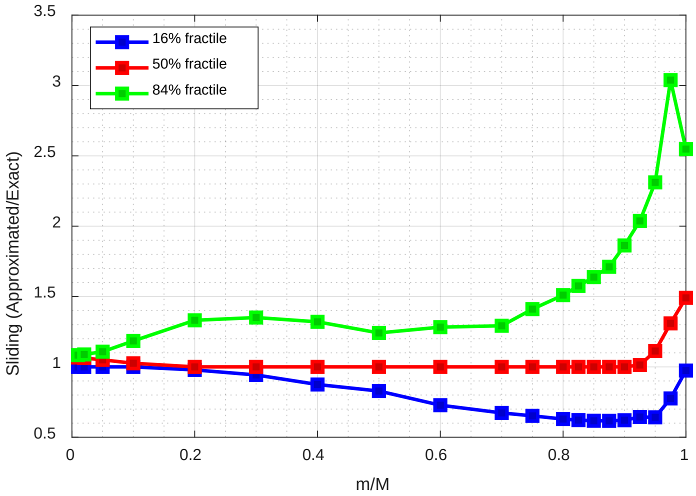

Figure 6.8: Comparison of NSBA ("Approximated") with a 2DOF slider-on-cantilever ("Exact"), in terms of the predicted sliding for a system with $T = 0.7$ sec and $\mu = 0.3$. The 16%, 50% and 84% fractiles of 30 ground-motions are shown, for m/M within 1% and 100%.

6.2.3 Equivalent damping ratio

From the previous analyses it was found that NSBA significantly overestimates the predicted sliding displacements on 2DOF systems with large percentage of sliding inertia, i.e., for systems with high values of m/M. Moreover, as CSSI is not explicitly simulated, the predicted stress resultants and displacements are also overestimated. Herein, we propose a simplified approach to capture CSSI in the context of an elastic response history analysis, which employs an equivalent damping ratio (ξ_{eq}) that replaces the e.g., 3% damping ratio typically used in racks. Inspired by Jacobsen (1960), ξ_{eq} does not have a solid physical explanation, but instead comprises a proxy to empirically adjust the elastic response, to account for the apparent reduction of inertial forces due to sliding. This approach was chosen over the numerical reduction of the structure's seismic mass, as it can mitigate the effect of the seismic excitation without changing the periods and modes of vibration of the system.

The equivalent damping ratio should depend both on the seismic motion under consideration and the friction constant. For relatively mild excitations, ξ_{eq} should be equal to the default 3% value and increase for more vigorous vibrations. Moreover, for the same seismic motion, a wooden pallet (lower μ) should have greater ξ_{eq} than a plastic or steel pallet. Additional parameters such as the pulse period of pulse-like ground motions, or the dominant period of the excitation in general, may be influential when considering the response under a specific record (Nikfar and Konstantidis, 2017). Still, they are not considered as they cannot be easily introduced in practical applications. Essentially, the sliding displacement, and consequently the ξ_{eq}, of a 2DOF system with $m = M$, period T, and friction constant μ, is tested against the single variable $Sa(T)/\mu$ that was selected as the normalized intensity measure (IM) for the effect of pallet sliding, with $Sa(T)$ being the spectral acceleration of a linear elastic oscillator with period equal to T. Our intention is to derive an expression for ξ_{eq} on the 2DOF and employ it to approximate the response of MDOF racking systems.

Eleven 2DOF systems with periods within [0.3, 2.5] sec were selected. A total of 105 "ordinary" (i.e., no directivity, no long duration) ground motion records were selected from the PEER-NGA strong motion database (Kazantzi et al., 2021) and scaled to eight normalized intensity levels of $Sa(T)/\mu$ in (1, 3]. Finally, four friction constants were employed to account for different contact surfaces between the pallets and the racking structure within [0.15, 0.40]. For each level and 2DOF system, the equivalent damping ratio was adjusted by steps of 0.5% until the mean sliding predicted by NSBA matched the flat slider model. Figure 6.9 shows an example of application for a 2DOF with T = 0.75 sec, $Sa(T)/\mu$ = 2.25, and μ = 0.3. Using linear regression analysis on the 352 individual points (11 models × 8 levels × 4 friction constants) of $Sa(T)/\mu - \xi_{eq}$ the following formula was derived (Figure 6.10):

$$\xi_{eq} = min\left\{3\%,\quad 5.82\%\frac{Sa(T)}{\mu} - 3.97\%\right\} \qquad \text{Eq. (6.3)}$$

with an error standard deviation of $\sigma_{\xi_{eq}}$= 0.0061 or 0.61%. It is noted that even though Eq. (6.3) was fitted for $1 \leq Sa(T)/\mu \leq 3$, the ξ_{eq} results are identical for different values of μ thanks to the normalization of the IM; thus, the validity of the expression can be extended to larger values of $Sa(T)/\mu$ if needed.

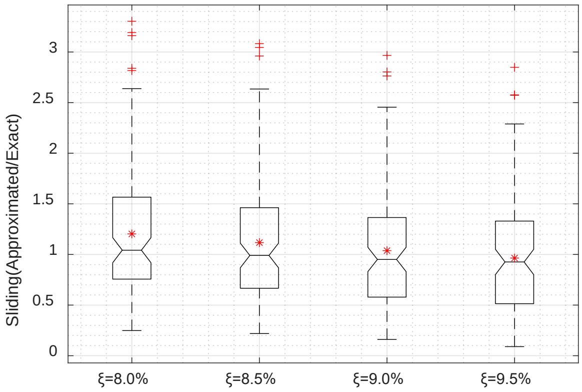

Figure 6.9: Boxplots of the ratio of the sliding displacement predicted by NSBA ("Approximated") over the estimate of the 2DOF slider-on-cantilever ("Exact"), for a system with $T = 0.75$ sec, $\mu = 0.3$ and $Sa(T)/\mu = 2.25$, using 105 ground motions (red asterisks indicate the mean values). The optimal $\xi_{eq} = 9.5\%$ results to a mean ratio ~1.0.

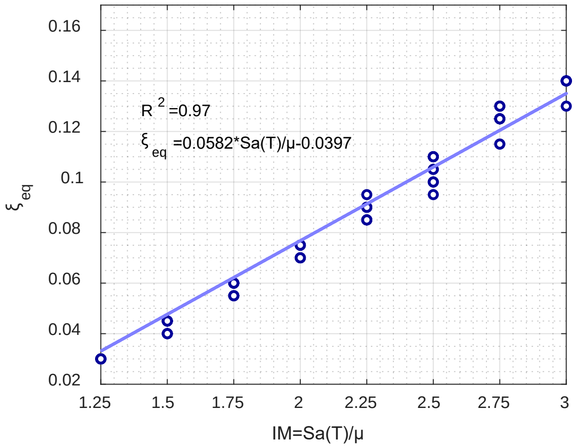

Figure 6.10: Linear regression analysis for the relation of $Sa(T)/\mu$ with the equivalent damping ratio, ξ_{eq}, selected to optimally match NSBA with the 2DOF slider-on-cantilever.

The results of the RHAs can also be used to investigate how the period of the system T affects the maximum sliding displacement. Figure 6.11 shows the mean values of sliding for the aforementioned eleven 2DOF slider-on-cantilever systems with $\mu = 0.3$, subjected to 105 ground motions and 8 levels of IM. In general, the higher the period of the 2DOF system, the greater the sliding (Konstantidis and Nikfar, 2017). Indeed, it has been shown analytically that the maximum displacement of a sliding mass depends approximately on the square of the dominant period of the excitation (Nikfar and Konstantidis, 2017), which for sliding of contents it is practically equivalent to the period of the supporting rack that dominates the narrow-band floor/level excitation (Kazantzi et al., 2020).

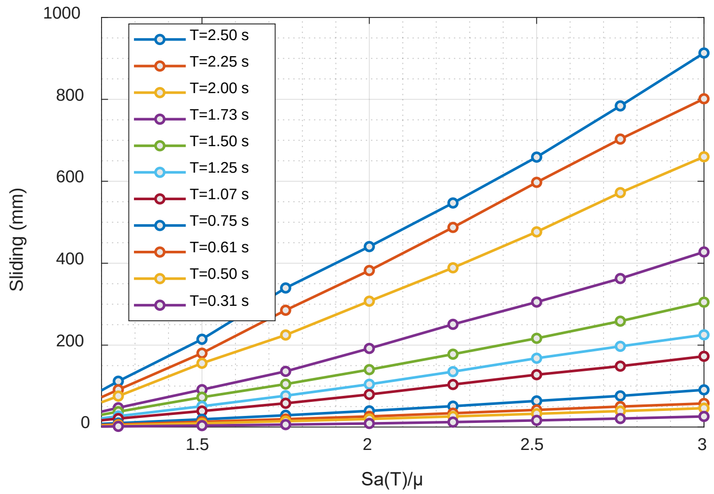

Figure 6.11: Mean values of sliding displacement for 11 2DOF systems with different periods of vibration and μ = 0.3, subjected to 105 ground motions and 8 levels of IM.

6.3 RHA for MDOF systems

6.3.1 CSSI for MDOF structures

Flat slider elements can be used in the numerical model of a MDOF racking system to explicitly account for the effect of CSSI. In the case of systems with one pallet resting on two pallet beams, like the cross-aisle direction of the well-known APRs, the horizontal force H acting on the unit load produces an overturning moment $H{\cdot}e_V$ (EN 16681, 2016), where e_V is the vertical eccentricity between the center of gravity of the unit load and the beams. Subsequently, this overturning moment is transferred as a pair of axial forces $H{\cdot}e_V$ on the supporting beams and uprights (Figure 6.12). A detailed simulation of this load transfer mechanism requires a sub-system of 5 nodes for each pallet; Nodes 1-3, 2-3 and 4-5 are connected by “rigid” beam elements, while nodes 3-4 by a flat slider element. As the stiffness of the supporting upright frame should not be affected, the entire sub-system is attached to the frame by rotational hinges in nodes 1 and 2. It should be stressed that this complex simulation is not always required. Indeed, there are cases, such as the down-aisle direction of APRs or the cross-aisle direction of multi-depth ARSWs, where the overturning forces are nullified by the adjacent pallets that also tend to overturn, as shown in Figure 6.13.

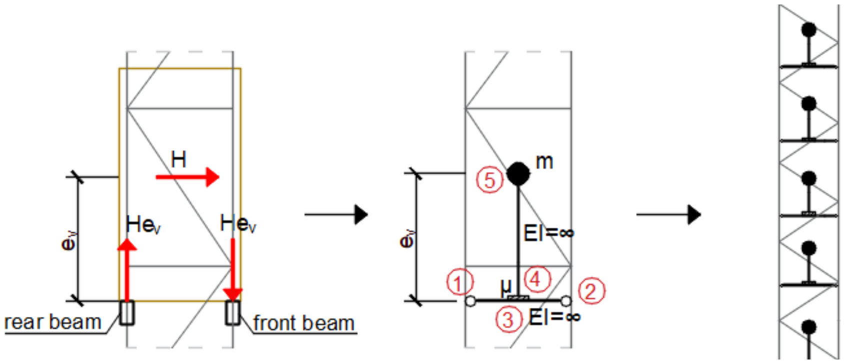

Figure 6.12: Modelling of pallets along the cross-aisle direction of an APR system using flat sliders and rigid elements.

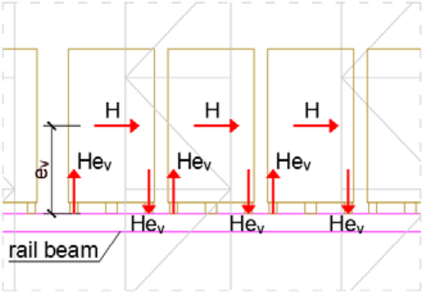

Figure 6.13: When multiple pallets are resting on pallet/rail beams, the pair of overturning forces $H{\cdot}e_V$ produced by the vertical eccentricity of the pallet and the supporting beams is cancelled by its adjacent pallets.

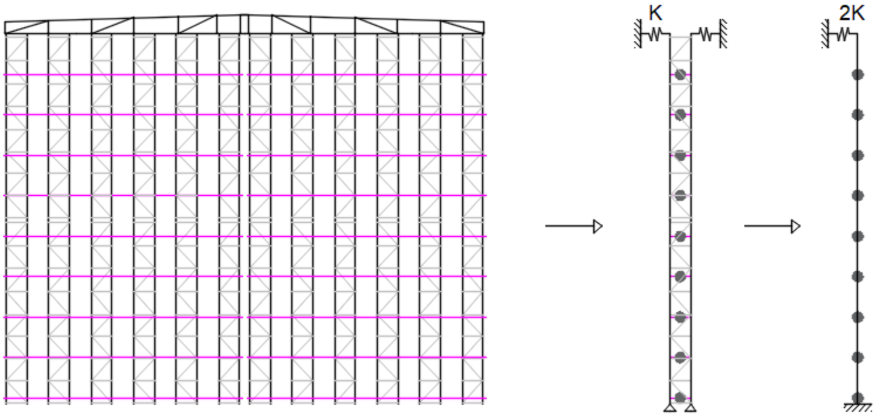

Figure 6.14: Substitution of the full cross-aisle frame of multi-depth systems with a single upright frame or a single stick that employs horizontal axial springs at the top, to simulate the lateral restraint offered by the roofing system.

For low-rise racking systems with a limited number of pallets, one can employ the aforementioned sub-system of flat sliders and dummy elements to simulate the behavior of each pallet, without affecting considerably the robustness of the numerical model. On the other hand, the numerical simulation of all pallets on a multi-depth high-rise racking system may require hundreds of flat slider elements, leading to convergence difficulties.

In general, as pallet sliding is an issue only in the cross-aisle direction (where pallets can slide off the rack), one can take advantage of the similar/repeated upright frames to substantially reduce the model size (Chapter 5, Tsarpalis et al., 2021). Herein, we chose to consider a single upright frame instead of the full cross-aisle frame, as they have very similar periods and modes of vibration. By closely matching the dynamic characteristics of the full frame, the sliding behavior of pallets can be well approximated. For the case of racking systems that also act as supporting structures for the roof, so-called automated rack supported warehouses (ARSWs), axial horizontal springs are considered at the top level of the single upright frame to account for the roof lateral restraint (Figure 6.14). The stiffness of the axial springs was calibrated to match the first five eigenmodes and eigenvalues of the full cross-aisle frame. Finally, another simplification strategy to reduce the number of DOFs of the numerical model is to substitute the single upright frame with a “stick” model comprising Timoshenko beam elements that account for the shear flexibility of the system (Tsarpalis et al., 2021). Due to the aforementioned issue of overturning forces, when the focus is on the design of the upright frame, rather than on the assessment of the sliding displacement, this final simplification can only be accurately applied in cases where said forces are counteracted by multiple pallets, e.g., multi-depth cross-aisle frames (Figure 6.14). When only sliding is concerned, the stick simplification is always a viable option.

6.3.2 Five modelling approaches

Five modelling approaches will be tested to simulate CSSI for MDOF systems in the context of a response history analysis, each characterized by a different level of accuracy and computational efficiency (Table 6.1). The first one, termed the full model (FM) approach, comprises flat sliders to simulate the contact surface between the rack and the unit loads. It is the benchmark modelling approach to assess the accuracy of the other simpler options. The second technique, the stick model (SM), also incorporates flat sliders but the upright frame is substituted with a stick model to decrease the number of DOFs. The third approach, the Newmark's block model (NM), does not use any special elements or implicit methods to account for the pallet sliding; the absolute floor accelerations are recorded and an NSBA is conducted for each load level.

The fourth approach, namely the Newmark's block with equivalent damping model (NDM), also uses NSBA together with an equivalent damping ratio to capture the isolation effects of pallet sliding. Specifically, for each record the first and second-mode spectral accelerations are calculated, namely $Sa(T_1)$ and $Sa(T_2)$, respectively. Then the corresponding $\xi_{1,eq}$ and $\xi_{2,eq}$, can be derived by Eq. (6.3) and a mean equivalent damping ratio is calculated as:

$$\bar{\xi}_{eq} = \frac{\xi_{1,eq} + \xi_{2,eq}}{2} \qquad \text{Eq. (6.4)}$$

A more natural choice would have been to apply $\xi_{1,eq}$ and $\xi_{2,eq}$ to the first and second mode instead of using a mean value. Indeed, Rayleigh damping formulation allows different damping ratios to form the damping matrix:

$$[C] = a_0[M] + a_1[K] \Rightarrow \begin{Bmatrix} \xi_i \\ \xi_j \end{Bmatrix} = \frac{1}{2} \begin{bmatrix} 1/\omega_i & \omega_i \\ 1/\omega_j & \omega_j \end{bmatrix} \begin{Bmatrix} a_0 \\ a_1 \end{Bmatrix} \qquad \text{Eq. (6.5)}$$

where:

$[C]$, $[M]$ and $[K]$ the damping, mass and stiffness matrix, respectively;

ω_i and ω_j the angular frequency of modes i and j (not necessarily the first and second mode);

ξ_i and ξ_j the damping ratio of modes i and j;

a_0 and a_1 the mass and stiffness coefficients of the Rayleigh damping formulation.

Solving Eq. (6.5) for a_0 and a_1 leads to:

$$a_0 = \frac{-2\omega_i\omega_j(\xi_i\omega_j - \xi_j\omega_i)}{\omega_i^2 - \omega_j^2}\ , \quad a_1 = \frac{2(\xi_i\omega_i - \xi_j\omega_j)}{\omega_i^2 - \omega_j^2} \qquad \text{Eq. (6.6)}$$

For $\xi_i = \xi_j = \xi$, the classical Rayleigh coefficients are derived (Chopra, 1995):

$$a_0 = \frac{2\omega_i\omega_j}{\omega_i + \omega_j}\xi, \quad a_1 = \frac{2}{\omega_i + \omega_j}\xi \qquad \text{Eq. (6.7)}$$

Table 6.1: Selected modelling approaches, indicating the use of flat slider elements, equivalent damping, or none.

#	Model	Description	Flat sliders	Equivalent damping ratio
1	FM	full model	✓	✗
2	SM	stick model	✓	✗
3	NM	Newmark’s block model	✗	✗
4	NDM	Newmark’s block model with mean ξ_{eq}	✗	✓
5	NWDM	Newmark’s block model with weighted mean ξ_{eq}	✗	✓

Using Eq. (6.7), a_0 and a_1 are always positive values as they involve multiplications and additions of positive terms. On the other hand, the coefficients derived from Eq. (6.6) can also be negative, which leads to negative damping matrices that are not physically meaningful. To illustrate this issue with an example, a typical case of a racking system is selected with periods of vibration T_1 = 1.5 sec and T_2 = 0.5 sec and a constant damping ratio in the first mode ξ_1 = 3%. Figure 6.15 illustrates the values of a_0 and a_1 for increasing ξ_2, using Eq. (6.6). As the difference between ξ_1 and ξ_2 grows, i.e., the ratio ξ_2/ξ_1 increases, the mass coefficient a_0 becomes negative and thus the contribution $a_0[M]$ to the damping matrix leads to a dynamically unstable system. To avoid such issues, applying the averaged damping of Eq. (6.4) uniformly to both modes is preferrable.

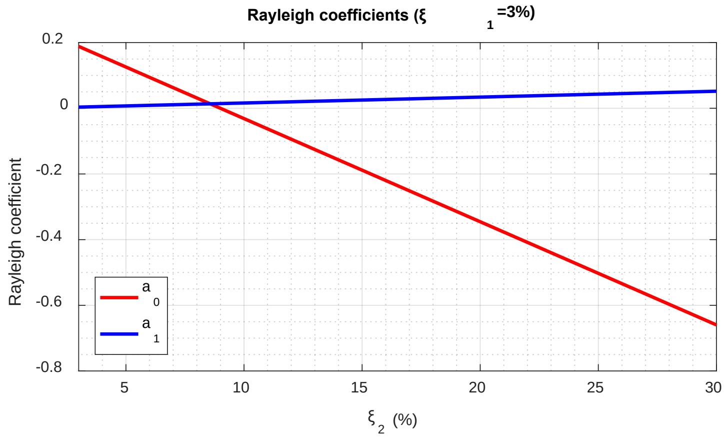

Figure 6.15: Rayleigh damping coefficients for ξ_1 = 3% and ξ_2 varying from 3% to 30%.

The fifth modelling approach, the Newmark’s block with weighted mean equivalent damping model (NWDM), also incorporates an NSBA framework together with an equivalent damping ratio, similarly to the NDM, with the difference that a weighted mean of the $\xi_{1,eq}$ and $\xi_{2,eq}$ is used:

$$\bar{\xi}_{w,eq} = w_1 \cdot \xi_{1,eq} + w_2 \cdot \xi_{2,eq} \qquad \text{Eq. (6.8)}$$

where w_1 and w_2 are weights for the first and the second mode, to take into account the higher influence of the first mode:

$$w_1 = \frac{m_1^*}{m_1^* + m_2^*}, \quad w_2 = \frac{m_2^*}{m_1^* + m_2^*} \qquad \text{Eq. (6.9)}$$

where m_1^* and m_2^* are the effective modal masses of mode 1 and 2, respectively.

6.3.3 Description of case studies

To illustrate the application of the proposed method, three case studies will be examined. The first example comprises the multi-depth case study CS2 of Chapter 3, but represented herein for convenience. Specifically, it has been designed by professional engineers according to EN 1993 (2005), EN 15512 (2009) and EN 16681 (2016) to be installed in the city of Van, Turkey, a site with 10%/50yr peak ground acceleration of a_g = 0.3 g and a friction constant μ = 0.3. The overall plan dimensions are 65.80 m × 71.50 m in the cross- and down-aisle direction, respectively, while the total height is about 25.60 m. There are nine load levels, each comprising four storage cells of 13 unit-load capacity (Figure 6.16), thus each cross-aisle pallet frame supports up to 468 pallets. Load levels 1 to 2 are for 1000 kg pallets, 3 to 5 for 800 kg and 6 to 9 for 600 kg.

Herein, a single cross-aisle pallet frame is considered, comprising 48 uprights, connected in pairs to form 24 “K-type” upright frames of 1.35 m width (Figure 6.16). The cross-section area of the diagonal braces of the upright frames was reduced to 10% to account for the reduced shear stiffness due to their bolted connection (Talebian et al., 2018). To decrease the number of involved flat sliders and corresponding DOFs, the simplification procedure discussed earlier is followed. Thus, a single upright frame is isolated and properly calibrated axial springs are employed at the top nodes of the model to account for the effect of the roof (Figure 6.14). Regarding the mass distribution, the most critical upright frames of a 13-pallet storage cell lie one frame away from its edges and they are assumed to support 2 pallets per load level.

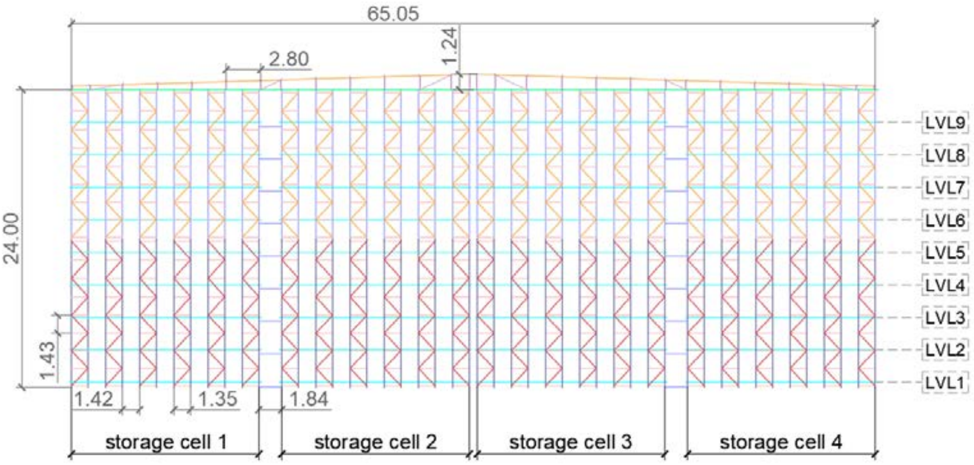

Figure 6.16: Cross-aisle view of the multi-depth Case Study 1, consisting of 24 “K-type” upright frames and a connecting shallow roof truss (units in meters).

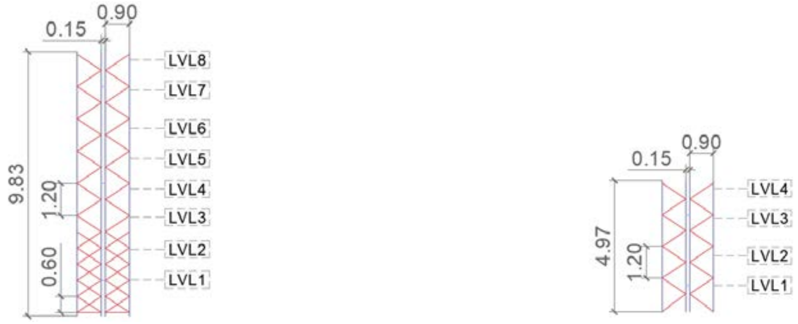

(a) (b)

Figure 6.17: Cross-aisle view of: (a) the medium-rise APR Case Study 2 and (b) the low-rise APR Case Study 3 (units in meters).

Table 6.2: Cross-section properties of structural members. Cross-section areas are rounded to the 3rd digit while moments of inertia to the 5th.

Member	**Case study**	**Section**	**Steel grade**	***A* (mm^2)**	***I* (mm^4)**
Lower bracing upright (reinforced)	1	Ω [*]	S350GD	1300	3000000
Lower bracing upright	1	Ω	S350GD	900	2000000
Upper bracing upright	1	C [**]	S350GD	500	150000
Lower pallet upright	1	C	S350GD	300	340000
Upper pallet upright	1	I [***]	S350GD	1640	5410000
Lower upright frame diagonal	1	Ω	S350GD	680	610000
Upper upright frame diagonal	1	C	S350GD	330	110000
Lower vertical bracing (floor-5th level)	2, 3	Ω	S350GD	580	480000
Lower vertical bracing (6th level-top)	2, 3	C	S280GD	100	20000

[*] Ω: Ω-type upright section; [**] C: channel section with lips; [***] I: I section.

Table 6.3: Periods and mass participation factors for the three considered case studies along the cross-aisle direction.

Mode #	**Case Study 1**		**Case Study 2**		**Case Study 3**	
	Period (sec)	**Mass Part.**	**Period (sec)**	**Mass Part.**	**Period (sec)**	**Mass Part.**
1	1.79	66%	1.02	75%	0.47	86%
2	0.62	17%	0.30	17%	0.16	11%
3	0.32	5%	0.17	4%	0.09	2%
4	0.23	2%	0.12	2%	0.08	1%
5	0.17	1%	0.09	0%	0.07	0%
6	0.07	8%	0.08	0%	0.06	0%

The second case study consists of a medium-rise back-to-back indoor APR system with eight load levels, designed to be installed in a facility at Aspropyrgos, Greece, a site with 10%/50yr peak ground acceleration a_g = 0.24 g and a friction constant μ = 0.3. Load levels 1 to 5 and 7 are designed to carry 3×480 kg unit loads per compartment, while load level 6 and 8 carry 3×640 kg and 3×240 kg, respectively. To accommodate a variety of unit loads, the vertical distance between the load levels is not constant. In the cross-aisle direction (Figure 6.17(a)) two upright frames are connected with 3 spacers (at 1.33, 4.93 and 8.53 m from the floor), to form the back-to-back storage system. Each individual upright frame has an X bracing pattern up to 3.13 m distance from the floor and it continues upwards with a D system, as the seismic loads are lower. The cross-section area of the diagonals was also reduced to 10% of their gross area, to account for the flexible bolted connection. Herein, a single upright frame is considered, assuming that the spacers do not offer adequate stiffness and the two upright frames can be analyzed individually. Finally, the third example comprises a low-rise back-to-back APR system which was derived by considering the four upper load levels of Case Study 2 (Figure 6.17(b)), but using a friction constant μ = 0.37. Table 6.2 summarizes the cross-sectional properties for the main structural members of all case studies, while Table 6.3 contains the periods and mass participation factors for the first six modes of each structure. The high-rise ARSW (Case Study 1) has a relatively low mass participation factor on the first mode and thus, the contribution of higher modes on the CSSI is expected to be more significant. On the other hand, the low-rise APR (Case Study 3) comprises a first-mode-dominant structure, while the medium-rise APR (Case Study 2) is an in-between scenario of the other two examples.

6.3.4 Seismic hazard and record selection

For each site, a set of 30 natural records was used (set #1 for Van (Kohrangi et al., 2018) and set #2 for Athens (Kohrangi and Vamvatsikos, 2016)), that match the conditional spectra (CS) (Baker, 2010; Lin et al., 2013a; Lin et al., 2013b) using the geometric mean of spectral accelerations, $AvgSa$ (Eq. (3.14)), as the IM (Kohrangi et al., 2017). We employed a single period range for both sites of [0.3s, 3.0 s] with an increment of 0.2 s. Figure 6.18 illustrates the $AvgSa$ hazard curves of Van and Athens. Crossing the hazard curves with a horizontal line at the design level (i.e., 10% in 50 years), the corresponding IM in Athens is equal to 0.11 g while in Van 0.24 g, or more than twice.

To compare the five modelling approaches, a series of RHAs is conducted using the aforementioned 30-records sets for multiple IM levels. Table 6.4 shows the selection of seismic input for each case study, presented in terms of probability of exceedance. In general, racks are characterized by low or non-existent ductility, therefore brittle failures tend to govern the response. For reasons of checking sliding displacements of large magnitude, we have chosen herein not to simulate such failures, assuming instead that members remain elastic and the only source of nonlinearity comes from geometric considerations (i.e., P-Δ effects). In general, this is considered to be a more severe test of the different modelling formulations, as it leads to larger sliding displacements. Allowing earlier failures or even material nonlinearity would either stop the analysis earlier, or reduce sliding due to the beneficial reduction of (absolute and relative) peak accelerations at each floor (see for example NIST (2017)).

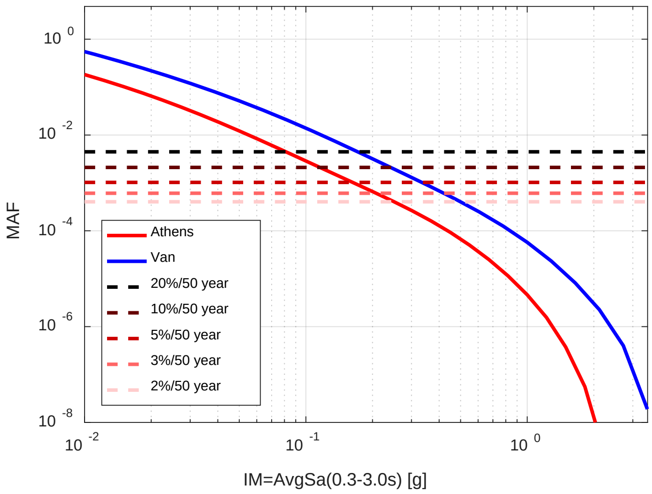

Figure 6.18: Hazard curves for the sites of Athens and Van, using $AvgSa$ as an IM.

Table 6.4: Selection of seismic input for Case Studies 1, 2 and 3.

Probability of exceedance	**Case Study 1**	**Case Study 2, 3**
2% in 50 years	-	set #2 [***] (IM = 0.25 g)
3% in 50 years	set #1 [*] (IM [**] = 0.43 g)	set #2 (IM = 0.21 g)
5% in 50 years	set #1 (IM = 0.33 g)	set #2 (IM = 0.16 g)
10% in 50 years	set #1 (IM = 0.24 g)	set #2 (IM = 0.11 g)
20% in 50 years	set #1 (IM = 0.19 g)	-

[*] set #1: 30-records set for Van; [**] IM: $AvgSa(0.30 - 3.0$ sec); [***] set #2: 30-records set for Athens

6.3.5 Comparison of modelling approaches

Each case study was analyzed using 4 scales of IM and 30 ground-motions (see Table 6.4), for a total of 360 RHAs. The four “Approximated” quantities, resulting from the SM, NM, NDM and NWDM approaches, were compared with the “Exact” approach, FM. From each RHA, the maximum (over height and time) base shear, roof drift, interstorey drift and sliding displacement were derived, and the “Approximated/Exact” (or A/E) ratios were estimated. A useful approximating approach would be considered to have a mean A/E close to 1.0, thus being unbiased, with low dispersion of the overall results, as large dispersions indicate higher uncertainties.

Figure 6.19(a)-(d) illustrate the resulting ratios using boxplots. It should be noted that the range of sliding ratios can be misleadingly large; low “Exact” values of pallet movement of, e.g., 0.1 mm coupled with an “Approximated” value of 0.3 mm will lead to an A/E of 3.0. This seems quite high, but it is of little engineering significance as the pallets in both models remain practically idle. To alleviate this issue, we chose to only consider sliding ratios corresponding to “Exact” displacements higher than 5 mm.

The SM approach shows excellent predictive ability, both in terms of mean value and coefficient of variation (CoV) for all recorded structural responses. The only statistic that may be cause for worry is the CoV = 0.41 in the pallet sliding ratio; this is expected, as the absolute floor accelerations are quite variable themselves (Miranda and Taghavi, 2005; Ramirez and Miranda, 2012). Nevertheless, as the record-to-record variability dominates the dispersion of pallet sliding, it is safe to consider this error to be of secondary importance. Thus, one can easily choose to substitute FM with the more frugal SM, reducing the computational cost and gaining in numerical robustness.

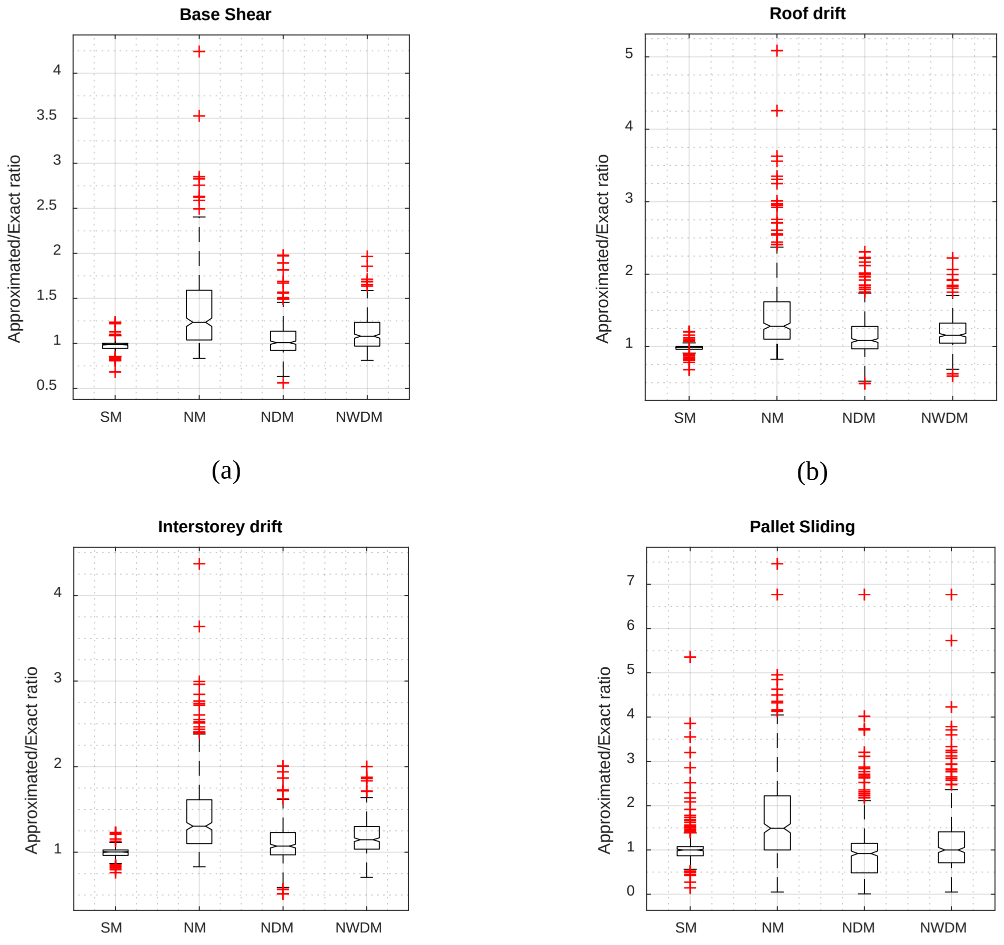

(a) (b)

(c) (d)

Figure 6.19: Boxplots of the “Approximated/Exact” ratio of (a) Base Shear, (b) Roof Drift, (c) Interstorey Drift and (d) Sliding, for all the 30x12 = 360 RHAs shown in Table 6.4 (the FM approach was considered the “Exact” solution, and the rest four “Approximated” were compared against it).

On the other hand, the NM approach overestimates all responses, giving a mean A/E of 1.37 for the base shear, 1.46 for the roof drift, 1.43 for the interstorey drift and 1.73 for the pallet sliding. Recalling Figure 6.8, NSBA on a 2DOF slider-on-cantilever with $T = 0.7$ sec showed a similarly mediocre performance, overestimating sliding by a factor of 1.70 when m/M is greater than 0.95, as expected for a typical rack. Instead, employing the equivalent damping ratio ξ_{eq} per the NDM approach reduces the bias and the variability, bringing mean A/E values closer to 1.0 and decreasing CoVs. Contrarily, the NWDM approach, where higher weight is applied to the first mode of vibration per Eq. (6.9), is inferior to the NDM. Perhaps this should not be totally unexpected as local responses (such as sliding) tend to be heavily influenced by higher modes, whereas the weighting of the modes in NWDM was derived per their contribution to the roof displacement, disproportionately favoring the fundamental mode.

6.4 MRSA for MDOF systems

6.4.1 Reduction of lateral loads for simplified CSSI

Targeting practical code-compatible design or assessment applications, where MRSA is the method of choice, the use of a lateral load reduction factor similar to E_{D1} (Eq. (6.1)) is a simple and effective way to account for CSSI. Comparing the results of the FM approach with NM, is equivalent to comparing the effect of sliding versus non-sliding masses. By dividing said results, one can calculate a reduction factor to convey the effect of CSSI per each RHA. When thus considering the resulting base shears, one can determine by proxy a reduction factor that can be applied to the design spectrum to estimate the “effective” lateral loads as $E_{N1} = V_{b,FM} / V_{b,NM}$, where $V_{b,FM}$ and $V_{b,NM}$ are the maximum recorded base shear of the FM and the NM approach, respectively. Three IMs were considered, namely $Sa(T_1)/\mu$, $Sa(T_2)/\mu$, and their geometric mean $\sqrt{Sa(T_1)Sa(T_2)}/\mu$. Figure 6.20(a)-(c) illustrates the E_{N1} – IM data points for all the 360 RHAs, fitted with a simple linear regression, $E_{N1} \approx b_0 + b_1 \cdot IM$. A higher $R^2 = 0.54$ (with an error standard deviation of $\sigma = 13.64\%$) is achieved using $\sqrt{Sa(T_1)Sa(T_2)}/\mu$ as the IM, with respect to $R^2 = 0.43$ and $R^2 = 0.36$ when using $Sa(T_1)/\mu$ and $Sa(T_2)/\mu$, respectively. The resulting expression for E_{N1}, bounded within [0.4, 1.0] for compatibility with EN 16681 (2016), is:

$$E_{N1} = max\left\{0.4, \ -0.1966 \cdot \sqrt{Sa(T_1)Sa(T_2)}/\mu + 1.0995\right\} \leq 1.0 \qquad \text{Eq. (6.10)}$$

In general, it should be understood that the code-compatible approach of E_{N1} is a practical yet fairly limited solution, compared to RHA with flat-sliders or ξ_{eq}. If Figure 6.20 is not enough warning, Figure 6.21 and Figure 6.22 illustrate the reduction of the roof drift and the maximum interstorey drift, respectively. One can observe that the reduction of the roof drift is strongly related to $Sa(T_1)/\mu$, a well-known behavior of any building-like structure with a relatively dominant first mode. On the other hand, the reduction of the maximum interstorey drift is also sensitive to $\sqrt{Sa(T_1)Sa(T_2)}/\mu$, as the effect of higher-order modes becomes significant locally, e.g., at the lower levels of a racking system where the maxima tend to appear. Thus, in general we expect the E_{N1} approach to work well for base shear, but become less accurate for roof drift, and even worse for story drifts.

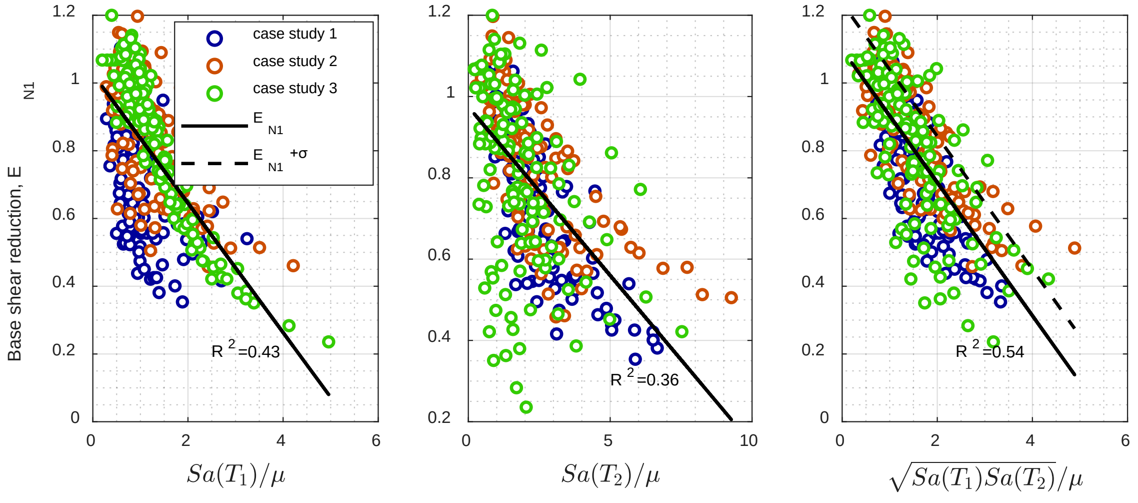

(a) (b) (c)

Figure 6.20: Linear regression analysis for E_{N1} (FM/NM base shear reduction) given the IM of (a) $Sa(T_1)/\mu$, (b) $Sa(T_2)/\mu$, and (c) $\sqrt{Sa(T_1)Sa(T_2)}/\mu$.

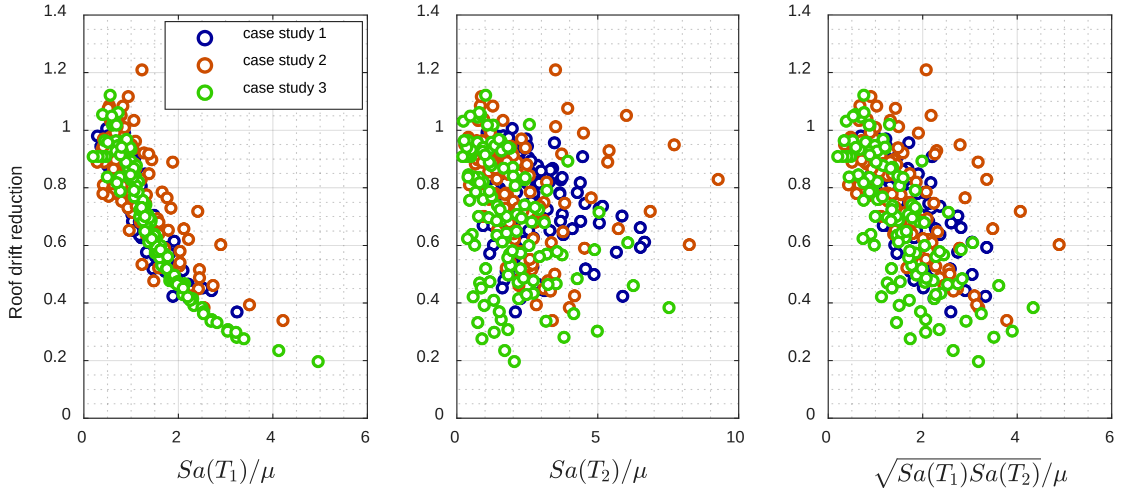

(a) (b) (c)

Figure 6.21: FM/NM roof drift reduction given the IM of (a) $Sa(T_1)/\mu$, (b) $Sa(T_2)/\mu$, and (c) $\sqrt{Sa(T_1)Sa(T_2)}/\mu$.

Finally, as a side note, Figure 6.23(a)-(c) show scatter plots of the maximum recorded pallet sliding for each of the 360 RHAs. These are the results of the FM models, as MRSA cannot be used to assess sliding. One can observe that sliding is loosely dependent on any of the three considered IMs. Essentially, there is a high record-to-record variability in sliding responses that cannot be easily captured: Small changes in the absolute floor accelerations may lead to large deviations on the corresponding goods movement. Another significant observation is that in most cases the taller rack experiences greater sliding displacements than the shorter, similarly to what was found for 2DOF systems of long versus short periods (Figure 6.11).

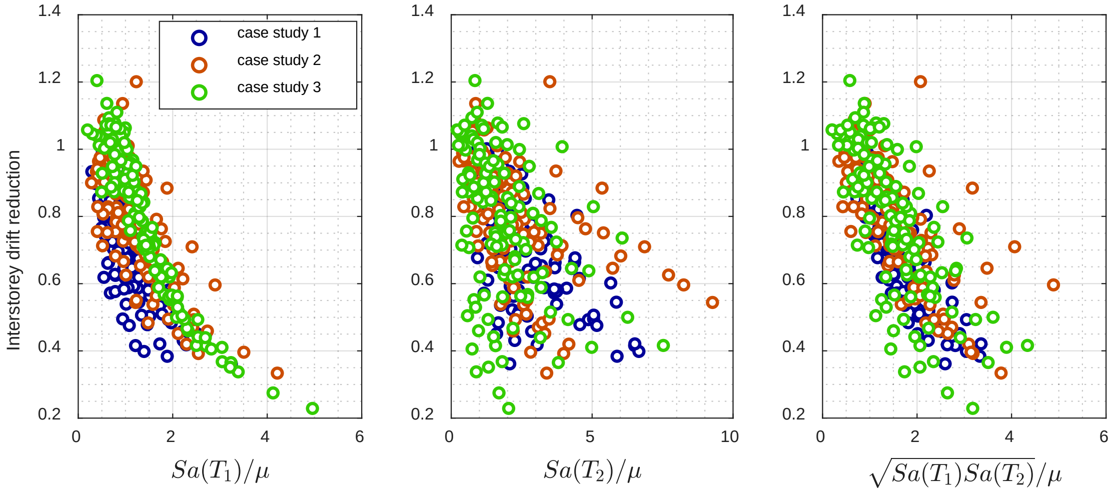

(a) (b) (c)

Figure 6.22: FM/NM maximum interstorey drift reduction given the IM of (a) $Sa(T_1)/\mu$, (b) $Sa(T_2)/\mu$, and (c) $\sqrt{Sa(T_1)Sa(T_2)}/\mu$.

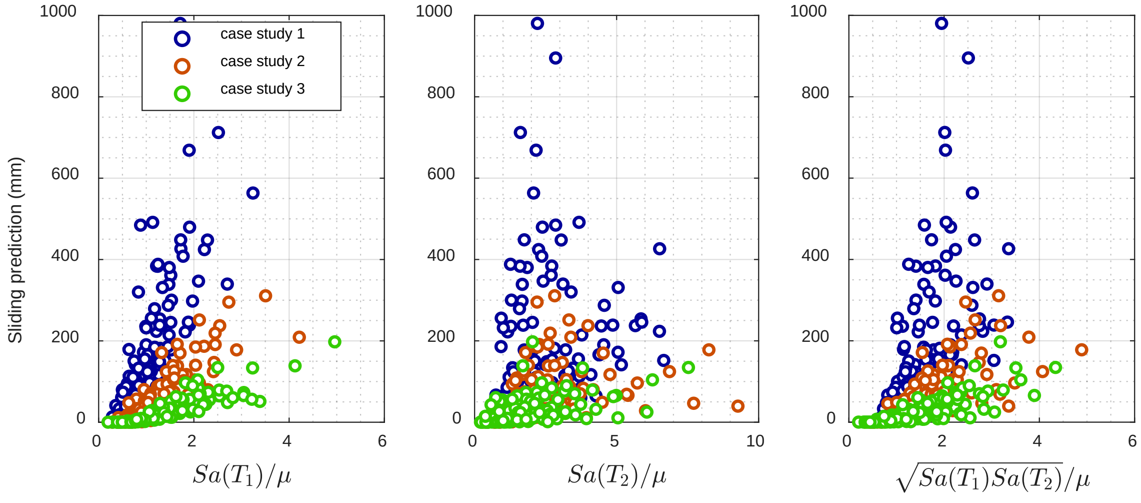

(a) (b) (c)

Figure 6.23: Pallet sliding prediction via RHA with flat sliders given the IM of (a) $Sa(T_1)/\mu$, (b) $Sa(T_2)/\mu$, and (c) $\sqrt{Sa(T_1)Sa(T_2)}/\mu$.

6.4.2 Comparison of MRSA approaches

As shown previously, the most efficient method to implicitly consider the positive effect of pallet sliding in the context of a RHA, without using any special slider elements, is to adopt the equivalent damping ratio of Eq. (6.4), i.e., the NDM approach. This equivalent damping ratio can also be used to modify the design spectrum in an MRSA, for example by using the damping modification η-factor of EN1998-1 (2004):

$$\eta = \sqrt{10/(\xi_{eq} + 5)} \geq 0.55 \qquad \text{Eq. (6.11)}$$

On the other hand, one may also use the E_{N1} reduction factor given in Eq. (6.10) to straightforwardly decrease the design seismic forces. To compare the two approaches, the high-rise ARSW Case Study 1 is used, employing the 30-records set for the city of Van

(Kohrangi et al., 2018), scaled to intensity levels corresponding to 3%, 5% and 10% in 50 years probability of exceedance. Five sets of analyses are conducted for all records:

(1) RHA: RHA using flat slider elements, which is considered as the benchmark.

(2) MRSA-E_{D1}: MRSA using the actual spectrum of each record with 3% damping ratio, a reduction factor E_{D1} according to EN 16681 (2016) given by Eq. (6.1) and a CQC modal combination.

(3) MRSA-ξ_{eq}: MRSA using the actual spectrum of each record with the equivalent damping ratio given by Eq. (6.4) and a CQC modal combination.

(4) MRSA-E_{N1}: MRSA using the actual spectrum of each record with 3% damping ratio, a reduction factor E_{N1} given by Eq. (6.10) and a CQC modal combination.

(5) MRSA-1.1E_{N1}: A modified version of (4), where the coefficients in Eq. (6.10) are multiplied by a factor of 1.10. While MRSA-1.1E_{N1} is expected to overestimate the average response of the rack, it is a conservative approach that may be preferrable for design.

Geometric nonlinearities (i.e., P-Δ effects) were treated explicitly in RHA via a first-order approximation, while in MRSA their effect was incorporated according to EN 16681 (2016). Specifically, modal analysis was performed by taking into account the geometric stiffness matrix, which makes the structure more flexible and thus elongates the periods of vibration. Moreover, the lateral seismic forces were multiplied by a factor $1/(1-\theta)$, where θ is the sensitivity coefficient, calculated as:

$$\theta = q_d \cdot P_E / P_{cr,E} \qquad \text{Eq. (6.12)}$$

where P_E is the total gravity load of the rack in the seismic design situation, $P_{cr,E}$ is the Euler critical load and q_d the displacement-related behaviour factor, assumed equal to 1.0 as the structural model does not incorporate any ductility. Figure 6.24(a)-(f) shows the A/E ratios, with RHA considered as the “Exact” result, for various response parameters.

The MRSA-E_{D1} analysis overestimates practically any parameter of interest, namely base shear, upright/diagonal axial forces, and roof drift, by 20% to 40%. MRSA-ξ_{eq} tends to decrease, but not nullify this overestimation, while MRSA-E_{N1} offers the best overall performance, both in terms of a nearly-unbiased mean value and smaller CoV. Given that the lower bound in MRSA-E_{N1} over RHA predictions tends to lie around 0.90, a 10% increase of E_{N1} can help achieve a higher level of safety, commensurate with the current norm represented by MRSA-E_{D1} over RHA. This is demonstrated by the MRSA-1.1E_{N1} approach, which achieves a code-like lower bound (i.e., similar safety), while having reduced dispersion (i.e., lower overestimation and higher economy) when compared with EN 16681 (2016).

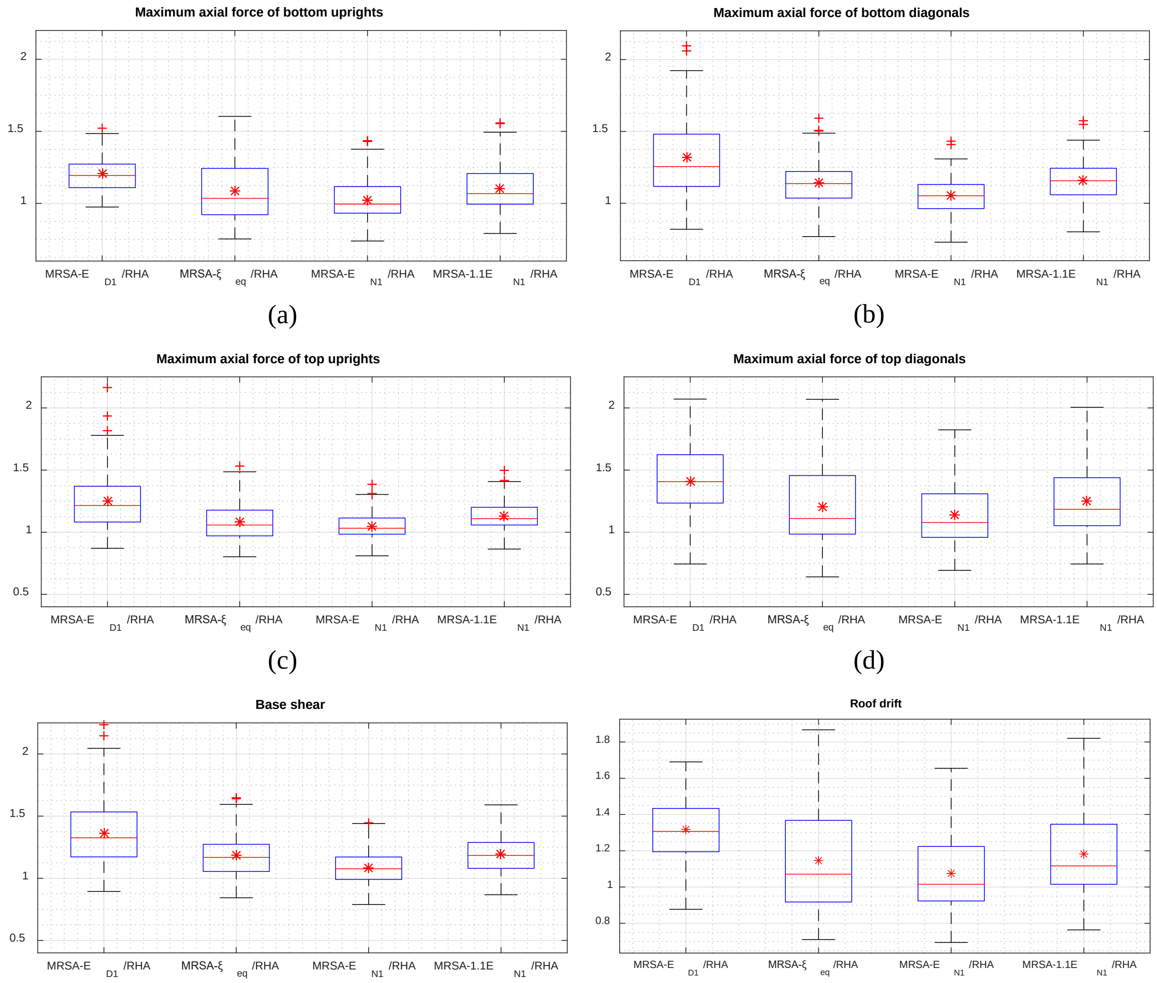
Maximum axial force of bottom uprights

Maximum axial force of bottom diagonals

Maximum axial force of top uprights

Maximum axial force of top diagonals

Base shear

Roof drift

(a) (b)

(c) (d)

(e) (f)

Figure 6.24: Boxplots of the MRSA/RHA ratio of (a) maximum bottom upright axial force, (b) maximum bottom diagonal force, (c) maximum top upright axial force, (d) maximum top diagonal axial force, (e) base shear and (f) roof drift, for the upright frame of Case Study 1, using the 30-records set #1, scaled to 3%, 5% and 10% in 50 years probability of exceedance (red asterisks indicate the mean value while red horizontal lines the median).

6.5 Conclusions

Three different methods for tackling CSSI are offered, distinguished by their need for RHA versus MRSA analysis, as well as the level of modelling detail, requiring friction slider elements versus adjustments of damping or lateral loads. A distinct advantage of RHA-based methods is their capability to assess content sliding displacement, at the cost of requiring ground motion records. From the RHA-based methods, definitely the best results are obtained by employing friction slider elements to simulate the sliding of the pallets, with the cost of increasing the numerical complexity of the model. On the other hand, completely excluding the effect of CSSI during the execution of RHAs leads to large overestimations on the predicted mean pallet sliding (+73%) and the corresponding base shear (+37%) and interstorey drift (+43%) of the rack. To alleviate this issue while keeping the numerical model as simple as possible, it was found that a good solution is to adjust the damping ratio of the model via a simple regression expression. Achieving the same feat of the RHA with MRSA is not easy, as it requires modal combination approaches to predict peak floor accelerations (presently available, e.g., by Moschen et al. (2016)), plus some (presently unavailable) approximation approach to convert such accelerations to sliding displacements. Still, even the lowly MRSA approach combined with the proposed empirical lateral-load reduction formula, can offer unbiased prediction of forces, moments and deformations, suitable for application within the code in tandem with the desired factor of safety. In the case study examined, the MRSAs using the E_{D1} factor of EN 16681 (2016), overestimate the forces on the uprights and diagonals by 20% – 40% on average, which means that lighter (and hence more economical) sections could be potentially used. On the other hand, using the proposed E_{N1} offers better overall performance, largely removing the bias and decreasing the dispersions, while reducing the overestimation of member forces to 2% – 15% on average for a more economical design. In any case, it cannot be stressed enough that the trend for taller racking systems leads to a higher propensity for excessive pallet displacement, as racks with longer periods of vibration tend to experience larger sliding. Thus, the structural design of high-rise racking systems may need to be accompanied by a series of RHAs (or some practical equivalent), to estimate the magnitude of pallet sliding and assess whether precautions have to be taken to arrest pallet movement.

6.6 References

Adamakos K., Sesana S., Vayas I. (2018). “*Interaction Between Pallets and Pallet Beams of Steel Storage Racks in Seismic Areas*”, International Journal of Steel Structures, **18**, 1018-1034. https://doi.org/10.1007/s13296-018-0041-y

Ancheta T.D., Darragh R.B., Stewart J.P., Seyhan E., Silva W.J., Chiou B.S.J., Wooddell K.E., Graves R.W., Kottke A.R., Boore D.M., Kishida T., Donahue J.L. (2013). “*PEER NGA-West2 Database*”, Technical Report PEER 2013/03. Pacific Earthquake Engineering Research Center, Berkeley, CA.

Baker J.W. (2010). “*Conditional Mean Spectrum: Tool for Ground-Motion Selection*”, Journal of Structural Engineering, **137**(3). https://doi.org/10.1061/(ASCE)ST.1943-541X.0000215

Chopra A. K. (1995). “*Dynamics of structures: theory and applications to earthquake engineering*”, Englewood Cliffs, Prentice Hall.

Clifton G.C., Bruneau M., Macrae G.A. (2011). “*Steel structures damage from the Christchurch earthquake series of 2010 and 2011*”, Bulletin of the New Zealand Society for Earthquake Engineering, **44**(4), 297-318. https://doi.org/10.5459/bnzsee.44.4.297-318

Coulomb C.A. (1776). “*Essai sur une application des règles de maximis et minimis a quelques problèmes relatifs à l’architecture*”, Mémoires de Mathématique et de Physique, **7**, 343-382, Académie Royale des Sciences.

EN 15512 (2009). “*Steel static storage systems - Adjustable pallet racking systems - Principles for structural design*”, European Committee for Standardization (CEN), Brussels, Belgium.

EN 16681 (2016). “*Steel static storage systems - Adjustable pallet racking systems - Principles for seismic design*”, European Committee for Standardization (CEN), Brussels, Belgium.

EN 1993 (2005). “*Eurocode 3: Design of Steel Structures*”, European Committee for Standardization, Brussels, Belgium.

EN 1998-1 (2004). *"Eurocode 8: Design of structures for earthquake resistance - Part 1: General rules, seismic actions and rules for buildings"*, European Committee for Standardization, Brussels, Belgium.

Gilbert B.P., Teh L.H., Badet R.X., Rasmussen K.J.R. (2013), *"The influence of pallets on the behaviour and design of steel drive-in storage racks - Part II Design"*, Faculty of Engineering and Information Sciences - Papers: Part A. 1927.

Gilbert B.P., Teh L.H., Badet R.X., Rasmussen K.J.R. (2014). *"Influence of pallets on behaviour and design of steel drive-in racks"*, Journal of Constructional Steel Research, **97**, 10-23. https://doi.org/10.1016/j.jcsr.2014.01.013

Jacobsen L.S. (1960). *"Damping in composite structures"*, Proceedings of the 2nd World Conference on Earthquake Engineering, **2**, 1029–1044.

Kazantzi A.K., Vamvatsikos D., Miranda E. (2020). *"Evaluation of seismic acceleration demands on building nonstructural elements"*, Journal of Structural Engineering, **146**(7). https://doi.org/10.1061/(ASCE)ST.1943-541X.0002676

Kazantzi A.K., Lachanas C.G., Vamvatsikos D. (2021). *"Seismic response distribution expressions for on-ground rigid rocking blocks under ordinary ground motions"*, Earthquake Engineering and Structural Dynamics, **50**(12), 3311-3331. https://doi.org/10.1002/eqe.3511

Kohrangi M., Vamvatsikos D. (2016). *"INNOSEIS ground motion set for high seismicity European sites"*. INNOSEIS Project. Link: http://innoseis.ntua.gr/high_record_set.rar

Kohrangi M., Bazzurro P., Vamvatsikos D., Spillatura A. (2017). *"Conditional spectrum-based ground motion record selection using average spectral acceleration"*, Earthquake Engineering and Structural Dynamics, **46**(10), 1667-1685. https://doi.org/10.1002/eqe.2876

Kohrangi M., Tsarpalis D., Vamvatsikos D. (2018). *"CS(AvgSA) consistent Records and Hazard curves for Van and Montopoli"*. STEELWAR Project. Link: http://users.ntua.gr/divamva/resources/Van_set_10_50yrs.rar

Konstantidis D., Nikfar F. (2017). *"Seismic response of sliding equipment and contents in base-isolated buildings subjected to broadband ground motions"*, Earthquake Engineering and Structural Dynamics, **44**(6), 865-887. https://doi.org/10.1002/eqe.2490

Lin T., Haselton C.B., Baker J.W. (2013a). *"Conditional spectrum-based ground motion selection. Part I: Hazard consistency for risk-based assessments"*, Earthquake Engineering and Structural Dynamics, **42**(12), 1847-1865. https://doi.org/10.1002/eqe.2301

Lin T., Haselton C.B., Baker J.W. (2013b). *"Conditional spectrum-based ground motion selection. Part II: Intensity-based assessments and evaluation of alternative target spectra"*, Earthquake Engineering and Structural Dynamics, **42**(12), 1867-1884. https://doi.org/10.1002/eqe.2303

MATLAB (2020). *"MATLAB version 9.9 (R2020b)"*, Natick, Massachusetts: The MathWorks Inc.

McKenna F., Fenves G.L., Scott M.H., Jeremic B. (2000). *"Open System for Earthquake Engineering Simulation (OpenSees)"*, Pacific Earthquake Engineering Research Center, University of California, Berkeley, CA.

Miranda E., Taghavi S. (2005). *"Approximate Floor Acceleration Demands in Multistory Buildings. I: Formulation"*, Journal of Structural Engineering, **131**(2). https://doi.org/10.1061/(ASCE)0733-9445(2005)131:2(203)

Moschen L., Adam C., Vamvatsikos D. (2016). *“A response spectrum method for peak floor acceleration demands in earthquake excited structures”*, Probabilistic Engineering Mechanics, **46**, 94-106. https://doi.org/10.1016/j.probengmech.2016.09.001

National Institute of Standards and Technology (NIST) (2017). *“ATC-120, Seismic Analysis, Design, and Installation of Nonstructural Components and Systems-Background and Recommendations for Future Work”*. https://doi.org/10.6028/NIST.GCR.17-917-44

Newmark N.M. (1965). *“Effects of Earthquakes on Dams and Embankments”*, Géotechnique, **15**(12), 139-160. https://doi.org/10.1680/geot.1965.15.2.139

Nikfar F., Konstantidis D. (2017). *“Peak Sliding Demands on Unanchored Equipment and Contents in Base-Isolated Buildings under Pulse Excitation”*, Journal of Structural Engineering, **143**(9). https://doi.org/10.1061/(ASCE)ST.1943-541X.0001811

Pozzi M., Der Kiureghian A. (2015). *“Response spectrum analysis for floor acceleration”*, Earthquake Engineering and Structural Dynamics, **44**(12), 2111-2127. https://doi.org/10.1002/eqe.2583

Ramirez C.M., Miranda E. (2012). *“Significance of residual drifts in building earthquake loss estimation”*, Earthquake Engineering and Structural Dynamics, **41**(11), 1477-1493. https://doi.org/10.1002/eqe.2217

RMI, ANSI MH16.1.12 (2012). *“Specification for the Design, Testing and Utilization for Industrial Steel Storage Racks”*, Rack Manufacturer’s Institute, Charlotte, NC.

Rosin I., Calado L., Proença J., Carydis P., Mouzakis H., Castiglioni C., Brescianini J.C., Plumier A., Degee H., Negro P., Molina F. (2007). *“Storage racks in seismic areas (SEISRACKS)”*, Final Report, RFSR-PR-03114, European Commission, DG Research, Brussels, Belgium.

Taghavi S., Miranda E. (2005). *“Approximate Floor Acceleration Demands in Multistory Buildings. II: Applications”*, Journal of Structural Engineering, **131**(2). https://doi.org/10.1061/(ASCE)0733-9445(2005)131:2(212)

Talebian N., Benoit P.G., Baldassino N., Karampour H. (2018). *“Factors contributing to the transverse shear stiffness of bolted cold-formed steel storage rack upright frames with channel bracing members”*, Thin-Walled Structures, **136**, 50-63. https://doi.org/10.1016/j.tws.2018.12.001

Tsarpalis D., Vamvatsikos D., Vayas I., Delladonna F. (2021). *“Simplified Modelling for the Seismic Performance Assessment of Automated Rack-Supported Warehouses”*, Journal of Structural Engineering, **147**(11). https://doi.org/10.1061/(ASCE)ST.1943-541X.0003153

Tsarpalis D., Vamvatsikos D., Deladonna F., Fabini M., Hermanek J., Dot Margotan P., Sesana S., Vantusso E., Vayas I. (2022). *“Macro-characteristics and taxonomy of steel racking systems for seismic vulnerability assessment”*, Bulletin of Earthquake Engineering. https://doi.org/10.1007/s10518-022-01326-x

7 Conclusions

7.1 Summary

The present dissertation attempted to fill gaps on several issues regarding the seismic behaviour of steel racking systems.

Following a brief introduction and problem statement, **Chapter 2** presents a comprehensive review of the macro-characteristics of various racking typologies, focusing on their structural behaviour under seismic actions. Based on the Building Taxonomy of the Global Earthquake Model (Brezv et al., 2013), an extensible taxonomic categorization for racking systems is proposed, comprising five basic “Attributes”, which are broken down to several “Attribute Levels”, and then further discretized to “Options”. The proposed taxonomy was designed to be user-friendly and intuitive, with the considered macro-characteristics being easily identifiable by non-experts. Finally, the classification of several analytical and experimental publications demonstrated that most case studies tend to conform to the low-rise APR systems. On the other hand, the semi- and fully-automated systems, like the multi-depth pallet shuttle racks or the high-rise ARSWs, have not yet received enough academic attention, despite being very popular systems in the market.

As a first step towards understanding the seismic behaviour of the innovative ARSWs, **Chapter 3** presents the seismic assessment of five multi-depth case studies, designed by professional engineers according to the current European standards. The study employed a series of 15 RHAs in each direction, using natural records that respect the hazard of the installation site. The calculation of the component resistances demonstrated the inadequacy of all case studies to develop reliable ductility, as brittle member/connection failure modes were dominant. Along the cross-aisle direction, the weakest components were typically the pallet uprights and their anchorage system. On the other hand, the pallet diagonals and their bolted connections were under-stressed, due to a capacity design rule foreseen by EN 16681 (2016). A non-ductile behaviour was also observed in the down-aisle direction, with the bracing anchors, diagonal connections, and uprights being first in the hierarchy of criticalities.

Subsequently, the effect of the cumulative seismic load multiplier was investigated, by realizing a series of “what-if” scenarios for each case study. It was found that, even if favorable design assumptions are adopted, one also has to employ (or essentially assume) a $q = \Omega$ between 1.5 and 2.0, to drop the UFs of the (pallet and bracing) uprights and diagonals under 1.0. However, the actual overstrength (Ω) of an ARSW may be lower than e.g., 1.5, as high optimization leads to razor-thin overstrength margins. Finally, it was found that a seismic design of anchorage systems using solely MRSA underlies significant uncertainties, as, even in the most pleasing scenarios, most RHAs (scaled at the design level) experienced a base failure.

To counter the issues arising from the application of standard design methods to unconventional rack typologies, such as the high-rise ARSWs, **Chapter 4** adopts a ductile approach for seismic designing along the cross-aisle direction, the plastic ovalization strategy (POS). POS relies on the bearing deformation of the diagonal bolt hole to “dissipate” the seismic excitation, while the rest structural components remain elastic by employing ten new capacity design rules. A parametric study, using existing analytical equations (EN 1993-1-8, 2005; prEN 1993-1-8:2021, 2021) and finite element models, demonstrated that a ductile connection behaviour can be accomplished, as long the diagonal is thick enough to prevent local buckling of its web. To assess the performance of POS, the cross-aisle frames of one double- and one multi-depth ARSW was examined by means of multi stripe analysis (Jalayer and Cornell, 2009), using 30 records and six IM levels. A clear advantage of the POS design was reported, especially for stripes that exceed the design level. This enhanced seismic behaviour was possible without necessarily increasing the overall cost of the structure. This is indeed a very promising finding, as POS sets the ground for resilient racking systems, while at the same time respects the principles of the rack industry that demands simple bolted connections and light steel members.

A simplified modelling approach for the seismic assessment of high-rise ARSWs is proposed in **Chapter 5**, which can reduce the size of the numerical problem by orders of magnitude. It is based on the substitution of truss beams and columns with equivalent Timoshenko beams (Belleri et al., 2017; Kalochairetis and Gantes, 2012), but surpasses previous methodologies by providing the ability for inelastic simulations. This is achieved with the use of link elements that incorporate distinct nonlinear springs to account for each of the modes of relative deformation of their two ends. To assess the robustness and efficiency of the simplified method, the cross-aisle frames of one multi- and one double-depth ARSW was investigated. The simplified models were validated by means of linear modal analyses, static pushover tests, and RHAs, showing a negligible loss of accuracy and remarkable time savings, decreasing the cost of one dynamic analysis from more than an hour down to few seconds. As the evaluation of ARSWs’ seismic behaviour is an on-going research process, the proposed simplified model can suitably fit in the context of performance-based assessment and design (Cornell and Krawinkler, 2000), where low complexity without loss of fidelity is a primary goal.

A comprehensive study on the effect of content-structure-sliding interaction (CSSI) is presented in **Chapter 6**, focusing on the case of steel racking systems. Three approaches were investigated to capture CSSI: (i) employing friction sliders per pallet and running nonlinear RHAs, (ii) increasing the model viscous damping and using elastic RHAs, and (iii) reducing the horizontal seismic loads in tandem with MRSA. Definitely, the most accurate way to simulate CSSI is approach (i), with the cost of increasing the numerical complexity of the model. On the other hand, completely disregarding CSSI during the execution of RHAs leads to large overestimations on the predicted response of the rack. To alleviate this issue while keeping the numerical model as simple as possible, it was found that approach (ii) is a good alternative, which adjusts the damping ratio of the model via a simple regression expression, but also negates the need for nonlinear slider elements.

Finally, a method to account for CSSI in the context of MRSA is proposed (approach (iii)), which is based on the reduction of the horizontal seismic loads by a calibrated E_{N1} factor. Contrarily to what current codes assume, it was found that the second mode of vibration majorly affects the magnitude of CSSI. In this sense, E_{N1} was fitted via linear regression by employing $\sqrt{Sa(T_1)Sa(T_2)}/\mu$ as input IM, instead of the $Sa(T_1)/\mu$ used by the E_{D1} factor of EN 16681 (2016). In the case study examined, E_{D1} overestimated the forces on the uprights and diagonals by 20% – 40% on average, while the proposed E_{N1} showed better overall performance and reduced the overestimation to 2% – 15%. In this sense, correctly considering CSSI can lead to lighter steel members and, thus, to a more economical design. Moreover, the 360 RHA data points were used to define a relationship between the rack's periods of vibration and the magnitude of sliding displacement. It was observed that the high-rise (and flexible) ARSWs are more vulnerable to excessive sliding than the low-rise, first-mode-dominant APRs. Thus, the structural design of racking systems with long periods of vibration may need to be accompanied by a series of RHAs, using approaches (i) and (ii) to estimate the magnitude of pallet sliding and assist decision-making on whether precautions should be taken.

7.2 Limitations and future work

While the results of the present study are based on solid methodologies and comprehensive analytical studies, they are still bound to limitations that call for improvements by future work. Chapter 2 described the structural configuration and macro-characteristics of most rack typologies, but there are several systems, like the mezzanine floor pallet racking systems, excluded from the discussion. In addition, the proposed taxonomy followed the principles of GEM's Building Taxonomy (Brezv et al., 2013), and thus was mainly designed for seismic vulnerability assessment, giving less heed to other hazards, like extreme rain or wind actions. However, the abstract and inclusive nature of the five basic "Attributes" renders the extension/modification of the taxonomy quite easy and straightforward.

The seismic assessment presented in Chapter 3 employed five multi-depth ARSWs case studies, disregarding completely their "sister" systems, the double-depth racks. In this sense, the hierarchy of criticalities is expected to be modified if additional double-depth ARSWs are considered, but only slightly, as the domination of brittle failure modes is prevalent in both systems. More refined results could have also been obtained if a larger set of records was used, i.e., 30 ground motions per case study instead of 15. Another limitation is related to the modelling method, as 2D models were employed to capture the seismic response of three-dimensional structures. Of course, 3D models of high-rise multi-depth ARSWs are extremely cumbersome for seismic assessment (Tsarpalis et al., 2021), but the simplification method presented in Chapter 5 is a promising tool that can shed light on whether the cross- and down-aisle direction can be simulated separately without loss of accuracy or important three-dimensional effects being ignored.

The plastic ovalization strategy proposed in Chapter 4 majorly improved the seismic response of the two case studies when examining global failure. In the future, additional damage states can be introduced, by defining engineering demand parameters that are applicable to racking systems, like excessive bearing deformation or pallet displacement. Indeed, defining additional damage states can be beneficial to the rack community, as it sets the ground for a performance-based earthquake assessment (Cornell and Krawinkler, 2000) of racking systems installed in high-seismicity areas. Moreover, the proposed capacity design rules shall be modified in the future, as the parametric finite element study demonstrated that the thickness of the diagonal plays an important role in the ductility of the connection. Thus, a more consistent comparison between the standard and the POS design can be achieved, if the POS models are re-designed by introducing an additional rule that limits the d/t ratio to be lower than e.g., 5. Finally, the finite element simulations presented in this thesis shall be verified by experimental tests, to determine whether all important connection details were captured. Indeed, in the context of the European project STEELWAR (2017) an experimental campaign that comprises several monotonic and cyclic tests is under way at the time of writing; this will offer a clearer view on the behaviour of the diagonal-to-upright connection and open fruitful discussions in the upcoming months.

The simplified modelling method proposed in Chapter 5 was validated by means of 3D elastic and 2D inelastic static and dynamic tests, respectively. However, the methodology has not been verified yet on 3D inelastic models, which will require the use of three-dimensional link elements and, consequently, the calibration of six translational and rotational springs. Moreover, in the present study the shear springs were calibrated to capture the buckling and yielding of the diagonals, while in the future the method can be extended to also simulate the bearing deformation of the bolt holes, for racks designed according to the POS.

Finally, the investigation presented in Chapter 6 examined the effect of CSSI by only considering cross-aisle case studies. Although pallet sliding is not so crucial in the down-aisle direction, as the uprights can arrest the contents from falling-off, additional studies are required to evaluate its actual effects, especially when weak and flexible MRFs are concerned. In addition, the proposed modelling approaches employed 2D models to capture CSSI, however it is understood that sliding is a complex three-dimensional phenomenon (Castiglioni et al., 2018). Future work, using 3D beam element models accompanied by detailed finite element analyses, may give a clearer view on the sliding problem along the complete horizontal space.

7.3 References

Belleri A., Torquati M., Marini A., Riva P. (2017). *“Simplified building models as advanced seismic screening tools for steel industrial buildings”*, Journal of Constructional Steel Research, **138**, 51-64. https://doi.org/10.1016/j.jcsr.2017.06.027

Brzev S., Scawthorn C., Charleson A.W., Allen L., Greene M., Jaiswal K., and Silva V. (2013). *“GEM Building Taxonomy Version 2.0”*, GEM Technical Report 2013-02 V1.0.0, 188 pp., GEM Foundation, Pavia, Italy.

Castiglioni C.A., Drei A., Kanyilmaz A. Mouzakis H.P. (2018). *“Earthquake-Induced pallet sliding in industrial racking systems”*, Journal of Building Engineeering, **19**, 122-133. https://doi.org/10.1016/j.jobe.2018.05.004

Cornell C.A., Krawinkler H. (2000). *“Progress and challenges in seismic performance assessment”*, PEER Center News, **3**(2), 1-4.

EN 16681 (2016). *“Steel static storage systems - Adjustable pallet racking systems - Principles for seismic design”*, European Committee for Standardization (CEN), Brussels, Belgium.

EN 1993-1-8 (2005). *"Eurocode 3: Design of Steel Structures - Part 1-8: Design of joints"*, European Committee for Standardization, Brussels, Belgium.

Jalayer F., Cornell C.A. (2009). *"Alternative non-linear demand estimation methods for probability-based seismic assessments"*, Earthquake Engineering and Structural Dynamics **38**(8), 951-972. https://doi.org/10.1002/eqe.876

Kalochairetis K. Gantes C.J. (2012). *"Axially and transversely loaded Timoshenko and laced built-up columns with arbitrary supports"*, Journal of Constructional Steel Research, **77**, 95-106. https://doi.org/10.1016/j.jcsr.2012.05.004

PrEN 1993-1-8 (2021). *"Eurocode 3: Design of Steel Structures - Part 1-8: Design of joints"*, European Committee for Standardization, Brussels, Belgium.

STEELWAR (2017). *"Advanced structural solutions for automated STEELrack supported WARehouses"*, The Steelwar Project Consortium, Pisa, Italy. https://www.unipi.it/index.php/risultati-e-prodotti/item/10663-steelwar

Tsarpalis D., Vamvatsikos D., Vayas I., Delladonna F. (2021). *"Simplified Modelling for the Seismic Performance Assessment of Automated Rack-Supported Warehouses"*, Journal of Structural Engineering, **147**(11). https://doi.org/10.1061/(ASCE)ST.1943-541X.0003153

Annex A: Spring stiffnesses of two-node link element

Given L, E, A and I the elastic properties of an Euler Bernoulli beam element, a triplet K_a, K_s and K_r resembling springs' linear stiffnesses has to be determined. In the consolidated system (Figure A.1), an axial nodal displacement δ_a leads to an equal axial spring-displacement $\delta_{a,spring} = \delta_a$, a potential energy U and axial force N related as:

$$U = \frac{1}{2} K_a \delta_a^2 \Rightarrow K_a \delta_a = \frac{\partial U}{\partial \delta_a} = N = \frac{EA}{L} \Rightarrow K_a = \frac{EA}{L} \qquad \text{Eq. (A.1)}$$

Similarly, a transversal nodal displacement δ_s leads to a shear force F:

$$U = \frac{1}{2} K_s d_s^2 \Rightarrow K_s \delta_s = \frac{\partial U}{\partial \delta_s} = F = \frac{12EI}{L^3} \Rightarrow K_{s,EB} = \frac{12EI}{L^3} \qquad \text{Eq. (A.2)}$$

On the other hand, a nodal rotation φ excites a coupled behaviour between the shear and rotational spring, producing both a shear displacement δ and rotation a φ (Figure A.1). For small displacements, it can easily be shown that $\delta = \varphi L / 2$ holds, leading to:

$$U = \frac{1}{2} K_s \delta^2 + \frac{1}{2} K_r \varphi^2 \Rightarrow K_s \frac{L^2}{4} \varphi + K_r \varphi = \frac{\partial U}{\partial \varphi} = \frac{4EI}{L} \Rightarrow K_r = \frac{EI}{L} \qquad \text{Eq. (A.3)}$$

Same procedure can be followed for the case of a Timoshenko beam element with the difference that Eq. (A.2) is transformed to account for a potential shear deformation:

$$K_{s,T} = \frac{12EI}{(1+\Phi)L^3}, \quad \Phi = \frac{12EI}{L^2 G A_s} \qquad \text{Eq. (A.4)}$$

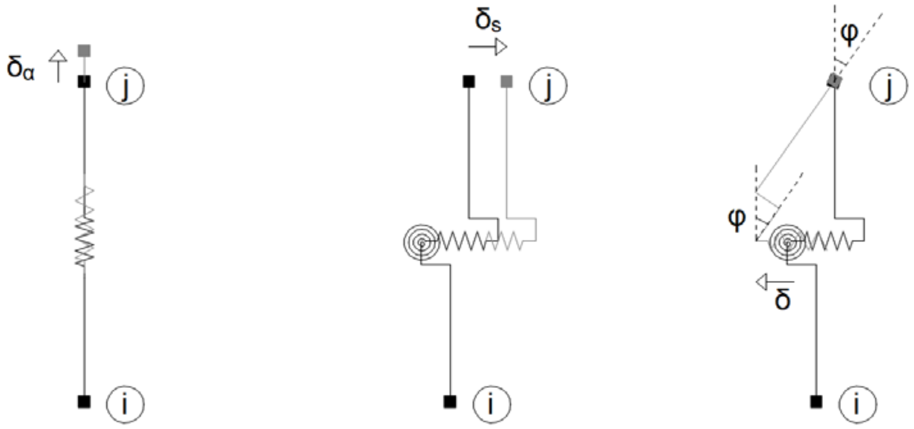

Figure A.1: Unit nodal displacement/rotation for the derivation of springs' elastic stiffnesses (axial, shear and rotational spring).

Annex B: MATLAB function for performing NSBA on an idealized body sliding on a moving platform

```
function [a_rel, v_rel, d_rel] =  NewmarkSlidingBlock(time, acc_plat, acc_y)

    %%---------------------------- INPUT --------------------------------%%
    % time: a vector of size N, containing the time-points to account for a
    % non-constant time step.
    %
    % acc_plat: a vector of size N, containing the absolute accelarations
    % of the platform.
    %
    % acc_y: the yield accelaration.
    %%-------------------------------------------------------------------%%

    %%---------------------------- OUTPUT -------------------------------%%
    % a_rel: a vector of size N, containing the relative-to-the-platform
    % accelaration of the body.
    %
    % v_rel: a vector of size N, containing the relative-to-the-platform
    % velocity of the body.
    %
    % d_rel: a vector of size N, containing the relative-to-the-platform
    % displacement of the body, i.e. the sliding.
    %%-------------------------------------------------------------------%%

    timesteps = size(time, 1);
    v_rel = zeros(timesteps,1);
    a_rel = zeros(timesteps,1);
    d_rel = zeros(timesteps,1);

    for i=2:timesteps
       dt = time(i) - time(i-1);

       if(v_rel(i-1) == 0.0)
          %idle condition
          a_rel(i) = acc_plat(i) - sign(acc_plat(i)) * acc_y;
          avg = 0.5*(a_rel(i)+a_rel(i-1));

          if(abs(acc_plat(i))>acc_y)
                % sliding occurs
                v_rel(i) = v_rel(i-1) + avg * dt;
          else
                % body remains stick to the platform
                a_rel(i)=0.0;
                v_rel(i)=0.0;
                avg = 0.0;
          end
       else
           a_rel(i) = acc_plat(i) - sign(v_rel(i-1)) * acc_y;
           avg = 0.5*(a_rel(i)+a_rel(i-1));
           v_rel(i) = v_rel(i-1) + avg * dt;

           if(v_rel(i)*v_rel(i-1)<0.0 && avg*v_rel(i-1) < 0.0)
               % body re-sticks to the platform
               a_rel(i)=0.0;
               v_rel(i)=0.0;
               avg = 0.0;
           end
       end

       d_rel(i) = d_rel(i-1) + v_rel(i-1) * dt + 0.5 * avg * dt * dt;

    end
end
```